N O T I C E

THIS DOCUMENT HAS BEEN REPRODUCED FROM
MICROFICHE. ALTHOUGH IT IS RECOGNIZED THAT
CERTAIN PORTIONS ARE ILLEGIBLE, IT IS BEING RELEASED
IN THE INTEREST OF MAKING AVAILABLE AS MUCH
INFORMATION AS POSSIBLE

Development of Cathodic Electro-
catalysts for Use in Low Temperature
H_2/O_2 Fuel Cells with an
Alkaline Electrolyte

Contract No. NASW-1233

Q-12

FINAL REPORT

Covering

July 1, 1965 to June 30, 1968

for

National Aeronautics and Space
Administration
Headquarters, Washington, D. C.

TYCO LABORATORIES, INC., BEAR HILL, WALTHAM, MASSACHUSETTS 02154

Tyco Laboratories, Inc.
Bear Hill
Waltham, Massachusetts 02154

DEVELOPMENT OF CATHODIC ELECTROCATALYSTS FOR USE IN LOW TEMPERATURE H_2/O_2 FUEL CELLS WITH AN ALKALINE ELECTROLYTE

Contract No. NASW-1233

Q-12

Final Report
Covering
July 1, 1965 - June 30, 1968

by
J. Giner
J. Parry
L. Swette
R. Cattabriga

NOTICE

This report was prepared as an account of Government sponsored work. Neither the United States, nor the National Aeronautics and Space Administration (NASA), nor any person acting on behalf of NASA:

A.) Makes any warranty or representation, expressed or implied, with respect to the accuracy, completeness, or usefulness of the information contained in this report, or that the use of any information, apparatus, method, or process disclosed in this report may not infringe privately owned rights; or

B.) Assumes any liabilities with respect to the use of, or for damages resulting from the use of any information, apparatus, method or process disclosed in this report.

As used above, "person acting on behalf of NASA" includes any employee or contractor of NASA, or employee of such contractor, to the extent that such employee or contractor of NASA, or employee of such contractor prepared, disseminates, or provides access to, any information pursuant to his employment or contract with NASA or his employment with such contractor.

Requests for copies of this report should be referred to:

National Aeronautics and Space Administration
Office of Scientific and Technical Information
ATTN: AFSS-A
Washington, D. C. 20546

DEVELOPMENT OF CATHODIC ELECTROCATALYSTS FOR USE IN LOW TEMPERATURE H_2/O_2 FUEL CELLS WITH AN ALKALINE ELECTROLYTE

CONTRACT OBJECTIVES

The research under contract NASW-1233 is directed towards the development of an improved oxygen electrode for use in alkaline H_2/O_2 fuel cells. The work is being carried out for the National Aeronautics and Space Administration, with Mr. E. Cohn as technical monitor. Principal investigators are Dr. J. Giner and Dr. J. Parry.

ABSTRACT

In the first phase of this program (section 1 of this report), a survey was carried out on the intrinsic activity of the transition metals, selected transition metal alloys and intermetallic compounds, and transition metal carbides, nitrides, borides and silicides for the electrochemical reduction of oxygen. Subsequently, alloy compositions known to be active were studied in detail. These included (section 2) gold alloys of the precious metals and silver magnesium alloys. Measurements made on finely divided catalysts and compounds of group VIII metals prepared by the Bureau of Mines are described in section 3, while catalysts prepared for life testing and the longevity tests are given in section 4. A coprecipitated platinum gold black was discovered which shows higher performance than platinum. Section 5 is the mathematical treatment of porous PTFE-bonded electrodes. A new model is proposed and the results indicate the possibility of very high power density electrodes.

SECTION 1: SUMMARY AND CONCLUSIONS

Survey of the Intrinsic Activity of Catalysts for the Cathodic Reduction of Oxygen (Solid Electrodes)

A summary of the data obtained in the survey is presented in Table II; the principal conclusions to be made from it are as follows:

A. The Elements

The activity for the reduction of O_2 was Pt ~ Pd > Au ~ Ag > Mn > C ≈Os. Of the remaining elements Fe, Re, Ir, and Rh were active below +675 mv; Ni, Ti, and Cu were active below +360 mv on the DHE scale (DHE ≈ -30 mv vs. RHE).

Metals most active for oxygen reduction were generally those with easily reduced surface oxides. The principal exception was manganese: A substantial O_2 reduction current was observed on MnO_2 at about +900 mv.

i

B. Alloys and Intermetallic Compounds of Transition Metals

The materials examined were alloys of transition metals. They are discussed under four groupings — alloys of (1) platinum, (2) nickel, (3) Ti, Zr, Hf, and (4) Ta.

1. Platinum Alloys

Alloys of platinum with base metals were generally less active than platinum, although a number of alloys equalled platinum in activity, e. g. Pt_2Ta and PtMn.

Alloys of platinum with metals that corroded in the pure state often developed a roughened or etched surface. However, the extent of corrosion was far less than that for the pure, base metal. For example, Pt_2Nb corroded at a substantially lower rate than Nb; similarly, Pt_3Co did not form the surface oxides found with pure cobalt. Alloys showing corrosion (e. g. PtNb) may show a high apparent activity because of surface roughening.

2. Nickel Alloys

Of the nickel-based metal alloys studied, only those with manganese and cobalt were significantly active for the reduction of O_2. In the former system the activity is associated with manganese. The activity of $NiCo_2$ is probably due to the formation of a surface layer of nickel-cobalt spinel. The activity is enhanced by holding the starting potential above + 1200 mv, where Co^{+3} is formed. Apparently Co^{+3} is reduced to Co^{+2} below +750 mv and the activity noted above this potential disappears below +750 mv. Returning the electrode to high potentials restores its performance. This effect was not observed for pure cobalt because of excessive corrosion current.

One of the more interesting characteristics of nickel alloys is the effectiveness of nickel in suppressing corrosion of the alloyed constituents. These effects were observed for alloys of at least 50 wt % nickel and either Mn, Co, Al, Nb, or Mo.

3. Titanium, Zirconium, and Hafnium Alloys

The corrosion behavior of these alloys was similar to that of nickel. No pronounced enhancement of O_2 activity was noted for alloys containing base metals. In fact, the small amount of activity associated with nickel was inhibited in Zr_2Ni and suppressed in $TiNi_3$.

The activity of $TiPt_3$ was less than that of platinum, while Ti_3Au was more active for the reduction of O_2 than gold, being comparable to platinum. The surface area of Ti_3Au increased with time, apparently yielding a surface having a higher Ti/Au ratio than the bulk material had. In spite of the higher surface concentration of non-noble metal, activity of the sample also increased. $ZrAu_3$, richer in gold than is Ti_3Au, showed a lower activity than gold itself and a stable surface.

4. Tantalum Alloys

The performance of alloys of tantalum showed very little interaction between the metals; i.e. the corrosion and O_2 activity were approximately what was expected from a mixture of the pure metals. $TaPt_2$ and $TaPd_3$ are essentially as active as platinum and palladium, respectively.

C. Carbides and Nitrides of the Transition Metals

The carbides and nitrides showed, in general, greater activity than the parent metal; even when the metal itself was inert (e. g. Zr, Hf, TaCr) the carbide showed some activity for O_2 reduction. The highest activities were observed for TiN, VC, Fe_2C, Ni_3C. The latter two materials are discussed in detail in section 3.

D. Borides and Silicides of the Transition Metals

The borides and silicides were characterized by rapid corrosion at O_2 reduction potentials. Exceptions were Ni_2B and Ni_3B, which experienced slight corrosion, and Pt_2B, which was resistant. The activities of these three materials were no greater than those of the parent metals.

E. Silicon Carbide Single Crystals

The 6H-α silicon carbide single crystal is of interest since opposite faces are monatomic and present either silicon or carbon atoms on polishing. The behavior of these faces would be expected to be similar or different, depending on the relative importance of continuum or atomic properties in the catalytic activity of this crystal. The two surfaces behave differently. Notably the first reduction current observed on the carbon side occurs at 525 mv vs. RHE and on the silicon side at 375 mv, suggesting that continuum factors are not dominant in this case.

F. Titanium, Nonstoichiometric TiO_2

The initial survey on solid electrodes showed Ti_3Au to have an activity comparable to platinum. In finely divided form the Ti_3Au intermetallic corroded rapidly and subsequently demonstrated low activity, probably due to the formation of TiO_2. Two approaches were adopted in an attempt to take advantage of the activity displayed by titanium gold intermetallics. One was a more extensive study to understand the electrochemistry of titanium and TiO_2 better, particularly in its nonstoichiometric form which has an electronic conductivity several orders of magnitude greater than the stoichiometric form. The second approach was to look at other alloys of titanium and gold.

The studies of titanium and nonstoichiometric TiO_2 showed that thin films of the nonstoichiometric oxide on titanium will cathodically reduce O_2 at potentials of 550 mv, 220 mv more positive than on the passive stoichiometric TiO_2 film normally formed. Measurements on single crystals of nonstoichiometric TiO_2 showed that the nonstoichiometric forms of reasonable conductivity (e. g. $TiO_{1.8}$) are stable (i. e. they do not revert to TiO_2 stoichiometry) under the experimental conditions of oxygen reduction. However, titanium powder, oxidized under conditions that should give rise to a nonstoichiometric oxide, produced an electrode of high ohmic resistance and negligible activity.

SECTION 2: SUMMARY AND CONCLUSIONS

The Activity of Gold Alloys of Precious Metals and
Silver Magnesium Alloys (Solid Electrodes)

A. <u>Gold Alloys of Ag, Pd, and Pt</u>

The rate of oxygen reduction was measured on gold, platinum, palladium and silver, and the alloys Au/Pd, Au/Pt, and Au/Ag at 10% increments of composition. The activity of the Au/Ag alloys decreased progressively as the silver content was increased. The Au/Pt alloys showed an almost constant activity over the whole composition range; the Au/Pd alloys, however, showed a broad maximum of activity (i. e. greater than that of the Au/Pt alloys) over the composition range. The order of activity was Au/Pd > Au/Pt > Au/Ag. For the 1:1 alloys the following potentials (E_{50}) were recorded at i = 50 $\mu a/cm^2$: Au/Pd - 926 mv, Au/Pt - 878 mv, Au/Ag - 856 mv, all <u>vs.</u> RHE. An interesting feature of the results is that at 25°C palladium (E_{50} = 922 mv <u>vs.</u> RHE) is more active than Pt (E_{50} = 880 mv <u>vs.</u> RHE). At 75°C these figures were 915 mv for Pd and 903 mv for Pt. In other words at 75°C and 50 $\mu a/cm^2$ Pd was more active (12 mv less polarization) than Pt.

B. <u>Silver Magnesium Alloys</u>

The enhanced intrinsic activity claimed in the literature for Ag 1.5% Mg alloys compared with pure Ag was not confirmed. The higher activity that we measured for the alloy was directly related to an increase in surface roughness.

SECTION 3: SUMMARY AND CONCLUSIONS

Preparation and Testing of Finely Divided Catalysts

A number of materials tested as solid electrodes were prepared as finely divided powders: Pd-Au alloys, Pt-Au, Pt-Ag, Pt-Os, and Ti_3Au. Other materials were tested only as powders. All of the materials were tested as plastic bonded electrodes in the floating electrode cell at 75°C, 35% KOH, for oxygen reduction activity.

Many preparations of Pd-Au were made in which the preparative method and alloy composition were changed. The formaldehyde reduction process for making the alloy blacks gave the best results and the 70% Pd alloy was better than other compositions. The Pt-Au and Pt-Os were also made by formaldehyde reduction. Pt-Ag electrodes were made from mixtures of commercial Pt and Ag_2O.

Many preparations of titanium gold, Ti_3Au and TiAu were attempted. Some of these were moderately successful, but the final composition of the powder is believed to be almost pure gold, due to the leaching process involved.

Thirty two samples of Ni_3C were also prepared (in addition to the Bureau of Mines' preparations). Three of these were moderately successful, i. e. about 100 ma/cm^2 at 750 mv vs. RHE.

Interstitial compounds of Fe, Ni and Co in finely divided form were prepared by the Bureau of Mines. These were made up as plastic bonded electrodes and tested at Tyco in 35% KOH at 75°C for activity as O_2 fuel cell electrodes. The activity observed is summarized in Table XV The best performances observed in terms of current at 600 mv were iron carbide — 32 ma/cm^2, iron nitrocarbide — 68 ma/cm^2, iron carbonitride — 3 ma/cm^2, nickel carbide — 94 ma/cm^2, nickel cobalt carbide — 125 ma/cm^2, nickel nitrocarbide — 68 ma/cm^2, and nickel cobalt nitrocarbide — 49 ma/cm^2. Of the nickel cobalt materials the pattern of activity was 3 Ni/Co > Ni/Co > Ni/3 Co. All the cobalt carbide samples tested corroded rapidly. The level of activity of nickel

carbide did not compare favorably with samples of nickel carbide (290 ma/cm^2) and nickel cobalt carbide (350 ma/cm^2) prepared by acetate decomposition in the laboratory. The most likely explanation for this difference is variation in the physical characteristics, particularly the porosity of the catalyst. Carbides and nitrocarbides of Raney alloys of nickel and cobalt with silver, gold and palladium showed greater activity (up to 180 ma/cm^2), but this was generally less than that observed for the uncarbided alloy, e. g. NiAuPd which gave a current of 315 ma/cm^2 at 750 mv.

The level of activity observed with the interstitial compounds of iron and nickel prepared by the Bureau of Mines (excluding those containing a precious metal) does not yet meet the requirements of a practical fuel cell catalyst. Nickel and nickel/cobalt carbides have demonstrated high activity, but reproducibility in terms of good electrode performance was not always obtained. If high activity nickel carbide catalysts could be prepared consistently and with reasonable electrode life, these materials would constitute catalysts of practical interest even though their performance is some 100 mv below that of platinum.

SECTION 4: SUMMARY AND CONCLUSIONS

Catalyst Life Testing

Twelve of the materials tested as floating electrodes were life tested for times ranging from 500 to 3000 hours. The materials tested were as follows:

American Cyanamid Pt AB-40 (system reference)

TYCO Platinum (electrode fabrication reference)

Pt-Au 70/30

Pt-Ag 30/70

Pt-Os 80/20

Pd-Au 40/60

Pd-Au 50/50

Pd-Au 70/30

Pd-Au 60/40 + 50 wt % Ag_2O

Au-Pt-Pd (B.O.M.)

Ag-Pt-Pd (B.O.M.)

Ni_3C (B.O.M.)

Ni_3C (TYCO)

The best results were obtained with Pt-Au 70/30, Pd-Au 40/60, and Pt-Ag 30/70. The Pt-Au alloy is particularly promising in that it showed a higher performance level than platinum at half the catalyst loading of the AB-40 electrode. The Pd-Au is also interesting in that there was no obvious performance loss that could be attributed to corrosion of Pd even after 3000 hours of operation.

SECTION 5: SUMMARY AND CONCLUSIONS

A Mathematical Treatment of the Porous PTFE Bonded Electrodes

A model for the Teflon-bonded electrode which differs considerably from the widely accepted Thin Film and Simple Pore models is proposed and analyzed.

In a Teflon-bonded electrode, the catalyst particles form porous (and electronically conductive) agglomerates which, under working conditions, are flooded with electrolyte. The catalyst agglomerates are bound together by Teflon which creates hydrophobic gas channels. As current is drawn from the electrode, reactant gas diffuses through the gas channels, dissolves in the electrolyte contained in the agglomerates and, after diffusing a certain distance, reacts on available sites of the catalyst particles.

The column of flooded agglomerates has been approximated in the mathematical treatment by a porous cylinder, perpendicular to the surface of the electrode. The catalyst particles and electrolyte in the column were considered to be homogeneously dispersed as a continuum. During operation, gas arrives at the cylinder in a direction perpendicular to its axis and diffuses to its center along the radius, with reaction on catalyst particles in the diffusion path. Ionic current is conducted in a direction parallel to the cylinder axis.

The results obtained with this model differ considerably from the results obtained with other published models. Thus, while the Thin Film Model and its variants predict that only a small fraction (1-10%) of the catalyst is utilized during operation, analysis of our model shows that under the studied conditions (O_2-reduction, $i \simeq 200$ ma/cm^2, 20 mg Pt/cm^2, 35% KOH and 80°C), it is possible to obtain almost 100% utilization of the catalyst. This is a consequence of a very small iR-drop between front and back of the electrode. For example, at 350 ma/cm^2 this iR-drop is typically only about 10 mv.

Because high utilization of catalyst can be obtained with relatively thick electrodes, our work shows that high power density (amps/cm^2) electrodes can be built.

The assumptions made in the treatment and the limitations of the model are discussed briefly. It is shown that with the present assumptions our model does not apply to reactions with higher i_o (such as the H_2-electrode), and modifications of the model are necessary.

CONTENTS

CONTENTS (Cont.)

CONTENTS (Cont.)

CONTENTS (Cont.)

LIST OF ILLUSTRATIONS

LIST OF ILLUSTRATIONS (Cont.)

LIST OF TABLES

LIST OF TABLES (Cont.)

SECTION 1

SURVEY OF THE INTRINSIC ACTIVITY
OF CATALYSTS FOR THE
CATHODIC REDUCTION OF OXYGEN
(SOLID ELECTRODES)

I. INTRODUCTION

The selection of alloys for experimental investigation as electro-
catalysts for oxygen reduction must be carried out in a systematic way.
Random selection is a questionable procedure, since the number of
possible systems is extremely large. For example, even if one restricts
the choice to about 30 transition metals that are generally good catalysts,
there are about 400 binary systems, 4,000 ternary systems, 28,000
quaternary systems, and so on, for a total of about a hundred million
systems. If we consider that, in addition, there are distinct intermetallics
and that even solid solutions of different concentration may have qualitatively
different properties, it is clear that in the available time we can study only
a tiny fraction of the possible compositions.

The intrinsic factor which determines the reactivity of an oxygen
electrode is its atomic composition and the subordinate crystal structure.
The composition ultimately determines both the desirable properties (viz.
electrocatalytic activity for reduction of oxygen) and the undesirable pro-
perties (viz. corrosion or other time-dependent failure mechanisms which
limit the efficiency or life of the electrode). The electrode activity may be
an inherent characteristic of the pure electrode surface, or it may be con-
ditioned by reactions with the electrolyte, e.g. through specific adsorption
or ions.

Previous work on catalysts has been treated within a theoretical
framework based on a consideration of two extreme points of view concerning
the source of surface activity. According to one view (which can be called

the "atomic approach"), the reactivity is determined by the intrinsic chemical properties of the individual surface atoms and is only slightly influenced by the neighboring atoms in the crystal bulk. The other extreme view (which can be called the "continuum approach") is that reactivity is determined primarily by the electronic energy states of the material as a whole, with the specific atomic chemistry being secondary. This approach has been used extensively to interpret chemisorption and catalysis on transition metal alloys where the surface activity has been correlated with d-band occupancy.

The oxygen reaction is admittedly a more complex process, the mechanism of which (i.e. the precise sequence and relative rates of the various elementary steps) still remains unresolved[1]. However, there is ample evidence for the existence of a special kind of oxygen-metal interaction during the electrolytic reduction of oxygen, even if knowledge of the precise nature of this interaction is scanty.

There is also little doubt that the disruption of the oxygen-to-oxygen bond is the slowest step in the over-all process and that hydrogen peroxide appears as an intermediate or by-product during reduction in alkaline solutions. Without going into the details of the reaction, we can thus safely assume that (a) electronic factors play an important role in the kinetics and (b) geometric factors are probably also involved in the catalytic breaking of the oxygen bond.

Catalysts were selected with both the "continuum" and "atomic" approaches in mind. Alloys of noble metals (Pt, Au) — which are good catalysts for O_2 reduction — with base metals were investigated, as well as alloys containing only base metals. The materials examined encompass a variety of crystal types; a partial listing is given in Table I. The validity of the continuum approach to the electrocatalysis of oxygen reduction would be established by alterations on the noble metal activity through alloy formation and/or by the development of high activity through alloying of low activity base metals.

TABLE I

Structure and Stoichiometry of Selected Alloys

Stoichiometry	Structure	Alloy
A_3B	"βW"	Ti_3Au
		Nb_3Pt
		Mo_3Pt
A_2B	$CuAl_2$ type	Zr_2Ni
	$MoSi_2$ type	Ti_2Cu
AB	C_5Cl type	TiCo
	AuCl-B19	NbPt
AB_2	Laves Phases	TaV_2
		HfW_2
		$TiCr_2$
	C.P. phases	$TaPt_2$
		$NbPt_2$
AB_3	$AuCu_3$ type	$TiPt_3$
		$CoPt_3$
	41	$ZrPt_3$
	12 lsh	$TiNi_3$
		$TaPt_3$
		$TaIr_3$
	2 lsh	$ZrAu_3$
		$TiCu_3$
	3 lsh	VPt_3
AB_n $n > 3$		$MoNi_4$
Variable	δ	NbPt
	μ	TaNi

II. EXPERIMENTAL

A. Introduction

A convenient method of testing a material for corrosion resistance and catalytic activity was to use it as a solid ingot. As such, it could be mounted in an alkali resistant resin and tested potentiostatically as a rotating disc electrode run consecutively in N_2- and O_2- saturated KOH-solution.

By potentiostatic measurement of the corrosion current under an inert atmosphere, it was possible to measure the corrosion rate over the whole potential region relevant to an oxygen electrode.

The advantages of this method are that the samples can be prepared with relative ease and have well-defined surfaces. They could therefore be tested unequivocally for corrosion and for O_2-activity under well-defined transport conditions (Levich equation). The main disadvantage of the method is the sensitivity of the electrode, with its low roughness factor, to poisoning by impurities. This disadvantage is minimized by the high electrode potential at which O_2 is reduced and by continuous surface renewal due to the small corrosion current present in most cases. The low concentration of surface defects on solid electrodes, in contrast to that on dispersed electrodes, may lead to lower specific activity, but this difference is probably irrelevant in a comparative study of the relative activity of a series of materials.

B. Testing of Solid Ingots as Rotating Discs

1. Preparation of the Disc Electrode

Carefully weighed mixtures of pure elements were arc-melted in a furnace with six water-cooled copper heaters (each one-inch in diameter), using a tungsten tip under an argon atmosphere. A Ti getter was fired before each run in order to eliminate traces of O_2. A maximum of six ingots weighing 5 to 10 grams could be obtained in one run.

If the alloy or compound was formed peritectically (i. e. during solidification the composition of the solid phase differs from the composition of the liquid phase), the ingot was annealed, generally overnight, at a convenient temperature. If the alloy or compound was formed congruently (i. e. the solidifying phase had the same composition as the molten phase), the ingot could be used without any subsequent thermal treatment.

The ingots were button shaped when removed from the furnace and were cut with a boron carbide or chromonel saw in order to expose two parallel, flat, circular faces. One part of the sawed button was used for metallographic analysis, according to standard procedures.

The part of the button with the two parallel, flat, circular planes was incorporated as shown in Fig. 1a with "Koldmount, " (an acrylic resin — including methylmethacrylate monomer — used for metallographic work, which erroded less than 0. 05 mg/cm^2 in 2N KOH at 80°C over a period of 80 hrs). This arrangement, besides isolating the electrical contact to the electrode from the electrolyte, also constituted an ideal configuration for controlling precisely mass transport to the electrode.

Electrical contact to the button was made by screwing a metal rod down on a spring-loaded contact in the threaded shaft of the Koldmount. The rod, spring, and contact were gold-plated and the rod was covered with heat shrinkable Teflon tubing (Fig. 1a). The electrode assembly was mounted in a Sargent 600 rpm synchronous motor designed for voltammetry with solid electrodes. Contact between the stirring rod and the fixed lead was made by dipping a wire into a pool of mercury in the hollow top of the rod.

A series of ductile materials was also tested in a demountable assembly described by Stern and Makrides[2], with only Teflon and glass exposed to the solution (Fig. 1b). Ductile materials tested in both electrode assemblies gave basically the same results. This confirms that the acrylic resin used in the rotating disc had no poisoning effect on the results.

METAL TUBE

TEFLON SLEEVE

BRASS SPACER

TEFLON SPACER

GLASS SLEEVE

METAL ROD

TEFLON SPACER

SAMPLE
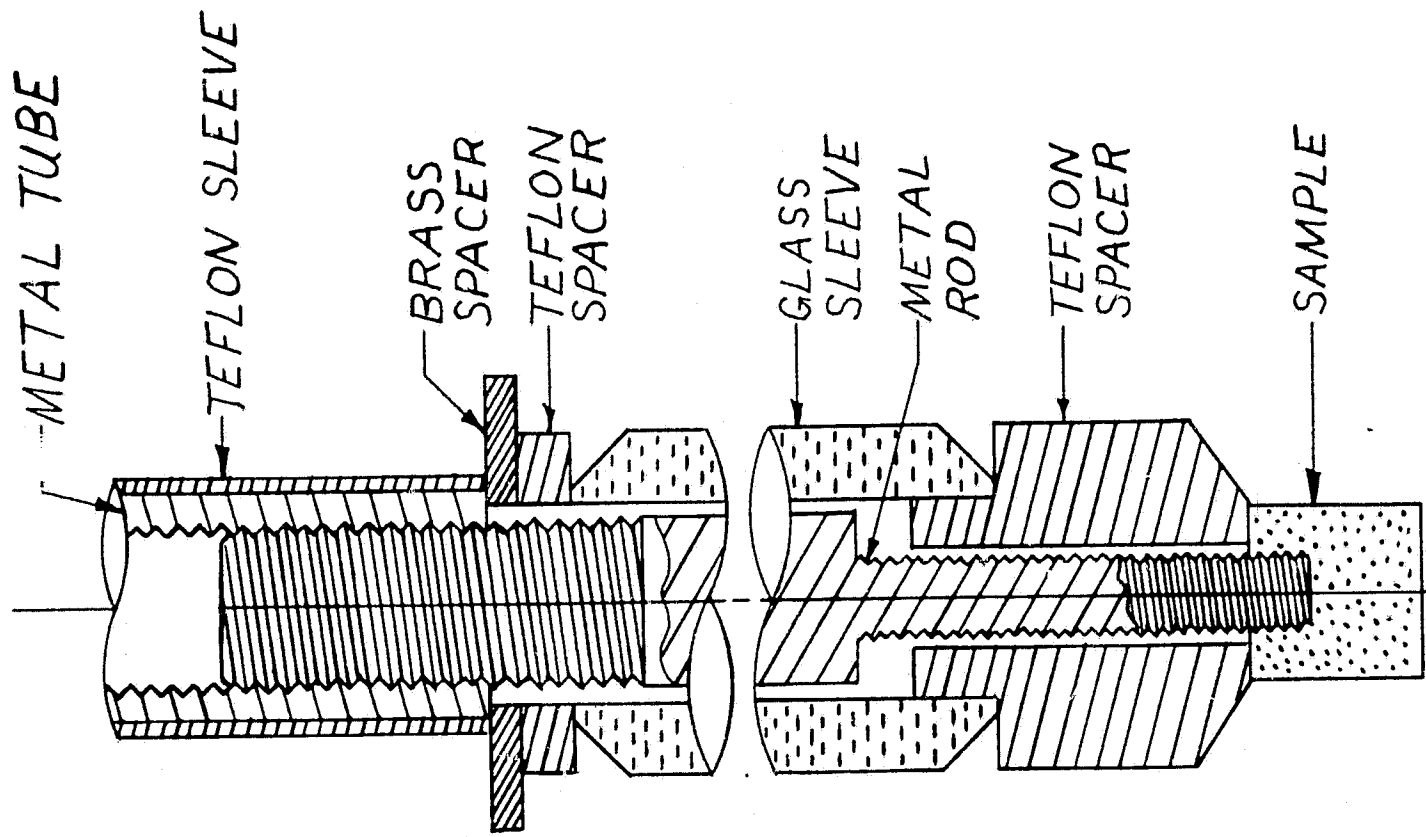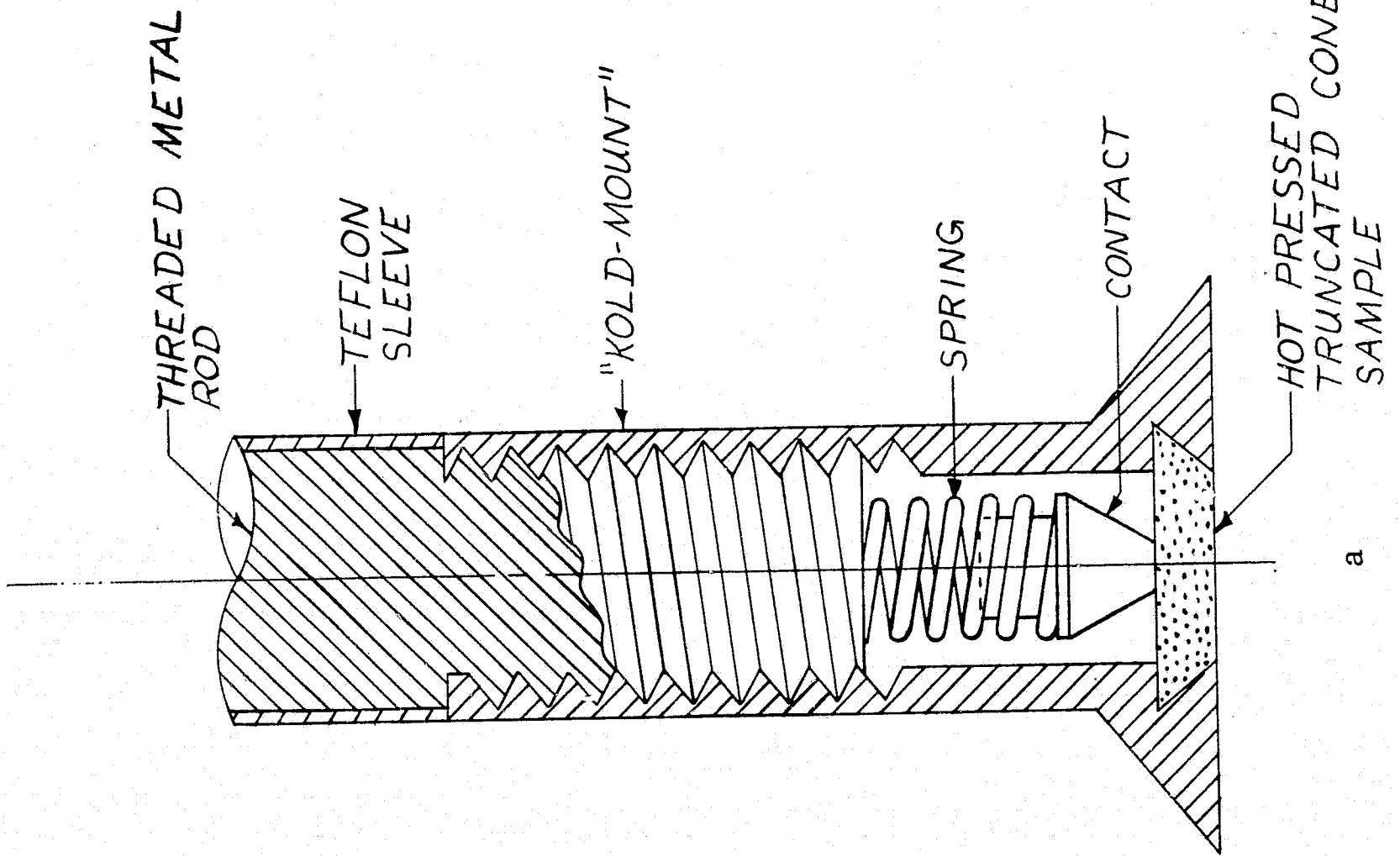
Fig. 1 "Makrides-Stern" holder

4 X ACTUAL SIZE

THREADED METAL ROD

TEFLON SLEEVE

"KOLD-MOUNT"

SPRING

CONTACT

HOT PRESSED TRUNCATED CONE SAMPLE

a

2. Test Cell

The cell shown in Fig. 2 was used. In this cell all the frits were eliminated since they dissolve in caustic solution. The lack of a frit between working and counter electrodes did not introduce a significant error, since during the cathodic oxygen reduction (with oxygen saturated solution) only oxygen was evolved at the counter electrode. The hydrogen evolved at the counter electrode during the corrosion test (N_2-saturated solution) which could dissolve and reach the working electrode was largely swept by nitrogen and therefore did not contribute significantly to the measured current.

The reference electrode was a Dynamic Hydrogen Electrode (DHE)[3] which under the cell-operating condition adopted a potential 30 mv $\pm$ 5 mv negative to the RHE.

The temperature of the cell was regulated $\pm$ 0.5°C by a heating mantle and a regulator with a temperature sensor inside the electrolyte. A temperature of 75°C was selected for the experiments.

The electrolyte concentration was set at 2M KOH after preliminary experiments with 35% (8.4 M) KOH. This concentration had a more favorable transport factor (D x C) than 8.3 M KOH solutions used in fuel cells. Since the screening electrolyte was milder, the chances of missing a possible catalyst were reduced.

3. Electrochemical Measurements

i(E)-curves were generated by imposing a linear potential scan on the working electrode by means of a slow linear potential signal to a Wenking potentiostat. The slow function generator was constructed with two standard batteries, two 10 turn, 10 K potentiometers, and a synchronous motor (Insco Corp., Groton, Mass.). The motor has a basic speed of 4 rpm and six gear ratios of 1:1, 2:1, 5:1, 10:1, 20:1, and 50:1. By changing these gear ratios and the peak voltage, scanning rates from 10 mv/min to 800 mv/min could be obtained. For the initial routine screening, a rate of 50 mv/min was selected.
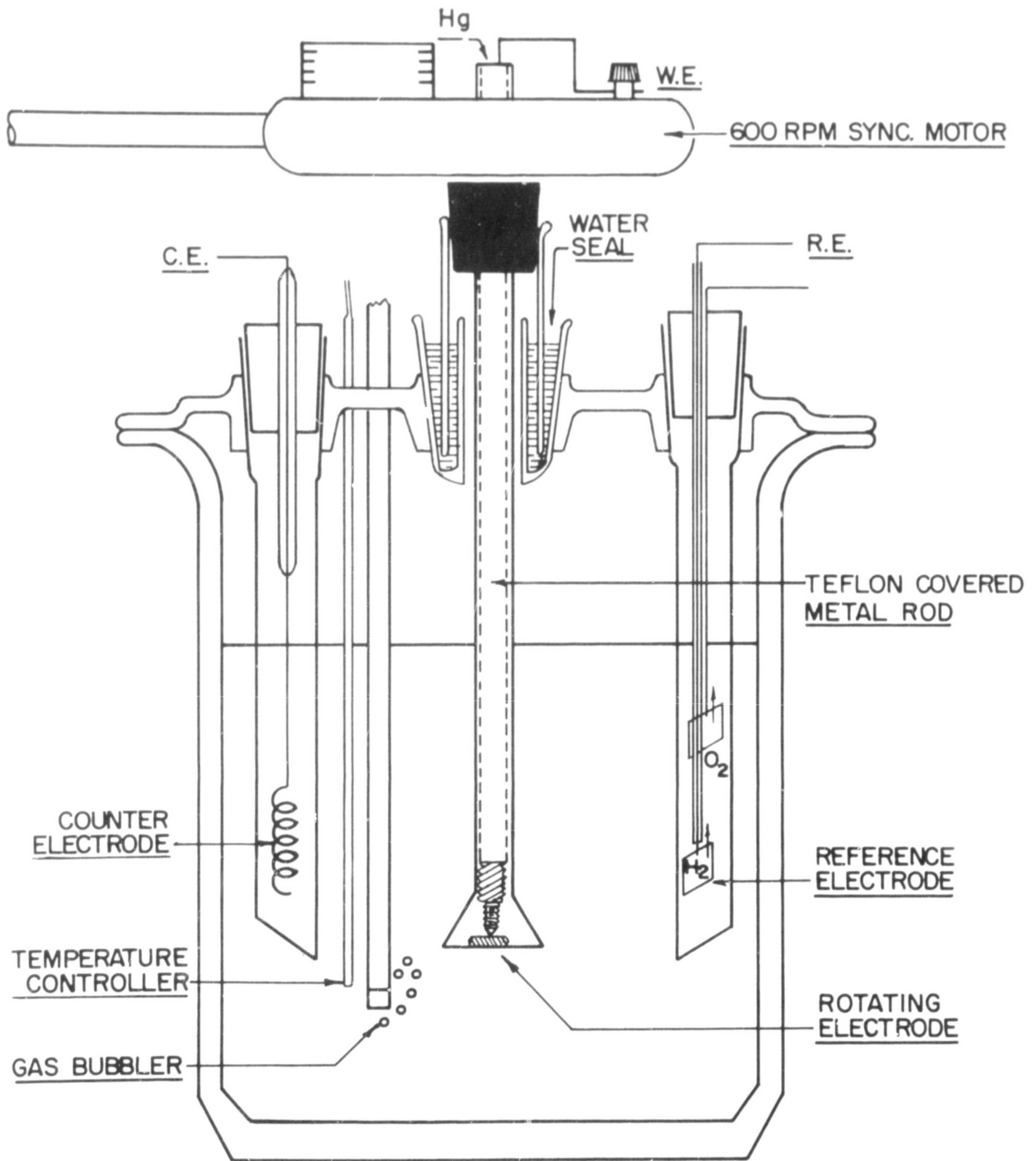
Fig. 2 Rotating electrode cell

572F

The current-potential curve was recorded directly on an x-y recorder. Current-time curves at constant potential for relatively long times could be recorded on the same recorder by using the slow function generator to feed the y-axis of the recorder.

Before an activity test experiment, the corrosion current under inert gas (N_2) was measured at a series of potentials. This corrosion current had to be measured with stirring in order to subtract it quantitatively from the O_2 reduction current. It was also measured without stirring in order to apply the results to a practical electrode. Also, the possibility of a decrease of the corrosion rate with time had to be investigated. As long as the corrosion current was small compared with the expected O_2-current, the O_2-curve was run, even if the corrosion rate was higher than useful for a practical cell.

In order to ascertain whether an observed performance represented the intrinsic activity of a material and not a mere increase of the surface area, the real surface area of the electrode had to be estimated. The only practical method of doing this during screening of a large number of flat electrodes was by measuring the double layer capacity of the electrode.

For the capacity measurements a method was selected in which a triangular wave of 50 cycles/sec and a peak-to-peak voltage of 100 mv (i.e. a sweep rate of 10 volts/sec), biased by a convenient dc voltage, was fed to the signal input of the potentiostat. The dc voltage was selected so that Faradaic currents were avoided. If the electrode behaves as a perfect capacitor (no Faradaic or ohmic resistance), the small triangular potential wave is transformed into a square current wave, with a peak-to-peak value which is proportional to the electrode capacity and therefore to the real surface.

C. Procedure

The following procedure was used for routine screening:

(1) N_2 Saturation

A freshly prepared 2M KOH solution was saturated with pure nitrogen for at least 45 minutes. The electrode was kept inside the cell but not exposed to the electrolyte until N_2 saturation was complete.

(2) Corrosion i(E)-Curve

The electrode was introduced into the solution at a potential of E = 0 mv. The potential scan was initiated within a minute at a rate of 50 mv/min and 600 rpm rotation. The potential scan was reversed between E = 0.8 volt and E = 1.23 volts, depending on the extent of corrosion in this range. If there was a high corrosion rate at the lower potentials, higher potentials were still investigated since there could be a region of passivation in the potential range of interest.

At several points of the i(E)-curve, stirring was stopped for 1 or 2 minutes without stopping the potential sweep (in order to observe the effect of stirring on corrosion).

(3) Measurements of the Double Layer Capacity

At several points in the i(E)-curve under N_2, the recording was interrupted and a double layer capacity measurement was made as described above.

The electrode potential was never left uncontrolled in order to control the history of the electrode from the moment it was immersed in solution. If, in addition to the i(E)-curve, the electrode had to be left for some time at a known potential, the time at this potential was kept as short as possible and noted. The electrode was removed from the solution during extended periods of inactivity, and any attached electrolyte was removed by rotating the electrode in the gas phase for a short time (about half a minute).

(4) O_2-Saturation

If the corrosion current was within tolerable limits, the test for O_2-activity was carried out. The electrode was removed from the system and repolished, and the solution was saturated with O_2 (at least 45 min).

(5) i(E)-Curve for O_2-Reduction

The repolished sample was introduced into the electrolyte at a high, passive potential where possible, but below any current wave

(usually between 0.8 volt and 1.23 volt), and the i(E)-curve was initiated in the direction of decreasing potentials. At E = 0, the direction of the potential sweep was reversed.

(6) Measurements of the double layer capacity in the region of the limiting current were necessary when doubts existed about the real surface increase during recording of the i(E)-curve.

(7) After recording the i(E)-curves, a micrograph of the electrode surface was taken and the sample was filed for subsequent study.

(8) The data presented in tabular form are corrected to the reversible hydrogen electrode (RHE) in the same electrolyte by subtracting 30 ± 5 mv from the recorded potentials (DHE).

D. Presentation of Data

Table II lists the following information for the transition elements and alloys and intermetallic compounds: $E_{\frac{1}{2}}$, the half wave potential; E_2, the potential at which cathodic current was first observed; i_L, the limiting current density; and C, the double layer capacities of the electrode. The significance of these measurements in defining the activities of a catalyst is established below. The detailed results from which these figures were derived were presented in the Fourth Quarterly Report[4]. Comment is also made in Table II on the corrosion (anodic currents) observed for the electrode measured in the absence of O_2.

The reduction of oxygen is an irreversible process, and in the absence of concentration polarization, the current potential curve is described by

$$i = i_o \exp\left(\frac{\alpha z F}{RT} \eta\right) \qquad (1)$$

where i_o is the exchange current, α the transfer coefficient, $z = \frac{n}{\nu}$ where n is the number of electrons involved in the electrode reaction

and ν the stoichiometric number, F is Faraday's constant, R the gas constant, and T the absolute temperature.

If, in addition to activation polarization, concentration polarization appears due to O_2 depletion at the electrode, equation (1) converts to:

$$i = i_o \left(\frac{C^E}{C^B} \right)^{z'} \quad \exp \quad \left(\frac{\alpha z F}{RT} \right) \eta \tag{2}$$

where C^E and C^B are the concentrations of oxygen at the electrode and in the bulk of the solution, respectively, and z' the stoichiometric factor[5] for the oxygen molecule in the reduction reaction.

Equation (2) can be rewritten as

$$\eta = \frac{RT}{\alpha z F} \ln \frac{i}{i_o} + \frac{z' RT}{\alpha 2 F} \ln \left(\frac{C^B}{C^E} \right) \tag{3}$$

It can be easily demonstrated that in case of diffusion-controlled limiting current (as is the case in most of our experiments), at the half wave potential (i. e. when $i = i_{d/2}$) $C^E = \frac{C^B}{2}$.

Equation (3) can then be rewritten as

$$\eta = \eta_{act} + \frac{z' RT}{\alpha z F} \ln 2 \text{ , or at } T = 75°C \tag{4}$$

$$\eta = \eta_{act} + \frac{z'}{\alpha z} \quad 0.018 \text{ (volt)} \tag{5}$$

Thus, for electrodes with similar hydrodynamic conditions (as exist in our experiments) at the half wave potential of a diffusion limited wave, $i = \frac{1}{2} i_L =$ const and the overvoltage ($\eta_{\frac{1}{2}} = E_{\frac{1}{2}} - E_o$) is equal to pure activation polarization plus a small numerical term. This term depends on the transfer coefficient, stoichiometric factor, and stoichiometric number.

It is apparent that the half wave potential is a very appropriate quantity for comparing catalysts studied under identical hydrodynamic conditions, since the normalization of the current to this potential is not subject to errors made in the measurement of electrode area.

In this system there are two complications which limit the rigor with which such a comparison can be made:

(1) The passivating effect of oxides and chemisorbed oxygen. Because of this effect, it is frequently found that above a given potential no current is seen, while below the potential at which the "oxide" is reduced, a very steep (purely diffusion controlled) wave appears. It is therefore possible that electrodes with little "oxide passivation" but large overvoltage due to other causes show a more negative half wave potential than do electrodes with very steep waves but with an "oxide inhibition" at low polarizations.

(2) The formation and accumulation of HO_2^- by partial reduction of O_2 during the following reaction sequence:

$$O_2 + H_2O + 2e^- \rightarrow HO_2^- + OH^- \tag{6}$$

$$HO_2^- + H_2O + 2e^- \rightarrow 3\,OH^- \tag{7}$$
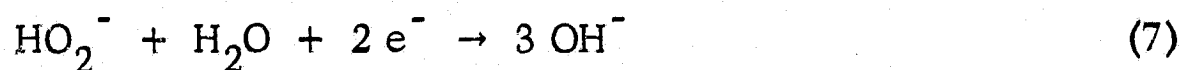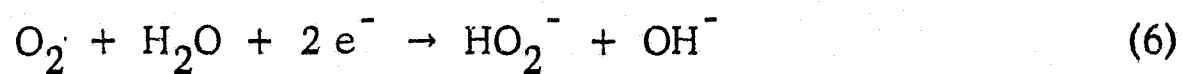
It is possible in principle that an electrode with completely reversible step (6) and very irreversible step (7) (i.e. with a very low half wave potential for the 4-electron O_2-reduction over-all wave) shows much more negative half wave potential than an electrode with less reversible reaction (6) but a more reversible reaction (7).

In order to eliminate this uncertainty, we have included in the tabulation the initial potential, i. e. the potential at which a net cathodic current is observed. This value is, at best, semiqualitative since it is dependent on the sensitivity of the ammeter and the presence or absence of corrosion current. Even with these limitations, it is a good complement to the half wave potential for comparing catalyst performance.

TABLE II

Master Table of Activity for O_2 Reduction and Corrosion Resistance

<u>ELEMENTS</u>

	$E_{\frac{1}{2}}$ mv	E_i mv	i_L $\mu a/cm^2$	C $\mu f/cm^2$	Corrosion
Ag	760	900	1800	60	
Au	785	900	1340	96	
Co					Corrodes
Cr		~200			Corrodes
Cu					Corrodes
Fe	300	645	780	52	
Graphite	370	810	390	410	
Hf					Inert
Ir	544	675	705	176	
Mn	820	900	150	604	Extensive oxide formation
Mo					Corrodes
Nb					Corrodes
Ni	<90	340	500	26	
Os	375	810	250	75	
Pd	835	900	1200	95	
Pt	845	925	1350	115	
Re	340	820	600	350	
Rh	545	820	1370	340	
Ru	545	670	1000		
Ta					Inert
Ti	160	250	600	100	Corrosion >950
V					Corrodes
W					Corrodes
Zr					Inert

TABLE II (Cont.)

ALLOYS AND INTERMETALLIC COMPOUNDS

	$E_{\frac{1}{2}}$mv	$E_i$mv	i_L μa/cm^2	Cμf/cm^2	Corrosion
$AuNb_3$	825	910	582		some corrosion
$AlNi$	130	300	800	17	
$AlNi_3$	100	700	225	18	
$AlNiCo$	175	400	140	212	slight corrosion
Al_3NiCo_2					corrodes
$AuPd$					see separate
$AuPt$					section
$Au_{1.5}Rh_{1.5}Ti$	825	920	658	225	slight corrosion
$AuTi$	745	925	746	51	
Au_2Ti	725	800	665	47	
$AuTi_3$	810	910	698	70	some corrosion
AuV_3					corrodes
Au_3Zr	575	875	360	22	slight corrosion
$AuZr_3$					corrodes
$CoAlNi$	175	400	140	212	slight corrosion
Co_2Al_3Ni					corrodes
$CoHf_2$					inert
Co_2Ni	810	880	500	87	slight corrosion
$CoPt_3$	815	900	680	133	some corrosion
$CoTi$					corrodes
Cr_2Ta					inert, corrosion >850mv
Cr_2Ti	130	270	1000	41	
Cr_4Ti					inert
$CuTi$					corrodes
$CuTi_2$	180	250	240	41	some corrosion
Cu_3Ti					corrodes
Fe_2Ta	230	390	1600	420	some corrosion
Hf_2Co					inert
$HfMo_2$					corrodes
HfW_2					corrodes
Ir_3Ti	550	750	1280	375	

TABLE II (Cont.)

ALLOYS AND INTERMETALLIC COMPOUNDS(cont.)

	$E_{\frac{1}{2}}$ mv	E_i mv	i_L $\mu a/cm^2$	C $\mu f/cm^2$	Corrosion
MnNi(2:1)					extensive oxide formation
MnNi(1:1)	150	820	1430	163	slight corrosion
MnPt(3:1)	820	920		1400	some corrosion
Mo_2Hf					corrodes
$MoNi_4$	150	250	600	19	slight corrosion
MoPt	560	810	1700	350	some corrosion
Mo_3Pt					corrodes
Mo_2Zr					corrodes
Nb_3Au	825	910	582		some corrosion
$NbPt_2$	810	860	1320	133	
NbPt	840	920	1400	820	some corrosion
$NbNi_3$	200	800	910	17	
NiAl	130	300	800	17	
Ni_3Al	100	700	225	18	
NiAlCo	175	400	140	212	slight corrosion
$NiCo_2Al$					corrodes
NiMn(1:1)	150	820	1430	163	slight corrosion
NiMn(1:2)					extensive oxide formation
Ni_4Mo	150	250	600	19	slight corrosion
Ni_3Nb	200	800	910	17	
Ni_2P	210	810	1550	27	slight corrosion
NiTa	120	225	410	30	
Ni_2Ta	175	280	575	80	
Ni_3Ta	160	720	630	65	
Ni_3Ti	90	260	200	15	
$NiZr_2$					inert
PdAg					see separate
PdAu					section
PdPt	840	900	1500	140	
Pd_3Ta	835	890	1250	180	slight corrosion
$PdZr_2$	730	830	1000	68	
Pt_3Co	815	900	680	133	some corrosion

TABLE II (Cont.)

ALLOYS AND INTERMETALLIC COMPOUNDS   (cont.)

	$E_{\frac{1}{2}}$ mv	E_i mv	i_L $\mu a/cm^2$	C $\mu f/cm^2$	Corrosion
PtMo	560	810	1700	350	some corrosion
PtMo$_3$					corrodes
PtMn	820	920	1400		some corrosion
PtNb	840	920	1400	820	some corrosion
Pt$_2$Nb	810	860	1320	133	
PtNb$_3$					corrodes
PtPd	840	900	1500	140	
Pt$_2$Ta	840	900	1205	112	
Pt$_3$Ta	840	890	1280		some corrosion
Pt$_3$Ti	820	870	1003	132	
Pt$_3$V	820	880	1000	132	some corrosion
Rh$_{1.5}$Au$_{1.5}$Ti	825	920	658	225	slight corrosion
Rh$_3$Ti	610	920	1266	129	slight corrosion
TaCr$_2$					inert-corrosion >850mv
TaFe$_2$	230	390	1600	420	some corrosion
TaNi	120	225	410	30	
TaNi$_2$	175	280	575	80	
TaNi$_3$	160	720	630	65	slight corrosion
TaPd$_3$	835	890	1250	180	
TaPt$_2$	840	920	1205	112	slight corrosion
TaPt$_3$	840	890	1280		corrodes
TaV$_2$					
TiAu	745	925	746	51	
TiAu$_2$	725	800	665	47	
TiAu$_{1.5}$Rh$_{1.5}$	825	920	658	225	
Ti$_3$Au	810	910	698	70	some corrosion
TiCo					corrodes
TiCr$_2$	130	270	1000	41	
TiCr$_4$					inert
TiCu					corrodes
Ti$_2$Cu	180	250	240	41	some corrosion

TABLE II (Cont.)

ALLOYS AND INTERMETALLIC COMPOUNDS (cont.)

	$E_{\frac{1}{2}}$mv	$E_i$mv	$i_L \mu a/cm^2$	$C\mu f/cm^2$	Corrosion
$TiCu_3$					corrodes
$TiIr_3$	550	750	1280	375	
$TiNi_3$	90	260	200	15	
$TiPt_3$	820	870	1000	132	
$TiRh_3$	610	920	1266	129	
VPt_3	820	880	1000	132	some corrosion
V_2Ta					corrodes
V_3Au					corrodes
W_2Hf					corrodes
W_2Zr					corrodes
Zr_3Au					corrodes
$ZrAu_3$	575	875	360	22	slight corrosion
$ZrMo_2$					
Zr_2Ni					inert
Zr_2Pd	730	830	1000	68	
ZrW_2					corrodes

TABLE II (cont.)

INTERSTITIAL COMPOUNDS - BORIDES AND SILICIDES

Electrode	Corrosion Behavior	E_I for O_2 Reduction
TiB_2	corrodes	<+200
Ti_5Si_3	corrodes	<+200
$TiSi_2$	corrodes	<+700 mv
ZrB_2	high corrosion current	----
$ZrSi_2$	high corrosion current	----
VB_2	high corrosion current	----
VSi_2	high corrosion current	----
NbB	high corrosion current	----
NbB_2	high corrosion current	----
$NbSi_2$	corrodes less than NbB, by order of magnitude	----
TaB	high corrosion current	----
TaB_2	high corrosion current	----
Ta_5Si_3	low corrosion current	----
$TaSi_2$	higher corrosion current	----
CrB	Cathodic current above +300; Anodic current below +700	----
CrB_2	similar to CrB	
Cr_5B_3	similar to CrB	
Cr_2B	low corrosion currents	low O_2 currents

TABLE II (Cont.)

Electrode	Corrosion Behavior	E_I for O_2 Reduction
Cr_3B	similar to Cr_2B	----
Cr_4B	similar to Cr_2B	----
$CrSi_2$	very low corrosion below lv	----
Cr_3Si	very low corrosion below lv	----
MoB	high corrosion currents above + 200	----
MoB_2	high corrosion currents above + 200	----
$MoSi_2$	high corrosion currents above + 200 (lower than MoB)	----
WB	high corrosion currents above + 100	----
W_2B	high corrosion currents above + 100	----
W_2B_5	high corrosion currents above + 100	----
WSi_2	high corrosion currents above 0	----
$MnSi_2$	high corrosion currents	
$CoSi_2$	corrosion	
Ni_2B	stable	+250
Ni_3B	stable	+150
Pt_2B	stable	+875
B_4C	stable	low +200

TABLE II (cont.)

INTERSTITIAL COMPOUNDS-CARBIDES AND NITRIDES

	E_i*mv	i $\mu a/cm^2$ at 500 mv	i $\mu a/cm^2$* at 150mv	C $\mu f/cm^2$	Corrosion
Ti	+250	----	0.24	100	
TiN	+770	0.27	1.13	540	
TiC	+820	0.1	0.26	220	
Zr	----	----	----	----	inert
ZrN	----	----	----	435	
ZrC	+400	----	0.48	46	
Hf	----	----	----	2	
HfN	+500	----	.01	----	
HfC	+500	----	0.80	17	
V	----	corrosion	----	----	corrodes
VN	+180			>500	
VC	+820	0.27	0.50	61	
Nb	~270	corrosion	1.0	----	
NbN	~270	----	0.4	----	
NbC	+600	0.29	1.1	169	
Ta	inert	----	----	----	
TaN	+100	corrodes	----	----	
TaC	+630	0.15	1.0	----	
Cr	+200	----	.01	22	
Cr_2N	+400	----	.01	266	
Cr_3C_2	+600	0.3	1.1	----	

* The E-i characteristics do not permit unequivocal definition of $E_{\frac{1}{2}}$ or i_L for most of these materials.

TABLE II (Cont.)

	E_i mv	$i\ \mu a/cm^2$ at 500mv	$i\ \mu a/cm^2$ at 150mv	$C\ \mu f/cm^2$	
Mo	----	----	----	----	corrodes
Mo_2C	----	----	----	----	corrodes
W	----	----	----	----	corrodes
WC	----	----	----	----	corrodes
WC-Co	----	----	----	----	corrodes
Fe	+645	0.14	0.70	52	
Fe_2C	+770	0.42	0.88	28	
Ni					
Ni_3N		Separate Section			
Ni_3C					
Carbon (graphite)	+820	0.55	0.56	410	
SiC					
(C-side)	+525				Inert
(Si-side)	+375				

III. RESULTS

A. Transition Metals and Intermetallics

Table II presents all the data accumulated on the activity and corrosion resistance of the elements of the transition series and of intermetallic and interstitial compounds. The intermetallic compounds are listed alphabetically for each component. Supplementary Tables III to IX group the materials in terms of activity, corrosion resistance, etc., and are discussed in detail below.

The first group (Table III) comprises those transition elements that show activity for O_2 reduction above + 800 mv.

TABLE III

Transition Metals Active for O_2 Reduction Above + 800 mv

Mn	Ag
	Au
Pd	(C)
Pt	Os

The performance curves indicate the order of activity (based on initial potential): $Pt \approx Pd > Au \approx Ag > Mn > C \approx Os$.

Of the remaining elements, Fe, Re, and Ir are active below +675 mv; Ni, Ti, and Cu are active below +360 mv.

A parallel grouping of the metals can be formed according to whether oxygen is reduced on an oxide or on "bare" metal. This correlation is shown in Table IV.

TABLE IV

Oxygen Reduction Activity vs. Surface Composition

Oxide Surface	Metal Surface
Ti	Pd
Nb	Pt
Fe	Ag
Mn	Au
Ni	Cu

The performances of the transition metals are summarized in Table V according to position in the periodic table, in Table VI, according to the potential region of activation controlled current, and in Table VII according to $E_{\frac{1}{2}}$ and E_i values.

The most active elements are those for which the metal itself catalyzes the O_2 reduction process. The low limiting currents and the slope of the performance curves for Fe, Ti, and possibly Ni and Re indicate that these materials have a low activity for the decomposition of HO_2^-. Nb also shows a two-step reduction; however, some ambiguity is introduced by corrosion.

Manganese dioxide is the one oxide which shows activity for oxygen reduction at high potentials.

TABLE V

O$_2$ Reduction Properties of the Elements

Group	Metal	E_i	$E_{\frac{1}{2}}$	i_1 (ma/cm^2)
IV B	Ti	250	160	0.66
	Zr		inert	
	Hf		inert	
V B	V		corrodes	1.36
	Nb		(2 190), corrodes	
	Ta		inert	
VI B	Cr	~ 200	< 0, corrodes > + 950	
	Mo		corrodes	
	W		corrodes	
VII B	Mn	900	~ 820	0.60
	Re	820	340	0.60
VIII B	Fe	645	300	0.78
	Ru	670	545	1.00
	Os	810	375	0.25
	Co		"corrodes"	1.37
	Rh	820	545	0.70
	Ir	675	544	
	Ni	340	<90	0.50
	Pd	900	835	1.2
	Pt	925	845	1.35
I B	Cu	900	oxide formation	1.33
	Ag	900	760	1.80
	Au		785	1.34
graphite		810	370	0.89

TABLE VI

Materials Active for O_2 Reduction

Potential Region of Activation Control Current

> + 700 mv	+ 700 to + 450	+ 450 to + 250	+ 250 to + 100	≤ + 100
Pt, TiPt₃, Co₂Ni	Re, MoPt	Ni*	Ti, Ti₂Cu	Cr
Pd, TaPt₃, ZrAu₃	Fe, TaNi₃	Cu, ZrC	Nb, TiNi₃	TiCr₂
Ag, VPt₃, Ti₃Au	Ru, TiIr₃	Ni₃Nb*, HfC	Ni₃Ti, TiCr₄	TiCo
Au, CoPt₃, TaPd₃	Ir, TiC	TiCu, NbC	NiTa, NbN	ZrN
Mn, TaPt₂, C	TiN	TiCu₃, Ni₃N*	TaNi₂, CrSi₂	HfN
Os, NiPt₂, Pt₂B	VC	TaFe₂, Cr₅B₃*	Ni₄Mo, Ni₂B	VN
TiAu₁.₅Rh₁.₅	TaC	Ni₂P	NiAl, Ni₃B	TaN
AuNb₃	Cr₃C₂	Fe₂Ta	Ni₃Al*, B₄C	Cr₂N
AuTi	Fe₂C		Alnico*	TiB₂
Au₂Ti	Ni₃C*			TiSi₂**
MnNi (3:1), PdZr₂	Ti₃Si			
MnNi*, Cr₂B	Cr₂B			

* The placement of these materials is not well defined by the data.

** Considerable corrosion also observed in this potential range.

TABLE VII

Classification of O_2 Reduction Catalysts According to $E_{\frac{1}{2}}$

(Materials Showing Activity Above + 700 mv)

Class 1 ~ 840 mv

Material	E_1	$E_{\frac{1}{2}}$
Pt	+925	+845
Pt_2Ta	920	840
Pt:Pd	900	840
Pt_3Ta	870	840
Os	810	375*
PtNb	920	840

Class 2 ~ 830 mv

Pd	900	835
$TaPd_3$	890	835
Pt_2B	875	830

Class 3 ~ 800 mv

$AuNb_3$	910	825
$Ti(Au_{1.5}Rh_{1.5})$	920	825
PtMn	920	820
Mn	900	820**

---

* Low $E_{\frac{1}{2}}$ due to slow reduction of HO_2^-.

** Limiting current was not observed due to oxide reduction.

TABLE VII (Cont.)

Class 3 ~ 800 mv (Cont.)

Material	E_1	$E_{\frac{1}{2}}$
Pt_3V	880	820
Pt_3Ti	870	820
Pt_2Nb	870	820
Pt_3Co	900	815
Ti_3Au	910	810

Class 4 < 800 mv > 700 mv

Au	900	785
Ag	900	760
AuTi	925	745
$PdZr_2$	830	730
$AuTi_2$	800	725

Class 5 < 700 mv

MnNi (3:1)	820	700
$TiRh_3$	920	610
$ZrAu_3$	875	575
PtMo	810	560
$TiIr_3$	750	550
C	810	370
MnNi	820	150

Finally, we group together those metals which either corrode substantially or are inert over the potential range 0 to +1200 mv. These metals are listed in Tables VIII, IX, X, and XI.

TABLE VIII

Elements Not Active as Oxygen Electrodes

Corrode	Inert
V	Zr
Nb*	Hf
Ta	Cr**
Mo	
W	
Co	

  * Active where corrosion is observed
** Corrodes above +900 mv.

TABLE IX

Materials Inert Between 0 and +1200 mv

Zr	Zr_2Ni
Hf	Hf_2Co
Ta	HfN

TABLE X

Materials Showing <u>Anodic</u> Current Between + 800 and + 1200 mv

Cr	Co_2NiAl_3	TiC	TaC	Cr_2B	Cr_3Si
Re	$TiCr_2$	VN	Cr_2N	Cr_3B	
Os	$TiCr_4$	VC	Cr_3C_2	Cr_4B	
Ag	$TaCr_2$	NbC	CrB	$CrSi_2$	
Rh	Ti_3Au				

TABLE XI

Materials Showing <u>Anodic</u> Current Below + 800 mv

V	NbPt (low)	TiCu*	ZrN	$TiSi_2$	TaB_2	W_2B
Nb	MoPt (low)	$TiCu_3$	HfC*	ZrB_2	$TaSi_2$	W_2B_5
Mo	Nb_3Pt	TiCo	NbN	$ZrSi_2$	Ta_5Si_3	WSi_2
W	Mo_3Pt	TaV_2	TaN	VB_2	CrB_2	$MnSi_2$
Co*	Co_2NiAl_3	$TaFe_2$	Mo_2C	VSi_2	Cr_5B_3	$CoSi_2$
Cu*	$ZrMo_2$	MnNi*	WC	NbB	MoB	
Mn*	$HfMo_2$		WC-Co	NbB_2	MoB_2	
	ZrW_2		TiB_2	$NbSi_2$	$MoSi_2$	
	HfW_2		Ti_5Si_3	TaB	WB	

---

* Apparent insoluble oxide

In a number of cases, the observed corrosion behavior was other than that predicted by thermodynamics. Consider the following specific examples:

a) Vanadium corroded at negative potentials, presumably due to the formation of $HV_2O_5^-$. A slight passivation occurred at $+$ 200 mv; the predicted transition to V_2O_5 or $H_3V_2O_7^-$ at about 600 mv was not observed.

b) Niobium is reported to be covered by an insoluble oxide at positive potentials. However, corrosion of niobium was observed above + 250 mv, presumably because of a soluble reaction product.

c) The formation of soluble $WO_4^=$ is predicted to occur at negative potentials. However, the formation of a soluble corrosion product was not observed below + 200 mv.

The remaining transition elements show some activity for O_2 reduction. Table IX lists elements which catalyze O_2 reduction above + 800 mv.

The borides, silicides, carbides, and nitrides of the transition metals were surveyed for their corrosion behavior and their activity for catalyzing the electrochemical reduction of oxygen.

The performances of materials within each grouping is discussed in terms of modifying the properties of the parent transition metal.

In a later section of this report, we discuss a more detailed study of highly dispersed carbides, nitrides, nitrocarbides, and carbonitrides of Fe, Ni, and Co. The data presented below are, except where noted, for solid electrodes.

B. Nitrides and Carbides

(1) Ti, TiN, TiC

A slight anodic corrosion current is observed for titanium. This current is much less for TiN even though the surface area of the nitride is much greater, as indicated by the capacitance (540 $\mu f/cm^2$). Substantial corrosion of TiC is observed above +830 mv. Judging from the absence of a passivating current, the reaction product is either partly soluble or porous.

The O_2 reduction activity of TiN is substantially higher than that of Ti. The current-potential curve has two waves, implying a difference in rate for O_2 and HO_2^- reduction noted for oxide coated metals. This material was also studied with a graphite counter electrode to eliminate the possibility of contamination of TiN by dissolved platinum. No difference in activity was found.

TiC is slightly more active than titanium and some O_2 reduction current is noted at +820 mv. However, its performance is less than that of TiN. Some of this could be ascribed to the large difference in surface area.

(2) Zr, ZrN, ZrC.

As noted previously, Zr does not corrode or reduce O_2 over the potential range studied. ZrN shows a slight activity and possibly corrosion at potentials above +600 mv.

Corrosion is not observed for ZrC; the material shows cathodic current for O_2 reduction below +400 mv.

(3) Hf, HfN, HfC.

Hafnium, like Zr, is inert over the potential range studied. The low capacitance ($2~\mu f/cm^2$) is consistent with an insulating oxide film. HfN is also essentially inert although there is a slight indication of activity below +500 mv.

HfC shows an anomalous anodic current peak at +630 mv. O_2 reduction is observed at potentials less positive than +500 mv.

(4) V, VN, VC.

Vanadium corrodes under the conditions of the experiment, presumably with the formation of a soluble product. Anodic corrosion current is observed for VN above +180 mv, and a small amount of oxygen activity is observed below +180 mv. These corrosion reactions are further suppressed in VC. Anodic current is observed only above +820 mv; the low capacitance ($60~\mu f/cm^2$) at +600 mv is consistent with a stable surface. Cathodic O_2 reduction current is observed below this potential.

(5) Nb, NbN, NbC.

Niobium corrodes above +170 mv, but is also active for O_2 reduction; a net cathodic current was observed below +270 mv. The corrosion behavior of NbN is similar to that of the metal; the O_2 activity may be less, although this point is difficult to establish because of the corrosion current.

NbC is more resistant to corrosion than is the metal; anodic current is observed only above +600 mv. Reduction of oxygen is observed below this potential; as with the other carbides studied, two waves are present.

(6) Ta, TaN, TaC.

Tantalum is essentially inert over the potential range studied. The nitride, on the other hand, shows substantial corrosion at potentials more positive than 0 mv. A small amount of oxygen activity is observed below + 100 mv. Corrosion is observed for TaC above + 630 mv, and O_2 reduction is observed below + 630 mv.

(7) Cr, Cr_2N, Cr_3C_2.

Chromium shows little activity for O_2 reduction and corrodes to soluble chromate above + 900 mv. The behavior of Cr_2N is essentially identical. The corrosion behavior of Cr_3C_2 is apparently more complex; anodic current is observed above + 350 mv. Net O_2 reduction activity is observed below + 600 mv.

(8) Mo, Mo_2C.

Substantial corrosion current is observed for both materials.

(9) W, WC, 94 WC - 6 Co, 80 WC - 20 Co.

The corrosion behavior of W and WC are essentially identical. This behavior appears to be somewhat suppressed by alloying with cobalt. Anodic current peaks are observed rather than continuous corrosion.

(10) Fe, Fe_2C.

Fe_2C is somewhat more active than Fe and cathodic current is observed at more positive potentials. Both limiting currents are low ($\sim 0.8 - 0.9$ ma/cm^2), indicating incomplete reduction of O_2. The electrical capacitances of the electrodes indicate stable surfaces on both samples.

(11) Ni, Ni_3N, Ni_3C.

It was difficult to prepare the carbide and nitrides as solid ingots; powder electrodes were therefore used; the preparative techniques are described elsewhere.

Ni_3N is slightly more active than nickel, and Ni_3C is two orders of magnitude more active than nickel. It is not clear whether this high activity is an inherent property of Ni_3C or due to a high surface area. Furthermore, the sample is not pure Ni_3C; nickel is also present as a major constituent.

The corrosion behavior of these compounds relative to the parent metals is given in Table XII. The data are qualitatively displayed in terms of increased or decreased corrosion.

TABLE XII

Relative Corrosion Behavior

Metal	Nitride	Carbide	Corrosion Level (Metal)
Ti	decreased	increased	low
Zr	small increase	small increase	none
Hf	no change	?	none
V	decrease	decrease	high
Nb	no change	decreased	high
Ta	increase	increase	none
Cr	no change	increase	at high potential
Mo	----	no change	high
W	----	no change	high

There are no systematic trends in corrosion behavior useful in predicting the behavior of other compounds or in correlating with other pertinent parameters such as O_2 activity. The corrosion rates of VC, VN, NbC, and TiN are lower than they are for the metals. However, Cr_3C_2, TiC, and TaC corrode faster than the parent materials. Apparently either porous or soluble products are formed since passivation currents are not observed. This effect implies that the composition of the surface oxide film normally present on the metal has been substantially altered by the presence of carbon.

The carbides are all more active than the parent metal for O_2 reduction, and some activity is found even when the metal itself is inert, e.g. Zr, Hf, Ta, and Cr. Except for the titanium compounds, the nitrides are less active than the carbides. The apparent limiting currents (at + 150 mv) for Cr_3C_2, Fe_2C, NbC, and TaC were significantly higher than for graphite, implying that the carbides are more effective in reducing HO_2^-.

The highest activities were observed for TiN, VC, Fe_2C, and Ni_3C. The relative activity of TiN may be misleading since the material had a high surface area (540 $\mu f/cm^2$). The use of VC cathodes is impractical because of corrosion at high positive potentials. Fe_2C is apparently stable over the voltage range studied so that its use is not ruled out by corrosion problems.

C. Borides and Silicides

Corrosion currents are observed for the borides and silicides of the refractory metals. Of interest are the high corrosion rates for the borides and silicides of metals which are inert in 2N KOH, e.g. Zr, Hf, and Ta. Evidently, the normally passivating film of insoluble oxide is substantially modified by the nonmetallic constituent, more so than for carbon or nitrogen.

The chromium compounds are the most stable in this group, although a small amount of corrosion current is observed for the high boron-content compounds, i.e. CrB, CrB_2, and Cr_5B_3. The first two of these materials also show cathodic currents. It is tempting to assign this current to reduction of soluble chromate. However, the stirring in these experiments should remove from the surface chromate produced at high potentials.

Because of these high corrosion currents, the refractory metal borides and silicides cannot be considered as possible oxygen electrodes.

The group VIII borides studied (Ni_2B, Ni_3B, Pt_2B) were relatively resistant to corrosion, although even in the case of Pt_2B anodic current was observed at high potentials. The measurement of O_2 activity indicated no enhancement due to the presence of boron.

D. Silicon Carbide

Single crystalline 6H-α-silicon carbide most frequently grows in the direction of the c-axis, and consequently the largest surfaces will be the {0001} planes. These surfaces are monatomic, one side showing silicon atoms and the opposing parallel surface only carbon atoms.

Both surfaces, carbon and silicon, of the SiC crystal showed activity for O_2-reduction. However, there are some differences between the two surfaces which could be related to the surface composition. The open circuit potential, though not a completely reliable parameter here, is higher on the carbon side of the crystal (700 mv vs. 500 mv). The initial cathodic current on the carbon side is observed at 525 mv vs. RHE, compared with 375 mv for the silicon side. The cathodic current at 0.0 mv is 34 μa for the carbon side and 15 μa for the silicon side.

These differences suggest that for SiC continuum factors are not the dominant factor in the rate of reduction of O_2.

E. Ti and TiO_2

The first measurements on titanium metal were made with a sweep from 1000 to 0 mv at 50 mv/min. O_2-reduction current was first observed at 400 mv. The diffusion limited current was not reached above zero mv. The corrosion current observed under nitrogen was of the order of 10-20 μa/cm^2.

The reaction obviously occurs on an oxide layer down to potentials of -450 mv. When the sweep is extended to -900 mv or held at -600 mv, O_2-reduction is apparently taking place on a clean titanium metal surface, as indicated by the large hysteresis and the exceptionally flat diffusion current plateau.

The paper of Bianchi, Mazza, and Trasatti[6] asserts that in alkaline solutions of hydrogen peroxide, the "black oxide" is formed in preference to the passive oxide film. We examined the behavior of this black oxide in the potential region of O_2 reduction. The titanium electrode was exposed in the first case to 0.1 molar peroxide solution for 120 hours. This electrode was then tested for O_2-reduction activity. The potential at which O_2-reduction occurs is shifted to more positive values, $E_{\frac{1}{2}}$ by about 70 mv and E_1 by about 200 mv. The double layer capacity increases by a factor of approximately two.

In a subsequent experiment the peroxide concentration was increased to 1M. The electrode was left in solution for 20 hours and then tested for O_2-reduction activity. It had a heavy, adherent black film on its surface. The shift in potential for O_2-reduction was ~ 200 mv more positive; the double layer capacity increased by a factor of 25.

Current voltage curves were measured on single crystals of TiO_2. Measurements were made on both the "a" and "c" crystals in the "as-received" condition. The as-received crystal was slightly oxygen deficient, but from the electrochemical behavior the stoichiometry was not far removed from TiO_2.

Interesting differences are already apparent between the two crystallographic orientations. The potential at which a reduction current is first discernible (E_i) is 100 mv greater for the c-axis crystal (at 375 mv vs. RHE) than for the a-axis crystal. The effect of the difference in conductivity can be seen in the less rapid increase of current with potential for the a-axis crystal below 275 mv.

The two samples were retested after reduction in H_2 at 1000°C for 3 hours. The temperature for this process was increased from room temperature to 1000°C in three hours. The cooling time was 15 hours; (these times were necessary to prevent thermal cracking). The resistance of this crystal (measured with a resistance meter across the electrode configuration) was about 50 ohms, which is considerably less than the original sample. The reduced sample shows an increase in activity over the original crystal. The initial cathodic current is observed in the present case at 500 mv, compared with 375 mv observed previously. The sample was subsequently swept through different potential ranges in a manner similar to the measurements made on pure titanium to check the effect of prepolarization. The results are essentially the same with one significant exception: Sweeping to -600 mv on pure titanium produces a clean metal surface and a flat diffusion current plateau on the return sweep. This was never observed on the titanium dioxide crystal.

Finally, a slow sweep was rerun at the end of this series, starting at the open circuit potential and going to 1000 mv before sweeping back to 0.0 mv. The initial potential at which cathodic current is seen occurs at a higher potential, ~ 750 mv, than that at which cathodic current occurs initially, ~ 550 mv.

Similar measurements were made with the c-axis crystal. Cathodic current on these crystals is first observed at 850 mv, i.e. approximately 100 mv more positive than in the a-axis crystal. Pre-polarization of the electrode in anodic and cathodic directions has no discernible effect.

IV. DISCUSSION

We can consider these catalysts mainly in terms of the role of the oxide film formed on the surface during the oxygen reduction process. There are three main groups.

The first includes metals on which oxygen reduction begins only when bare metal surface becomes available - that is after substantial reduction of an oxide or chemisorbed oxygen layer. The reduction of oxygen proceeds directly to water on the bare surface with very little hydrogen peroxide accumulation. Examples of metals of this type include those of the Pt group and silver. Within this group Pt has the highest activity at low temperatures. The metals Zr, Ta, Hf, and Nb can be included in this group insofar as an oxide layer is present at all potentials and no appreciable O_2^- reduction occurs.

The next group contains elements such as Ti, Ni, Fe, and graphite. Oxygen is reduced on these materials on oxide-covered surfaces with varying degrees of reversibility. For example, reduction of oxygen on passivated Ti requires an overvoltage of about 1 v, while on graphite (which is completely covered by oxygen) oxygen can be reduced to hydrogen peroxide with a high degree of reversibility.

The third group includes elements such as Mn and Co on which redox reactions of the type

$$Mn^{4+}/Mn^{3+} \text{ or } Co^{3+}/Co^{2+}$$
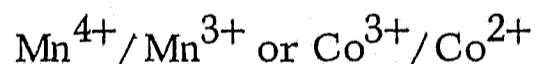
have specific effect on oxygen reduction. In these cases, a maximum activity is found in the range of potentials where these reactions occur. A maximum can be observed directly on pure Mn but is masked on pure cobalt by a corrosion current. It is, however, observed on Ni-Co alloys where the corrosion current is very small. The activity of the $NiCo_2$ alloy may be additionally due to a synergistic effect related to the spinel Co_2NiO_4.

Gold is a special case since it is the only metal essentially free of oxide or chemisorbed oxygen below the reversible O_2^- potential (1.23 v). Reduction of oxygen to hydrogen peroxide is virtually reversible on gold, while the further reduction of HO_2^- to water (or OH^-) is slow.

In the case of the intermetallic compounds, we were principally concerned with the influence of alloy or compound formation on the intrinsic catalytic activity for the electrochemical reduction of O_2. Again for most of these we are examining the influence of the bulk catalyst composition on the surface oxide formed under the test conditions, rather than the activity of the intermetallic itself.

Our experiments show that enhancement of the catalytic properties by formation of a new phase is generally small. The catalytic properties of the components of an alloy appear to be more important than the electronic or crystallographic structure of any phase that may be formed. However, compounds or alloys may show substantially higher activity and stability than do the components. This result is generally due to the effect of the electronic or crystallographic structure of the compound on the properties of the surface oxide formed during oxygen reduction on all nonnoble metals.

A substantial effect of chemical compound formation is also apparent in corrosion.

Of the specific systems studied, the intermetallic compounds of platinum and nickel and the interstitial compounds of the transition elements with carbon and nitrogen are of particular interest.

From our study of intermetallic compounds of Pt with nonnoble metals we may conclude that:

(a) Appreciable dilution by a nonnoble metal (e.g. Pt_2Ta) causes no decrease of the platinum activity for comparable surface roughness factors.

(b) Considerable surface increase can be obtained in some intermetallic compounds, probably by leaching of the nonnoble metal component. This effect may be useful in obtaining platinum particles with a high and stable surface for practical electrodes.

(c) Although addition of cobalt to nickel imparts a considerable increase in activity, $PtCo_3$ does not show a corresponding improvement. This may be due to the high intrinsic activity of Pt. This conforms to the general pattern observed, namely that no intermetallic compound tested to date shows more activity than platinum.

Nickel alloys with Co and Mn show improvement in performance over nickel. The corrosion resistance of a metal which corrodes in alkali is improved, on the other hand, by addition of Ni. This general trend was noticed for all nickel alloys; the best example was NiAl which behaved exactly as nickel.

Ti_3Au is a particularly interesting intermetallic compound. Its initial performance is higher than titanium or gold (but somewhat lower than platinum). With time, this performance increased to a level higher than platinum, but it was accompanied by a pronounced increase in double layer capacity, implying roughening of the surface. This was confirmed by electron microscopy. Analysis of the surface with an electron micro-probe showed the surface exposed to the electrolyte to be more rich in titanium than was the bulk of the sample. This is discussed in more detail later.

Of the "interstitials" of the refractory metals, borides and silicides generally exhibited high corrosion currents, which eliminated them as possible oxygen electrodes in caustic electrolytes.

The nitrides and carbides are another matter, especially in the cases of VC, VN, NbC, and TiN all of which are more resistant than their parent metals. The carbides (and the nitrides to a lesser extent) are all more active for O_2^- reduction than the parent metals; some activity is found even when the metal itself is inert, for instance with Hf, Ta, and Cr.

Another example of interest is Ti and TiN. The decrease of corrosion current and of overvoltage for O_2^- reduction (about 500 mv) observed with TiN is hard to explain as a pure surface area effect and must be due to the favorable effect of an oxynitride of titanium covering the TiN surface.

The essential points to come out of the measurements on the single crystals of TiO_2 are that the reduced form (particularly the c-axis crystals) does support a cathodic current corresponding to reduction of oxygen at potentials > 500 mv and is stable (i. e. does not revert to TiO_2 stoichiometry during the time interval of the experiments in the potential range of interest (600-1200 mv). This latter point is well demonstrated by the fact that pre-polarization to both cathodic and anodic potentials beyond this range has no effect on the current voltage characteristics. The anodic (and cathodic) currents noted in the potential range 300 to 1000 + mv with the fast sweep method can be attributed to the double layer charging current, both from the dependence on the direction of the sweep and the fact that the current decays rapidly when the sweep is stopped or the sweep rate reduced. The magnitude of this charging current indicates a significant roughness factor for these crystals.

The behavior of the black oxide on titanium and the nonstoichiometric TiO_2 is quite similar and even if the absolute activities are low considerable increases can be obtained by modification of stoichiometry.

Sufficient electronic conductivity exists in the oxide to sustain relatively high rates of O_2 reduction on single crystal surfaces and on thin films on the metal surface when the total amount is small. However, this conductivity is not high enough to provide the current paths for the high currents to be expected in the finely divided form in PTFE bonded electrodes. This would account for the inactivity of the finely divided Ti_3Au electrode.

SECTION 2

THE ACTIVITY OF GOLD ALLOYS OF PRECIOUS METALS AND
SILVER MAGNESIUM ALLOYS
(SOLID ELECTRODES)

I. GOLD ALLOYS OF SILVER, PALLADIUM, AND PLATINUM

A. Introduction

These alloys are of interest because of the gradual changes in electronic configuration and lattice parameters which can be induced by alloying. In addition, some new surface-oxide characteristics may exist for these alloys. It has been found that oxide layers of Pt, Pd, and Ag do not catalyze O_2-reduction to the same extent as the bare metal does. Consequently alloying with gold, which does not form surface oxides, may lend some noble characteristics to the alloys. It should be noted, however, that the absence of an oxide layer does not ensure catalytic activity for O_2-reduction. Gold, for example, catalyzes the reduction of O_2 to HO_2^- quite reversibly but shows considerable irreversibility in the second step, the reduction of HO_2^- to OH^-.

One of the purposes of this work was to try to distinguish between the electronic effects and the influence of the oxide layer. Special precautions were taken (a) to keep the composition of the surface constant (i. e. avoiding selective segregation of components), (b) to control diffusion conditions and (c) to minimize the effect of impurities.

B. Experimental

The rate of oxygen reduction was measured on gold, platinum, palladium and silver and the alloys Au/Pd, Au/Pt, and Au/Ag at 10% increments of composition. The electrodes were machined and polished cylinders 0. 6 cm high and 0. 6 cm diameter and were mounted in a holder described by Makrides and Stern[2]. The actual geometric surface area was determined accurately in

each case. All tests were made in 2M potassium hydroxide (Baker
Analyzed) at 25°C $\pm$ 0.1°C. Further tests on selected alloys were made
at 75°C. The reference electrode was a reversible H_2 electrode separated
by a Teflon frit. After preliminary tests with Pt and graphite the counter
electrode was changed to a large folded piece of Pd-Ag foil precharged
cathodically with hydrogen in order to maintain its potential below 100 mv
vs. RHE for the duration of the test. (The reason for selecting this counter
electrode is discussed later.) The solution was presaturated with nitrogen
for corrosion tests and with oxygen for the activity determination. The
electrode was rotated at 600 rpm.

Mass transport to an electrode of the described configuration cannot
be strictly defined by a simple equation such as the Levich equation for
rotating disc electrodes. Consequently, an experiment was performed to
determine the transport contribution from the sides and the bottom of the
electrode to the total current. The implications of this information are
discussed in the next section.

Three experimental techniques were used to establish the characteristics
of the alloys:

(1) Fast potential sweeps (500 mv/sec) carried out in the presence
of a N_2 saturated solution to determine the nature of surface oxidation of the
alloys.

(2) Slow sweeps (50 mv/min) in an O_2 saturated solution to define
the current voltage relationship for the O_2-reduction reaction.

(3) Capacity measurements to determine the relative surface
roughness.

The electrode potential was controlled at all times with a potentiostat, and
the signal source was either a fast or slow function generator. The E (I)-curves
were followed on an X-Y recorder, or an oscilloscope in case of fast sweeps
and capacity measurements.

Typical fast sweeps are shown in Figs. 3a, 3b, and 3c. The potential range for these fast sweeps was 0 to 1600 mv vs. RHE except for the gold palladium alloys. For these alloys the potential was kept above 400 mv vs. RHE to avoid the absorption of H_2 by palladium, since the subsequent oxidation of the H_2 masks the surface oxidation processes being studied. Particular precautions were taken to prevent surface roughening and changes of surface composition of the alloys. The samples were repolished for each experiment; in addition, the number of potential cycles applied to the electrode, before the fast sweeps were recorded, was restricted to four sweeps, the first three being used to align the trace on the oscilloscope. For the slow sweep, the electrode was again polished and the potential restricted to 600-1000 mv. The higher limit was set to avoid surface composition changes due to oxidation above 1000 mv, and the lower limit was intended to minimize the duration of the experiment and thus avoid accumulation of peroxide in the electrolyte. A typical example of a slow sweep curve is shown in Fig. 4.

The capacity of each electrode was measured in N_2-saturated solution prior to the O_2-reduction activity determination. The technique consisted of the application of a small triangular wave (25 mv, peak to peak) to the electrode at 600 mv vs. RHE (to conform to the potential restriction mentioned above). The resulting square wave of current was used to calculate the double layer capacity.

Effect of Impurities

Gold was chosen as the electrode material for the investigation since it allows the most sensitive measurements of side reactions.

In the initial tests, there were two unexpected features in the experimental curves. These were (1) an unusual cathodic peak in the limiting current during the return sweep (increasing potential) at 250-500 mv and (2) an anodic current, also observed with gold, at potentials > 900 mv, which varied with time and immediate past history of the system. Both of these factors were important in considering our present objectives.

GOLD ALLOYS -
FAST POTENTIAL
SWEEPS

Fig. 3a

Fig. 3b

Fig. 3c

GOLD (Makrides-Stern Elec.)

25°C , 2 N KOH , Oxygen

Ref. Elec. - Pd-Ag/H$_2$ (+30 mv vs. R.H.E.)

Counter Elec. - Platinum

Sweep: 400 mv/min

——— 1st sweep 0 → 1000 mv

- - - - 2nd sweep 1000 → 300 → 1000 mv

E vs. Pd-Ag/H$_2$ (mv)

Fig. 4

I
(μa)

I
(μa)
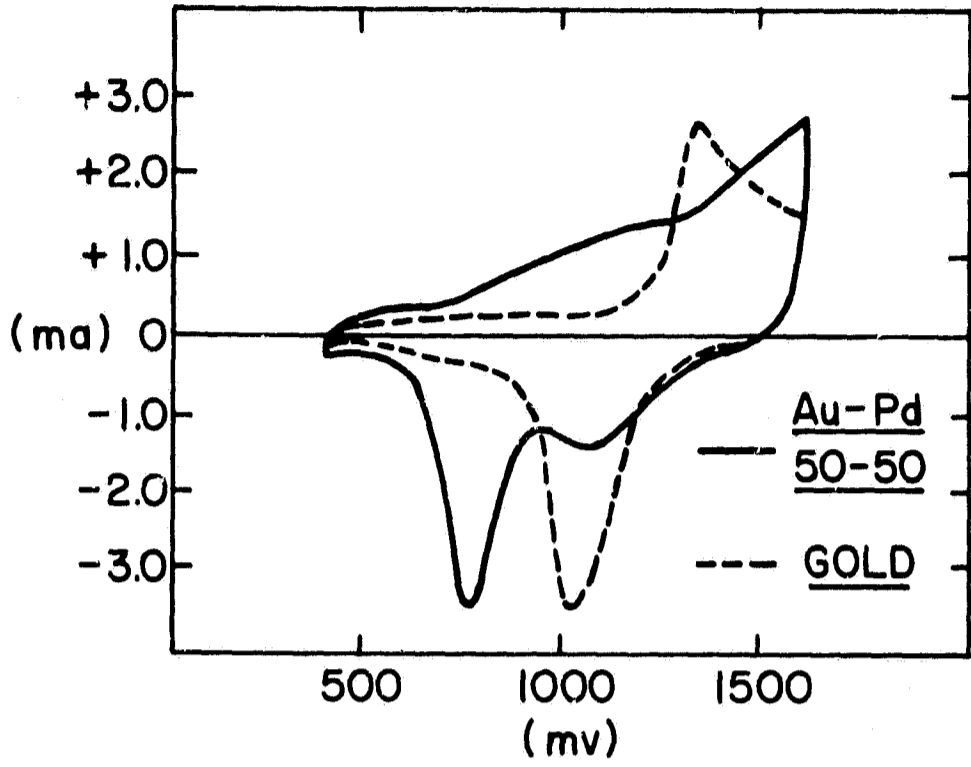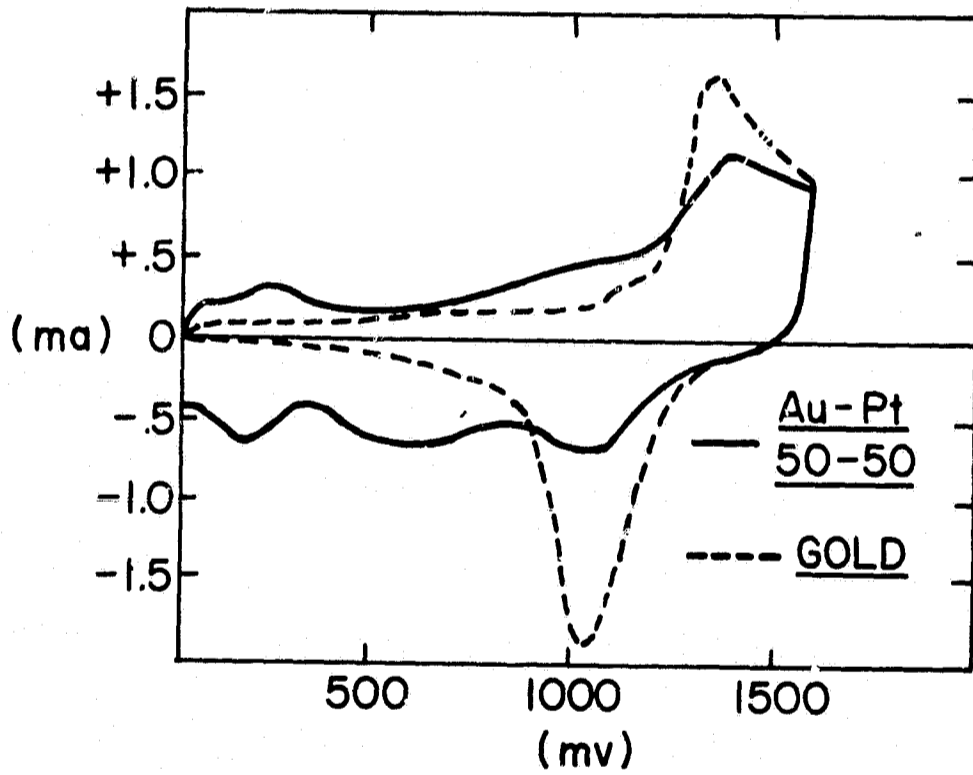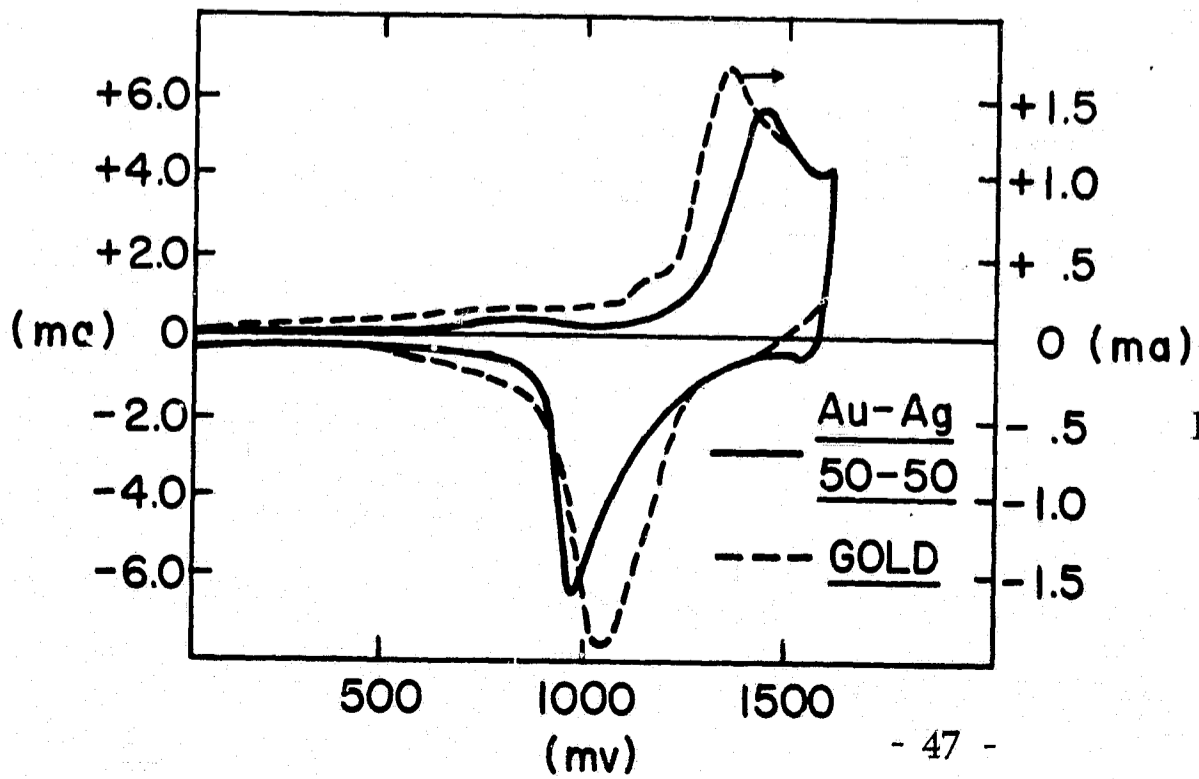
The peak in the limiting current was undesirable because it prevented precise definition of $E_{\frac{1}{2}}$ and because it was an indication of an impurity in solution that was actively involved in the oxygen reduction reaction. The anodic current was undesirable because it occurred in the potential region where the O_2 reduction process is activation controlled. The activation controlled region (Tafel region) of the current voltage curve is that where the surface reaction, which is dependent on the catalytic activity of the electrode, controls the over-all rate of the reduction reaction. Measurements of the rate, the current density per real square centimeter of the surface as a function of potential in this region, is a means of assessing the activity of the electrocatalyst. Therefore, the presence of a simultaneous anodic process of any magnitude restricts precise determination of the electrocatalytic activity toward the O_2 reduction process (further discussion below). Prior to making the experimental measurements on the three systems, the possible causes of the anodic current and the cathodic peak were investigated.

The anodic current occurred at all potentials > 800 mv under N_2. Under O_2 the anodic current was not observed until higher potentials (~ 950 mv), but it was assumed that the anodic reaction occurred simultaneously at the lower potentials, affecting the magnitude of the observed cathodic current. The anodic current tended to increase with time and frequently showed a sharp increase after the determination of a current voltage curve under O_2.

This behavior corresponds to the accumulation in the electrolyte of H_2O_2 (or more precisely HO_2^-) produced by the incomplete reduction of O_2. This is particularly the case when the electrode material is not a good peroxide decomposition catalyst. To check the effect of peroxide accumulation, hydrogen peroxide was added to the electrolyte to make a 10^{-3}M solution. The anodic current increased by a factor of 10^3. If it is assumed that the current is diffusion controlled, then the anodic currents usually observed correspond to a solution 10^{-6}M in peroxide. This level of concentration may occur under the normal operating conditions, particularly since the electrode is at low positive potentials for quite long periods during the slow sweep measurements. A large

gold scavenger electrode was introduced to the system and maintained at a potential of 1000 mv vs. RHE, in order to consume accumulated peroxide. However, this electrode was apparently not as efficient as was expected in the oxidation of HO_2^-, since it did not reduce the magnitude of the anodic current, possibly because of poor transport of HO_2^- to its surface.

The anodic currents have been minimized by working with fresh electrolyte for every determination, by conducting the measurements in the shortest possibly time, and by using a restricted potential range for the slow sweep studies (see below) thereby reducing the amount of peroxide produced.

The cathodic peak in the limiting current of O_2-reduction to HO_2^- is a catalytic peak. It did not appear when the potential was maintained above 300 mv vs. RHE. Furthermore, the current peak never exceeded the theoretical limiting current to be expected from reduction of O_2 to H_2O. This suggests that the effect was possibly due to the complete reduction of O_2 to OH^- catalyzed by a metal deposited at the low potential. Kronenberg[7] has reported a 1M solution of KOH containing 1-10 ppm of Fe, Ag, Cu and Cr. For iron, a 5 ppm impurity level corresponds to a 10^{-4}M solution.

Another source of impurities that was considered was the counter electrode. Initially, Pt was excluded from the system because of its possible dissolution and deposition on the surface of the working electrode, which could change its character, including oxygen film formation at lowered potentials. Measurements carried out with a graphite counter electrode indicated that it contained leachable impurities. Gold was excluded on the same basis as Pt. Any gold deposited on the working electrode would not show the difference in activity expected of Pt but could give rise to a continuously changing surface composition in the case of the alloys. The system selected for the counter electrode was a large piece of Ag/Pd foil charged with H_2. The anodic process that occurs to complement the cathodic reduction of O_2 is hydrogen oxidation, and since this occurs at < 100 mv vs. RHE, no metal dissolution can occur.

C. Results

A typical E-log i curve is presented in Fig. 5. The linearity of the curve for over a decade of current suggests that in this particular region the reaction is activation controlled.

The activities of the complete range of alloys are presented in Figs. 6 and 7 at the potential corresponding to a particular current density in the Tafel region; the current was normalized for the real surface area of the electrodes using the double layer capacities measured previously. Also shown in Fig. 8 are the activities defined in terms of potential at a constant current density (per geometric square centimeter). The pattern of activity is the same.

The order of activity was Au/Pd > Au/Pt > Au/Ag; for the 1:1 alloys the following E_i values were recorded for i = 50 $\mu a/cm^2$: Au/Pd - 926 mv, Au/Pt - 878 mv, Au/Ag - 856 mv vs. RHE. The Au/Pd series exhibit a flat maximum of activity over the range 70/30 - Au/Pd to 30/70 - Au/Pd; the Au/Pt and Au/Ag alloys show, with some scatter, a steady transition from the activity of one pure component to the other. The activity patterns are approximately the same at 75°C (Fig. 9). The enhanced activity of the Au/Pd alloys is not unexpected and has been reported in the literature[8,9]. An interesting feature of these results is that at 25°C pure Pd (E_{50} = 922 mv vs. RHE) is more active than pure Pt (E_{50} = 880 mv vs. RHE). As the temperature was increased from 25°C to 75°C, the activity (E_{50}) of pure Pt increased from 880 to 903 mv, while that of Pd decreased from 922 to 915 mv. In other words, at 75°C and 50 $\mu a/cm^2$ Pd was still somewhat more positive (12 mv) than Pt.

An important reason why Pd has not been extensively used in practical fuel cells is that it is known to corrode at a significant rate at positive potentials in KOH (or in acid) at 75°C and above. The anodic current observed at 1000 mv was 3 $\mu a/cm^2$ for Pd compared with 1 $\mu a/cm^2$ for Pt, though no great significance should be attached to the absolute value of these figures. It is therefore of considerable interest to note that the activity of Pd is

25°C, 2 N KOH
SWEEP: 50 mv/ min
E vs. REV. H_2 ELEC.
CTR. ELEC.: Pd-Ag/H_2

PLATiNUM

Fig. 5

$\log i^*$ ($\mu a/ \mu f$)

E
(mv)

1000

950

900

850

800

750

.01

0.1

1.0

10

- 52 -

572F

Potential at $i^* = 0.5\ \mu a/\mu f$ vs. % Au
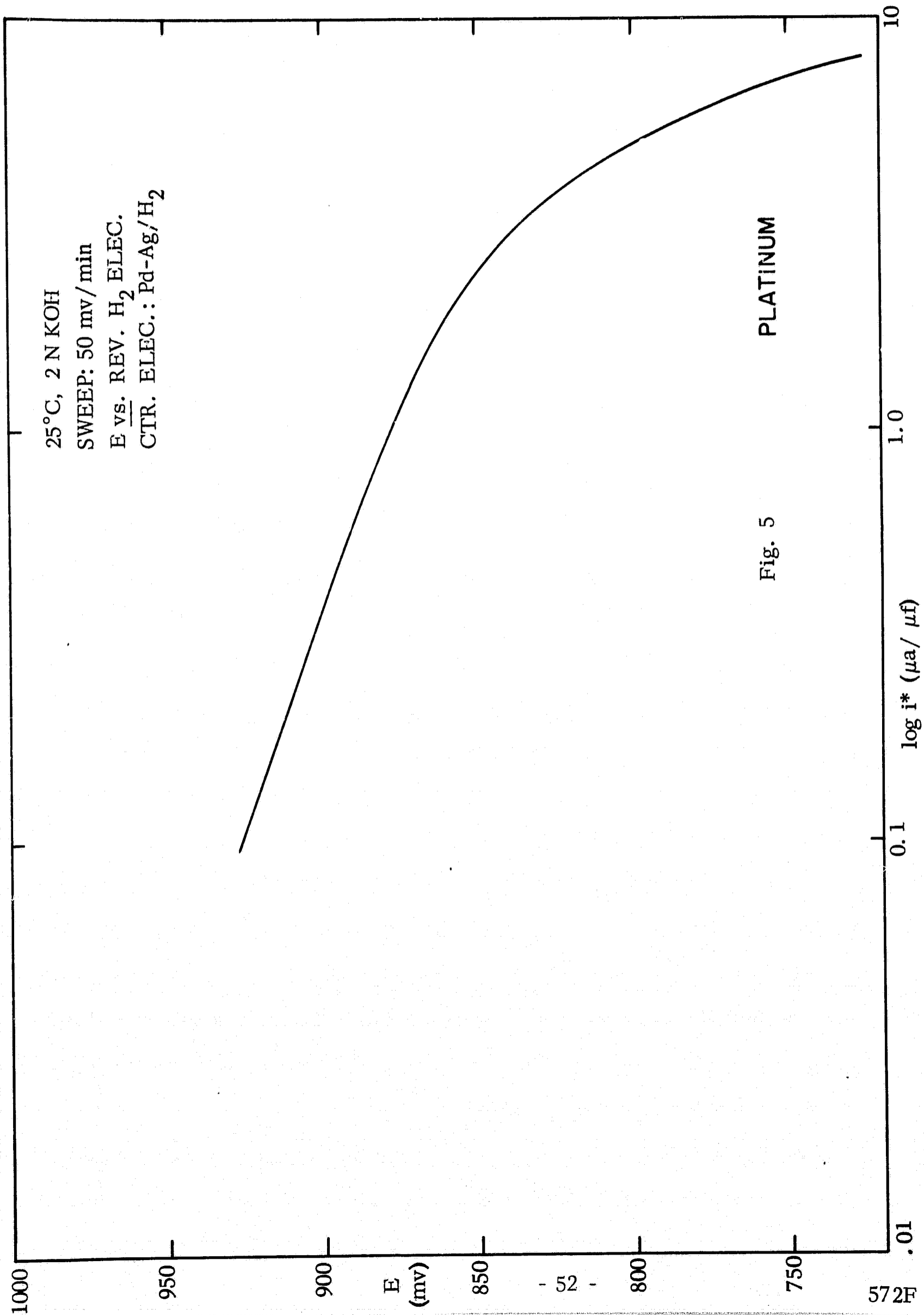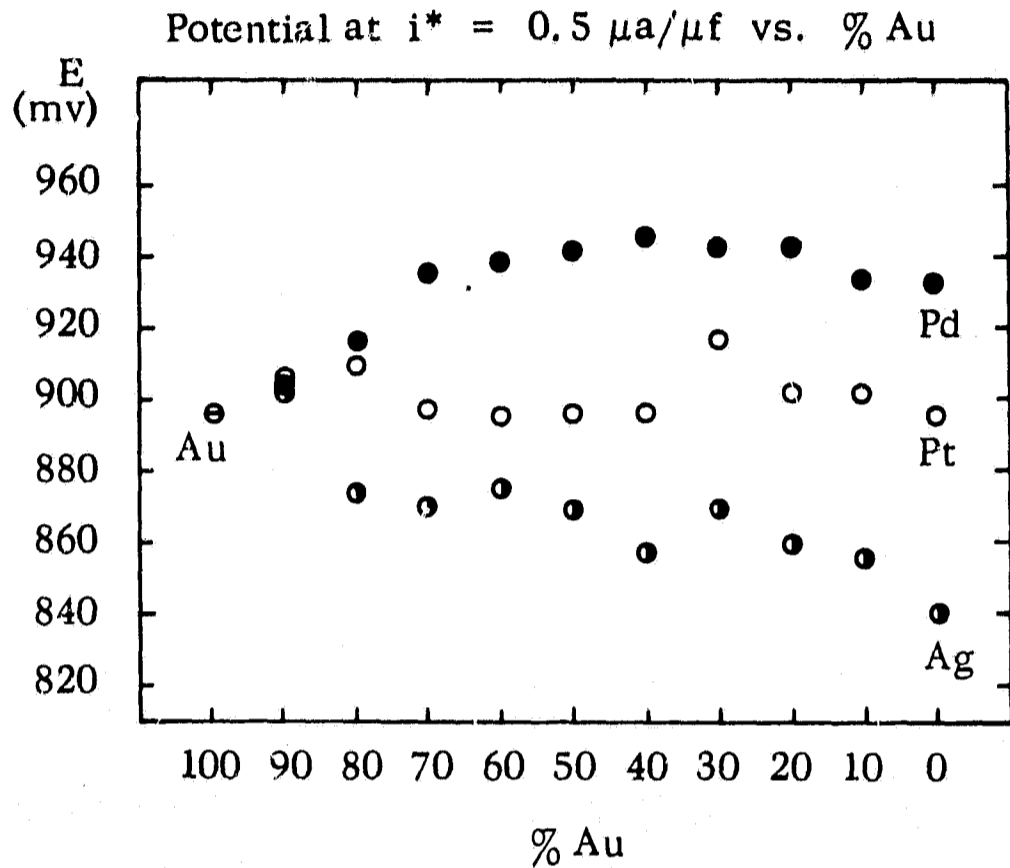
Fig. 6 Gold alloys: Composition vs. activity.

Potential at $i^* = 1.0\ \mu a/\mu f$ vs. % Au

Fig. 7 Gold alloys: Composition vs. activity.

- 53 -

572F

Potential at 50 $\mu a/cm^2$ vs. % Au
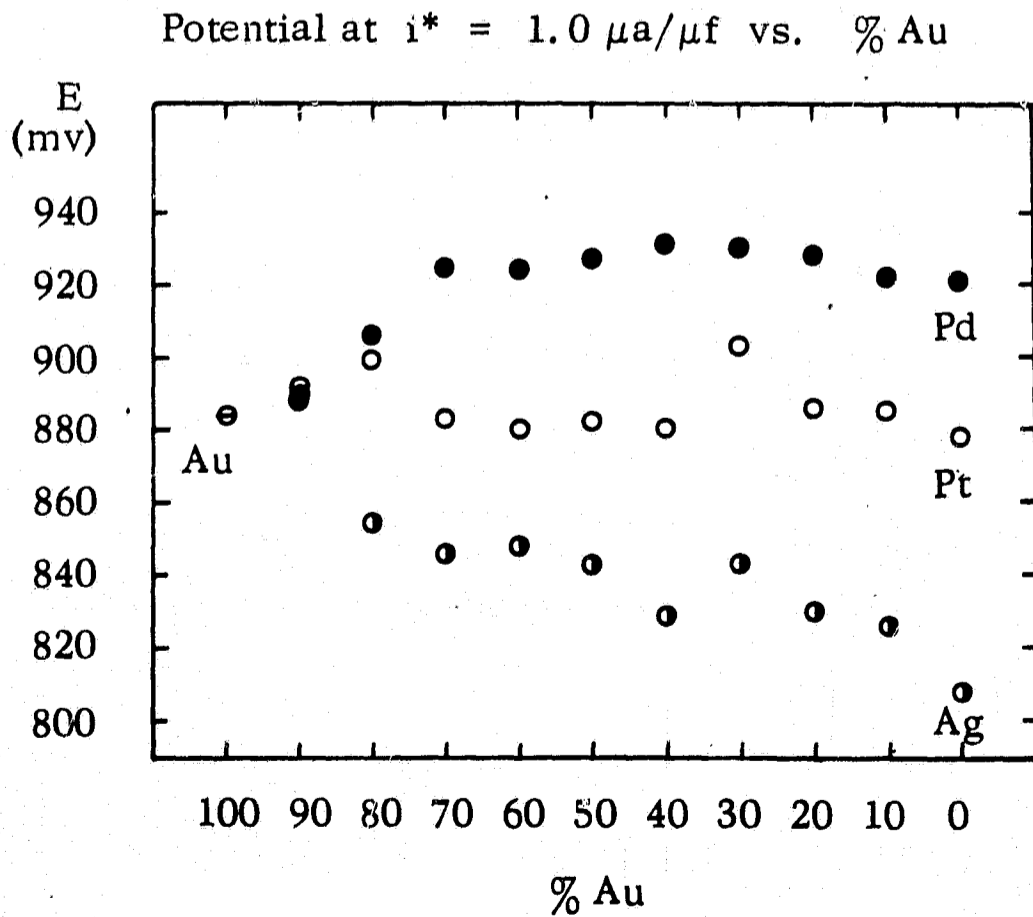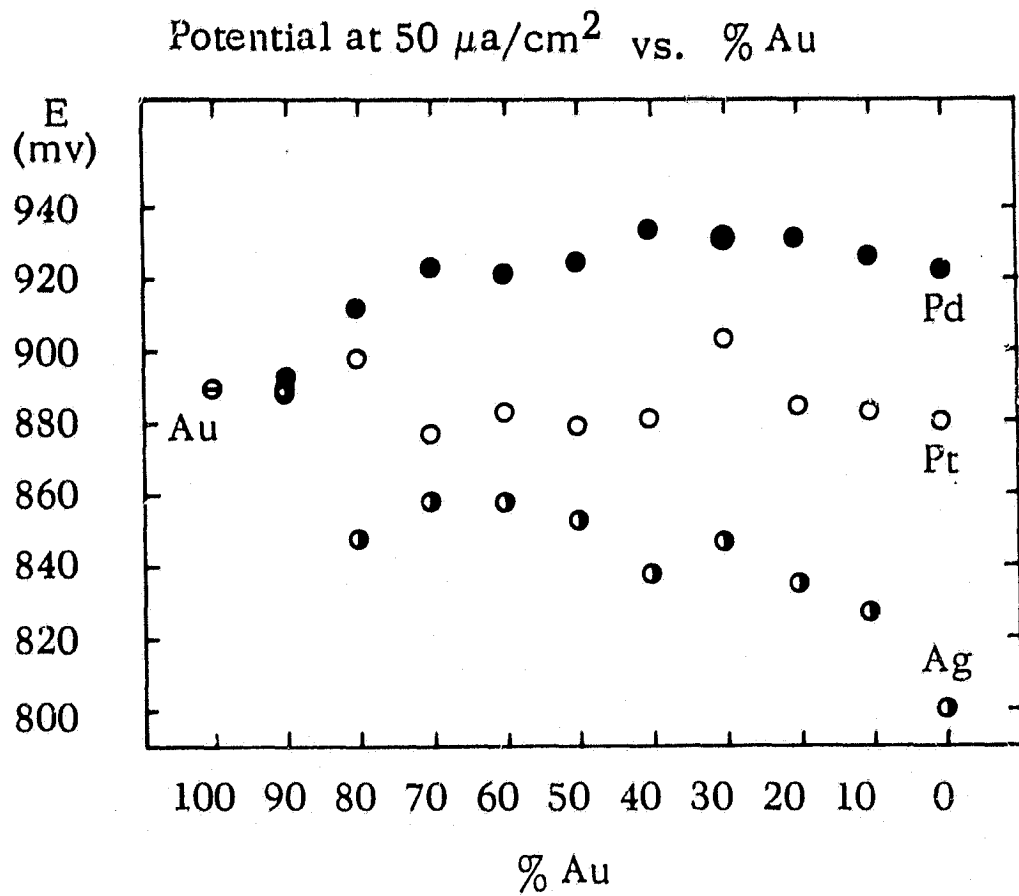
Fig. 8 Gold alloys: Composition vs. activity.

Potential at 1.0 $\mu a/\mu f$ vs. % Au
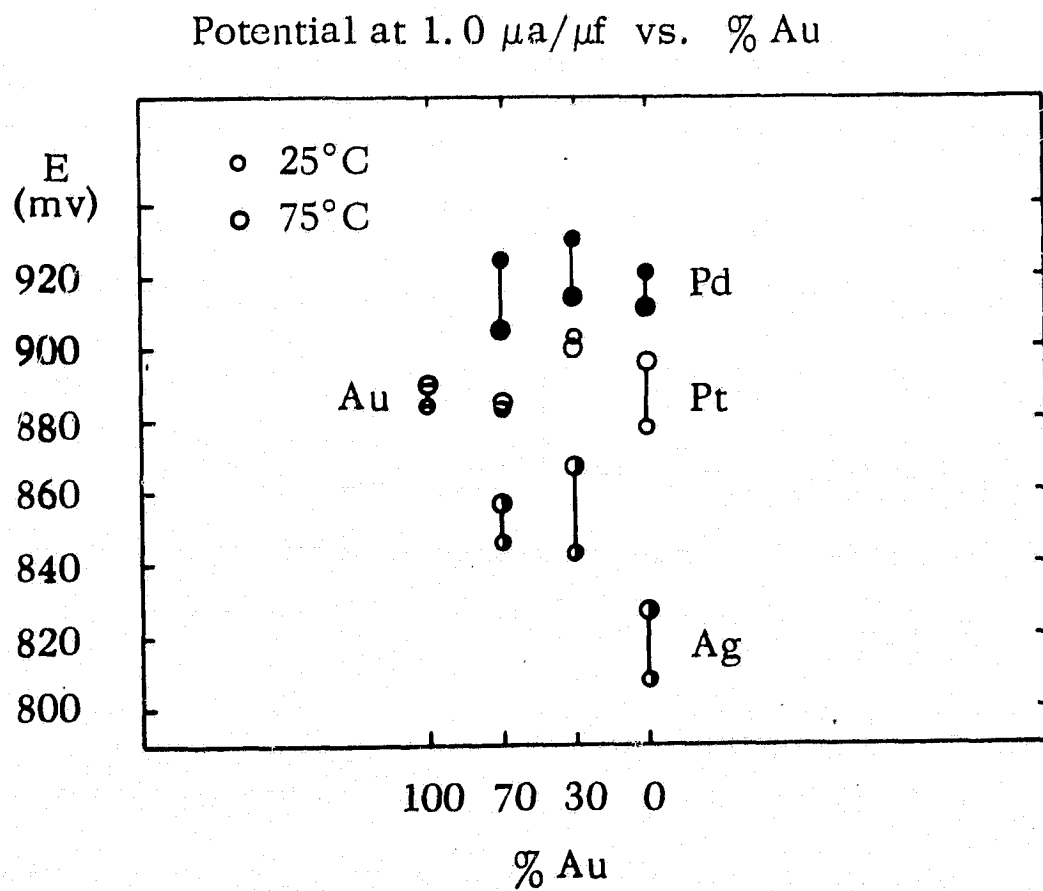
Fig. 9 Gold alloys: Composition vs. activity.

maintained or even enhanced in the gold alloys up to 70% Au, particularly since it might be expected that the corrosion resistance of the alloys would be better than that of pure Pd, as is the case for the Ni alloys of Mn and Co[4].

In the fast potential sweeps separate peaks for the O_2 desorption process (cathodic current) are observed on the Au/Pd and Au/Pt alloys (Figs. 10-12), the relative magnitudes changing with the alloy composition. This indicates that for the most part, as shown in our study of intermetallic compounds, the component metals retain their individual characteristics with respect to oxide reduction and do not exhibit any composite properties. There is less differentiation of peaks, except in magnitude, among the Au/Ag alloys since the pure metals under these conditions behave in a similar manner. Another indication that the component metals retain their individual characteristics is the observed differences in limiting current density for 10% additions of Ag, Pd, or Pt. At room temperature the reduction of O_2 on gold proceeds only to peroxide at low polarization, wheras platinum, palladium, and silver are all effective peroxide decomposition catalysts. It is interesting to note that the limiting currents are doubled for only a 10% addition of these components to Au. See Table XIII.

A number of these alloys have been prepared in a finely divided form and tested as practical fuel cell electrodes (sections 3 and 4).
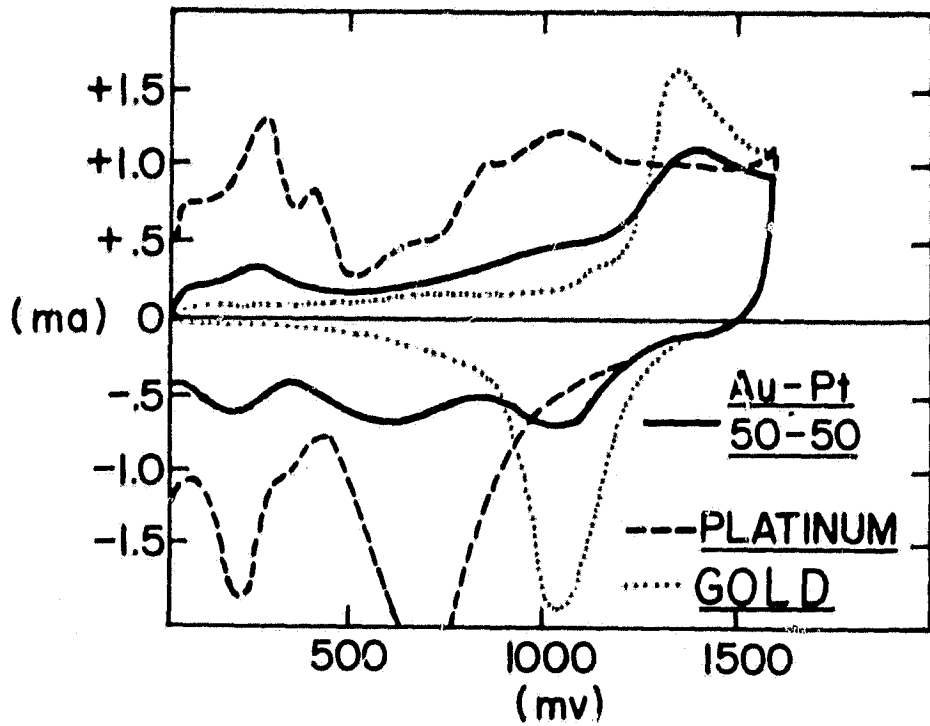
GOLD ALLOYS -
FAST POTENTIAL
SWEEPS

Fig. 10

Fig. 11

Fig. 12
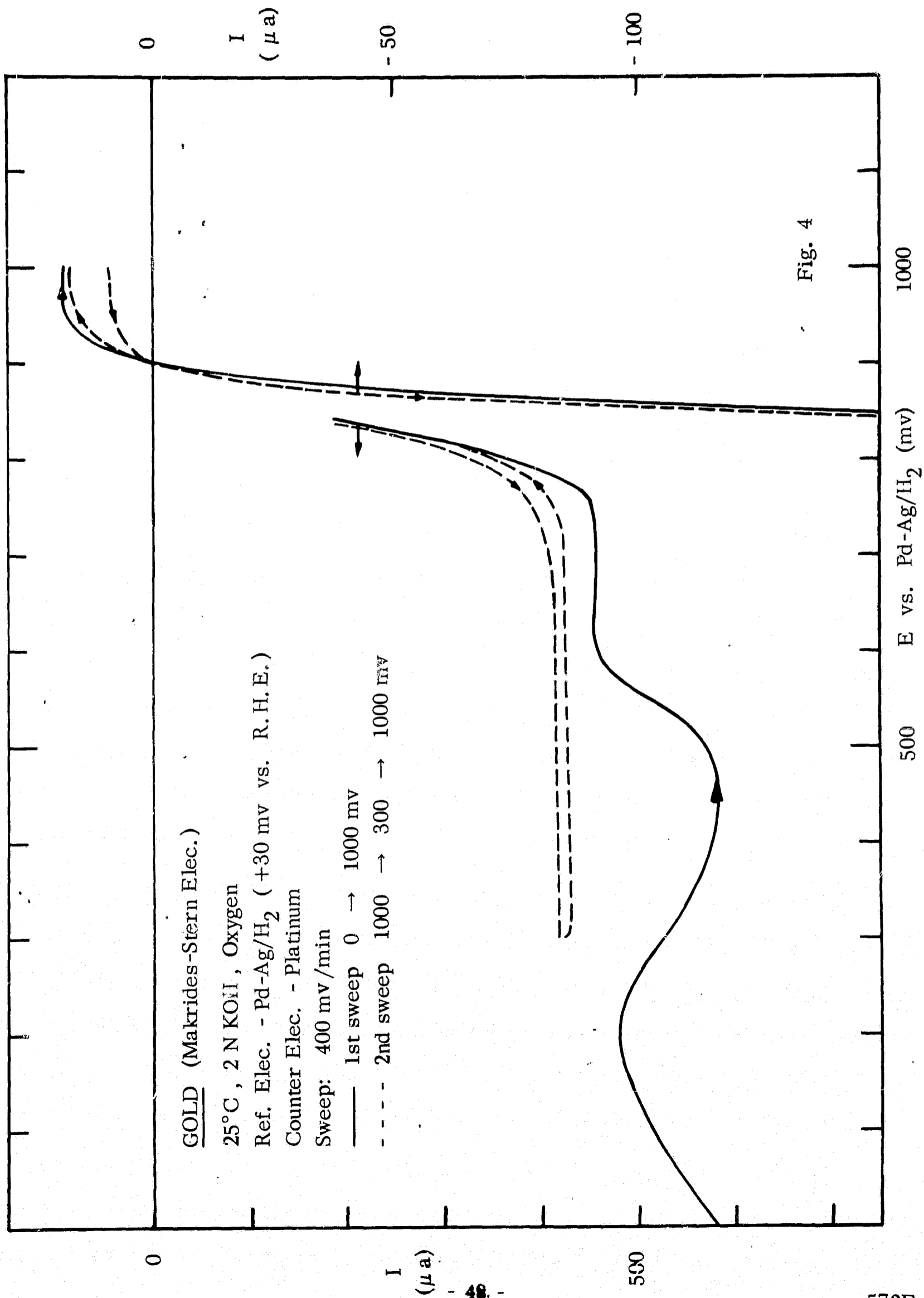
572F
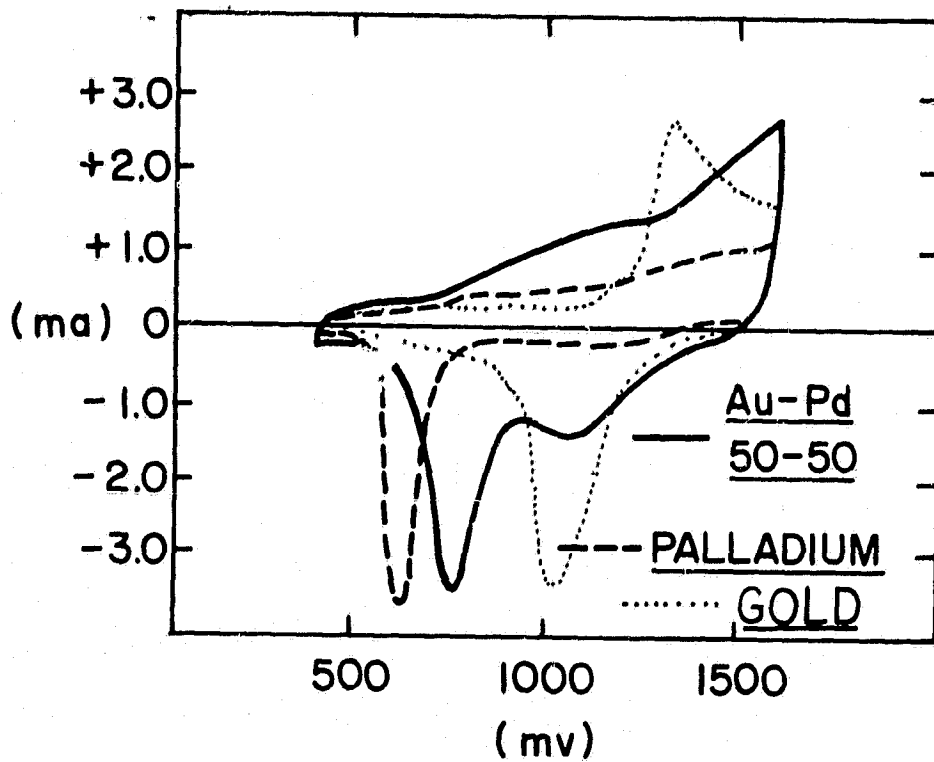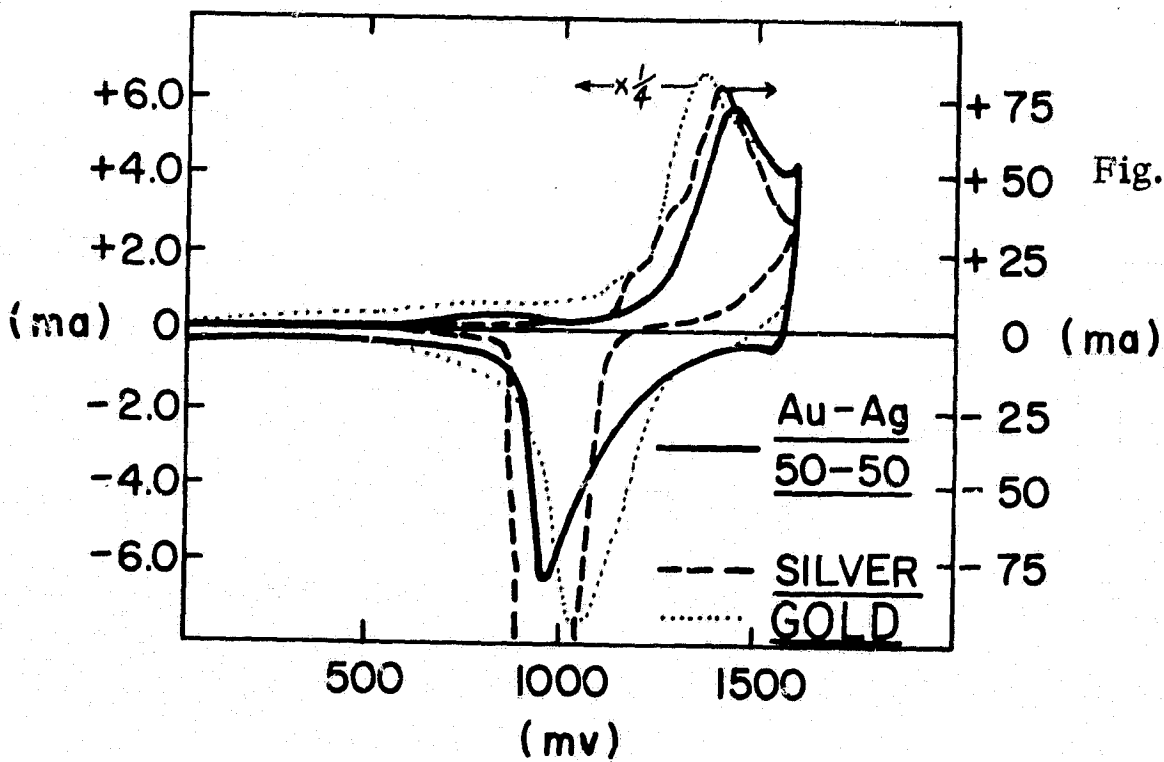
TABLE XIII

Activities of Platinum, Palladium, and Silver Alloys of Gold

Atom % Au	Au-Pt		Au-Pd		Au-Ag	
	i_L/A ($\mu a/cm^2$)	$E_{\frac{1}{2}}$ (mv)	i_L/A ($\mu a/cm^2$)	$E_{\frac{1}{2}}$ (mv)	i_L/A ($\mu a/cm^2$)	$E_{\frac{1}{2}}$ (mv)
100	340 (Au)	860				
90	623	820	558	840	508	825
80	766	826	662	860	491	750
70	636	787	781	877	650	755
60	615	804	637	877	675	750
50	599	795	845	873	701	739
40	763	785	1006	880	634	717
30	808	837	1037	876	693	737
20	686	795	984	878	623	728
10	802	787	926	877	628	713
	676 (Pt)	780	1000 (Pd)	854	436 (Ag)	700

II. SILVER-MAGNESIUM ALLOYS

A. Introduction

We have tested silver-magnesium alloys under similar experimental conditions to those described for the gold alloys. The principal reason for this was that Beer and Sandler[10] have examined these catalysts for the oxygen-reduction reaction, with different surface pretreatments, and have reported improved performance for a 1.7% Mg:Ag alloy. This was considered to be related to its enhanced secondary electron emission. This work did not include a determination of the real surface area of these materials. A comparison of the real surface areas of Ag and the alloy was carried out in this laboratory in conjunction with activity tests on these materials.

B. Experimental

The silver-magnesium alloy was obtained as foil from Handy and Harman Co., New York, and silver foil was purchased from Williams Metals. The foils, welded to an Ag-wire and sealed in glass, were polished to a bright finish with alumina and tested in a rotating electrode cell as 1 cm by 1 cm squares.

C. Results

The current potential curves for these materials are shown in Figs. 13 and 14. A comparative figure for the real surface areas of the Ag and Ag:Mg foils was obtained from the ratio of their double-layer capacities. The capacities were measured with a 50 mv triangular sweep at 400 and 700 mv at the beginning and at the end of each activity determination. The ratio of the real surface areas ranged from 3.2 to 6, the Ag:Mg alloy having the higher surface area. A series of experiments at different sweep rates showed that the surface was substantially free of adsorbed impurities.

A comparison of the potentials at a current density of 200 $\mu a/cm^2$ (corrected for the difference in surface roughness), where there are no mass transfer limitations, shows no greater intrinsic activity for the Ag:Mg alloy (Table XIV).

Fig. 13   Ag/1.7 Mg and Ag

572F

i (ma/cm^2)

Fig. 14

Ag 1.7% Mg and Ag

2N KOH, O$_2$, 75°C
Sweep Rate 200 mV/min
E vs. RHE

Current Scale x 0.1

Double Layer   Ag   230 μF
Capacity   Ag/Mg 1080 μF

—·—·— Ag 1.7% Mg

———— Ag

572F
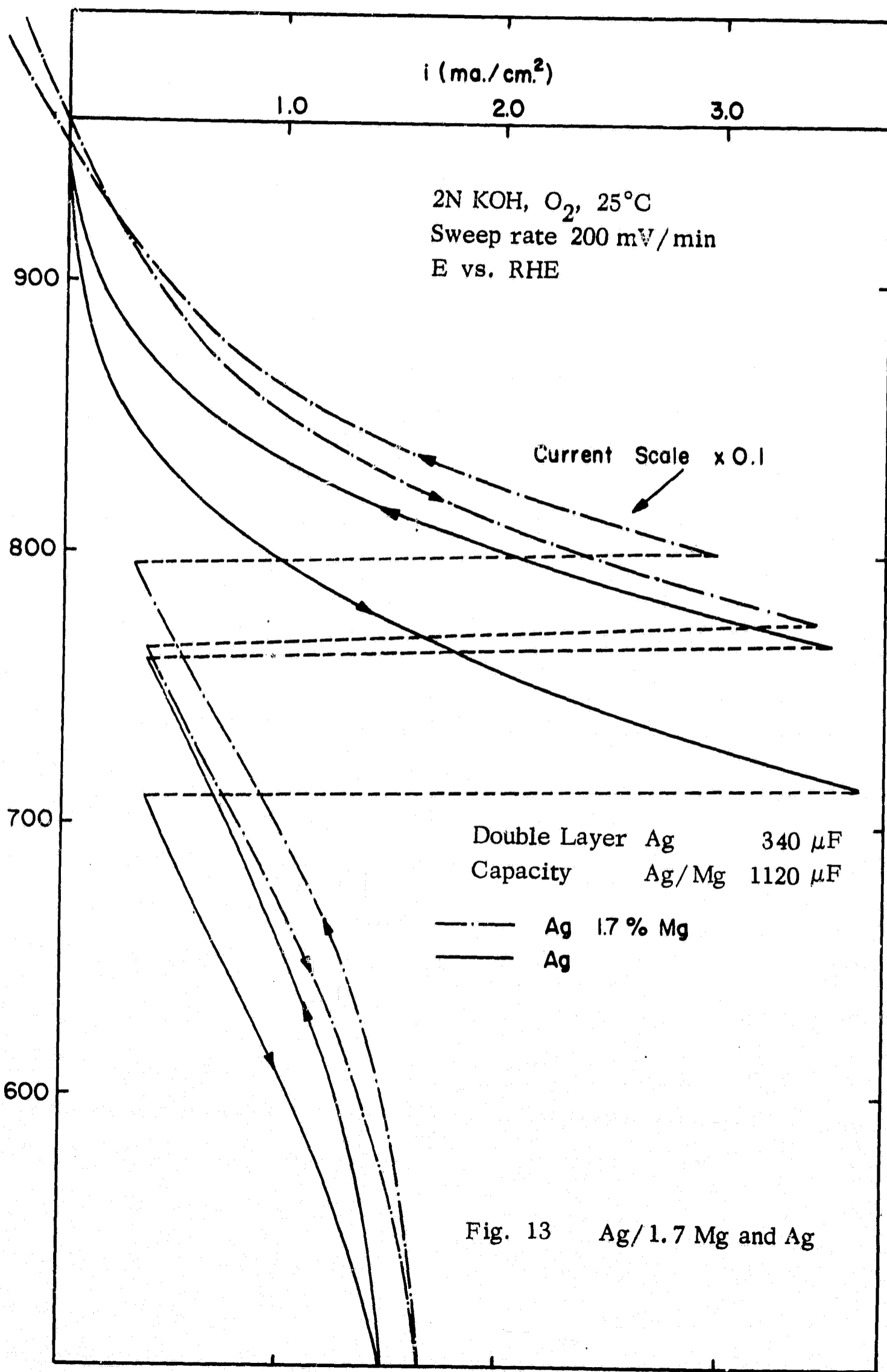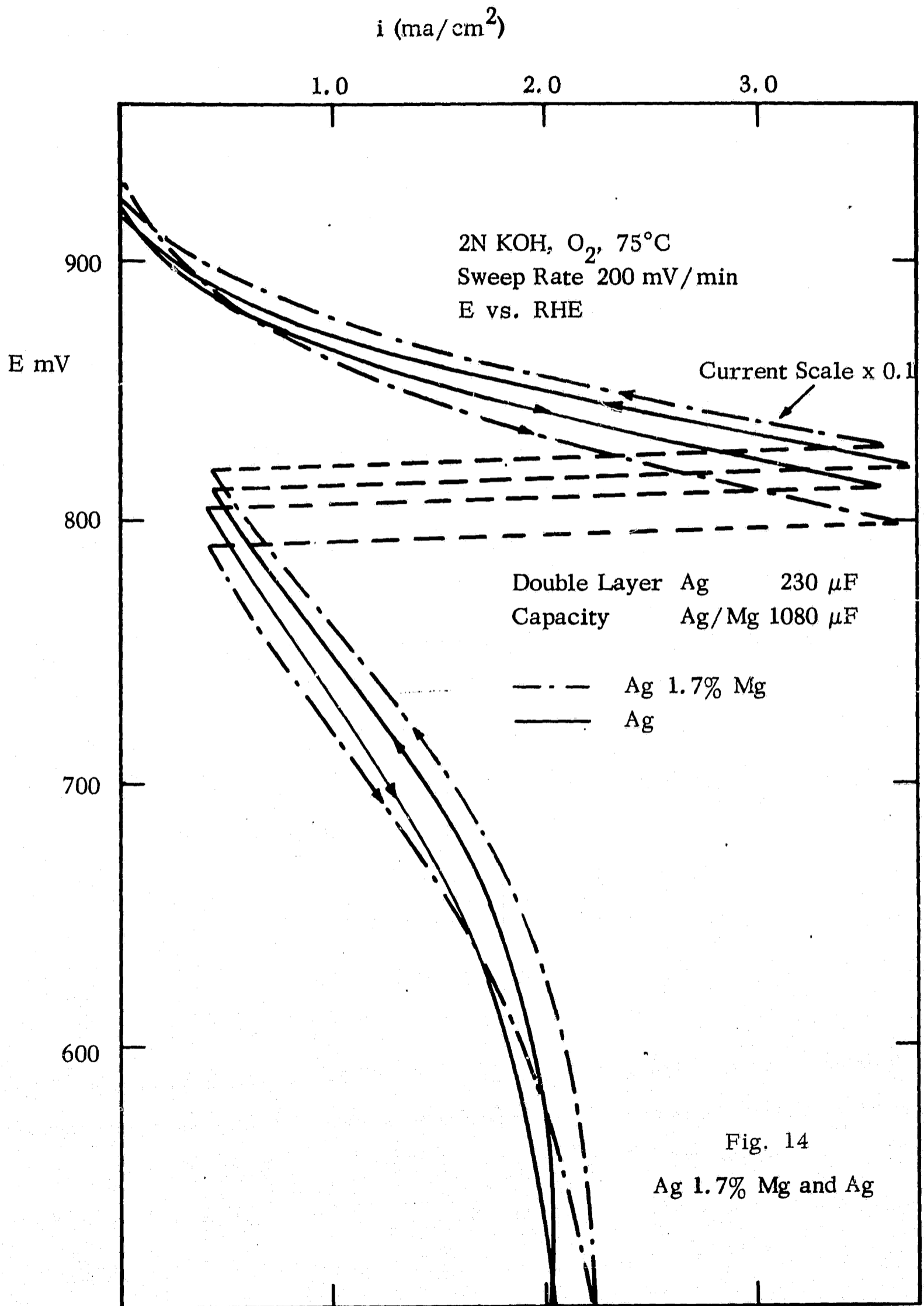
TABLE XIV

Comparison of Silver and Silver-Magnesium Alloys

$$\underline{E \text{ vs. RHE}}$$

		$\underline{\text{Ag}}$	$\underline{\text{Ag:Mg}}$
25°C	i = 200 μa/cm^{2*}	863	858 mv
75°C	i = 200 μa/cm^{2*}	900	880 mv

* Corrected for difference in surface roughness.

SECTION 3

PREPARATION AND TESTING OF FINELY DIVIDED CATALYSTS

I. PREPARATION OF FINELY DIVIDED CATALYSTS

The screening program described in the first two sections of this report indicated that a number of materials were potentially good catalysts for oxygen reduction. In order to verify this, it was necessary to prepare these materials in a finely divided state. In some cases, as with the gold alloys, a variety of precipitation methods were available but for other materials, such as titanium gold and nickel carbide, more complex techniques were needed. These preparative techniques are described below for Au-Pd, Au-Pt, Pt-Os, Ti_3Au, TiAu, TiN, Ni_3N, and Ni_3C.

A. Gold-Palladium Alloys

Previous measurements on gold alloys of Pt, Pd, and Ag showed the Au/Pd alloys to have the highest activity for O_2 reduction. Furthermore, this high activity (higher than pure Pt and pure Pd) extended over a wide range of alloy composition from 20 to 70% gold. The high activity of the gold rich alloys is particularly encouraging since these alloys are more corrosion resistant than pure Pd. Pure Pd is active for O_2 reduction but does not show the corrosion free behavior of pure Pt.

The following alloy compositions were chosen for preparation: Pd-Au 40/60, Pd-Au 50/50, Pd-Au 60/40, and Pd-Au 70/30. Three precipitation methods were used -- formaldehyde reduction, hydrazine reduction, and hydroxylamine reduction.

1. Formaldehyde Reduction

The formaldehyde reduction of a solution of $H\ AuCl_4$ and $PdCl_2$, for preparation of the black, avoids the complications of the widely

used borohydride reduction, which has two disadvantages: the possible introduction of boron into the product and the difficulty of predicting the composition of the product. The formaldehyde reduction has been used extensively at Tyco for the preparation of Pt blacks in a reproducible manner. The key to reproducibility is the control of the nucleation and mixing stages of the preparation. The method is based on the work of Turkevich, Hillier and Stevenson[11] and has been described in detail elsewhere[12]. Briefly, precipitation occurs in strongly alkaline solution by an electrochemical mechanism on preformed nuclei in solution; formaldehyde is oxidized at one site and the metal ion is reduced at another site on any given nucleus. The formation of nuclei, a slower molecular reaction, can be induced at lower pH where the rate of the electrochemical process is negligible. By separating the nucleation step and the growth (electrochemical) process by adjusting the pH, a more uniform product can be prepared.

The experimental procedure was to take a portion (1/4) of the gold palladium solution (6.160 g of $H AuCl_4$ and 6.465 g of $PdCl_2$ in 475 ml of water filtered through a Millipore filter)* and add twice the stoichiometric requirement of formaldehyde followed by sufficient sodium carbonate to bring the pH to 8.5. After ten minutes, during which time (as shown for Pt) the number of nuclei has reached a constant value, this solution and the remainder of the gold palladium solution (plus formaldehyde) is added rapidly (< 2 sec) to a vigorously stirred solution of NaOH at 90°C. The precipitation of the black, including agglomeration, was complete in 3 min. Oxygen was bubbled through the system during the reaction and for ten minutes afterwards. The black was collected, washed free from sodium chloride, and allowed to dry in air.

---

* All solutions were passed through a Millipore filter capable of removing particles down to 0.2μ; this reduced the possibility of heterogeneous nucleation, a source of irreproducibility.

2. Hydrazine Reduction

In this method hydrazine was added to the Au and Pd salts dissolved in methanol. Five preparations were made, the first at 90°C and the rest at room temperature. The blacks were collected, washed free of chloride, and dried in air.

3. Hydroxylamine Reduction

Hydroxylamine hydrochloride was added dropwise to the chosen alloy composition of Au and Pd salts (Pd-Au 40/60). The reaction was carried out at room temperature, 75°C, and 85°C. The blacks were collected, washed, and dried in air.

B. Au-Pt

In the testing of the gold alloy series as solid electrodes, it was found that, unlike the gold palladium series, the gold platinum alloys showed little if any improvement over the performance of platinum for oxygen reduction, with the exception of the 70% Pt composition. A black was made of this composition, Pt-Au 70/30, by the formaldehyde reduction method described above.

C. Platinum

Since the formaldehyde reduction method seemed to be the most promising, a platinum black was prepared with formaldehyde as a testing reference. The technique was originated as a platinum black preparation, as described in the gold palladium section above.

D. Pt-Os

Three platinum-osmium preparations were made, two by formaldehyde reduction and the other by mechanically mixing platinum and osmium powders. The precipitated material, theoretically Pt-Os 80/20, possibly had less osmium than indicated due to its difficult reduction. X-ray analysis was inconclusive. The mechanical mixture was impractical because of the large differences in particle size of the platinum and osmium.

E. Platinum-Silver

Platinum-silver electrodes (Pt-Ag 30/70) were made by mechanically mixing Englehard Pt black with Fisher Ag_2O powder. These electrodes were made in order to study the improved performance, apparently due to structural effects, observed previously with this composition.

F. Ti_3Au

Measurements on solid rotating electrodes of Ti_3Au showed it to be intrinsically more active than Pt. Several attempts were made early in the program to take advantage of this high intrinsic activity with a practical, high surface area form of the catalyst. It was found then that a Ti_3Au powder (-325 mesh), prepared by grinding and made up as a PTFE bonded electrode, effervesced vigorously on contact with 35% KOH. The catalyst/PTFE mixture expanded 50% in volume and separated from the support screen. No activity was observed either during or after effervescence.

An electrode prepared from Ti_3Au powder that had been leached in 35% KOH at 60°C for 50 hours (at which time all effervescence had stopped) was also inactive. This powder had a large content of a voluminous white component, probably TiO_2. A large TiO_2 content could explain the low conductivity of the leached powder and might also account for the absence of catalytic activity for O_2 reduction. Since TiO_2 is soluble in dilute acids, an acid wash (25% H_2SO_4) was introduced into the catalyst pretreatment to decrease the TiO_2 content.

In all, twenty-four preparations were made in which the KOH leaching conditions and acid washing conditions were varied.

G. TiAu

TiAu, when exposed to KOH, does not leach to the same extent as does Ti_3Au. In addition, it also shows high oxygen reduction activity. However, unlike Ti_3Au which is brittle, TiAu cannot be broken up by the usual pulverizing techniques. In order to obtain a powder, the vacuum

deposition technique was used. A small ingot of TiAu was brought to a
suitable temperature in an evaporator at a helium pressure greater
than one Torr. The powder which accumulated on the walls of the bell
jar was collected by brushing the surface with a camel hair brush. Half
of the sample was given a dilute sulfuric acid wash (which removed a
large portion of the material).

H. TiN

The preparation of the titanium nitride involved the evaporation of
titanium metal in a N_2 atmosphere at 50μ pressure. The titanium nitride
was blue-grey in color; (stoichiometric TiN is a golden yellow). Since
the N_2 pressure during evaporation controls the condensation rate and
therefore the particle size, it is unlikely that the stoichiometric form of
TiN can be prepared in finely divided form using this method.

I. Nickel Nitride

Only one successful preparation of nickel nitride was made. This
was based on the reduction of carbonyl nickel in H_2 at 450°C for 24 hours,
followed by nitriding at 300°C with NH_3 for 48 hours. X-ray measurements
showed 58% Ni_3N. Five other attempts to reproduce this preparation were
unsuccessful.

J. Nickel Carbide Prepared by Acetate Decomposition

Thirty-two samples of Ni_3C and two samples of Ni/Co were prepared
at Tyco by thermal decomposition of nickel and cobalt acetates in N_2,
according to the method of Leicester and Redman[13]. The initial experi-
ments based on this method were to a large extent responsible for the
interest in the survey of interstitial compounds prepared by the Bureau of
Mines.

The acetate crystals were first dehydrated by heating to 100°C on a
hot plate for 1 hour. The thermal decomposition was carried out in a furnace
with N_2 flowing over the sample. The times and temperatures of decomposi-
tion of the active samples are listed in Table XXVII. The inactive samples,

many of which were prepared under conditions apparently identical to the active catalysts, are not listed. For the Ni/Co alloy carbides the starting material was either a solution of the acetates evaporated to dryness or the crystals ground together in a pestle and mortar.

K. Bureau of Mines' Catalysts

The carbides, nitrides, carbonitrides and nitrocarbides of iron, nickel, and cobalt are an interesting group of catalysts many of which have been investigated in detail in connection with the Fischer-Tropsch reaction[14]. Because of their metallic properties and their possible enhanced resistance to oxidation as compared with their parent metals, this class of materials presented attractive possibilities as oxygen reduction electrocatalysts. Measurements with porous Ni_3C electrodes described in the previous section showed very high activity for O_2-reduction, at least for short-term measurements. In addition, initial measurements on an iron rod carbided on the surface demonstrated that iron carbide had a somewhat higher activity than pure Fe.

A range of interstitial compounds of Fe, Ni, and Co in finely divided form were prepared by the Bureau of Mines as part of a cooperative program. The preparation of these materials, as described in the Bureau of Mines' quarterly reports[15] are reproduced below.

TABLE XV

Pretreatment and Carbiding

Run no	Charge	Charge wt	% Fe in charge	Pretreatment Gas	Pretreatment Hourly space velocity, hr⁻¹	Pretreatment Reaction temp, °C	Pretreatment Reaction time, hrs	Carburization Gas	Carburization Hourly space velocity, hr⁻¹	Temperature Start of bed	Temperature Middle of bed	Temperature Rear of bed	Duration of carbiding, hrs	Discharge weight, g	Qualitative x-ray diffraction	Chem. Total Fe	Chem. Total C	Chem. Free C
1C	Leached Raney iron	43.44	93.50	--	--	--	--	10H₂+100	3000	190-212 (177)a/	--	190-240 (231)a/	40	45.01	Fe₃O₄, ε-Fe₂C, x-Fe₂C, α-Fe	----	cancelled	----
2C	do	46.78	92.01	--	--	--	--	do	do	164-210 (210)	--	164-241 (215)	45	50.56	ε-Fe₂C, Fe₃O₄	78.50	6.60	3.60
3C	do	46.62	91.20	--	--	--	--	do	do	190-270 (262)	190-320 (304)	190-290 (277)	48	53.05	x-Fe₂C, Fe₃O₄	77.80	4.90	3.45
4C	1C	--	--	--	--	--	--	do	do	167-220 (216)	167-288 (265)	165-250 (246)	24	39.81	x-Fe₂C, Fe₃O₄	84.37	7.50	3.34
5C	b/	--	--	H₂	2500	450	10	do	do	--	252-253 (252)	233-238 (228)	44	37.20	x-Fe₂C, α-Fe	90.27	5.30	3.12
6C	Leached Raney iron	45.28	85.62	do	do	460	10	do	do	163-212 (195) 282-330 (322)	188-240 (230) 316-365 (361)	170-245 (236) 324-400 (385)	14 / 31	-- / 55.94	x-Fe₂C, θ-Fe₃C	--	--	--
7C	do	45.78 43.74	89.10	do / He	do	460 / 340	22 / 40	do	do	190-225 (207)	215-268 (241)	227-270 (249)	52 / 40	45.89 / 42.37	x-Fe₂C, ε-Fe₂C / x-Fe₂C	--	--	--
8C	Magnetite	131.32	67.40	do	do	460	41	∞ / He	100 / --	143-300 (152) 474-487 (481)	158-322 (226) 496-510 (505)	154-304 (209) 496-502 (498)	23 / 3	-- / 106.91	θ-Fe₃C, ε-Fe₂C	81.57	9.25	4.39
9C	do	131.30		do	do	460	49	∞	100	150-180 (172) 180-260 (235) 260-309 (290)	169-199 (190) 199-288 (261) 288-349 (322)	143-182 (167) 182-258 (236) 258-305 (267)	16 / 24 / 6	109.31	x-Fe₂C	--		
10C	do	63.35		do	do	460	48	∞ / He	100 / --	174-260 (235) 260-324 (292) 498-502 (501)	206-266 (235) 470-474 (472)	137-206 (183) 206-266 (235) 470-474 (472)	7 / 8 / 3	47.58	θ-Fe₃C, α-Fe	--	--	
11C	do	128.50		do	do	450	44	∞	100	165-233 (206) 233-338 (318)	150-217 (178) 217-302 (292)	173-240 (206) 240-352 (338)	20 / 25	114.77	x-Fe₂C	17.31	11.81	--
12C	Leached Raney iron	107.68		do	do	458	10	1GH₂+100	3000	230-272 (242)	230-242 (235)	225-250 (241)	10	107.78	ε-Fe₂C, α-Fe	--		

a/ First figure is temperature at which reaction started, second figure is maximum temperature, third figure is the average temperature of carbiding.
b/ This is a rerun of an earlier preparation that had been oxidized during discharging.

TABLE XV   (Cont.)

Nitride Preparations

Run no	Iron source	Hourly space velocity of NH_3, hr^{-1}	Average bed temp, °C	Duration of nitriding, hrs	Discharge wt, g	Phases by x-ray diffraction	Chemical analyses, wt-%	
							Total Fe	Total N
1N	Magnetite	750	356	6	49.1	ϵ-Fe_3N, γ'-Fe_4N	89.90	5.92
2N	do	750	366	6	51.3	γ'-Fe_4N, ϵ-Fe_3N	83.20	5.47
4N	do	1000	339	7	48.9	ϵ-Fe_3N, γ'-Fe_4N	81.90	7.61
5N	do	1000	340	7	52.3	ϵ-Fe_3N, γ'-Fe_4N	82.80	6.57
6N	do	1000	338	12	51.5	ϵ-Fe_3N, ζ-Fe_2N	82.4	6.35
7N	do	1000	381	6	50.2	γ'-Fe_4N	83.53	5.04
8N	Raney iron	1000	347	7½	46.5	γ'-Fe_4N		
9N	Magnetite	1000	342	24	46.6	ζ-Fe_2N		7.94
10N	do	1000	345	24	55.5	ϵ-Fe_3N	80.28	4.85
11N	Coprecipitated 3Fe/1Ag	1000	350	25	50.5	ϵ-Fe_3N, Ag		
13N	Raney iron	1000	350	12	46.1	ϵ-Fe_3N	86.47	9.75
14N	do	1000	347	24	44.6	ϵ-Fe_3N		9.61
15N	Coprecipitated 1Fe/1Ag	1000	352	24	58.1	ϵ-Fe_3N, Ag		4.35
16N	do	1000	349	24	57.7	Ag, ϵ-Fe_3N		2.81
17N	Raney iron	1000	352	12	49.1	ϵ-Fe_3N		9.12
18N	do	1000	294	24	99.1	ζ-Fe_2N, ϵ-Fe_3N		

*   Taken from Bureau of Mines Quarterly Report - Contract No. NASW 12300

TABLE XV (Cont.)

Nitriding of Iron Carbides

Run no	Charge	Charge wt, g	X-ray analysis	Gas	Hourly space velocity, hr^{-1}	Average bed temp, °C	Duration of nitriding, hrs	Discharge wt, g	X-ray analysis	Chemical analysis, wt-%		
										Total C	Free C	Nitrogen
1NC	3C	50.41	x-Fe₂C, Fe₃O₄	NH₃	1000	345	28	-	ε-Fe₂X(C,N), Fe₃O₄	-	-	-
2NC	9C	107.85	x-Fe₂C	NH₃	1000	349	24	109.18	x-Fe₂X(C,N), ε-Fe₂X(C,N)	11.76	5.93	2.26
3NC	8C	101.58	θ-Fe₃C, ε-Fe₂C	NH₃	1000	352	24	104.40	ε-Fe₂X(C,N)	-	-	-

Carbiding of Iron Nitrides

Run no	Charge	Charge wt, g	X-ray analysis	Gas	Hourly space velocity, hr^{-1}	Bed temp, °C	Duration of carbiding hrs	Discharge wt, g	X-ray analysis	Chemical analysis, wt-%		
										Total C	Free C	Nitrogen
1CN	4N	46.05	ε-Fe₃N,γ'-Fe₄N	CO	100	309-346 (335) / 302-352 (347) / 292-315 (3?7)	11	46.67	ε-Fe₂X(C,N)	-	-	-
2CN	7N	43.14	γ'-Fe₄N	CO	100	210-295 (273) / 295-343 (319)	4 9	43.32	ε-Fe₂X(C,N)	-	-	-
3CN	14N	42.51	ε-Fe₃N	CO	100	180-350 (249) / 350	4 7	43.43	ε-Fe₂X	-	-	-

a/ First figure is temperature at which reaction started, second figure is maximum temperature of carbiding, third figure is the average temperature of carbiding.

* Taken from Bureau of Mines Quarterly Report - Contract No. NASW 12300

TABLE XV   (Cont.)

Carbiding of Iron Nitrides

Run No.	Charge	Charge wt.,g.	X-ray analysis	Gas	Hourly space velocity hr.⁻¹	Bed temp., °C a/	Duration of carbiding, hrs.	Dis-charge wt.,g.	X-ray analysis	Chemical analysis, wt.-%		
										Total C	Free C	Nitrogen
6CN	11N	30.4	ϵ-Fe$_3$N, Ag	CO	100	225-350(319) 350	3 5	30.4	ϵ-Fe$_2$X(C,N), Ag			
7CN	15N	37.6	ϵ-Fe$_3$N, Ag	CO	100	185-350(306) 350	5 5	37.6	ϵ-Fe$_2$X(C,N), Ag			
8CN	16N	37.6	Ag, ϵ-Fe$_3$N	CO	100	202-350(305) 350	4 6	37.2	Ag, ϵ-Fe$_2$X(C,N)			
9CN	21N	40.1	γ'-Fe$_4$N, ϵ-Fe$_3$N	CO	100	200-250(243) 250	½ 3½	40.1	γ'-Fe$_4$X(C,N)			
10CN	8N	17.7	γ'-Fe$_4$N, ζ-Fe$_2$N	CO	100	200-250(223) 250	1 3	17.1	γ'-Fe$_4$X(C,N)			

a/ First figure is temperature at which reaction started, second figure is maximum temperature of carbiding, third figure is the average temperature of carbiding.

* Taken from Bureau of Mines Quarterly Report - Contract No. NASW 12300

TABLE XV (Cont.)

Nitriding of Iron Carbides

Run No.	Charge	Charge wt.,g.	X-ray analysis	Gas	Hourly space velocity, hr.$^{-1}$	Average bed temp.,°C	Duration of nitriding, hrs.	Discharge, wt., g.	X-ray analysis	Chemical analysis, wt.-% Total C	Free C	Nitrogen
4NC	5C	34.5	χ-Fe$_2$C, α-Fe	NH$_3$	1000	350	20	35.3	ε-Fe$_2$X(C,N)	3.84	1.09	6.64
5NC	14C	35.1	θ-Fe$_3$C	NH$_3$	1000	294	6	35.0	θ-Fe$_3$X(C,N)	8.13	3.53	0.78
6NC	7C	15.0	χ-Fe$_2$C	NH$_3$	1000	280	15	14.7	χ-Fe$_2$X(C,N)	7.35	6.0	1.13
7NC	15C	29.9	θ-Fe$_3$C	NH$_3$	1000	300	6	29.8	θ-Fe$_3$X(C,N)			
8NC	21C	13.0	Ag, χ-Fe$_2$C	NH$_3$	1000	280	19	13	Ag, χ-Fe$_2$(C,N)			
9NC	22C	15.0	Ag, χ-Fe$_2$C	NH$_3$	1000	280	15	14.9	Ag, χ-Fe$_2$(C,N)			
10NC	24C	15.0	Ag	NH$_3$	1000	280	15	14.9	Ag			0.37[a]

a/ Fe 25.0%.

* Taken from Bureau of Mines Quarterly Report - Contract No. NASW 12300

TABLE XV (Contd.)

Coprecipitation and Reduction of Mixed Oxides of Iron and Silver

Run no	Reactants other than H_2O, g			Washings	Fe/Ag weight ratio of product	Charge, g	Reduction			
							Gas	Hourly space velocity, hr^{-1}	Average bed temp, °C	Duration of reduction, hrs
I-CP	$Fe(NO_3)_3 \cdot 9H_2O$ 46.62	$AgNO_3$ 3.38	Na_2CO_3 150	H_2O, acetone, ethanol, and ether	3.04/1	65.35	H_2	2,500	450	18
II-CP	$Fe(NO_3)_3 \cdot 9H_2O$ 41.07	$AgNO_3$ 8.93	Na_2CO_3 150	H_2O, acetone, ethanol, and ether	1/1	71.12	H_2	2,500	453	7
III-CP	$Fe(NO_3)_3 \cdot 9H_2O$ 30.25	$AgNO_3$ 19.75	Na_2CO_3 150	H_2O, acetone, ethanol, and ether	1/3.0	66.25	H_2	2,500	450	3.3

* Taken from Bureau of Mines Quarterly Report - Contract No. NASW 12300

TABLE XV (Contd.)

Pretreatment and Carbiding

Run No.		Pretreatment					Carburization						
	Charge	Charge wt., g.	Gas	Hourly space velocity, hr.⁻¹	Temp., °C.	Time, hr.	Gas	Hourly space velocity, hr.⁻¹	Temperature, °C. (Front of bed)	Temperature, °C. (Rear of bed)	Time, hr.	Discharge, wt., g.	X-ray diffraction
21C	38CP	33.95	H_2	2500	443	14	CO	100	170-357	157-329	45	27	Ag, X-Fe_2C
22C	39CP	42.41	H_2	2500	446	11	CO	100	170-350	167-343	45	36	Ag, X-Fe_2C
24C	40CP-	57.61	H_2	2500	452	13	CO	100	170-350	151-329	45	49	Ag
17C	Leached Raney nickel	44.78					CO	100	160-249(232)	155-244(229)	7	46.1	Ni_3C, Ni trace
		42.80					CO	100	250	228	24	43.8	Ni_3C, Ni trace
		43.2					CO	100	250	228	48	49.8	Ni_3C, Ni trace
									300	257	24		
18C	Leached Raney cobalt	40.54					CO	100	200-300	185-297	22	47.2	Co_2C, Co
									300	297	49		
19C	Leached Raney nickel	53.19					CO	100	180-250	161-236	29	55.2	Ni_3C, Ni
		54.33					CO	100	250	236	48	55.2	Ni_3C, Ni trace
									251	233	20		
20C	Leached Raney cobalt	49.95					CO	100	180-250	167-240	4	51.0	Co_2C, Co
		50.41					CO	100	250	240	48	50.1	Co_2C, Co
									260	241	27		

* Taken from Bureau of Mines Quarterly Report - Contract No. NASW 12300

TABLE XV   (Contd.)

Preparation of Carbides

Carbiding gas --------- CO
Hourly space velocity -   100

Run No.	Charge [1]	Duration of carbiding, hrs.	Temperature, °C	Chemical analysis, weight percent	
				Total C	Free C
25C	RAL-1 (1Ni-1Co)	13 216	170-225 250	9.78	6.18
26C	RAL-2 (1Ni-3Co)	13 144	170-228 250	8.86	4.86
27C	RAL-3 (3Ni-1Co)	13 144	170-225 250	9.33	7.48
29C	RAL-4 (1Ni-3Ag)	5, 104	170-230 250	1.21	0.7
30C	RAL-5 (1Ni-1Ag) 60-250 mesh	6 102	160-220 250	2.31	1.12
31C	RAL-5 (1Ni-1Ag)	6 100	160-220 250	2.04	1.06
32C	RAL-6 (3Ni-1Ag)	5 102	160-220 250	3.42	0.8
33C	RC-1 (Raney Co)	26 72	160-240 250	3.59	0.54
34C	RAL-9 (3Co-1Ag)	5 105	160-220 250	4.67	1.75
35C	RN-2B2 (Raney Ni)	22 72	160-220 250	10.78	6.55
36C	RNL-4 (Raney Ni, <mesh)	11 72	160-220 250		
38C	RAL-7 (1Co-3Ag)	6 100	160-220 250	1.82	0.72
39C	RAL-8 (1Co-1Ag)	13 100	160-230 250	2.56	0.66
40C	RAL-10 (1Ni-1Co-1Ag)	13 100	160-230 250	0.84	0.33
41C	RAL-11 (1Ni-1Co-1Au)	22 102	160-220 250		
42C	RAL-1 (1Ni-1Co)	21 101	160-220 250		
43C	RAL-5 (1Ni-1Ag)	4 102	160-250 250		
44C	RAL-12 (1Ni-1Ag-1Au)	4 103	160-250 250		

1/ Mesh size 150-250, unless otherwise stated.

* Taken from Bureau of Mines Quarterly Report - Contract No. NASW 12300

TABLE XV (Contd.)

Preparation of Carbides

Carbiding gas: CO
Hourly space velocity: 100

Run no.	Charge[1]	Duration of carbiding, hrs.	Temp., °C	Chemical analysis, weight-percent		X-ray analysis
				Total C	Free C	
53C	1Ni-1Ag	5 102 106	160-250 250 260	1.92	0.12	Ni₃C, Ag
56C	Ni	6 102 36	160-250 250 260	0.94	0.20	Ni₃C, Ni
57C	1Ni-1Pd	6 37 103	160-250 250 260	1.19	0.95	
59C	Co	5 100	160-250 250			Co₂C

[1] Reduced precipitated/coprecipitated hydroxides.

Space velocity of CO: 100 hr^{-1}

Run no.	Charge	Duration of carbiding, hrs	Temp, °C
45C	1Co-1Ag-1Au	4 104	160-250 250
46C	3Ni-1Ag	6 101	160-250 250
55C	1Ni-1Pd	4 106	160-250 250

TABLE XV   (Cont.)

Preparation of Nitrocarbides

Nitriding gas -------------- NH3
Temperature -------------- 260 °C
Hourly space velocity ----- 1000

Run No.	Charge	Duration of nitriding, hrs	Chemical analysis, weight-percent		
			N	Total C	Free C
11NC	19C (Ni$_3$, trace of Ni)	15	1.08		
12NC	20C (Co$_2$C, α-Co, Cub. Co)	39	0.90	5.33	2.50
13NC	26C (Carbided 1Ni-3Co)	48	0.92	8.88	4.50
15NC	27C (Carbided 3Ni-1Co)	48	1.01	9.30	6.38
16NC	25C (Carbided 1Ni-1Co)	48	0.87	9.45	6.46
17NC	29C (Carbided 1Ni-3Ag)	48			
18NC	30C (Carbided 1Ni-1Ag, 60-250 mesh)	48			
19NC	31C (Carbided 1Ni-1Ag, 150-250 mesh)	48			
20NC	32C (Carbided 3Ni-1Ag)	58			
21NC	33C (Co$_2$C, α-Co)	48			
22NC	34C (Carbided 3Co-1Ag)	48			
23NC	35C (Ni$_3$C)	48			
24NC	36C (Ni$_3$C, <250 mesh)	48			
25NC	38C (Carbided 1Co-3Ag)	48			
26NC	39C (Carbided 1Co-1Ag)	48			
27NC	40C (Carbided 1Ni-1Co-1Ag)	48			
28NC	42C (Carbided 1Ni-1Co)	48			
29NC	41C (Carbided 1Ni-1Co-1Au)	48			
30NC	44C (Carbided 1Ni-1Ag-1Au)				

TABLE XV (Cont.)

Preparation of Nitrocarbides

Nitriding gas: NH$_3$
Space velocity: 1,000 hr^{-1}
Time: 48 hours
Temperature: 260°C

Run No.	Charge	Total C	Free C	N
*39NC	54C$^{1/}$ (carbided Ni)	6.63	0.41	0.47
40NC	55C (carbided 1Ni-1Pd, Raney alloy)	7.65	6.91	1.69
41NC	56C (carbided Ni)	1.07	0.17	0.84
42NC	57C (carbided 1Ni-1Pd)	0.60	0.48	2.21
43NC	59C (carbided Co)	10.36	4.92	0.58
44NC	60C (carbided 1Ni-1Ag-1Au)	1.37	0.40	1.41
45NC	61C (carbided 3Ni-1Co)	0.37	0.24	0.65
46NC	62C (carbided 3Ni-3Pd)	0.29	0.24	0.38
47NC	63C (carbided 3Ni-1Pd)	2.14	1.40	2.45
48NC	64C (carbided 1Ni-1Au-1Pd)			

Run No.	Charge	Total C	Free C	N
49NC	65C (carbided 1Ni-1Au-1Pt)			
50NC	66C (carbided 1Ni-1Ag-1Pt)	0.50	0.32	0.15
51NC	67C (carbided 1Ni-3Ag)	0.56	0.15	0.94
52NC	75C (carbided 1Ni-1Ag-1Pd)			
53NC	76C (carbided 1Ni-3Au)			
54NC	74C (carbided 3Ni-1Au)			
55NC	77C (carbided 1Ni-1Au)			
56NC	78C (carbided 1Ni-4Cr)			
57NC	79C (carbided 1Ag-3Pd)			

*The letters NC stand for nitrocarbide.
1/ Nitrided at 250°C.

TABLE XV (Cont.)

Preparation of Nitrocarbides

Nitriding gas: NH₃
Space velocity: 1,000 hr⁻¹
Time, hours: 48
Temperature: 260 °C

Nitriding gas: NH_3
Space velocity: $1{,}000 \text{ hr}^{-1}$
Time, hours: 48
Temperature: $260\,°\text{C}$

Run No.	Charge	Chemical analysis, weight percent		
		Total C	Free C	N
58NC[1]	80C (carbided 3Ni-1Pt)	5.36	3.57	0.47
59NC	81C[2] (carbided 1Ni-1Pt)	3.57	2.86	0.26
60NC	82C (carbided 1Ni-3Pt)	1.11	0.88	0.24
61NC	84C (carbided 3Ni-1Ag)	5.42	0.34	0.57
62NC	85C (carbided 1Ag-1Pd)			
63NC	86C (carbided 3Ag-1Pd)			
64NC	88C[2] (carbided 1Au-3Pd)			

1/ The letters NC stand for nitrocarbide.
2/ Space velocity: $1{,}500 \text{ hr}^{-1}$.

TABLE XV (Cont.)

Preparation of Carbides

Carbiding gas: CO
Space velocity: 100 hr^{-1}

Run No.	Charge [1]	Duration of carbiding, hrs.	Temp., °C	Chemical analysis, weight percent	
				Total C	Free C
*60C	1Ni-1Ag-1Au	5 102	160-260 260	1.57	0.39
61C	3Ni-1Co	5 102	160-260 260	0.28	0.17
62C	1Ni-3Pd	6 100	160-260 260	0.35	0.25
63C	3Ni-1Pd	5 100	160-260 260	2.34	1.93
64C	1Ni-1Au-1Pd	5 104	160-260 260		
65C	1Ni-1Au-1Pt	5 100	160-260 260		
66C	1Ni-1Ag-1Pt	6 102	160-260 260		
67C	1Ni-3Ag	6 98	160-260 260	0.92	0.21
68C [2]	3Ni-1Co	5 120	160-260 260		
69C	3Ni-1Co	5 120	160-240 240		
70C	3Ni-1Co	.4 72	160-260 260		
71C	3Ni-1Co	4 72	160-240 240	4.15	0.53
72C	3Ni-1Co	4 24	160-260 240		
73C	3Ni-1Co	4 24	160-240 240	2.13	0.26
74C	3Ni-1Au	5 100	160-260 260	1.01	0.20
75C	1Ni-1Ag-1Pd	5 102	160-260 260		
76C	1Ni-3Au	4 103	160-260 260		
77C	1Ni-1Au	5 100	160-260 260		
78C	1Ni-4Cr	4 100	160-260 260		
79C	1Ag-3Pd	4 100	160-260 260		

*The letter C stands for carbide.
1/ Reduced coprecipitated hydroxides.
2/ The carbides 68C to 73C were all prepared from 3Ni-1Co but the conditions of carbiding were different in each case.

TABLE XV (Cont.)

Preparation of Carbides

Carbiding gas: CO
Space velocity: 1,000 hr^{-1}

Run No.	Charge[1]	Duration of carbiding, hrs.	Temp., °C	Chemical analysis, weight-percent	
				Total C	Free C
80C[2]	3Ni-1Pt	4 105	160-260 260	5.96	3.40
81C	1Ni-1Pt	5 100	160-260 260	3.66	2.57
82C	1Ni-3Pt	4 105	160-260 260	1.21	0.97
84C	3Ni-1Ag	4 103	160-260 260	5.75	0.35
85C	1Ag-1Pd	5 104	160-260 260	0.29	0.10
86C	3Ag-1Pd	4 105	160-260 260	0.5	0.23
87C	4Cr-1Mo	5 103	160-260 260		
88C	1Au-3Pd	4 104	160-260 260		

1/ Reduced coprecipitated hydroxides.
2/ The letter C stands for carbide.

TABLE XV (Cont.)

Reduction of Mixed Metals Hydroxides

Reducing gas: H_2
Space velocity: 1,000 hr^{-1}
Time: 85 hours

Run No.	Temperature of reduction, °C	Composition of reduced material
*61R	275	3Ni-1Co
62R	250	1Ni-3Pd
63R	250	3Ni-1Pd
64R	250	1Ni-1Au-1Pd
65R	250	1Ni-1Au-1Pt
66R	250	1Ni-1Ag-1Pt
67R	250 - 11 hrs. 275 - 74 hrs.	1Ni-3Ag
74R	250	3Ni-1Au
75R	250	1Ni-1Ag-1Pd
76R	250	1Ni-3Au
77R	275	1Ni-1Au
78R	275	1Ni-4Cr
79R	250	1Ag-3Pd

Run No.	Temperature of reduction, °C	Composition of reduced material
80R[1/]	250	3Ni-1Pt
81R	"	1Ni-1Pt
82R	"	1Ni-3Pt
84R	275	3Ni-1Ag
85R	250	1Ag-1Pd
86R	"	3Ag-1Pd
87R	275	4Cr-1Mo
88R	250	1Au-3Pd
89R	"	1Au-1Pd
90R	"	3Au-1Pd

1/ The letter R stands for reduced material.

TABLE XV   (Cont.)

92R 1Ag-1 Pt.   An alkaline aqueous suspension of Pt-black was treated with a solution of silver nitrate at room temperature with vigorous stirring. The solid was washed, dried and reduced with hydrogen at 2500 hourly space velocity, 250°C for 89 hours.

93R 1Ag-1Pt.   Silver hydroxide precipitated on Pt-black, as in 92R. Reduced with hydrogen at 2500 hourly space velocity, 250°C for 89 hours.

94R 1Pt-1Pd.   A mixed solution of Pt and Pd in aqua regia was made alkaline with NaOH, and then treated with a solution of sodium formate with vigorous stirring at 90°C. The solid was washed, dried and reduced with hydrogen at 1000 hourly space velocity, 250°C for 85 hours.

95R 3Pt-1Pd.   Preparative method as in 94R. Solid reduced with hydrogen at 1000 hourly space velocity, 250°C for 85 hours.

96R 3Pd-1Pt.   Preparative method as in 94R. Solid reduced with hydrogen at 1000 hourly space velocity, 250°C for 85 hours.

97R 1Au-1Pd-1Ag.   A mixed solution of Au and Pd in aqua regia was made alkaline with NaOH and the precipitate so obtained was washed free of chloride ions. The material was then suspended in water, made alkaline, and treated with a solution of silver nitrate with vigorous stirring. The solid was washed, dried, and reduced with hydrogen at 1000 hourly space velocity, 250°C for 85 hours.

98R 1Ni-1Pt-1Pd.   A mixed solution of Pt, Pd, and Ni was made alkaline with NaOH and then treated with sodium formate, with vigorous stirring at about 90°C. The dried powder was reduced with hydrogen at 2000 hourly space velocity, 250°C for 85 hours.

99R 1Ag-1Au-1Pt.   Gold as hydroxide and platinum as Pt-black were prepared separately and washed free of chloride ions. They were then mixed together and suspended in water. The suspension was made alkaline and treated with a solution of silver nitrate, with vigorous stirring at room temperature. The washed and dried solid was reduced with hydrogen at 2000 hourly space velocity, 250°C for 85 hours.

TABLE XV (Cont.)

100R 1Ag-1Pd-1Pt. A mixed solution of Pt and Pd in aqua regia was made alkaline with NaOH and then treated with a solution of sodium formate with vigorous stirring at 90°C. The solid was washed free of chloride ion, suspended in water, made alkaline with NaOH and treated with a solution of silver nitrate with vigorous stirring. The three-component precipitate was washed, dried, and reduced with hydrogen at 1000 hourly space velocity at 250°C for 85 hours.

101R 3Ag-1Au. Washed and dried, separately prepared hydroxides of silver and gold were mixed mechanically, and the mixture reduced with hydrogen at 1500 hourly space velocity, 250°C for 89 hours.

102R 3Au-1Pt. Pt-black and gold hydroxide were precipitated separately. Calculated amounts of the washed and dried powders were mixed mechanically, and the mixture reduced with hydrogen at 1500 hourly space velocity, 250°C for 80 hours.

103R 1Au-3Pt. Prepared as 102R. Reduced with hydrogen at 3000 hourly space velocity, 250°C for 92 hours.

104R 1Au-1Pt. Prepared as 102R. Reduced with hydrogen at 1500 hourly space velocity, 250°C for 82 hours.

105R 1Ag-3Au. Prepared as 101R. Reduced with hydrogen at 1000 hourly space velocity, 250°C for 89 hours.

106R 1Ag-1Au. Prepared as 101R. Reduced with hydrogen at 1000 hourly space velocity, 250°C for 90 hours.

107R 1Au-1Pt-1Pd. A mixed solution of Pt and Pd in aqua regia was made alkaline with NaOH and then treated with a solution of sodium formate at 90°C with vigorous stirring. The washed and dried powder was mixed mechanically with a separately prepared powder of gold hydroxide and the mixture reduced with hydrogen at 1000 hourly space velocity, 250°C for 86 hours.

---

*Taken from Bureau of Mines Quarterly Report - Contract No. NASW 12300

II. ELECTROCHEMICAL TESTING OF FINELY DIVIDED CATALYSTS

The testing of highly dispersed catalysts presents many problems that are not experienced with the testing of solid electrodes. These are discussed in detail before the presentation of the data, because the interpretation of the data depends to a great extent on an appreciation of these problems.

The high area surface of a catalyst is not used to its full advantage unless the electrode structure into which it is incorporated offers good mass transport characteristics to all regions of the surface. The plastic (PTFE) bonded electrode[16] undoubtedly comes closest to realizing this objective for a practical catalyst.

In these electrodes the catalyst is mixed with a dispersion of PTFE and spread on a nickel screen. The effectiveness of this structure depends on (a) the hydrophobic nature of the binder to provide gas contact to the interior surfaces of the electrode and (b) the porosity of the catalyst (the pores fill with electrolyte by capillary action) to provide electrolyte contact at all the reaction sites of the surface. Thus a catalyst of good intrinsic activity, in a highly dispersed form, must also have a pore structure conducive to the mass transport requirements of normal operation.

In more detail, most of the spaces between the agglomerates are wetproofed by the PTFE dispersion and provide good gas transport; some remain hydrophillic (depending on the % PTFE in the catalyst mix) and permit electrolyte penetration in depth into the electrode. However, contact between the electrolyte and a large percentage of the catalyst surface depends on a network of fine pores (pore diameter $< \sim 500$ Å) in the catalyst. These do not become wetproofed because the particle size of the PTFE dispersion (~ 0.1 μ) is larger than the pore diameter.

Even with a catalyst of good activity and ideal structure, the performance of a PTFE bonded electrode can vary with its method of preparation. The main variables are the percentage of plastic binder, the sintering time, and the sintering temperature. The distribution of the catalyst binder mixture on the supporting metal screen can also be carried out in several

ways. Before catalysts were tested, a familiarization program was carried out with platinum and carbon to explore these variables. Brief details are presented below.

A. Effect of Manufacturing Techniques on Performance of Porous Electrodes

1. Platinum Electrodes

Platinum electrodes were prepared by spraying, brushing, spreading, and rolling methods. All preparations to date have been made with approximately 30% Teflon, considered from previous work to be optimum, and a Pt loading of about 10 mg/cm^2. Deviations from the 10 mg/cm^2 loading are due to uncertainties in the expected loss of material for each fabrication method. All electrodes are cut from larger pieces to 1 cm^2 for testing.

2. Catalyst Distribution Methods

a. Spraying Technique

Electrodes numbered 1, 2a, TR-1, TR-2, TR-3A, TR-3B, TR-4A, TR-4B, TR-6, TR-7, and TR-8 were sprayed with an air gun to determine the relation between loading and spraying techniques. Electrodes 1 and 2a were prepared on 100 cm^2 of screen, and 50% excess platinum was used for a projected 10 mg/cm^2 loading after losses. These electrodes were sintered at 260°C and had 10 mg/cm^2 Pt. Electrodes TR-1, TR-2, TR-3 and TR-4 were prepared on 36 cm^2 of screen, and 20% excess platinum was used for a projected 10 mg/cm^2. These electrodes had approximately 3-7 mg/cm^2 of platinum. Electrodes TR-3A and TR-4A were sintered at 260°C and showed extremely low performance; subsequently, electrodes TR-3B and TR-4B, sintered at 310°C, showed improved performance. Electrodes TR-6, TR-7 and TR-8 were also sprayed on 36 cm^2 screens with 20% excess platinum but with the following changes in technique: Cab-o-SiL was added to the platinum-Teflon mix on a 1:1 volume ratio. Since this extended the liquid volume and produced a thicker spraying mix, continuous drying was employed. These electrodes had a good uniform physical appearance and loadings (8-10 mg/cm^2) were

closer to the projected loading. However, the Cab-o-SiL may have had an adverse effect on the wetting characteristics of the electrodes. The electrodes were sintered at 285°C, since 260°C seems to be on the borderline of the critical minimum sintering temperature. The influence of sintering temperature is considered in more detail below.

b. Spreading Technique

It has been found that spraying produces the most uniform distribution of catalyst but does not work well with a small quantity of material. The spreading process (spreading a thick paste with a spatula) lends itself better to small quantities but usually does not yield uniform electrodes. Electrode TR-5 was made in this manner on 8 cm^2 of screen starting with no excess material; 13% of the material was lost.

c. Brushing Technique

Electrode TR-9 was made by applying a paste with a small brush to 12 cm^2 of screen mounted on a portable jig for weighing "in situ." An excess of 100% was used in order to work with a paste of the same consistency throughout application. The performance of the electrode was exceptionally high, surpassing all previous runs. This method, however, has proved to be of limited application, being restricted to very finely divided catalysts.

d. Rolling Technique

Electrode TR-10 was made by forming the platinum-Teflon into a rubbery dough and rolling it between Teflon sheets over the defined area of screen. This electrode was not made specifically for this program and consequently did not have a 10 mg/cm^2 loading. It has been found that the rolling method produces uniform electrodes with no loss of material, but they show comparatively low performance. No duplication of runs has been made.

The results are summarized in Fig. 15. The variation in performance was assumed to be mainly related to sintering temperature. This was examined as described below.

Floating Electrode, 35% KOH, 75°C, O_2

E vs. RHE   All curves iR corrected

All electrodes, 30% TFE, Englehard Pt black

No.	Type	Loading (mg/cm^2)	Sint. °C
#1	spray	10	260
#2a	spray	10	260
TR-1	spray	6.3	260
TR-2	spray	7.7	260
TR-3B	spray	3.2	310
TR-4B	spread	2.8	310
TR-5	spread	8.7	285
TR-6	spray	7.7	285
TR-7	spray	10.1	285
TR-8	spray	9.8	285
TR-9	brush	9.8	285
TR-10	rolled	18.4	260

E (mv)

1100 1000 900 800

i (ma/cm^2)

100 200 300 400

TR-9
Am. Cy.
#2a
TR-1
#1
TR-5
Chemcell
TR-10
TR-8
TR-4B
TR-7
TR-2
TR-6
TR-3B

Fig. 15   Comparison of Platinum Electrodes

572F

B. Effect of Sintering Temperatures

A number of electrodes cut from a single sheet of electrode material prepared by the spray method were sintered at 250°C, 275°C, 300°C, and 325°C for five-minute and fifteen-minute intervals. The sintering temperatures in these experiments were accurately defined. In previous work the thermocouple controlling the sintering furnace was influenced by radiant heat. Since the electrodes were effectively shielded from the radiant heat by aluminum foil, the true sintering temperature was some 26° lower than that registered on the controller/indicator.

The two electrodes sintered at 250°C were not hydrophobic and were not tested. On the basis of these results summarized in Table XVI the sintering technique was improved and made more reliable and the optimum sintering conditions (for platinum) defined as 275°C for 15 minutes. Results obtained under these conditions compare favorably with the best previously reported for electrodes prepared in the same way. The change in real surface area during this sintering process at 275°C was measured by a BET technique. The figures before and after sintering were 22.6 m^2/g and 15.6 m^2/g respectively; the platinum black from which the electrodes were prepared had a surface area of 29.0 m^2/g.

C. Carbon and Graphite Electrodes

The performance of carbon and graphite powders were initially of interest as a basis for comparison of metal carbides. They also present a good opportunity for studying techniques of preparing high surface area electrodes, because of the wide range of samples available with such different physical properties as bulk density and surface area. They were consequently used to examine the influence of PTFE/catalyst ratio on performance. The bulk densities of the catalysts were measured to discover if a better correlation could be made in terms of a volume rather than a weight ratio. The following samples were examined; graphite with 22.5%, 25%, 27.5%, 30%, 35%, 40% PTFE content and acetylene black with 45%, 50%, 60%, 70% PTFE content. A summary of performance is given in

<div align="center">

TABLE XVI
</div>

<div align="center">

Effect of Sintering Time and Temperature
</div>

		E = 950 mv	E = 900 mv
250°C	------------- not tested -------------------------
275°C	5 min	i = 4	5 ma/cm^2
	15 min	28	242 "
300°C	5 min	5	10 "
	15 min	18	130 "
325°C	5 min	20	214 "
	15 min	25	230 "

Table XVII. The optimum PTFE contents were deduced to be 27.5% for graphite and 50% for acetylene black, although the curves showed fairly flat maxima so that these figures are not too critical.

The bulk densities were measured after vibration and after centrifuging. Each method is reproducible to about 5%, but as can be seen from Table XVIII, the agreement between the two methods is not good. This is not an unusual occurrence in the determination of bulk densities, since the particle shape factor has a different effect in the various methods of measurement[17]. The data available to correlate bulk density and PTFE content are shown in Fig. 16. It is apparent that the correlation is a useful guide and that the centrifuging method gives the more consistent data.
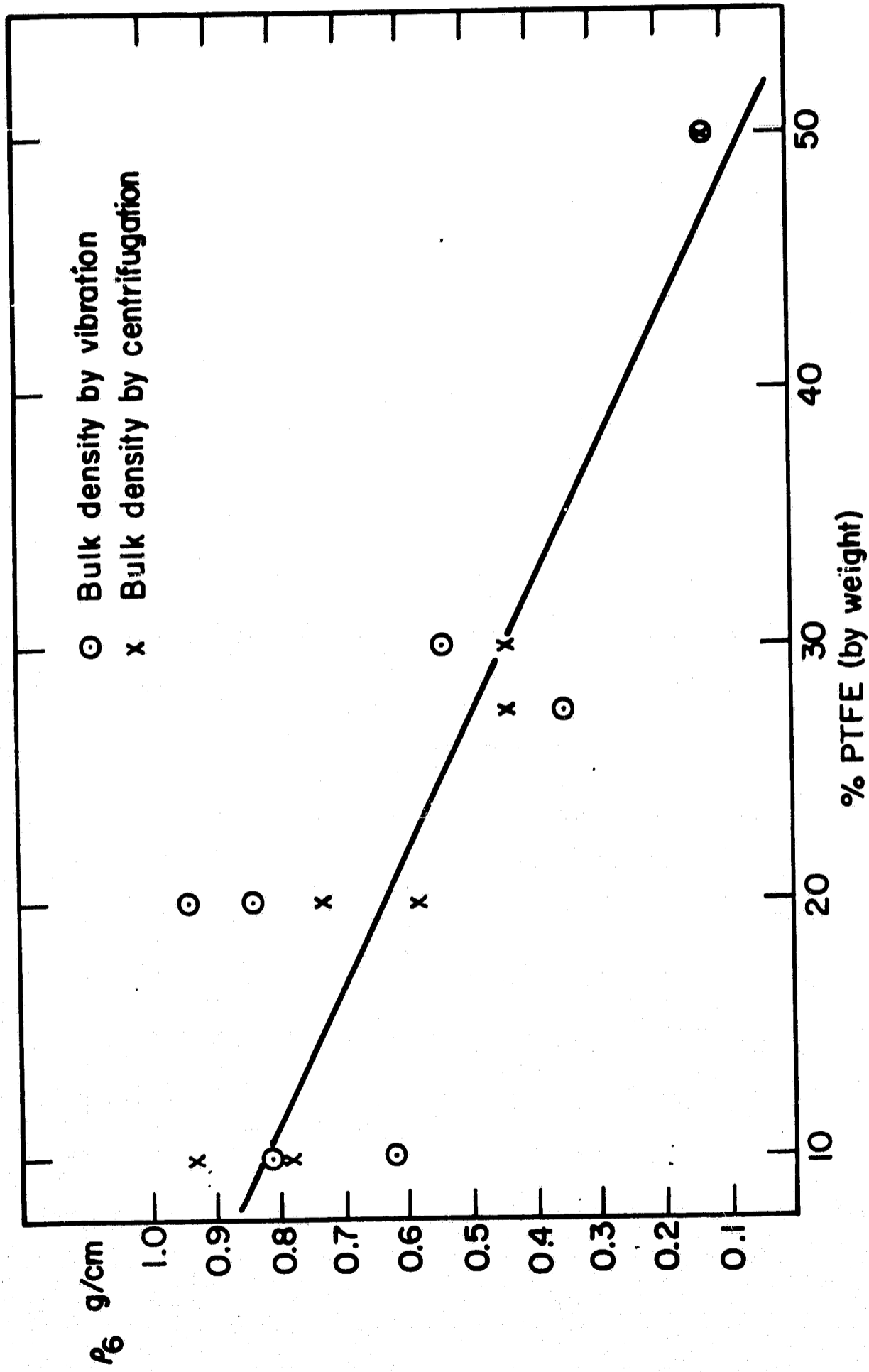
Fig. 16 Plot of Bulk Density vs. PTFE Content of Electrodes

572F

TABLE XVII

Performance as a Function of PTFE Content

Graphite	20	22.5	25	27.5	30	35	40	% PTFE
Current at 800 mv	----	9	7	22.2	5	61	4	ma/cm^2
Current at 600 mv	----	44.5	78	95.5	68	26.6	22	ma/cm^2

Acetylene Black	45	50	55	60	70	% PTFE
Current at 800 mv	2.4	7	5	4	3	ma/cm^2
Current at 600 mv	21.4	94.5	45	48	42	ma/cm^2

TABLE XVIII

Bulk Density Measurements

Bulk Density (gm/cc)

Material	Vibration	Centrifuge	% PTFE
Acetylene black	0.125	0.130	50
Graphite	0.350	0.425	27.5
Engelhard Pt black	0.540	0.435	30
Carbon #7706	0.940	0.735	20
Carbon #8946	0.830	0.580	20
Ni_3C	0.689	0.927	10
$Ni_3C + Co_2C$	0.814	0.780	10

D. Electrode Preparation

Electrode fabrication consisted of the mixing of the catalyst (after induction or exposure, see below) with a dispersion of PTFE (DuPont, Teflon 30) in a known weight ratio. This mixture was pasted on a nickel screen (100 mesh) to produce an electrode of ~ 6 cm^2 area. The electrodes were dried in a vacuum oven at 100°C and subsequently sintered in a stream of N$_2$ at 275°C. Several test electrodes of 1 cm^2 area could be cut from the sintered structure.

E. Electrochemical Testing

The fabricated electrodes were tested in a floating electrode cell configuration (Fig. 17)   in 35% KOH at 75°C using as reference a dynamic hydrogen electrode. Current-voltage curves were determined under potentiostatic conditions using the following procedures. The electrode made contact with the electrolyte at a controlled potential of 1000 mv; the potential was almost immediately reduced to 850 mv and the current noted. The current was measured again after five minutes, the potential was adjusted to 750 mv, and the current measured as before. The current voltage curve was then determined at 50 mv intervals, each held for 5 min in the sequence 750 mv → 400 mv → 850 mv. For the cobalt and nickel-cobalt alloys the procedure was modified to include an anodic induction at 1600 mv for 10 min. The anodic pretreatment induction should produce complete oxidation of the surface and effectively reduce the corrosion rate during oxygen reduction, particularly with the cobalt catalysts. In the case of the nickel-cobalt alloys, the high pretreatment potentials (which may be imagined as being equivalent to heating in an oxidizing atmosphere) could contribute to the formation of a surface spinel (NiCo$_2$O$_4$), reported[18] to exhibit good conductivity and catalytic activity for oxygen reduction. The complete E (i) curve 850 mv → 400 mv → 850 mv was measured as before.

Further modifications to the technique were introduced when experiments described in detail below showed that the activity of these electrodes
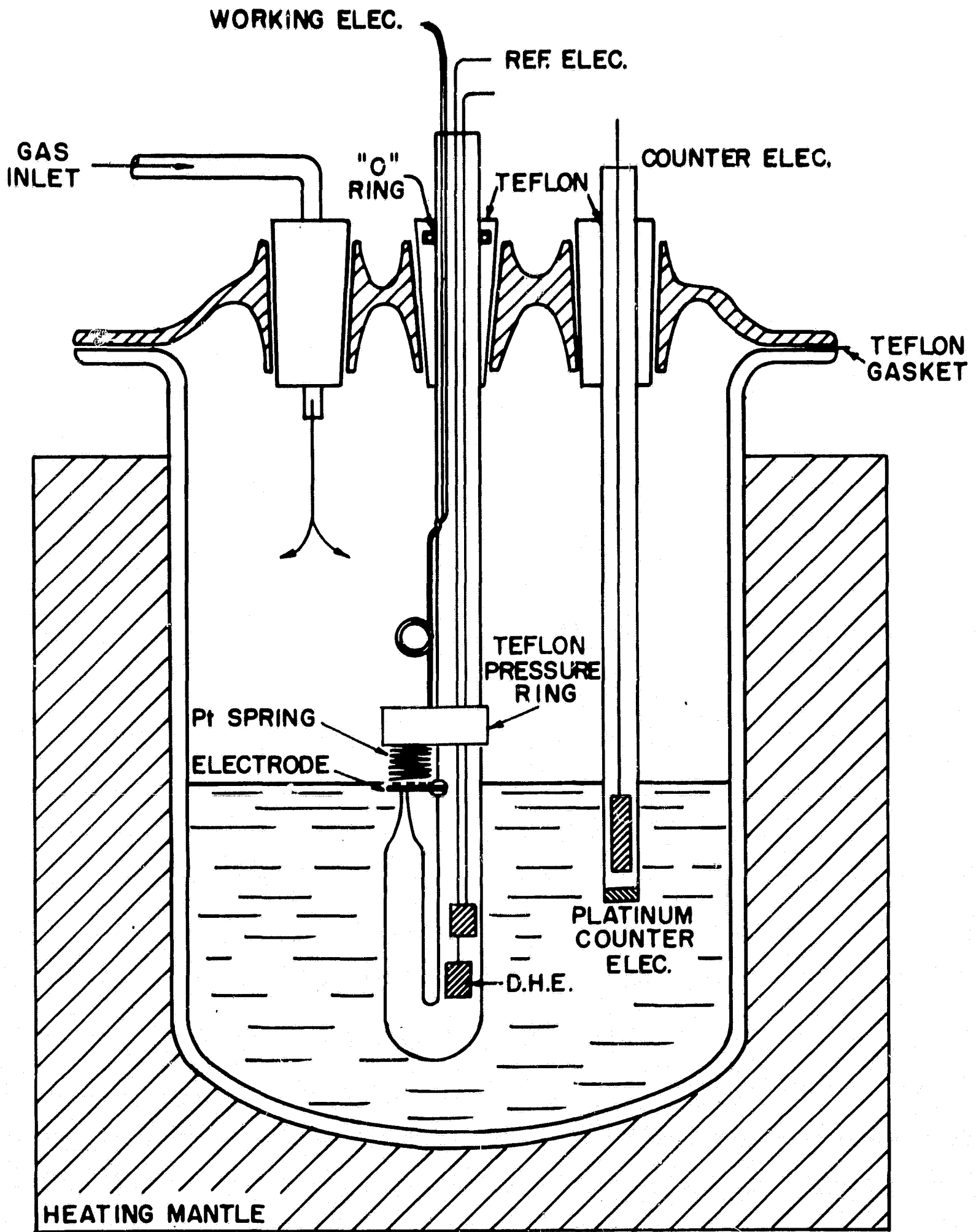
Fig. 17 Floating electrode cell.

572F

varied with time in an unusual manner (see Fig. 18). The current at constant potential initially increased, then remained constant for a period of time before decaying to a constant value somewhat below the initial current.

In order to compare the catalytic activity of individual samples, it was obvious that the measurements had to be made at identical points on this time curve. Since this behavior must be related to the surface oxide, two factors probably need to be taken into account: the total time the catalyst was exposed to air before testing (whether inducted or directly exposed) and the total time of exposure to electrolyte during tests.

After the initial examples the first factor was easily eliminated by preparing each electrode individually and testing as soon as possible (usually within 24 hours). Total contact time with the electrolyte was more difficult. If the fabricated electrodes were fully reproducible, complete information could have been obtained by measuring first a decay curve on one electrode and then the E (i) characteristic on another. Since good reproducibility cannot be guaranteed with PTFE bonded electrodes, the approach adopted was to make several successive determinations of the E (i) curve sufficiently rapidly to display the pattern of the activity change with time. This necessitated the use of a slow potential sweep method. After preanodization the electrode was subjected to a 100 mv/min potential sweep between 1000 mv and 400 mv. A complete curve of increasing and decreasing potential could then be obtained in about ten minutes. The sweeps were continued until the pattern of increase and decrease in current at a particular potential was observed; the tabulated values (see below) represent the highest observed activity. A careful comparison was made of the manual and sweep methods to ensure that the E (i) curves were equivalent.

F. Material Handling

The Bureau of Mines materials were delivered in sealed containers under an atmosphere of CO_2; the first process was to divide the sample into eight approximately equal lots. The subdivision was carried out in a glove box in a

35% KOH 70°C O_2
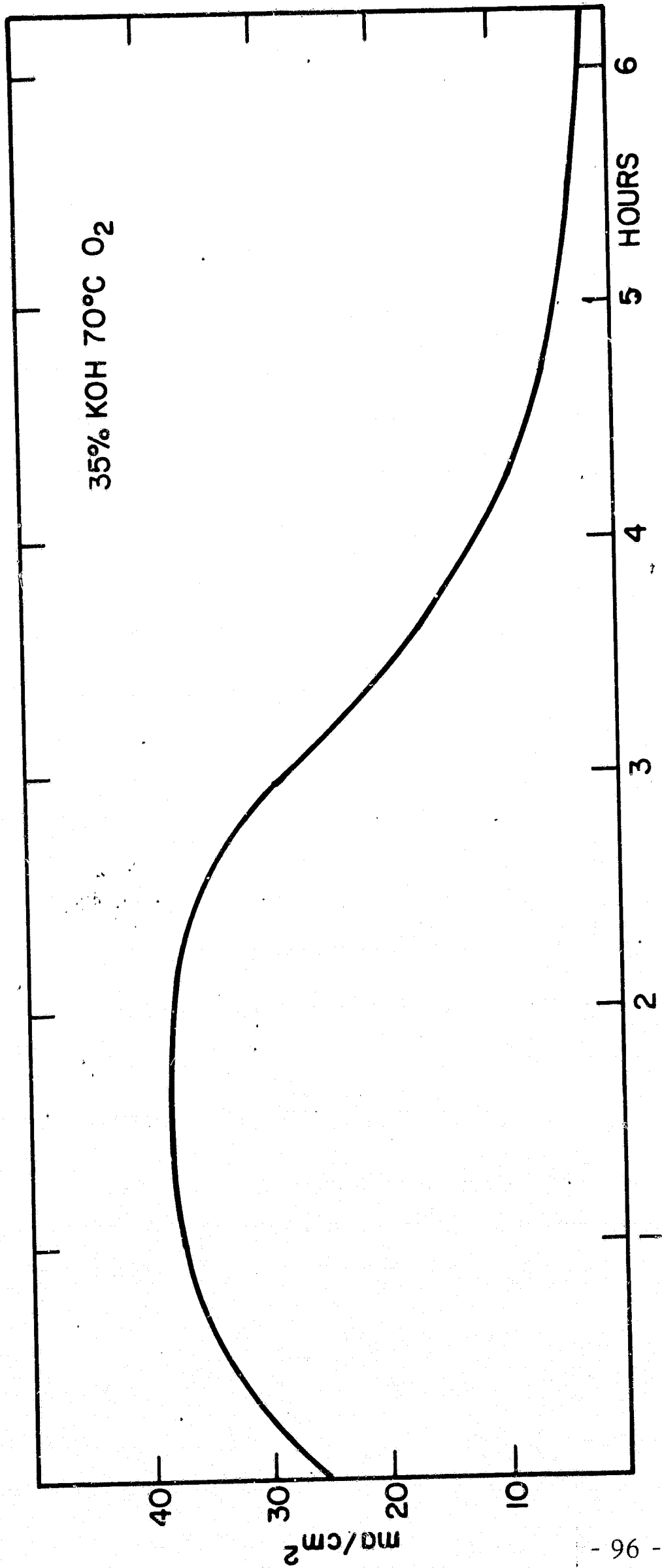
CURRENT AT 750 mv (vs RHE) vs TIME

ma/cm^2

HOURS

Fig. 18 #47 Ni$_3$C

572F

nitrogen atmosphere; the individual samples were contained in plastic snap top bottles that were further sealed in paraffin wax as the bottles were brought out of the inert atmosphere. A freshly prepared sample of Raney nickel was subjected to exactly the same procedures as the Bureau of Mines' materials up to the stage of wax sealing. The Raney nickel was then exposed to air and on each occasion the sample was pyrophoric, indicating the effectiveness of the glove box in each case. (The surface of Raney nickel is easily passivated by exposure to very small amounts of O_2 and becomes nonpyrophoric.)

Also, during the subdivision of the samples, the resistance of the powder was measured. The sample was contained between two pieces of Pt foil by an O ring 1/2" O.D. and 5/16" I.D. The sample was then compressed at constant pressure in a jig using a torque wrench (Sturtevant Model F-21-1 at 15 inch pounds) and the resistance measured. The resistance of exposed and inducted samples was measured in an attempt to measure the need for, or the effectiveness of, the induction procedure. The method was only used to determine major changes in conductivity (see below).

G. Induction Methods

In a finely divided state (BET surface areas in the range 10-27 m^2/g) many of these materials were pyrophoric. Pyrophoric oxidation probably results in the complete oxidation of the sample and, for finely divided materials, the loss of a large proportion of their surface area. Special techniques were developed to induct the materials prior to exposure to oxygen during electrochemical testing. The basis of these techniques was to carry out the initial oxidation process as slowly as possible. Thus it was hoped to limit the extent of oxidation and any significant increase in temperature to avoid appreciable loss of surface area by sintering. Some loss of surface area of the catalyst could also be expected from the heat treatment of the electrode to sinter the PTFE. This factor was examined simultaneously with the development of the induction procedure. The

induction procedure was based on the fact that the rate and extent of the initial oxidation of the surface was thought to be dependent on how and at what stage of the electrode fabrication process the catalyst was first exposed to air.

The experiments carried out are detailed in Table XIX. The effect of exposure to air when covered with methanol or water is believed to produce slow oxidation of the surface, either by reaction with dissolved O_2 or by progressive exposure to air during evaporation of the liquid layer. Elvax (a duPont polyvinyl resin) was substituted for PTFE as a plastic binder in the tests to investigate the effect of sintering. Elvax electrodes were prepared by dissolving the appropriate quantity of the resin in trichloroethylene at 70-80°C; after cooling to 35°C, the catalyst was added and the mix distributed on a nickel screen. The electrodes required no sintering and were tested after evaporation of the residual solvent. The results obtained with Elvax bonded Pt electrodes were equivalent to some of the better results obtained with PTFE bonded Pt electrodes, indicating that this was an effective method of catalyst testing. The life of the Pt electrode was, however, limited to about two hours, probably due to oxidation of the Elvax under the test conditions (35% KOH at 75°C). The life of Elvax-bonded electrodes prepared from the interstitial compounds was somewhat longer (3-4 hours). Other plastic binders are being examined in order to obtain longer lived electrodes.

The main conclusion drawn from these experiments was that careful induction of the catalyst produces a more active electrode and also that resistance measurements as described earlier on the dry powder are not sensitive enough to relate to activity.

The electrodes made with PTFE, in which the catalyst was exposed to air in the first case (#3, Table XIX) after sintering and in the second case (#4, Table XIX) before sintering, showed no signficant difference. Both were comparable to electrode #1 (i) made with Elvax. However, this

TABLE XIX

Inducting Methods For Catalysts 11-C

	Activity ma/cm^2 at 600 mv
ELVAX ELECTRODES	
1. Electrode made in N_2 then	
(i) Exposed to air slowly	10
(ii) Exposed to air in water	4
(iii) Exposed to air in methanol	4
2. Catalyst inducted by	
(i) Exposure to air slowly ⎫ Electrodes	10
(ii) Exposure to air in water ⎬ made in	3
(iii) Exposure to air in methanol ⎭ air	32
PTFE ELECTRODES	
3. Electrode made and sintered in N_2	10
4. Electrode made in air sintered in N_2 using catalyst 2 (iii)	12

cannot be regarded as a conclusive indication that the sintering process is not detrimental, since the test was not conducted with the catalyst in its most active form.

The induction method was further refined by the use of the following techniques:

(1) Slow oxidation in the gas phase

(2) Extension of the liquid phase induction in methanol to a sequence of organic solvents (petroleum, ether, diethyl ether, acetone and methanol), a sequence in which the reactivity and solubility of oxygen increases.

The slow gas phase oxidation was carried out by the Bureau of Mines with a second sample of material 11C. Three samples of 11C were supplied: an untreated sample, one that had been oxidized in 0.1% O_2 in N_2 for 100 hours at room temperature, and another in 1% O_2 in N_2 for 100 hours at room temperature. All were tested as Elvax bonded electrodes and compared with further samples that had been subjected to the liquid phase induction described above. The details of the tests and the results are presented in Table XX. The uniformity of the results (all except one produced close to 20 ma/cm^2 at 600 mv) indicates that all attempts, both at Tyco and at the Bureau of Mines, to induct this material were of no consequence. This is in direct contrast to the results reported previously. Further, the activity of the uninducted sample A is higher than previously observed, suggesting that the surface was in some way conditioned prior to the induction processes. The improved efficiency of the extended liquid phase induction process was demonstrated by the induction of the original sample of 11C to produce an activity of 40 ma/cm^2 at 500 mv; this compares to 33 ma/cm^2 observed with simple methanol induction.

The induction method for the protection of the activity of Raney nickel described in German Patent 1,185,589 (Doehren and Jung to Varta Petrix-Union G.m.b.H.), in which the catalyst was immersed in a polyhydric alcohol such as ethylene glycol, was not successful for induction of catalyst 11C.

TABLE XX

11C — Oxygen Induction Series (B. O. M.).

Sample	A	B	C	A	B	C
B.O.M. Pretreatment	None	Inducted in N_2 with 0.1% O_2 100 hours	Inducted in N_2 with 1.0% O_2 100 hours	None	Inducted in N_2 with 0.1% O_2 100 hours	Inducted in N_2 with 1.0% O_2 100 hours
Tyco Pretreatment	None	None	None	Catalyst Induced in Pet. Ether etc.	Catalyst Induced in Pet. Ether etc.	Catalyst Induced in Pet. Ether etc.
Binder	10% Elvax	10% Elvax	10% Elvax	10% Elvax	10% Elvax	10% Elvax
Electrode Activity ma/cm^2 at 600 mv	19.3	18.2	18.0	18.4	14.4	19.8

III. TEST RESULTS

A. Au-Pd Alloys

It can be seen from Tables XXI, XXII, and XXIII that there is a wide variation in the activity of the blacks depending on the preparation, the percent of Teflon, the loading, etc. , as described in the previous section on testing methods. The preparations made by hydrazine reduction (Table XXII) show the least activity — at 950 mv, < 1 ma/mg and < 35 ma/cm^2. The blacks prepared by hydroxylamine reduction are generally better — at 950 mv, > 1, < 2 ma/mg and < 70 ma/cm^2 (Table XXIII). The blacks prepared by formaldehyde reduction are generally the best, in spite of the erratic results of some electrodes — averaging, at 950 mv, higher than 2 ma/mg and less than 5 ma/mg (70-100 ma/cm^2), Table XXI.

The first results with the formaldehyde preparation indicated that, in contrast to the measurements of intrinsic activity, the 70% Pd alloy (F4) was in general more active than the 30% Pd alloy (F5 and F6). The 70% alloy showed a maximum activity of 5. 23 ma/mg at 950 mv (corresponding to 68 ma/cm^2), with typical results of the order of 3 ma/mg. The 30% Pd alloy gave typical results that were below 1 ma/mg at 950 mv <u>vs</u>. RHE; however, two electrodes — F6 vi(a) and vi(b) — prepared by the rolling technique (as opposed to the spreading technique used for the other electrodes) produced values of 3. 9 and 4. 1 ma/mg (67 and 87 ma/cm^2 respectively). This difference illustrates the difficulty associated with the testing of practical catalysts. Optimum performance from a particular catalyst demands several experiments to define the best method of electrode fabrication, the PTFE content, and possibly the sintering condition.

In sample F7 the palladium content was increased to 40%; since it was possible that in samples F5 and F6 the actual palladium content in the precipitated black was below 30%, the 40% Pd preparations permit some margin of error. (The original solutions contain the stoichiometric ratio of gold and palladium salts for a particular alloy. X-ray analysis of the early preparations showed the alloy black to have the desired composition; however, this was not tested for every preparation.) The activity level of 3. 0 ma/mg is comparable to that of the 70% Pd alloy.

TABLE XXI

Floating Electrode Performance Pd-Au Blacks (Formaldehyde Prep.)

Catalyst No.	Catalyst Preparation			Electrodes			Activity	
	Initial Concentrations	Final Volume	T°C	#	% PTFE*	Loading mg/cm^2	ma/cm^2 at 950 mv	ma/mg at 950 mv
F-1 Pd-Au 70-30	Au .03M Pd .07M NaOH 1.25M HCOH 0.33M	479 ml	90	(i)	20	47.0	55	1.18
				(ii)	30	21.0	36	1.73
F-3 Pd/Au 30/70	Au-0.07M Pd-0.03M NaOH-1.61M HCHO-0.42M	372 ml	70	(i)a	20	27.0	12	.45
				(iv)a	20	32.0	20	.64
				(v)a	30	29.0	1	.01
				(vi)a	20	23.0	5	.80
				(vii)a	20	24.0	36	1.58
				(viii)a	20	32.0	24	1.0
F-4 Pd-Au (70/30)	Au-.054M Pd-.126M NaOH-2.05M HCOH-.53M	400 ml	90		30	13.0	68	5.23
F-5 Pd/Au 30/70	Au-0.104M Pd-0.044M NaOH-2.37M HCHO-0.619M	378 ml	100	(i)	30	25.0	8	.32
				(ii)	20	26.0	12	.5

* All electrodes sintered at 275°C for 5 min.

TABLE XXI (Cont.)

| | Catalyst Preparation | | | | Electrodes | | | Activity | |
Catalyst No.	Initial Concentrations	Final Volume	T°C	#	% PTFE*	Loading mg/cm²	ma/cm² at 950 mv	ma/mg at 950 mv
F-6 Pd/Au 40/60	Au-0.06M Pd-0.04M NaOH-2.5M HCOH-.56M	420 ml	98	(i)	30	21.5	8	0.37
				(ii)	30	15.0	9	0.60
				(iii)	30	22.0	19	0.86
				(iv)	20	25.0	20	0.80
				(v)	20	28.0	37	1.3
				(vi)a	20	16.9	67	3.9
				(vi)b	20	20.9	87	4.1
				(vii)	10	23.7	3	0.13
				(viii)	10	22.2	19	0.86
				(ix)	30	18.0	50	2.8
				(x)	20	33.0	55	1.6
F-7 Pd/Au 40/60	Au-.06M Pd-.04M NaOH-1.0M HCOH-.56M	420 ml	90	(i)	30	17.4	52	.3
				(ii)	20	22.0	16	.7
				(iii)	30	20.0	56	2.8
				(iv)	20	27.0	65	2.6
				(v)	40	29.6	4.5	.15
				(vi)	40	27.8	80	2.8
				(vii)	40	26.0	80	3.0

* All electrodes sintered at 275°C for 5 min.

TABLE XXI (Cont.)

Catalyst No.	Catalyst Preparation			Electrodes			Activity	
	Initial Concentrations	Final Volume	T°C	#	% PTFE*	Loading mg/cm²	ma/cm² at 950 mv	ma/mg at 950 mv
F-8	Au-.05 M	1260	98	(i)	30[2]	23	5	.2
Pd-Au	Pd-.033 M			(ii)	30[1]	42	5	.12
(40-60)	NaOH-2.45 M			(iii)	30[1]	45	60	1.33
	HCOH-.56 M							
F-9	Au-.063 M	1000 ml	95	(i)	30[1]	41	90	2.2
Pd-Au	Pd-.042 M			(ii)	20[1]	51	15	.3
(40-60)	NaOH - 2.4 M			(iii)	15[1]	45	105	2.33
	HCOH - .56 M			(iv)	15[2]	58	66	1.14
				(v)	15[3]	44	78	1.8
				(vi)	20[1]	38	42	1.1
				(vii)	20[2]	34	36	1.1
				(viii)	20[3]	45	28	.6
				(ix)	25[1]	33	8	.24
				(x)	25[2]	32	12	.37
				(xi)	25[3]	35	13	.37
F-10	Au-.065 M	390	96	(i)	15	33	60	1.8
Pd-Au	Pd-0.043 M			(ii)	30	43	13	0.3
(40-60)	NaOH - 5.4 M			(iii)	15	45	145	3.2
	HCHO-1.2 M			(iv)	30	32	100	3.1
F-(8, 9, 10)[4] Pd-Au (40-60)					20[4]	28	128	4.6

(1) Sintered 250°C - 5 min (2) Sintered 275°C - 5 min

(3) Sintered 300°C - 5 min (4) Mixture of samples 8, 9, and 10 (~ 1:1:1).

TABLE XXI (Cont.)

Catalyst No.	Initial Concentrations	Initial Volume	T°C	#	% PTFE*	Loading mg/cm²	ma/cm² at 950 mv	ma/mg at 950 mv
F-11 Pd-Au (40-60)	Au-.169 M Pd-.114 M NaOH-10.5 M HCOH - (excess)			(i)	15	25	100	4
				(ii)	20	27	58	2.1
				(iii)	25	29	84	2.8
F-12 Pd-Au (40-60)	"			(i)	10	48	72	1.5
				(ii)	10	26	37	1.4
				(iii)	15	11	62	5.6
				(iv)	20	30	54	1.8
F-13 Pd-Au (40-60)	"			(i)	20	28	104	3.7
				(ii)	15	40	104	2.6
F-15 Pd-Au (50-50)	Au-.028 M Pd-.028 M HCOH (excess)			(i)	20	19.3	62	3.2
F-16 Pd-Au (60-40)	Au.198 M Pd.263 M NaOH 10.5 M HCOH (excess)			(i)	20	27	65	2.4
F-17 Pd-Au (70-30)	Au.143 M Pd.332 M NaOH 10.5 M HCOH (excess)			(i)	10	33	154	4.7

TABLE XXII

Floating Electrode Performance of Pd-Au Blacks (Hydrazine Prep.)

Catalyst Preparation			Electrodes			Activity	
Initial Concentrations	Vol. N_2H_4 Added	T°C	#	% PTFE*	Loading mg/cm²	ma/cm² at 950 mv	ma/mg at 950 mv
H1-a Pd-Au 40/60 Au-.020 M Pd-.013M 100 ml	0.1 ml	90	(i)	20	32.0	35	1.1
			(ii)	30	33.0	.5	0.01
H1-b Pd-Au 40/60 Au-.028 M Pd-.019M 100 ml	0.07 ml	23	(i)	20	24.0	9	0.4
			(ii)	30	27.0	15	0.55
H1-c Pd-Au 40/60 Au-.028 M Pd-.019 M 230 ml	.08 ml	23	Electrodes burned during sintering				
H1-d Pd-Au 40/60 Au-.028 M Pd-.019 M 230 ml			(i)	20	25	22	0.9
			(ii)	30	28	20	0.7
H1-e Pd-Au 40/60 Au-.028 M Pd-.019 M 230 ml	.32 ml	23	(i)	20	19	15	0.8
			(ii)	30	28	10	0.36

* All electrodes sintered at 275°C for 5 min.

TABLE XXIII

Floating Electrode Performance of Pd-Au Blacks (Hydroxylamine Reduction)

Catalyst No.	Initial Concentration	Final Volume	T°C	#	% PTFE*	Loading mg/cm²	ma/cm² at 950 mv	ma/mg at 950 mv
HY-1	Au-.1 M	125 ml	20	(ii)	20	69	105	1.5
Pd-Au	Pd-.068 M			(iii)	25	61	80	1.3
(40-60)	HONH$_2$· HCl-SAT			(iv)	15	50	106	2.1
				(v)	20	57	80	1.4
HY-2	Au-.1 M	125 ml	75	(i)	20	48	40	.83
Pd-Au	Pd-.068 M			(ii)	25	45	30	.66
(40-60)	HONH$_2$· HCl-SAT			(iii)	15	51	40	.8
				(iv)	20	77	38	.5
HY-3	Au-.1 M	125 ml	20	(i)	15	22	36	1.7
Pd-Au	Pd-.068 M			(ii)	20	36	36	1.3
(40-60)	HONH$_2$· HCl-SAT			(iii)	25	21	18	.86
				(iv)	30	15	40	2.66
HY-4	Au-.1 M	125 ml	85	(i)	15	27	30	1.1
Pd-Au	Pd-.068 M			(ii)	20	36	18	.5
(40-60)	HONH$_2$· HCl-SAT			(iii)	25	55	12	.22

* Sintered 250°C 5 min.

In preparation F8, a portion of the reactants was brought slowly to a pH of 8.5 in an attempt to induce nuclei formation prior to the growth stage in NaOH. This was omitted in preparation F9. There is a marked difference in activity of the two catalysts, indicating that these initial factors do influence activity. The preparation without the deliberate nucleation step was the more active.

Subsequent preparations were made by simply adding dropwise the metal salts mixed with formaldehyde into the hot stirred sodium hydroxide. Preparations F15, F16 and F17 represent variations in alloy composition. F17 (Pd-Au 70/30), like F4, shows a very high specific activity, 4.7 ma/mg. F15 and F16 are better than the average of previous preparations.

B. Pt-Au, Pt, Pt-Os, Pt-Ag (Table XXIV)

The Pt-Au alloy (70-30) exhibited very good activity, 4 ma/mg at 950 mv. No other preparations, perhaps unfortunately, were attempted with this alloy system.

Pt-73-70, prepared as a testing reference for the formaldehyde preparation method, had a specific activity of 4.6 ma/mg. Many of the Pd-Au preparation discussed above, such as F-4, F-6, F-12, F-17 and the Pt-Au, compare quite favorably with this result. In addition, all of the above mentioned compare quite well with the results obtained with Englehard Pt (3.8-5.5 ma/mg).

The Pt-Os electrodes did not perform as well as expected, < 2 ma/mg; however, as mentioned under the preparation section, the percentage of osmium may have been considerably lower than indicated.

The Pt-Ag 30/70 electrodes showed widely different activity, .3 ma/mg-4.5 ma/mg. It is apparent that structure had a very significant effect on the performance of this catalyst composition.

C. Ti_3Au

In the initial experiments, #1 and #2 of Table XXV, the powder prepared by leaching in the earlier work was subjected to the acid wash. As indicated, there was no improvement in activity.

TABLE XXIV

Floating Electrode Performance of Pt-Os, Pt-Ag and Pt-Au Preparations

Catalyst No.	Catalyst Preparation Initial Concentrations	T°C	Electrodes #	% PTFE*	Loading mg/cm²	Activity ma/cm² at 950 mv	ma/mg at 950 mv
F-2 Pt-Os (80-20)	Pt-.16 Os-.04	75	1b	20	40	60	1.5
	NaOH-3.18 M HCOH-1.39 M		3a	20	12	22	1.8
F-18 Pt-Os (80-20) NaOH-10.5	Os - .045 Pt - .181 HCOH - Excess	90	L-1	30	22	45	2
Pt-Ag (30-70)	Englehard Pt Mech. Mixt. Fisher Ag₂O		L-1	20	22	100	4.5
Pt-Ag (30-70)	"		L-2	20	27	8	.3
F-20 Pt-Au (70-30)	Au-.049 Pt-.116 NaOH-10.5 HCOH (excess)	90	L-1	20	22	87	4
73-79	Pt (Tyco)		L-1	30	27	124	4.6
Englehard	Pt		(i)	30	25	95	3.8
			(ii)	30	21	116	5.5
			(iii)	30	23	110	4.8
			(iv)	30	46	210	4.6

TABLE XXV

Floating Electrode Performance of Ti$_3$Au (Leached Powders)

| | Pretreatment | | | | Electrode | | Activity | |
| | 35% KOH | | 24% H$_2$SO$_4$ | | | | | |
	°C	time	°C	time	% PTFE	Loading	mg/cm^2 at 950 mv	ma/cm^2 at 900 mv
#1	60	50 hr	60	30 min	20	47	3	4.5
#2	--	--	60	100 hr	23	38	inactive	.92
#3	60	50 hr	--	--	30	17	inactive	.31
#4	60	50 hr	60	1 hr	27	40	32 (see Fig.	145
#5	50	50 hr	60	1 hr	27	21	6	22
#6	60	50 hr	60	15 min	27	24	3.5	10
#7	60	50 hr	60	2 hr	27	22	4.0	12
#8	60	50 hr	(5% HF at 25°C)		27	41	1.2	2.04
#9	60	45 hr	--	--		Not Tested		
#10	60	45 hr	50	30 min	20	37	inactive	.07
#11	60	45 hr	50	1 hr (i)	20	22	0.15	27
				(ii)	30	22	0.04	.09
#12	60	45 hr	50	2 hr (i)	20	29	0.79	1.3
				(ii)	30	27	0.08	1.3

*a (brace spanning rows #1–#8)

*b (brace spanning rows #10–#12)

* Varying H$_2$SO$_4$ washings of the same Ti$_3$Au sample leached in KOH a) 50 hr at 60°C, b) 45 hr at 60°C.

TABLE XXV (Cont.)

	Pretreatment				Ti$_3$Au Electrode		Activity	
	35% KOH		24% H$_2$SO$_4$					
	°C	time	°C	time	% PTFE	Loading	mg/cm^2 at 950 mv	ma/cm^2 at 900 mv
#13	60	50 hrs	50	1 hr	20	38	.755	2.04
#18[1]	60	19 hrs	25	10 min	20	35	----	----
#19[1]	60	19 hrs	25	1 hr	20	43	17	40
#20[1]	60	50 hrs	25	10 min	20	45	----	----
#21[1]	60	50 hrs	25	1 hr	20	33	.24	.56
#22[1]	60	3 hrs	25	1 hr	20	49	----	----
#23[2]	60	16 hrs	25	30 min	20	46	17	44
#24[3]	60	16 hrs	25	30 min	20	48	.3	1.25

(1) Ti$_3$Au ingot #4
(2) Ti$_3$Au ingot #7
(3) Ti$_3$Au ingot #5.

However, when this procedure was applied to a freshly prepared sample (#4), the activity was 32 ma/cm^2 at 950 mv vs. RHE. The complete current voltage curve is shown in Fig. 19. Three further attempts to prepare an active catalyst by acid washing were made (#5, #6, and #7); in these, the activity was lower but still significant. It was considered that the time interval between the KOH leaching and acid wash might be important. Further experiments were carried out with another batch of KOH leached powder (#9). The results of these tests — #10, #11, and #12 — are given in Table XXV; we did not succeed in reproducing the results of the earlier preparation. Sample #8, which was etched in HF, showed a low level of activity.

The remaining preparations of titanium gold consisted of variations in KOH-leaching time and acid washing conditions. The use of separate ingots as starting materials was also investigated. Two preparations #19 and #23, showed some activity. Weight loss calculations indicated that the leached product was very nearly pure gold; its structure, however, did not resemble the pure gold powder obtained by any precipitation methods tried, and it was more active than such precipitated preparations. This may have been due to the presence of residual titanium which prevented sintering and reduced malleability, yielding an electrode with a greater available surface.

D. TiAu and TiN

None of the samples of TiAu or TiN prepared by vacuum deposition showed significant activity for oxygen reduction. Free titanium may have been available in all samples, and this has been shown to be detrimental (Table XXVI).

E. Ni$_3$N

The activity of the Ni$_3$N + Ni catalyst as a PTFE bonded electrode was quite low (16 ma/cm^2 at 600 mv vs. RHE).
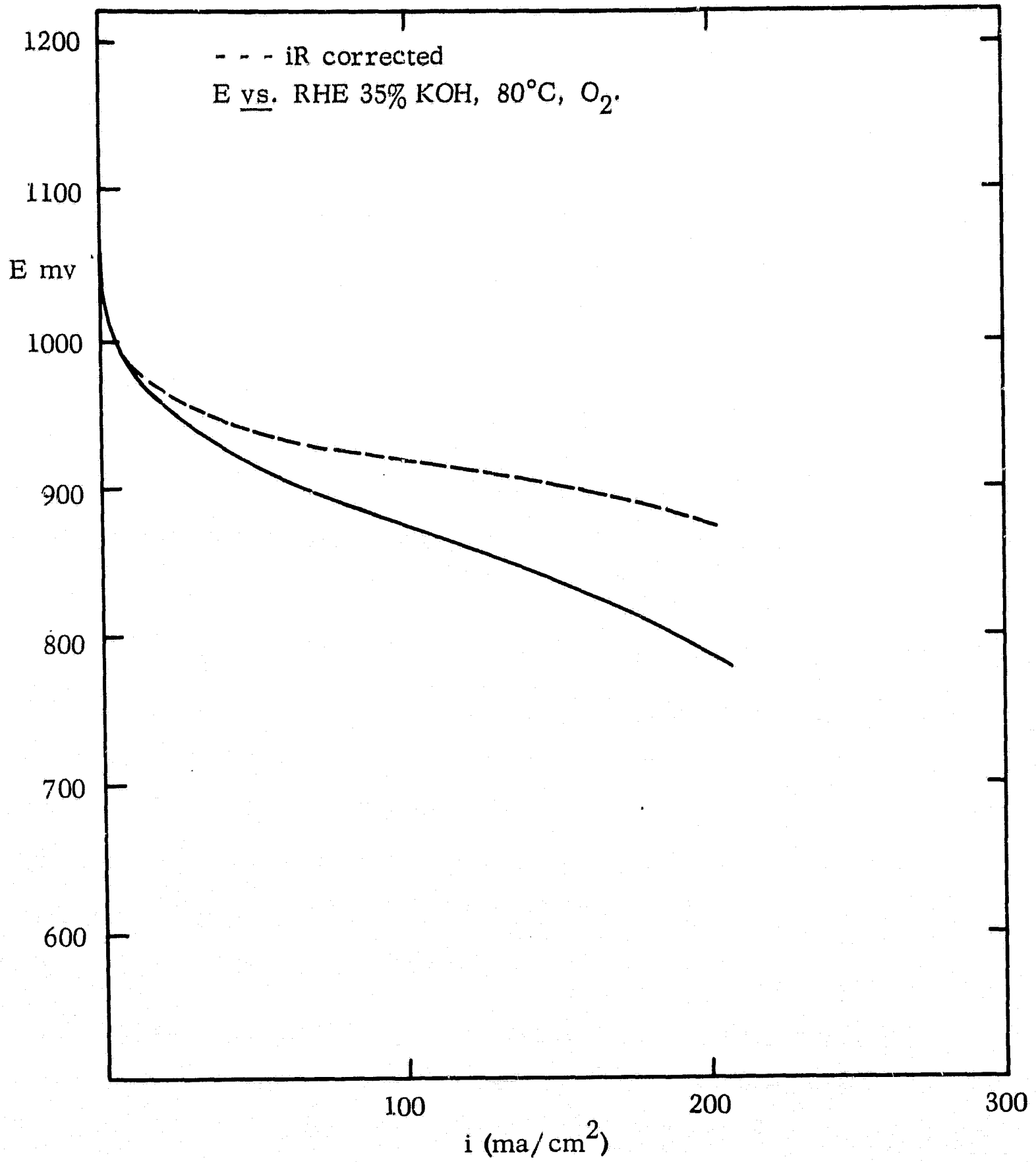
Fig. 19 Ti$_3$Au (leached).

TABLE XXVI

Floating Electrode Performance of Vacuum Evaporated Materials

Electrode		% PTFE	Loading mg/cm²	Activity		
				ma/cm² at 950 mv	ma/mg at 950 mv	ma/cm² at 600
TiN (i)	Evaporated Titanium Nitride	42	7.2			4.2/4.7 (1)
(ii)	Evaporated Titanium Nitride	52	7.7			3.3/3.5
Ti$_3$Au (i)	Evaporated Titanium Gold	27	5.7			1.6/2.9
(ii)	Evaporated Titanium Gold	40	5.3			2/2
Pd/Au	Evaporated 40/60 Pd/Au	27	44	40	0.9	

(1)   Oxidized to white powder during test.

F. Nickel Carbide

The best result obtained with Ni_3C catalysts was an activity of 100 ma/cm^2 at 750 mv vs. RHE, with a limiting current > 300 ma/cm^2. Figures 20, 21, and 22 show the current voltage curves of the most active catalysts. Other results are presented in summary form in Table XXVII. For the nickel cobalt catalysts $(Ni_3C + Co_2C)$, activities of 45 and 105 ma/cm^2 were measured at 750 mv vs. RHE. The latter electrode showed a limiting current greater than 350 ma/cm^2. Ten samples of Ni_3C and two samples of Ni/Co carbide showed very low activity $(i_L < 50$ ma/cm$^2)$.

The observed activities of these catalysts were very encouraging. However, the irreproducibility of the performance of electrodes and catalysts prepared in an apparently identical manner is difficult to explain. Where variations do exist in terms of the preparation of the catalysts' method of induction or electrode fabrication, no logical pattern was observed. It is possible that in the preparation of the catalyst the position of the sample in the furnace or the gas flow rate was critical. These factors were not rigidly controlled.

The discrepancy between the best results obtained with these catalysts and nickel and nickel cobalt carbides prepared by the Bureau of Mines is of greater significance and can probably be related to physical differences between the catalysts. The main difference was probably that of pore structure, which is of considerable importance in the efficient operation of the PTFE bonded electrode.

G. Bureau of Mines Materials

A complete listing of the activity of the interstitial compounds is presented in Table XXVIII. The electrodes are described by identification numbers — the first number and letter, e. g. 2C, corresponds to the Bureau of Mines' identification number of the catalyst. The italic number in parenthesis describes the electrode preparation, i.e. 2C (ii), and the final letter identifies the test (e. g. 2C (ii)a and 2C (ii)b are tests carred out on

Floating Electrode, 35% KOH, 75°C, O$_2$
8.32 mg/cm^2, 20% TFE
E vs. RHE   -----iR corrected curve

Fig. 20   Ni$_3$C, Sample #39

i(ma/cm²)

E(mv)

- 117 -

572F

30.5 mg/cm^2, 10% TFE
Floating Electrode, 75°C, 35% KOH, O$_2$
E vs. RHE ---- iR corrected curve
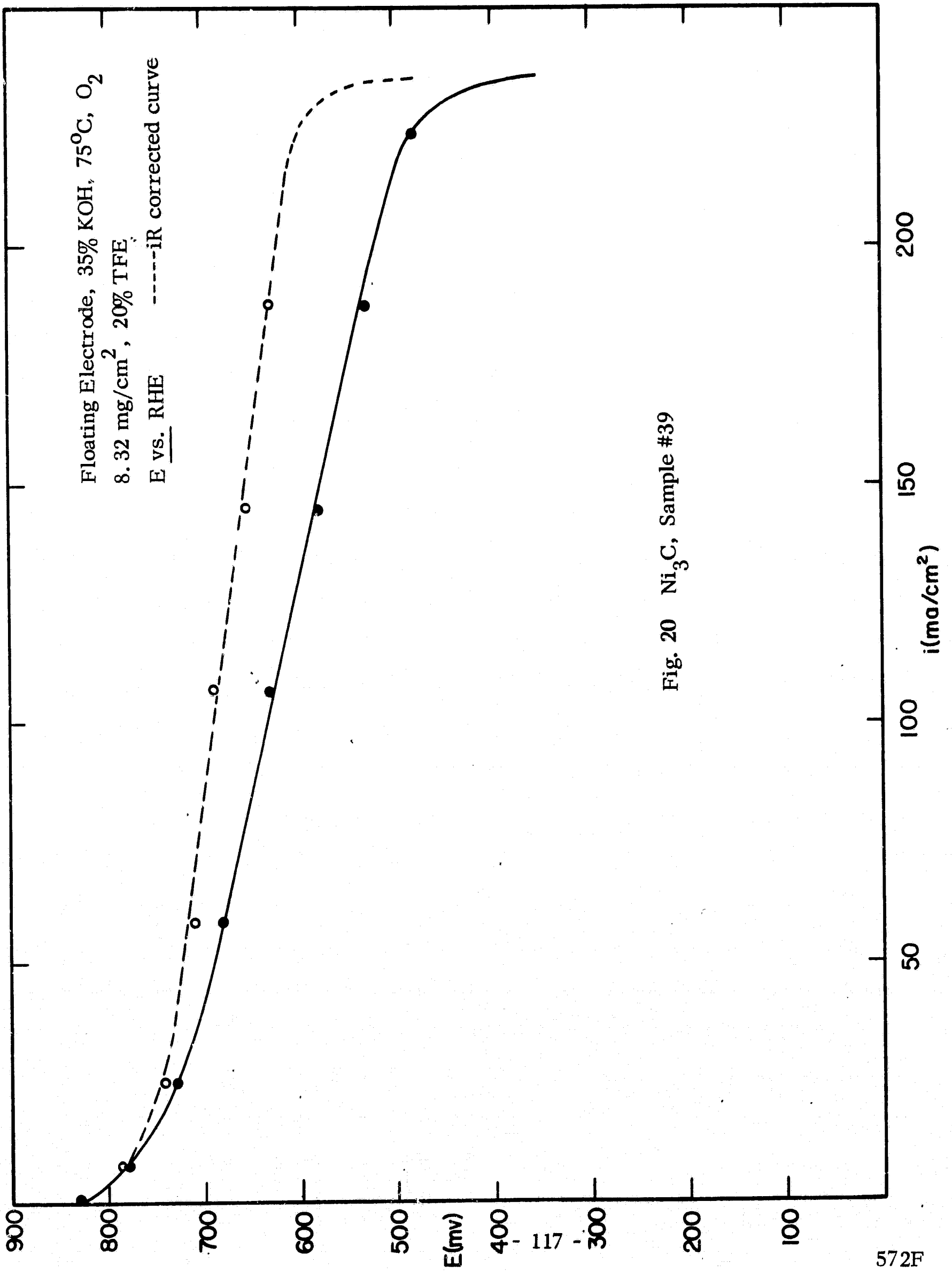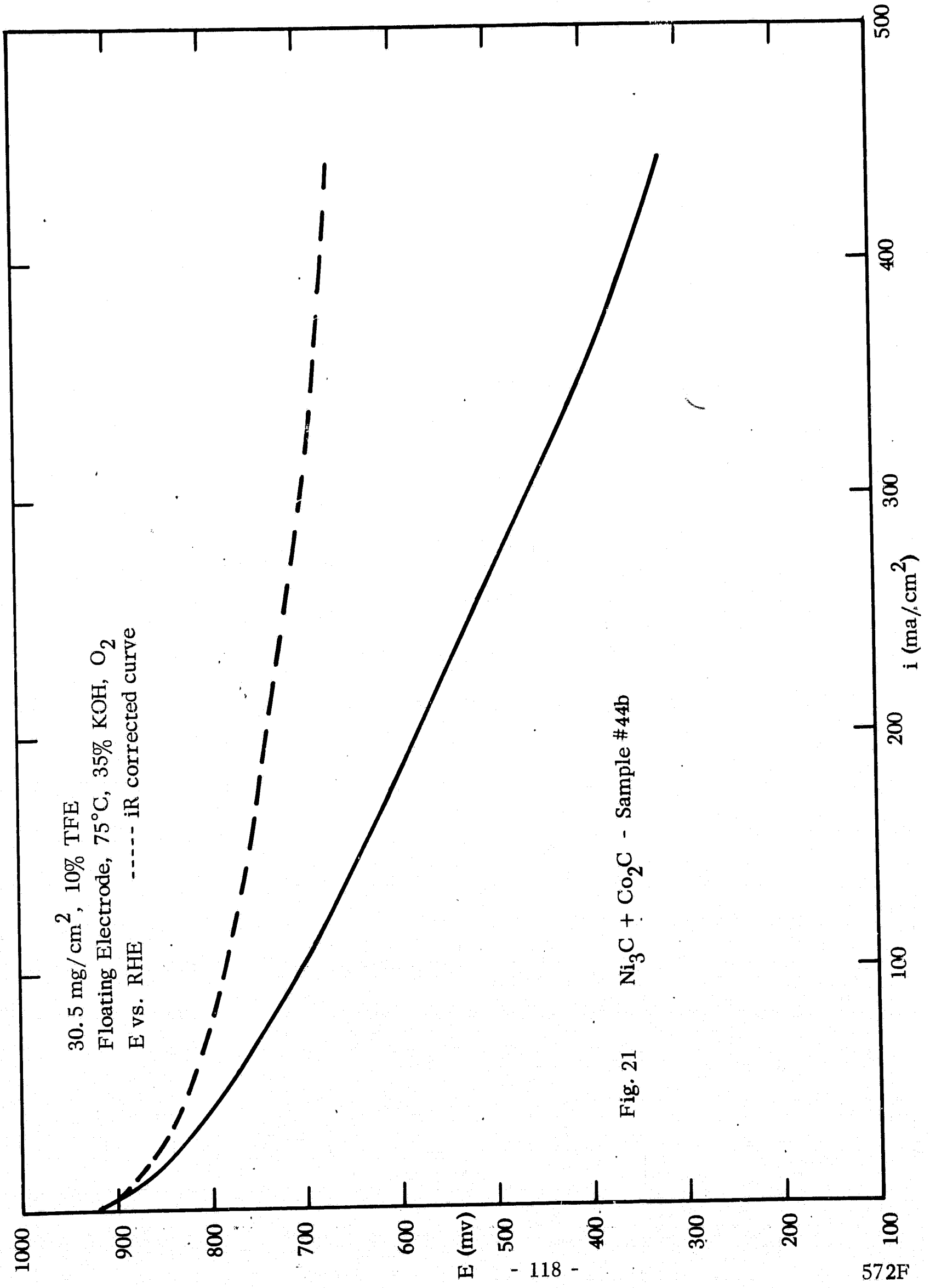
Fig. 21   Ni$_3$C + Co$_2$C - Sample #44b

i (ma/.cm^2)

E (mv)

572F

Ni$_3$C #63 (ii) 9.76 mg/cm^2
Floating Electrode, 35% KOH, 75°C, O$_2$
E vs. RHE ----- iR corrected curve

Fig. 22 Ni$_3$C #63 (11)

i (ma/cm^2)

E (mv)

1000
900
800
700
600
500
400

100
200
300
400

- 119 -

572F
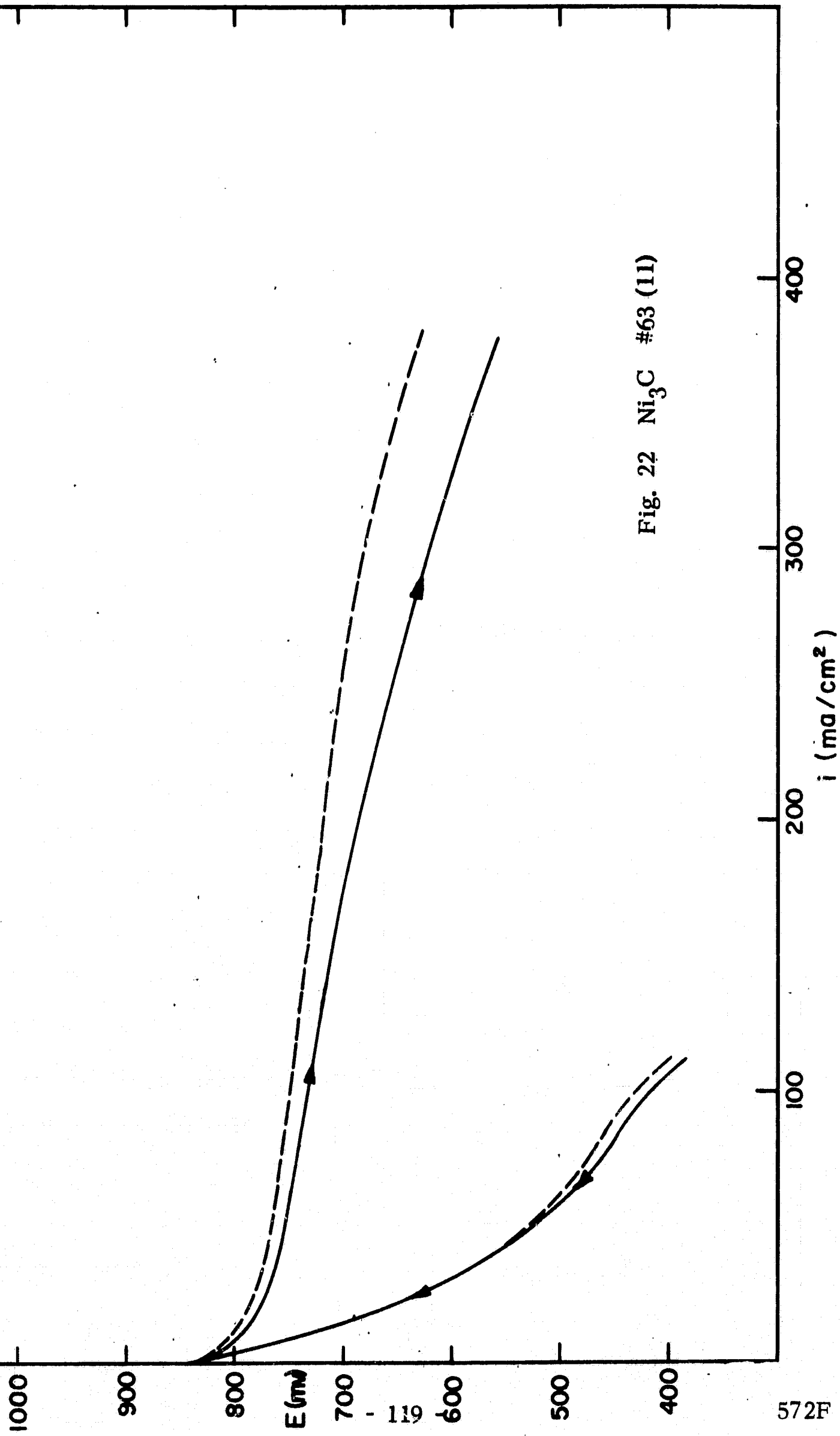
TABLE XXVII

Floating Electrode Performance of Ni_3C (Prepared by Acetate Decomposition in N_2)

Sample No.	Catalyst Preparation[1]				Loading mg/cm^2	Electrode[2] Activity ma/cm^2[3]	
	Time hrs.	Temperature °C	Induction	% PTFE		at 750 mv	at 600 mv
20	3	200	No	20	27	20	210
	4	275					
	4	300					
39	3	300	No	20	24	90	290
44[4]	6	300	No	20	30	105	>350
48[4]	6	300	No	20	26	50	150
53	3	300	No	20	30	44	310
55	3	350	No	20	43	20	87
56	3	350	No	20	9	18	58
58	3	300	Yes	20	28	30	125
59	3	300	Yes	20	23	16	82
62	3	300	No	20	27	40	300
63	3	300	Yes	20	10	100	>350

TABLE XXVII (Cont.)

Sample No.		Time hrs.	Temperature °C	Induction	% PTFE	Loading mg/cm²	Activity ma/cm² [3] at 750 mv	at 600 mv
67	L-1	3	@ 300		10	31	--	--
67	L-2	4	@ 325		10	71	--	--
68	L-1	5-3/4	300		10	69	--	--
69	L-1	22	300		10	38	59	178
69	L-1				15	69	56	260
70	L-1	97	280		10	69	9	21
71	L-1	5	300		30	38	7	22

(1) All preparations based on Liecester & Redman

(2) All electrodes contained 20% PTFE and were sintered 5 mins at 275°C

(3) Best figures when more than one electrode tested

(4) 3 Ni/Co carbides.

separate samples cut from electrode 2C (ii). The tables also record the induction of the catalyst, and the nature and amount of the plastic binder used. The activity is presented as the current density at selected potentials. The less active materials (mainly Fe interstitials) are compared at 600 mv; most others are compared at 750 mv, with additional figures at 900 mv for those catalysts containing Ag, Au, or Pd. When two figures are quoted, these are the current densities for increasing and decreasing potentials respectively. These can differ due to differences induced in the oxide films at the lower potentials (minimum potential for these tests was 400 mv). In the case of Ni interstitials, it was noted that the pattern of activity was an initial increase, followed by a plateau of steady current and steady decay. To insure that peak activity was recorded in these cases the repetitive potential sweep method described earlier was used. The results obtained by this method are identified in Table XXVIII.

The results obtained for the <u>interstitial compounds of iron</u> were disappointingly low. The highest activities were 53 and 58 ma/cm^2 at 600 mv <u>vs</u>. RHE for samples 5N and 6N.

After the initial low results with the carbides, the testing method was examined closely to eliminate all possible steps in the process that could be detrimental. These were the oxidation of the catalyst surface and the possible sintering of the catalyst at the "curing" temperature of PTFE bonded electrodes. The experimental approach to these problems was described in the previous section, together with an assessment of their effectiveness. For the testing of the nitrides, carbonitrides, and nitrocarbides, all the electrodes were prepared by the preferred method using an inducted catalyst with Elvax as a binder. In addition, several uninducted samples were tested and occasional electrodes were prepared with PTFE. The results were uniformly bad with only one electrode showing a current density > 10 ma/cm^2. This electrode 2 NC (ii)a showed an activity of 68 ma/cm^2 on first test, but this figure was not reproduced in a subsequent test. Though this activity represents the best observed for this class of materials, it does not approach the activity required of a practical catalyst. The general picture of activity for these materials, though not clearly defined, is nitrides > carbonitrides > carbides > nitrocarbides. Except where noted

in Table XXVIII, these materials did not show significant currents under N_2. Prolonged exposure to air (after induction) for several days was found to have an adverse effect on performance.

Poor physical structure of the catalyst, particularly in the form of pore size distribution, could contribute to the low activity shown by these electrodes, but it is unlikely that a substantial increase in current density could be expected even if this were improved. The results are considered to be a reliable guide to the activity of the iron interstitials, and it must be concluded that these materials do not meet the requirements for a practical catalyst of the reduction of oxygen in a basic electrodes.

Three catalysts prepared by the coprecipitation of $Fe(OH)_3$ and Ag_2O showed relatively high activity, particularly for the two high Ag content materials (92 and 59 ma/cm^2). This is most probably related to the silver content. The nitride and carbonitride forms of these catalysts showed lower activity $\sim$ 20 ma/cm^2 and 11 ma/cm^2 respectively, probably due to the adverse effect of the heat treatment associated with the nitriding and carbiding processes.

The carbides of nickel, and nickel cobalt alloys were in general, more active than were the iron compounds. The best activity of a series of tests with Ni_3C (19C(v)) was 94 ma/cm^2 at 600 mv. This does not compare with the activity obtained with catalysts prepared by decomposition of nickel acetate which give currents in excess of 300 ma/cm^2 at 600 mv (as discussed below). Cobalt carbide (20C) showed lower activity coupled with substantial corrosion (electrolyte became blue), preanodization at 1600 mv for 10 mins reduced the extent of corrosion but did not result in improved activity.

The carbided nickel cobalt Raney alloys (25C, 26C, 27C) showed activities in the range 20 to 70 ma/cm^2 at 600 mv, the order of activity being 3 Ni/Co > Ni/Co > 3 Ni/Co. All these materials were preanodized at 1600 mv. Conditions that could give rise to the formation of the nickel cobalt spinel at the surface improved conductivity and enhanced catalytic activity, as has been reported for the spinel. The nitrocarbides of nickel and cobalt 11 NC, 13 NC, 15 NC, 16 NC showed activity of the same order of magnitude as that of the carbides, though in the case of the nickel cobalt alloys the

TABLE XXVIII

Iron Carbides

	Catalyst	Inducted	mg/cm²	% PTFE	ma/cm² at 900 mv	ma/cm² at 750 mv	ma/cm² at 600 mv	Comments
2C (i)	ϵ-Fe$_2$C/Fe$_3$O$_4$	No	~10	10%*	---	---	---	Anodic
2C (ii)a		Yes	~10	10%	---	---	1.0	
2C (ii)b		Yes	~10	10%	---	---	11.0	
4C	χ-Fe$_2$C/Fe$_3$O$_4$	No	~10	10%*	---	---	1.0	
6C (i)	χ-Fe$_2$C + θFe$_3$C	Yes	~10	10%*	---			Anodic
6C (ii)		No	~10	19%		---	4.0	
10C	θ-Fe$_3$C + Fe	Yes	~10	10%*	---	---	3.4	
11C	See TABLE XIX							

* Elvax bonding

TABLE XXVIII (Cont.)

Iron Nitrides

Electrode	Catalyst	Inducted	mg/cm²	% PTFE	ma/cm² at 900 mv	ma/cm² at 750 mv	ma/cm² at 600 mv	Comments
2N (i)	γ-Fe_4N+ϵ-Fe_3N	Yes	~30	10*			0.6	
2N (ii)	"	No	~30	19			3	
5N (i)	ϵ-Fe_3N+γ-Fe_4N	Yes		10*			0.6	
5N (ii)	"	No		10			58	
6N (i)a	ϵ-Fe_3N+ζ-Fe_2N	Yes		10*			1.3	
6N (i)b	"	Yes		10*			2.2	
6N (ii)a	"	No		19			53.0	
6N (ii)b	"	No		19			2.6	
8N	γ'-Fe_4N	Yes		10*			6.4	
9N (i)	ζ-Fe_2N	Yes		10*			3.0	
9N (ii)		No		10			27.0	
11N	ϵ Fe_3N + Ag	Yes		10*			14.8	Fe/Ag = 3/1
13N (i)a	ϵ Fe_3N	Yes		10*			12.4	
13N (ii)a	"	Yes		10			Anodic	
15N	ϵ-Fe_3N+Ag	Yes		10*			19.4	Fe/Ag = 1/1
16N	ϵ-Fe_3N+Ag	Yes		10*			14.4	Fe/Ag = 1/3
18N	ζ-Fe_2N+ϵFe_3N	Yes		10*			Anodic	

* Elvax bonded

TABLE XXVIII (Cont.)

Iron Nitrocarbides

Electrode	Catalyst	Inducted	mg/cm² PTFE	%	ma/cm² at 900 mv	ma/cm² at 750 mv	ma/cm² at 600 mv	Comments
1 NC (i)	$\epsilon Fe_2X + Fe_3O_4$	Yes		10*			3.2	
1NC (ii)		Yes		10			3.2	
2 NC (i)a	$\chi Fe_2X + \epsilon Fe_2X+C$	Yes		10*			3.5	
2NC (i)b		Yes		10*			0.4	
2NC (ii)a		Yes		10			68.0	
2NC (ii)b		Yes		10			5.2	
3NC	ϵFe_2X	Yes		10*			1.6	
4NC	ϵFe_2X	Yes		10*			Anodic	
5NC	θFe_3X	Yes		10*			5.4	
6NC	χFe_2X	Yes		10*			1.2	
7NC (i)	θFe_3X	Yes		10*			Anodic	
7 NC (ii)		Yes		10			Anodic	

* Elvax bonded
X = C, N

TABLE XXVIII (Cont.)

Iron Carbonitrides

Electrode	Catalyst	Inducted	mg/cm²	% PTFE	ma/cm² at 900 mv	ma/cm² at 750 mv	ma/cm² at 600 mv	Comments
1CN	ϵ Fe$_2$X	No		10			1.0	
2CN (i)	ϵ Fe$_2$X	Yes		10			2.9	
2CN (ii)	"	Yes		10*			Anodic	
3CN	ϵ Fe$_2$X.	Yes		10*			Anodic	
6CN	ϵ-Fe$_2$X + Ag	Yes		10*			7.0	Fe/Ag = 3/1
7CN	ϵ-Fe$_2$X + Ag	Yes		10*			11.6	Fe/Ag = 1
8CN	ϵ-Fe$_2$X + Ag	Yes		10*			5.4	Fe/Ag = 3/1
9CN	γ'-Fe$_4$X	Yes		10*			Anodic	
10CM	γ'-Fe$_4$X	Yes		10*			1.9	

* Elvax bonded
X = C, N

TABLE XXVIII (Cont.)

Coprecipitated Iron and Silver Catalysts

Electrode	Catalyst	Inducted	mg/cm^2	% PTFE	ma/cm^2 at 900 mv	ma/cm^2 at 750 mv	ma/cm^2 at 600mv	Comments
1 CP	Fe(OH)$_3$ + Ag$_2$O	No	20	5*			1.0	Fe/Ag = 3/1
2 CP	"	No	20	10*			92	Fe/Ag = 1/1
3 CP	"	No	20	8*			59	Fe/Ag = 1/3

* Elvax bonded

TABLE XXVIII (Cont.)

Raney Alloys of Ni and Co

(with A Silver Gold Palladium and Platinum)

Electrode	Catalyst	Inducted	mg/cm²	% PTFE	ma/cm² at 900 mv	ma/cm² at 750 mv	ma/cm² at 600 mv	Comments
RAL 1 (i)a	Ni/Co	No	37.0	20		17/2	5/5.6	
RAL 1 (ii)a	"	Yes	51.0	20		3.4/2	6.3/3.5	
RAL 1 (ii)b	"	Yes	37.0	20		3.6/2.8	7.0/6.0	
RAL 2 (i)a	Ni/3Co	No	45.2	20		2.6/3.2	13/12	
RAL 3 (ii)a	"	Yes	45.0	20		1/0.5	2.3/3.6	
RAL 2 (ii)b	"	Yes	34.0	20		3.6/3.6	10.8/13.5	
RAL 3 (i)a	3 Ni/Co	No	36.0	20		32/36	60/64	
RAL 3 (ii)a	"	Yes	32.0	20		4.8/6.0	12.9/16.2	
RAL 3 (ii)b	"	Yes	35.0	20		7/11.5	19/26.5	
RAL 4 (i)a	Ni/3 Ag	Yes	31	20	10/11	39/44	39/44	

TABLE XXVIII (Cont.)

Electrode	Catalyst	Inducted	mg/cm²	% PTFE	ma/cm² at 900 mv	ma/cm² at 750 mv	ma/cm² at 600 mv	Comments
RAL 4 (i)b	Ni/3Ag	Yes	33.0	20	27/32			
RAL 4 (ii)a	"	No	46.3	20		26/26	76/84	
RAL 4 (i)c	"	Yes	33.0	20		40/82	140/191	
RAL 5	Ni/Ag	No	35.9	20		4/4	12/30	
RAL 5	"	Yes	38.0	20	18/75			
RAL 5	"	Yes	31.0	20	11.5/27.5	96/168		
RAL 14 (i)a	Ni Pd	No	21.0	30		0	0.25	
RAL 14 (ii)a	"	Yes	26.0	30		0.2	0.2	
RAL 17 (i)a	Ni Au Pd	No	3	30		80/100	145/162	
RAL 17 (ii)a	"	Yes	18	30	45/65	300/315		
RAL 21 (i)a	Ni Ag Pd	No	21	30	22.5/17	170/250		
RAL 21 (ii)a	"	Yes	20	30	15/48	132/232		

TABLE XXVIII (Cont.)

Carbides of Nickel and Cobalt

Electrode	Catalyst	Inducted	mg/cm²	% PTFE	ma/cm² at 900 mv	rna/cm² at 750 mv	ma/cm² at 600 mv	Comments
19C (i)	Ni_3C	Yes	51	20	---	/4	21/14	
19C (ii)		No	49	20	---	/3.5	46/18	
19C (iii)		No	68	10	---	13/2.5	19/7	
19C (iv)		No	48	20	---	14/10	55/29	
19C (v)		No	60	15	---	37/14	94/44	
19C (vi)		No	79	10		16/8	38/18	
19C (vii)		No	58	10		20/9	69/38	
20C (i)	Co_2C	Yes	35.5	10	---	0.4/0.4	0.8/1.0	electrolyte turned blue
20C (ii)		No	57.4	10	---	10/9	43/35	"
25C (i)a	Ni/Co C	Yes	60.4	20	---	16/2	43/6	
25C (ii)a		No	49.5	20	---	6/2	19/6	

TABLE XXVIII (Cont.)

Electrode	Catalyst	Inducted	mg/cm^2	% PTFE	ma/cm^2 at 900 mv	ma/cm^2 at 750 mv	ma/cm^2 at 600 mv	Comments
26C	Ni/3 CoC	No	45.5	30	---	12/6	28/15	
26C (i)b	Ni/3 CoC	No	41.0	30		6/10	16/23	
26C (ii)a	"	Yes	55.0	30		4/anodic	11/2	
26C (iii)a	"	No	56.0	20		7/anodic	13/1	
26C (iv)a	"	Yes	61.0	20		anodic	18/2	
26C (iv)b	"	Yes	39.0	20		7/0.3	16/1	
27C (i)a	3 Ni/CoC	Yes	46.7	20		24/24	72/72	sweep method
27C (i)b	"	Yes	51.4	20		14/15	44/44	"
27C (ii)a	"	No	63.4	20		13/14	36/40	"
27C (ii)b	"	No	45.1	20		14/13	34/34	"
28C	Ni$_3$C+Ni	Yes	----	Partially Impregnated		1.2/12	5/19	Carbided Ni plaque
28C (ii)	Ni$_3$C+Ni	No		Partially Impregnated		1.8/7.2	5/8.5	

TABLE XXVIII (Cont.)

Electrode	Catalyst	Inducted	mg/cm^2	% PTFE	ma/cm^2 at 900 mv	ma/cm^2 at 750 mv	ma/cm^2 at 600 mv	Comments
28C (iii)	Ni$_3$C + Ni	No		None		0.3/0.6	0.7/1.1	
	Ni			Partially Impregnated		0.9/2.9	3.8/10.8	
36C (i)a	Ni$_3$C	Yes	38.0	20		3/3	8/8.5	
36C (ii)a	"	Yes	22.0	40		10/12	29/30	sweep method
36C (iii)a	"	No	40.0	20		0.25/0.25	0.5/0.5	"
36C (iv)a	"	No	29.0	40		1.5/2	5.5/6.5	"
40C (i)a	Ni/Co/AgC	Yes	24.0	20		2.5/4	7.0/9.5	"
40C (ii)a	"	No	30.0	20		1.5/1.5	2.5/2.5	"
40C (iii)a	"	No	26.0	30		0.7/0.7	1.0/1.0	"
40C (iv)a	"	Yes	32.0	30		0/0.2	0.5/1	"
40C (iv)b	"	Yes	25.0	30		2/2.5	2.5/3.0	"
41C (i)a	Ni/Co/AuC	No	24.0	30		3/2	6/4.5	"
41C (ii)a	"	Yes	31.0	30		19/35	53/72	"
41C (ii)b	"	Yes	36.0	30		20/25	44/51	"

TABLE XXVIII (Cont.)

Electrode	Catalyst	Inducted	mg/cm²	% PTFE	ma/cm² at 900 mv	ma/cm² at 750 mv	ma/cm² at 600 mv	Comments
44C (i)a	Ni/Ag/AuC	No	18.0	30	17.5/18.5	90,95	177/180	sweep method
44C (ii)a	"	Yes	20.0	30	48/48	355/355		limiting current at 750 mv
45C (i)a	Co/Ag/AuC	No	15.0	30		40/60	113/140	sweep method
45C (ii)a	"	Yes	12.0	30		28/39	82/95	"
50C (i)a	3 Ni/Co C	No	10.9	30		4/8	11/17	"
50C (i)b	"	No	5.2	30		12/14	28/31	"
50C (ii)a	"	Yes	9.7	30		14/16	33/37	"
50C (ii)b	"	Yes	11.3	30		3.5/4	7.5/9	"
53C (i)a	Ni/AgC	No	20.6	30		18/26	41.5/50	"
53C (ii)a	"	Yes	24.4	30		23/12	25/21	"
54C (i)a	Ni₃C	No	23.4	20		22.5/49	100/126	"
55C (i)a	Ni/Pd C	No	20.2	30		0.5/0.5	1/1	"
55C (i)b	"	No	16.4	30		23/34	48/64	"
55C (ii)a	Ni/Pd C	Yes	24.8	30		10/14	19/23	slow sweep method
58C (i)a	3 Ni/Co C	No	10	30		52/50	125/120	"
58C (ii)a	"	Yes	13.4	30		3/3	3.5/3.5	"

TABLE XXVIII (Cont.)

Nitrocarbides of Nickel and Cobalt

Electrode	Catalyst	Inducted	mg/cm²	% PTFE	ma/cm² at 900 mv	ma/cm² at 750 mv	ma/cm² at 600 mv	Comments
11 NC (i)a	Ni$_3$NC	Yes	45.4	20		8/1.5	23/5	
11 NC (ii)a	"	No	57.4	20		10/9	43/35	
12 NC (i)a	Co$_2$NC	No	45.5	10		0.1	0.7	
12 NC (ii)a	"	Yes	37.0	10		0.2	0.5	
13 NC (i)a	Ni/3 Co NC	No	45.0	20		anodic/5	49/12	
13 NC (ii)a		Yes	50.0	20		10/anodic	27/1	
15 NC (i)a	3 Ni/Co NC	Yes	56.4	20		14/11	33/28	sweep method
15 NC (i)b		Yes	52.0	20				corrosion test see Fig.
15 NC (ii)a	3 Ni/Co NC	No	49.2	20		18/16	44/42	sweep method
16 NC (i)a	Ni/Co NC	Yes	49.7	20		11/13	37/27	"
16 NC (ii)a	"	No	53.2	20		25/22.5	68/68	"
24 NC (i)a	Ni$_3$NC	No	23.0	30		3/3	7/7.5	"

TABLE XXVIII (Cont.)

Electrode	Catalyst	Inducted	mg/cm²	% PTFE	ma/cm² at 900 mv	ma/cm² at 750 mv	ma/cm² at 600 mv	Comments
24 NC (ii)a	Ni₃NC	Yes	28.0	30		2.5/3	7.5/9	sweep method
27 NC (i)a	Ni/Co/Ag NC	No	23.0	30		3/4	6.5/9.5	"
27 NC (ii)a	"	Yes	28.0	30		1/1.5	2/2.5	"
27 NC (ii)b	"	Yes	17.0	30		1/3	4/8.5	"
29 NC (i)a	Ni/Co/Au NC	No	30	30		0.5/0.5	1/1	"
29 NC (ii)a		Yes	25	30		5/6.5	11.5/13.5	"
29 NC (ii)b	Ni/Co/Au NC	Yes	34.0	30		5.5/7	12.5/15	"
30 NC (i)a	Ni Ag Au NC	No	22.0	30	45/45	325/325		"
30 NC (ii)a	"	Yes	23.0	30	49/49	340/340		"
33 NC (i)a	Co Ag Au NC	No	16.0	30		82/115	230/257	"
33 NC (ii)a	"	Yes	20.0	30		70/90	200/225	"
37 NC (i)a	3 Ni/Co NC	No	10.2	30		9/21	28/49	"
36 NC (ii)a	"	Yes	20.6	30		18/26	41.5/50	"

TABLE XXVIII (Cont.)

Electrode	Catalyst	Inducted	mg/cm²	% PTFE	ma/cm² at 900 mv	ma/cm² at 750 mv	ma/cm² at 600 mv	Comments
37 NC	3 Ni/Co NC	No	16.7	30		3/3	4/4	sweep method
37 NC	"	Yes	9.4	30		1.5/2	3.5/4	"

TABLE XXVIII (Cont.)

Catalysts from Alternative Starting Materials to Raney Alloys

Electrode	Catalyst	Inducted	mg/cm²	% PTFE	ma/cm^2 at 900 mv	ma/cm^2 at 750 mv	ma/cm^2 at 600 mv	Comments
50R (i)a	3 Ni/Co	No	8.2	30		33/37	85/92	sweep method
50R (i)b	"	No	9.9	30		40/46	105/112	"
50R (ii)a	"	Yes	10.1	30		22/22	44/44	"
50R (ii)b	"	Yes	11.5	30		43/90	185/225	"
53R	Ni/Ag	No	22.6	30		95/100	195/207	"
53R	"	Yes	16.3	30		100/105	200/210	"
54R	Ni	No	22.5	30		43/48	100/105	"
54R	Ni	Yes	22.7	30		83/92	150/160	"

TABLE XXVIII (Cont.)

Interstitial Compounds

Electrode	Catalyst	Inducted	mg/cm²	% PTFE	ma/cm² at 750 mv	ma/cm² at 600 mv
60C (i)a	NiAuAgC	No	34.6	30%	0.1	
(ii)a	"	Yes	39.5	30%	0.1	
61C (i)a	3 Ni/CoC	No	46.6	30%	0.4	
(ii)a	"	Yes	37.0	30%	0.2	
63C (i)a	3 Ni/PdC	No	33.0	30%	44/44	100/100
		Yes	39.2	30%	38/38	74/74
39 NC (1)a	Ni (NC)	No	19.0	30%	70/70	130/145
39 NC (2)a	Ni (NC)	Yes	38.6	30%	25/50	130/145
(54C)	Ni_3C	No	23.4	20%	23/49	100/126
41 NC (1)a	Ni(NC)	No	19.8	30%	32/32	63/63
41 NC (2)a	Ni(NC)	Yes	25.6	30%	20/20	45/47
(56C)	Ni_3C	No	33.4	20%	32/35	56/60
42 NC (1)a	Ni/Pd (NC)	No	37.4	30%	60/70	130/187
42 NC (2)a	Ni/Pd (NC)	Yes	32	30%	67/130	162/220
(57C)	Ni/PdC	No	40	30%	100/137	215/230
45 NC (1)a	Ni/Co (NC)	No	39	30%	.5/.5	1/1
45 NC (2)a	Ni/Co (NC)	Yes	46	30%	.5/1	1/1.5

TABLE XXVIII (Cont.)

The Influence of Preparative Conditions on the Activity 3 Ni/CoC

	Catalyst		Electrode			Activity	
	Duration of Carbiding (hrs.)	Temperature	Induction	Loading	% PTFE	ma/cm^2 at 750 mv	ma/cm^2 at 600 mv
68C	5 120	160-260 260	No	18.0	30	34/35	69/72
68C	"	"	Yes	14	30	13/13	30/30
69C	5 120	160-240 240	No	12.3	30	6/8	13/15
69C	"	"	Yes	25	30	8/8	1.5/1.5
70C	4 72	160-260 260	No	16.0	30	7/8	12.5/14.5
70C	"	"	Yes	16.0	30	106/146	>300 ma/cm^2
71C	4 72	160-240 240	No	17.0	30	22/25	44/53
71C	"	"	Yes	19	30	3/3	4/4
72C	4 24	160-260 260	No	20.0	30	4.5/6	9/11
72C	"	"	Yes	14	30	3/1	3/2
73C	4 24	160-240 240	No	13.0	30	30/23	68/61
73C	"	"	Yes	21	30	5/2	3/3

TABLE XXVIII (Cont.)

Electrode			% PTFE	Loading mg/cm^2	Activity[1]		
	Catalyst	Induction			ma/cm^2 at 950 mv	ma/cm^2 at 750 mv	ma/cm^2 at 600 mv
74 R (i)	3 Ni/Au	No	30	44		32/32	55/54
74 R (ii)	3 Ni/Au	Yes	30	41		16/16	32/32
74 R (iii)	3 Ni/Au	No	30	48		20/25	38/40
74 R (iv)	3 Ni/Au	No	10	54		15/15	25/25
74 C (i)	3 Ni/Au C	No	30	38		14/13	24/25
74 C (ii)	3 Ni/Au C	Yes	30	41		17/19	32/35
54 NC (i)	3 Ni/Au NC	No	20	39		9/14	23/23
54 NC (ii)	3 Ni/Au NC	Yes	20	56		5/5	13/23
76 R (i)	Ni/3 Au	No	10	90		1.0	1.0
76 R (ii)	Ni/3 Au	Yes	10	90		1.0	1.0
76 C (i)	Ni/3 Au C	No	10	94		1.0	1.0
76 C (ii)	Ni/3 Au C	No	10	94		1.0	1.0
53 NC (i)	Ni/3 Au NC	No	10	116		4/4	4/4
53 NC (ii)	Ni/3 Au NC	Yes	10	111		1.0	1.0
79 R (i)	Ag/3 Pd	No	10		5/5	375	(limiting current)
85 R (i)	Ag/Pd	No	20	50	3.5/5	7300	(limiting current)
86 R (i)	3 Ag/Pd	No	20	48	9/18	205	(limiting current)

- 141 -

TABLE XXVIII (Cont.)

Electrode		Induction	% PTFE	Loading mg/cm^2	Activity[1]		
	Catalyst				ma/cm^2 at 950 mv	ma/cm^2 at 750 mv	ma/cm^2 at 600 mv
80 R(i)[2]	3 Ni-1 Pt	No	30	41		25/30	55/58
80 R(ii)	3 Ni-1 Pt	Yes	30	45		28/32	53/54
80 C(i)	3 Ni-1 Pt C	No	30	47		16/18	36/40
80 C(ii)	3 Ni-1 Pt C	Yes	30	46		19/26	46/58
58 NC(i)	3 Ni-1 Pt NC	No	30	42		8/13	24/3?
58 NC(ii)	3 Ni-1 Pt NC	Yes	30	62		8/8	18/19
82 R(i)	1 Ni-3 Pt	No	30	55		10/10	17/17
82 R(ii)	1 Ni-3 Pt	Yes	30	66		7/7	13/13
54 NC(iii)	3 Ni-1 Au NC	Yes	30	46		4/5.5	9/12
76 R(iii)	1 Ni-3 Au	Yes	30	34		2/2	3.5/3.5
76 C(iii)	1 Ni-3 Au C	Yes	30	39		2/2	3.5/3.5
53 NC(iii)	1 Ni-3 Au NC	Yes	30	39		1/1	2/2
79 R(iii)	1 Ag-3 Pd	Yes	30	57	3.5/5	275/307	
84 R (i)	3 Ni-Ag	No	20	28		28/29	51/51
84 C (i)	3 Ni-Ag C	No	20	40		10/9	22/20
61 NC (i)	3 Ni-Ag NC	No	20	53		Anodic	
84 R (ii)	3 Ni-Ag	Yes	20	30		70/75	137/140
84 C (ii)	3 Ni-Ag C	Yes	20	36		4/4	12/12
61 NC (ii)	3 Ni-Ag NC	Yes	20	46		Anodic	

(1) Activity expressed as current at decreasing potential
    Current at increasing potential

TABLE XXVIII (Cont.)

Electrode Catalyst	% PTFE	Loading mg/cm^2	Activity			
			ma/cm^2 at 950 mv	ma/mg at 950 mv	ma/cm^2 at 900 mv	ma/mg at 900 mv
88 C (1a) 1 Au-3 Pd	20	64	24	.37	120	1.8
88 R (1a) 1 Au-3 Pd (Carbide)	20	50	5	.1	14	.28
64 NC (1a) 1 Au-3 Pd (Nitrocarbide)	20	54	2	.05	6	.1
89 R (1a) 1 Au-1 Pd	20	58	13	.24	42	.7
90 R (1a) 3 Au-1 Pd	20	57	25	.44	60	1.05
91 R (1a) 3 Ag-1 Pt	20	59	18	.3	70	1.2

TABLE XXVIII (Cont.)

Electrode / Catalyst	% PTFE	Loading mg/cm^2	ma/cm^2 at 950 mv	ma/mg at 950 mv	ma/cm^2 at 900 mv	ma/mg at 900 mv
93R (19) 1 Ag-1 Pt	20	50	38	.76	100	2
95R (19) 3 Pt-1 Pd	20	29	44	1.5	200	7
98R (19) 1 Ni-1Pt-1Pd	20	48	5	.1	26	.5
99R (19) 1 Ag-1Au-1Pt	20	60	23	.4	48	.8
100R (L-1) 1 Ag-1Pt-1Pd	20	27	20	.8	130	5
102R (L-1) 3 Au-1 Pt	20	43	37	.8	130	3
107R (L-1) 1 Au-Pt-1 Pd	20	28	80	2.9	116	4

observed order of activity was Ni/Co > 3 Ni/Co > Ni/3 Co. It should also be noted for the uncarbided Raney nickel cobalt alloys (RAL 1, 2 and 3) the activity was in the same range, the Ni/3 Co alloy giving 60 ma/cm^2 at 600 mv. For the Raney alloys the activity pattern was Ni/3 Co > Ni/Co = Ni/3 Co.

In view of the demonstrated capabilities of Ni$_3$C catalysts prepared from the acetate, the much lower activity of the alloys prepared from the Raney alloys was unexpected. X-ray characterization showed the catalysts from both sources to be very similar. The acetate material had a higher free nickel content; the Raney material was obviously composed of smaller crystallites as evidenced by the line broadening of the X-ray pattern. The difference in activity can most probably be attributed to differences in the physical structure of the catalysts prepared by the two methods. A second sample of Ni$_3$C (36C) was prepared from the Raney alloy pulverized to < 250 mesh, to check whether gross particle size could affect electrode performance. The results, a maximum activity of 30 ma/cm^2 at 600 mv, were not encouraging. Sample 50C represented an attempt to carbide a Ni/Co alloy obtained by decomposition of nickel formate and cobalt acetate. The activity was still very low (33 ma/cm^2), but a second sample carbided at a lower temperature showed considerable improvement at 125 ma/cm^2 at 600 mv.

Several catalysts were prepared in which gold, silver and palladium were added to the Ni and Co. The performance of these catalysts themselves and as carbides was, in some cases (e.g. 44C), very good. Probably this is due to the activity of the precious metal itself, though the presence of the precious metal could improve the utilization of the nonnoble metal component by providing a lower resistance current path in the electrode structure. In these cases the structure of the Raney alloy catalyst was capable of supporting limiting currents of 350 ma/cm^2 (44C (ii) but this could easily be adversely affected by the carbiding process. Carbided porous nickel plaques were used for three tests on Ni$_3$C (28C). This electrode configuration gives a high surface area catalyst without the possibility of the high resistance that could occur with the particle-to-particle contact of the highly dispersed catalyst. The difficulty in testing

these electrodes was to establish the gas electrolyte interface throughout the electrode structure. In the results reported, this was attempted by partial wetproofing, with PTFE dispersion, so that the electrodes could be run in the floating electrode cell. The recorded performance shows that the attempt to produce an extended interface was not very successful. The material was tested in a conventional fuel cell configuration with a matrix electrolyte (see section 4). Under these conditions the pressure differential between the electrode and the electrolyte was varied to obtain optimum performance.

The unusual decay pattern associated with the activity measurements on nickel and nickel cobalt catalysts was described above. A tentative explanation for this can be given as follows:

Initially, in addition to the cathodic reduction of O_2, there is a simultaneous anodic process associated with further oxidation of the surface. This falls rapidly to a low value when the surface is completely covered and produces an apparent increase in the net cathodic current. The oxygen reduction process is assumed to occur on the oxide surface and not on the bare metal. (However, it is surprising that the surface oxidation is not complete during pretreatment of these electrodes at 1600 mv for 10 minutes.) The decay process that was then observed may be related to an increase in the resistance of the electrode. The operation of PTFE bonded electrodes depends on good electrical conductivity between individual catalyst particles, and since conductivity of the oxide is considerably lower than that of the metal, the electrode resistance increases. The points or faces of contact probably oxidize more slowly than the exposed surfaces, so that this process would not be complete within the time span of the surface oxidation responsible for the apparent increase in current described above.

The above argument suggests that some of the iR corrections made to the earlier results might be too large. The ohmic resistance was measured by the interrupter technique (resolution time 0.2 μ sec). The over-all resistance measured for the nickel and nickel cobalt electrodes is approximately twice that measured with a Pt electrode, indicating a

significant contribution from the resistance of the electrode. This resistance, in contrast to the bulk electrolyte resistance, is inevitable in the practical operation of the electrode and may not be a valid experimental correction of the E(i) curve. The over-correction, about $0.6\,\Omega$ or 60 mv at 100 ma/cm^2, is important only for those electrodes with high activity. In the results presented in Table XXVIII, this factor has been taken into account.

Sample 39 NC, nickel nitrocarbide, represents one of the best nickel catalysts tested. An unusual feature of this result (70 ma/cm^2 at 750 mv vs. RHE) is that it is higher than that recorded for the carbide from which it was prepared (49 ma/cm^2 at 750 mv vs. RHE). In most cases either the values for the corresponding carbide and nitrocarbide are of the same order of magnitude or the nitrocarbide shows a lower result, e. g. 41 NC = (32 ma/cm^2) and 56C (35 ma/cm^2), and 42 NC (130 ma/cm^2) and 57 C (137 ma/cm^2). Samples 57C and 42 NC, nickel/palladium carbide and nitrocarbide respectively, show the highest activity yet observed for an interstitial compound, disregarding the 350 ma/cm^2 observed for nickel silver gold carbide in which most of the activity can probably be attributed to the silver and gold. A comparison of 57C with 55C (34 ma/cm^2), a nickel palladium carbide prepared from the Raney alloy, emphasizes the better physical characteristics that are obtained when the carbide is prepared from the reduced coprecipitated hydroxides. (In contrast the Ni Ag Au carbide prepared by coprecipitation showed little activity, whereas the Raney alloy derivative was very active, see above).

The nickel cobalt nitrocarbide (45 NC) and carbide (61C) prepared from the reduced coprecipitated hydroxides, however, showed negligible activity (< 1 ma/cm^2 at 750 mv vs. RHE).

Catalysts 68C to 73C were prepared by carbiding a reduced coprecipitated 3 Ni/Co alloy at different temperatures and times. A summary of the preparative conditions and the activities is given in Table XXVIII.

- 147 -

From Table XXVIII it can be seen that at 240°C the activity decreases with increasing time of carbiding. It is possible that at 240°C no carbide was formed and that progressive sintering of the sample occurred. At 260°C the exposed samples exhibited an increase in activity with carbiding time. It would appear that the first sample (72C) was already substantially sintered after 24 hours; (its activity was below that of the initial sample (73C) at 240°C). The subsequent increase in performance can be attributed to carbide formation.

The behavior of the inducted samples does not follow the same pattern. The performance of the catalysts carbided at 240°C for 24 hours also showed low activity, but the 72 hour sample (70C) gave 146 ma/cm^2 at 750 mv $\underline{vs}$. RHE. Catalysts 68C carbided for 120 hours gave a lower activity of 30 ma/cm^2. Although attempts to reproduce the results obtained with 70C were unsuccessful, duplicate measurements on the rest of the series confirmed the activity pattern described above. The level of activity in this second examination was lower than that of the first, probably related to the total time of exposure of the catalyst to air (~ 2 weeks) before the second tests were carried out.

Tests on catalyst 50R, a 3 Ni/Co alloy prepared in an almost identical manner to the starting material for the carbides 68C to 73C, demonstrated an activity of 225 ma/cm^2 at 600 mv. This is much higher than the results for the carbides, excepting the unconfirmed figure for 70C.

Another series of compounds tested were the alloys, carbides and nitrocarbides of 3 Ni/Au, Ni/3, 3 Ni/Pt, Ni/3 Pt, and 3 Ni/Ag; and the 3 Pd/Ag, and Pd/Ag alloys. The silver palladium alloys 3 Pd/Ag and Ag/Pd showed very high currents (> 300 ma/cm^2) at 750 mv $\underline{vs}$. RHE, but activity at 950 mv (of the order of 5 ma/cm^2) was lower than that observed with Pt or Au/Pd alloys. This is in accord with the results presented for solid electrodes of these alloys in the Fourth Quarterly Report of this contract. The 3 Ag/Pd alloys showed better, but still low, activity at 950 mv; however, the current at 750 mv was much reduced (190 m /cm^2).

The Ni/Au alloys showed disappointing activity, with the Ni/3 Au alloys giving lower activity than the 3 Ni/Au alloys. This surprising result was reproduced in a re-examination at Tyco with electrodes of different PTFE content and in measurements made at the Bureau of Mines. The carbides and nitrocarbides of 3 Ni/Au were much less active than the parent alloy; the same compounds of Ni/3 Au were marginally more active (4 ma/cm^2 compared with 1 ma/cm^2 at 750 mv $\underline{vs}$. RHE) than the alloy.

The Ni/Pt alloys showed a very much lower activity than might be expected for a Pt based catalyst. The series of materials showed the same pattern of activity, as has been described before, of alloy > carbide > nitrocarbide. As with the Ni/Au alloys the activity of the nickel rich alloy was greater than that of the Ni/3 Pt alloys. The 3 Ni/Ag catalysts were very similar in performance to the 3 Ni/Au catalysts.

The gold palladium alloys showed promising activity; however, the performance level is well below that observed with a good Pt catalyst or the better examples of palladium gold prepared at Tyco. The carbide and nitrocarbide of 3 Pd/Au showed lower activity than the alloy. The range of alloy compositions 3 Pd/Au, Pd/Au and Pd/3 Au did not show the exact pattern of activity established with solid electrodes. The 3 Pd/Au alloy showed the highest activity, but the activity of the Au/Pd catalyst was below that of the 3 Au/Pd. This behavior can be accounted for in terms of differences in the structure of the finely divided catalyst.

The silver platinum (3 Ag/Pt) catalyst showed much lower activity than might have been expected for a platinum based catalyst.

SECTION 4

CATALYST LIFE TESTING

I. INTRODUCTION

In order to verify the activity for O_2-reduction of catalysts tested as floating electrodes in the previous phase of this program, as well as to check for possible long term degradation, it was necessary to life test the various materials investigated.

One of the first steps in this procedure was the development of techniques for fabricating sufficiently large electrodes and facilities to handle them. Previously, electrodes had been made on the order of $5\text{-}10 \text{ cm}^2$, sufficient for one cm^2 test pieces needed for the floating electrode tests. For life testing it was decided that 50 cm^2 electrodes would be used. This required both modified techniques for making electrodes and a larger sintering oven.

In order to approach practical fuel cell conditions as closely as possible, a working fuel cell design was chosen rather than a driven cell. The particular design chosen, a reservoir cell, although impractical in size, weight, volume, etc., ensured that the catalyst material rather than the fuel cell system was being tested. The cell is essentially an asbestos matrix cell with special provisions for electrolyte control.

One of the most significant problems in extended fuel cell operations is the controlled removal of product water. Inadequate control results in flooding or drying out of the electrolyte matrix. A frequently used method of control employs the continuous flow of one or both gases at a controlled rate to remove the excess moisture. Other techniques which have been tried are flowing electrolyte systems, wicking arrangements, and the vapor pressure control system of Allis Chalmers.

The free electrolyte system requires very special electrodes and cell construction not suited to our present tests. The continuous gas flow system is simply constructed but somewhat difficult to control. The vapor pressure control system is easier to control but is very sensitive to leaks

and is still prone to the problem of irreversible electrolyte loss during extended operation.

The fuel cell life test system was designed to take advantage of each of the above systems to yield a simple but more reliable testing device. The large reservoir of electrolyte, with its surface just below the gas side of the H_2 anode, maintained a constant water vapor pressure in the anode space. Since the O_2 electrode was dead-ended, this vapor pressure defined the concentration of the electrolyte in the cell in the same manner as the Allis Chalmers system.

The concentration of electrolyte in the reservoir was relatively unaffected by fluctuations in the water removal rate. Water was removed at a known rate in the H_2 exhaust. When deviations from the normal operating conditions resulted in loss of electrolyte, porous nickel wicks in contact with the anode and the electrolyte reservoir permitted the slow replacement of KOH.

Thus the reservoir cell simulated a free electrolyte system without the interface problem and had the advantage that it reduced the gas flow rate sensitivity of the water removal mechanism.

II. PREPARATION OF LARGE ELECTRODES

The first requirement for making large electrodes was a larger sintering oven. This was accomplished by constructing a closed "drawer" device which could be moved in and out of a standard oven through a hole in the door. This chamber was constructed of thin gauge aluminum with a nitrogen preheater on the outside and a gas distribution system inside. Electrodes (12" x 12" max) were placed in the chamber through a door on the front and the chamber was flushed with nitrogen for about 15 minutes. The chamber was then pushed into the preheated oven for the Teflon sintering program.

Two platinum catalysts — Pt(a) and Pt(b) — (Table XXIX) are samples of the same electrode preparation; the former was sintered by our established method in the small sintering oven and the latter, in the new oven designed to accommodate large electrodes. The large oven gave a minimum warm-up time of 8 minutes to 275°C and cool-down time of 12 minutes. These times are greater than those of the small oven, but it is apparent from the results in Table XXIX that in the case of Pt there was no detrimental effect. This was confirmed with several large electrodes, also listed in Table XXIX.

Another problem related to large electrode fabrication is the method of distributing the catalyst on the screen. A number of methods were described in section 3, such as spraying, brushing, rolling or spreading. For the massive screening programs described in section 3, the spreading technique was chosen because of the simplicity and economy in making the very small electrodes required. It was found, however, that this technique was very difficult to scale up, especially with regard to uniformity of distribution. Consequently the rolling method was chosen and was used to prepare all electrodes except the Ni_3C (which had to be spread, at the cost of uniformity, due to its high bulk density).

The catalyst preparations made into large electrodes are listed in Table XXX, along with the results of a floating electrode test of one cm^2 of the outer edge of the large electrode. Of the Pd-Au alloy preparations, only the formaldehyde preparations were deemed sufficiently active to warrant further testing.

TABLE XXIX

Platinum Electrodes

Electrode		% PTFE[1,2]	Loading[3] mg/cm^2	Activity	
				ma/cm^2 at 950 mv	ma/mg at 950 mv
Pt(a)	sintered in large furnace	20	15.2	97	6.3
Pt(b)	sintered in regular furnace	20	15.9	48	3.0
Pt-L(i)	Engelhard Platinum	30	25	95	3.8
Pt-L(ii)	Engelhard Platinum	30	21	116	5.5
Pt-L(iii)	Engelhard Platinum	30	23	110	4.8
Pt-L(iv)	Engelhard Platinum	30	46	210	4.6
Pt-L(v)	Engelhard Pt	20	13	51	3.1
Pt-L(vi)	Tyco #73-79	30	27	124	4.6

TABLE XXX

Performance of Large Electrodes Tested as Small Samples

Electrode Catalyst[1]	Electrode	% PTFE[2]	Loading[3] mg/cm^2	Activity ma/cm^2 at 950 mv	ma/mg at 950 mv
F-8 Pd-Au (40-60)	L-1	30	43	--	--
	L-2a	30	69	32	.5
	L-2b	30	64	57	.9
F-9 Pd-Au (40-60)	L-1	30	60	52	.9
	L-2	10	71	160	2.2
F-10 Pd-Au (40-60)	L-1	30	51	37	.7
F-11[4] Pd-Au (40-60)	L-1	30	30	86	2.8
	L-2	15	58	100	1.8
F-12[4] Pd-Au (40-60)	L-1	15	60	93	1.5
F-13[4] Pd-Au (40-60)	L-1	20	28	104	3.7
	L-2	15	40	104	2.6
F-(8,9,10)[5] Pd-Au (40-60)	L-1	20	28	128	4.6
F-15 Pd-Au (50-50)	L-1	20	19.3	62	3.2

TABLE XXX (Cont.)

Electrode Catalyst[1]	Electrode	% PTFE[2]	Loading[3] mg/cm²	Activity	
				ma/cm² at 950 mv	ma/mg at 950 mv
F-16 Pd-Au (60-40)	L-1	20	27	65	2.4
F-17 Pd-Au (70-30)	L-1	10	33	154	4.7
	L-2	15	28	126	4.1
	L-3	20	27	64	2.4
F-18 Pt-Os (80-20)	L-1	30	22	45	2
Pt-Os (80-20)[6]	L-2	30	27	68	2.5
Pt-Ag$_2$O (30-70)	L-1	20	27	8	.3
	L-2	20	22	100	4.6
F-20 Pt-Au (70-30)	L-1	20	22	87	4
Pd-Au 40/60					
Ag$_2$O 50 wt. %[7]	L-1	20	30	40	1.3
102R 3 Au/1Pt (B. O. M.)	L-1	20	43	37	.8
100R Ag-Pt-Pd (B. O. M.) 1-1-1	L-1	20	27	20	.8
107R Au-Pt-Pd (B. O. M.) 1-1-1	L-1	20	28	80	2.9

TABLE XXX (Cont.)

Catalyst No.	Catalyst[1] Composition	Electrode	% PTFE[2]	Loading[3] mg/cm²	ma/cm² at 750 mv	ma/cm² at 600 mv
54C	Ni$_3$C (B. O. M.)	L-1	20	78	15	60
67	Ni$_3$C + Ni (Tyco)[8]	L-1	10	31	--	--
67	"	L-2	10	71	--	--
68	"	L-1	10	69	--	--
69	"	L-1	10	38	59	178
69	"	L-2	15	69	56	260
70	"	L-1	10	69	9	21
71	"	L-1	30	38	7	22

(1) All electrodes made on expanded nickel screen.

(2) All electrodes sintered at 275°C for 15 minutes.

(3) Loading here is for one cm²; average loading of large electrode may be slightly different.

(4) Prepared by adding, dropwise, a mixture of Pd salts, Au salts, H$_2$O, and 13M HCHO to 10.5 N NaOH at 90°C (see section 3).

(5) Mixture of samples 8, 9 and 10 ($\sim$ 1:1:1).

(6) Mechanical mixture of Pt and Os powders; water proofing very non-uniform.

(7) Sintered in air 275°C, 15 minutes.

(8) All preparations made by acetate decomposition.

Most of the 40 large electrodes prepared, with the exception of the nickel carbide, were quite active — between 2 and 5 ma/mg. The nickel carbide preparation performed poorly compared with the other catalysts, as expected, and also in comparison to earlier Ni_3C preparations. However, of the 32 preparations of Ni_3C, only about 3 were successful, i.e. $\sim$ 100 ma/cm^2 at 750 mv.

III. LIFE TESTS

A. Experimental

Eight reservoir type cells were set up for life testing. The individual test station is conventional in design (see Figs. 23-26), providing for the control and measurement of gas pressures and flow rates and for the collection and measurement of the water produced. Particular attention was paid to carrying out the tests under realistic conditions but under circumstances (not necessarily feasible in a practical cell) that avoid the more common failure modes of a H_2/O_2 cell. Decay in performance can then be directly attributed to the cathode catalyst.

Maintaining the water balance is probably the most critical variable in the operation of a matrix cell. This was achieved by having a large reservoir of electrolyte immediately behind the anode (see Fig. 26). This reservoir defined the water vapor pressure in the anode gas space (i. e. no presaturation was necessary) and therefore controlled the water content of the electrolyte trapped in the matrix. Since the reservoir electrolyte concentration could not change very rapidly even with relatively high H_2 flow rates, the water vapor pressure remained constant for relatively long periods of time (say several hours). An effective water balance could then be maintained by comparing the total amount of water removed with that produced (calculated from the current-time curve) and by making the necessary adjustments in the gas flow rates. Product water was removed primarily by the flow of excess hydrogen. A further refinement was the provision of porous nickel wicks from the electrolyte reservoir to the matrix. Then, in the event of loss of KOH from the matrix (e. g. lost as a result of gross deviations in the water balance which result in drowning), the KOH could be replaced by diffusion through the wicks.

The reservoir cell, therefore, simulated a free electrolyte system but without the associated interface problem and had the advantage that it reduced the gas flow rate sensitivity of the water removal mechanism.
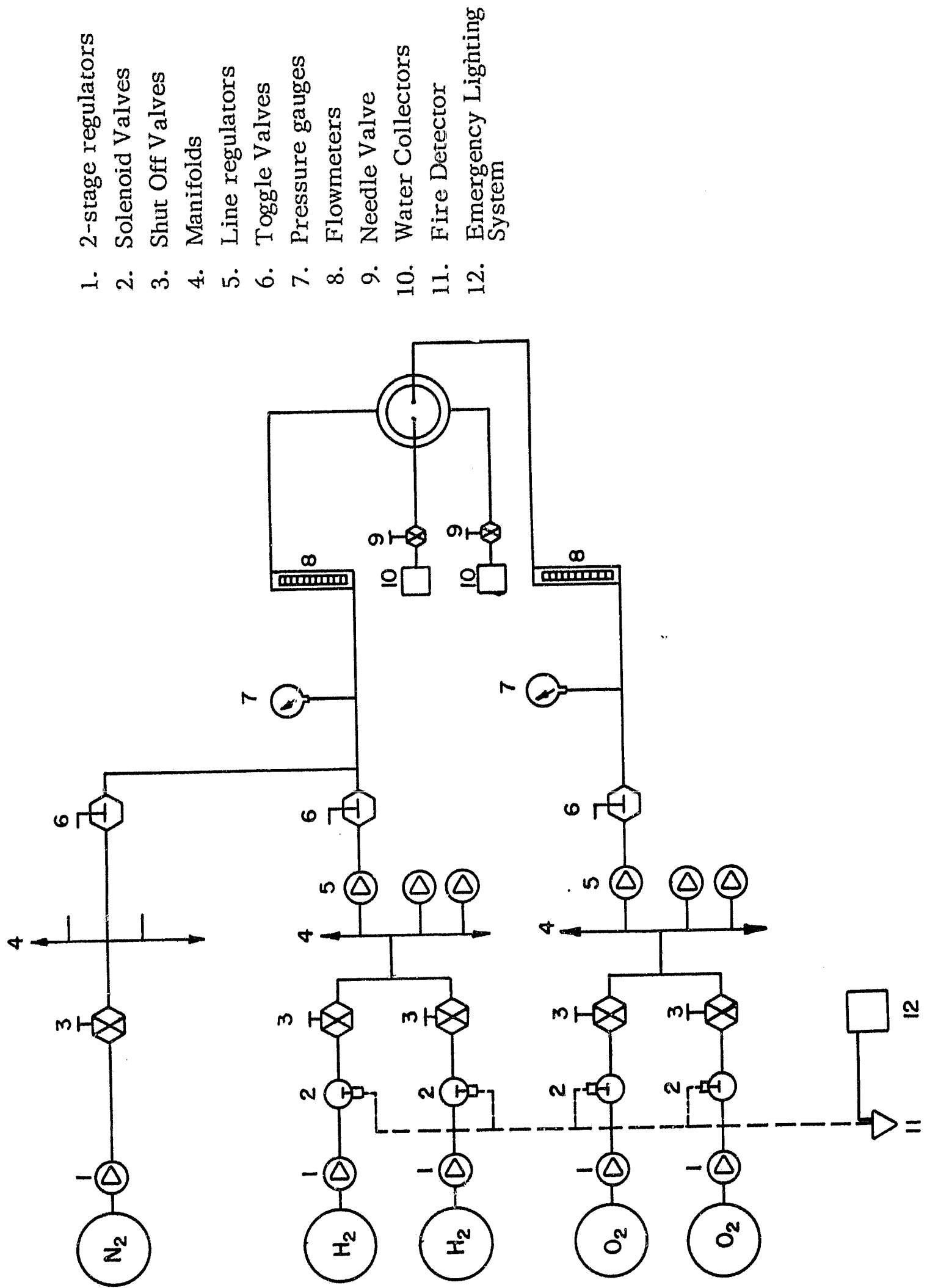
1. 2-stage regulators
2. Solenoid Valves
3. Shut Off Valves
4. Manifolds
5. Line regulators
6. Toggle Valves
7. Pressure gauges
8. Flowmeters
9. Needle Valve
10. Water Collectors
11. Fire Detector
12. Emergency Lighting System

Fig. 23 Flow diagram of test rig.

572F
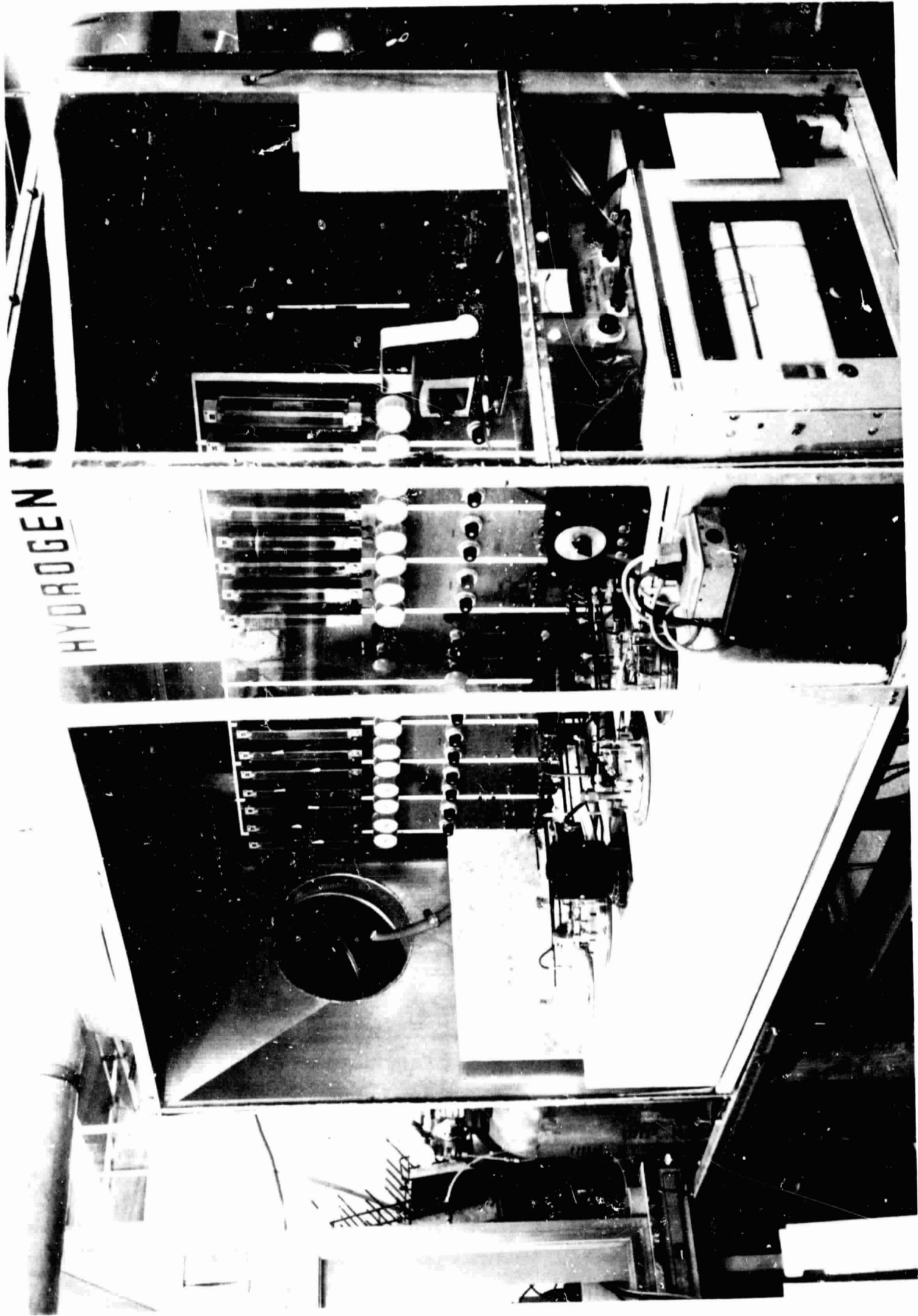
Fig. 24   Test rig.
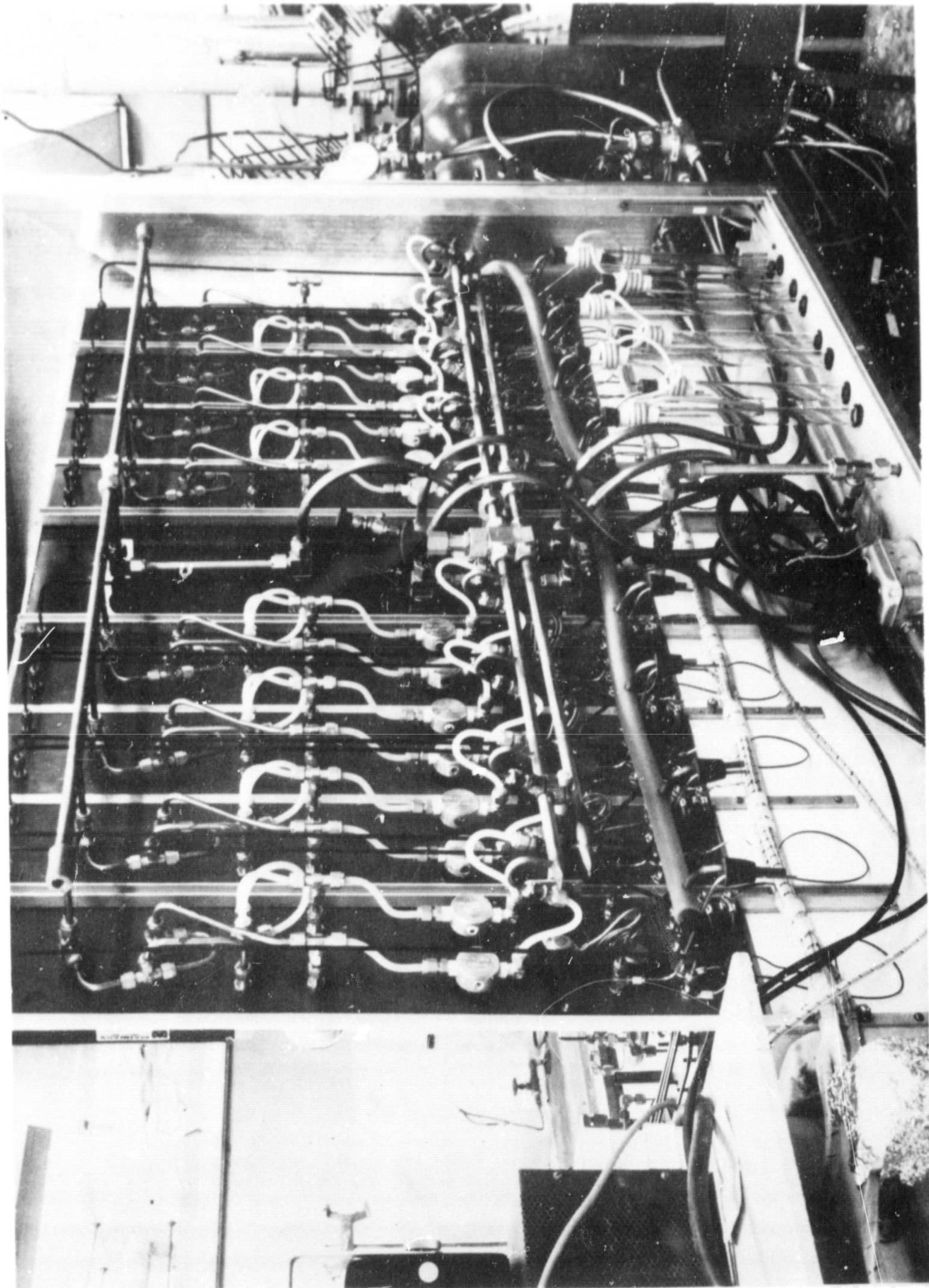
Fig. 25   Test rig - rear view.
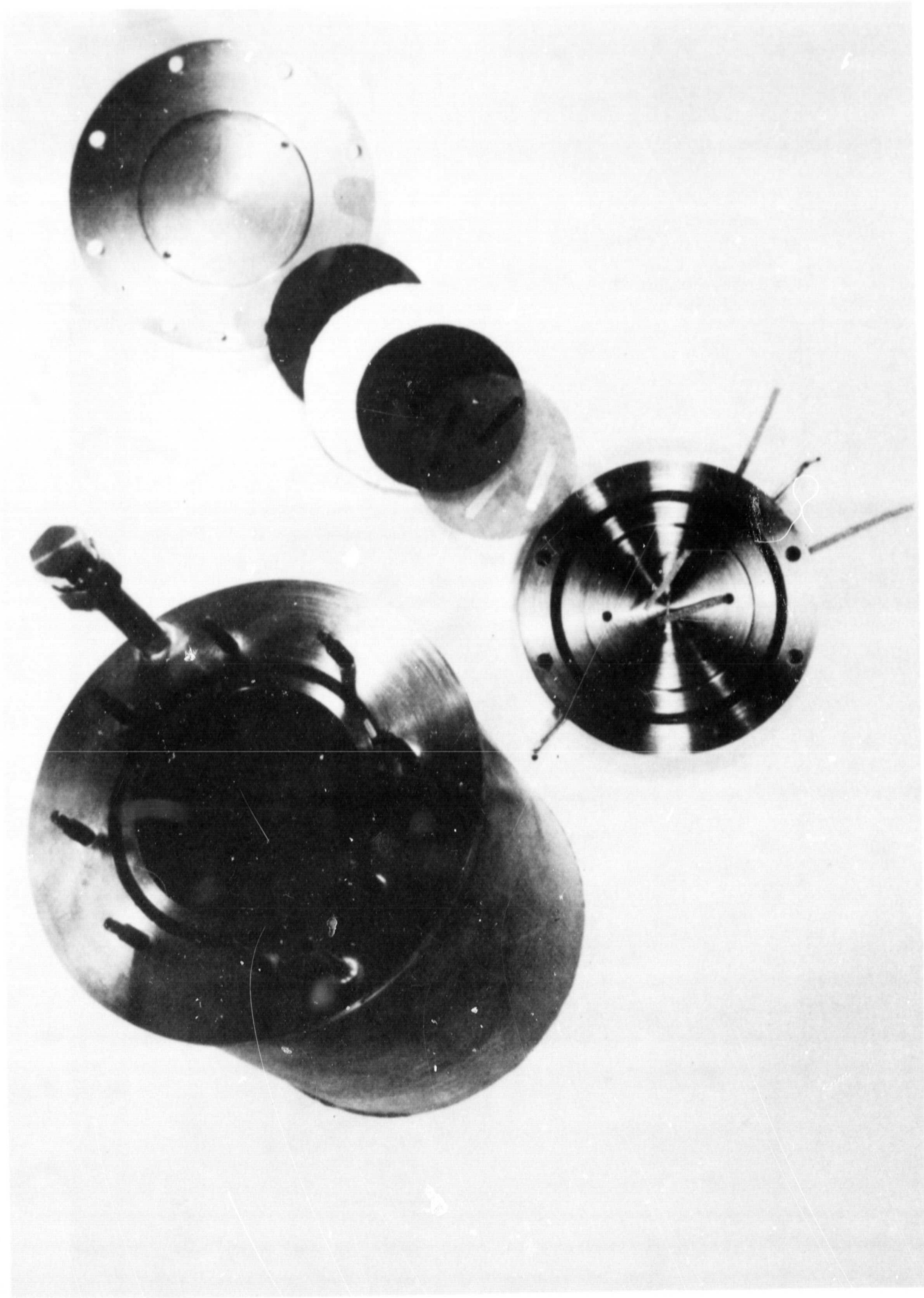
Fig. 26 Reservoir test cell - exploded view.

The catalysts were tested as PTFE bonded electrodes, 50 cm^2, formed on gold plated expanded nickel screen. The electrolyte was 35% KOH and the cells were run at 80°C. In all cases the anode was a commercial platinum electrode (American Cyanamid AB-40). This electrode with a Pt loading of 40 mg/cm^2 on a gold plated nickel screen is specifically designed to give long life and reliability.

B. Preliminary System Tests

Two cells were set up initially, one with an American Cyanamid AB 4X cathode, the other with a cathode made at Tyco from a commercial platinum black (37 mg/cm^2). The anodes of both cells were American Cyanamid AB-40 electrodes.

Both cells were run with 40% KOH in the temperature range 77 to 79°C. The patterns of performance for both cells are shown in Figs. 27 and 28. The principal difference between the two life tests is that cell #2 failed three times during the course of the test but was successfully restored to the original performance level by blowing out the cathode vent lines. This action removed large quantities of electrolyte (compared with the amount of water normally removed by the gas glow) and accounts for the difference between the theoretical and measured quantities of water shown in the plots in Figs. 27 and 28. The problem was considered to be due, in part, to the difficulty of controlling the low gas flow rates, and the pressure differential across the cell, with the needle valves originally fitted on the vent lines. These were replaced to alleviate this difficulty. It is also possible that the electrolyte accumulated in the cathode space because of some transport mechanism (e. g. electro-osmosis) that is a critical function of the structure and PTFE content of the electrode. This accumulation of electrolyte could be avoided by applying a pressure differential across the cell. This was difficult to control in the initial test because of the difficulties associated with the adjustment of the needle valves in the vent line.

Maximum current from the cells was < 3A until copper leads were added as the current carriers to the load devide (a transistor bias circuit)
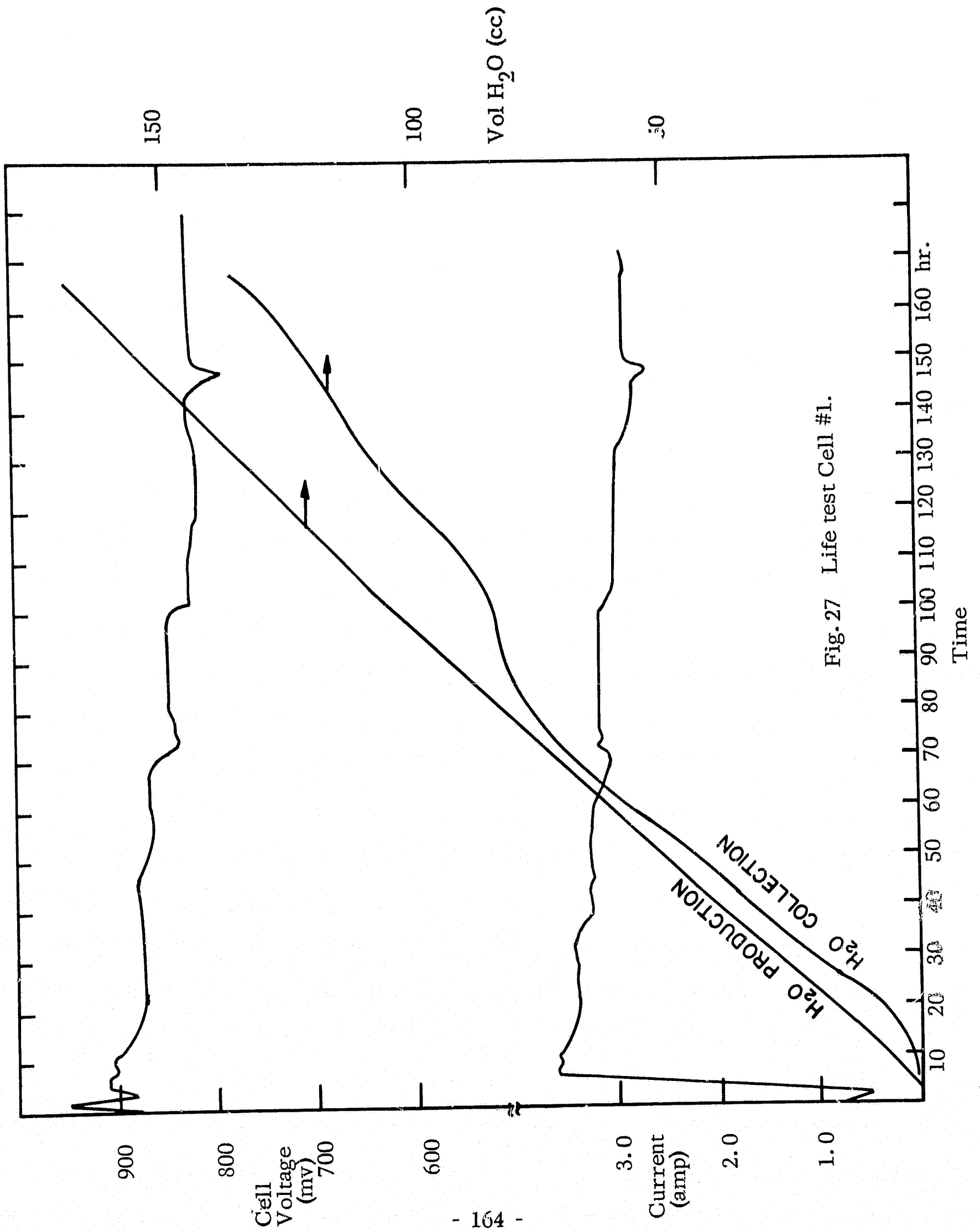
Fig. 27   Life test Cell #1.

- 164 -

572F
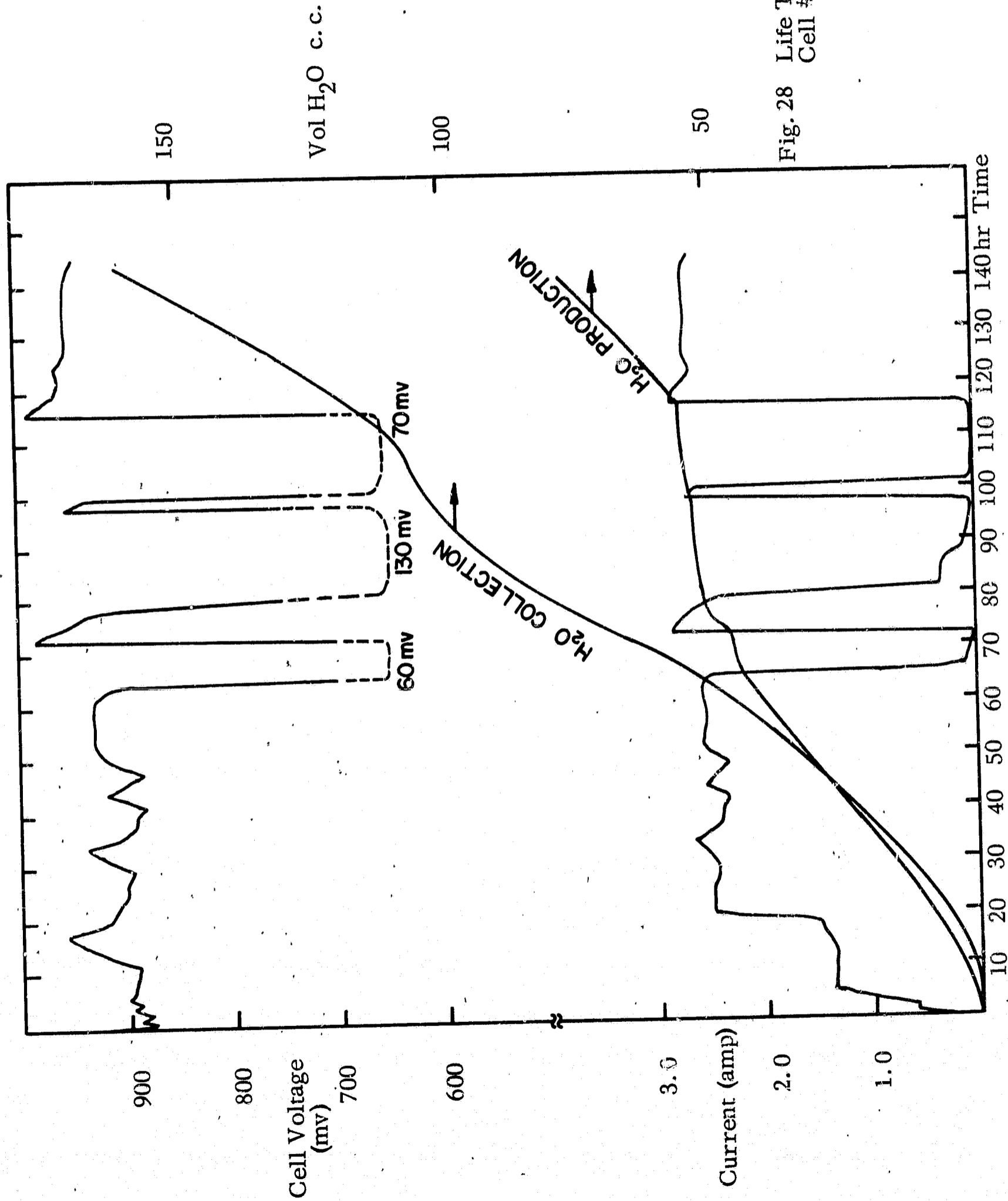
Fig. 28 Life Test
Cell #2.

- 165 -

572F

in place of the stainless steel gas lines. To improve current collection at the cathode, the nickel screen current collectors and the cell back plate were gold plated. These changes permitted loads of up to 8 amps (160 ma/cm^2). In order to make the modifications listed above, tests on cells #1 and #2 were terminated after about 250 hours.

After these modifications were made, all eight cells were gradually put into operation. Since the temperature specification was lowered from 90° to 80°C, the KOH concentration was also lowered from 40% to 35%. The cells were operated continuously at about 5 amps (100 ma/cm^2). For the sake of stability, the cells were operated below the optimum performance level. Maximum performance was obtained by allowing electrolyte to flood the oxygen cavity, with simultaneous removal by excess oxygen flow. This behavior can be explained by assuming that electrolyte pumping without removal caused deterioration by flooding, while if pumping was avoided by excess oxygen pressure, the oxygen electrode was not optimally wetted by electrolyte and the performance decreased. Periodically the cells were brought up to maximum performance for purposes of comparison.

The following materials were life tested as oxygen reduction catalysts.

(1) American Cyanamid - Type AB-40
Pt 40 mg/cm^2

This cell was used as a system reference.
Was operated for 3000 hours.

(2) TYCO - Platinum #73-79 (L-6)
20 mg/cm^2, 30% PTFE

Electrode fabrication reference - 1750 hours.

(3) Pt-Au 70/30 #F-20 (L-1)
20 mg/cm^2, 20% PTFE

Cell rebuilt at ~ 1100 hours due to power failure damage - 1500 hours.

(4) Pt-Ag 30/70 (Englehard Pt and Fisher Ag$_2$O)
22 mg/cm^2, 20% PTFE

2275 hours.

(5)   Pt-Os 80/20 #F-18 (L-1)
        25 mg/cm^2, 30% PTFE

        1570 hours.

(6)   Pd-Au 40/60 #F-13 (L-1)
        28 mg/cm^2, 20% PTFE

Operated for 3000 hours to investigate the effects of palladium alloy corrosion.

(7)   Pd-Au 50/50 #F-15 (L-1)
        23 mg/cm^2, 20% PTFE

Test terminated at 1250 hours in order to begin testing other materials.

(8)   Pd-Au 70/30 #F-17 (L-1)
        24 mg/cm^2, 10% PTFE

        1610 hours.

(9)   Pd-Au 60/40 + 50 wt % Ag$_2$O
        32 mg/cm^2, 20% PTFE

        1470 hours.

(10)   Au-Pt-Pd (B. O. M.) #107-R-(L-1)
        39 mg/cm^2, 20% PTFE

        1584 hours.

(11)   Ag-Pt-Pd (B. O. M.) #100-R-(L-1)
        38 mg/cm^2, 20% PTFE

        1584 hours.

(12)   Ni$_3$C (B. O. M.) #54-C
        56 mg/cm^2, 20% PTFE

Terminated at 646 hours to begin testing a second sample of Ni$_3$C.

(13)   Ni$_3$C (TYCO) #69 (L-1)
        25 mg/cm^2, 10% PTFE

Terminated after 530 hours due to low performance.

C. Results

The results of the life testing are shown graphically in Figs. 29-31. Voltage current curves were taken periodically (Table XXXI), and cell voltages at 100 ma/cm^2 are given in the figures. None of the cells tested failed, although some were terminated before 1500 hours due to low performance or redundancy.

The best results were obtained with the Pt-Au 70/30, Pt-Ag 30/70, and Pd-Au 40/60. The platinum-gold alloy is particularly promising since it showed a higher performance level than pure platinum at the same loading (Tyco Pt) and higher than Pt at twice the loading (AB-40). Since Pt-Au was one of the last materials tested, there was not sufficient time to prepare and test other alloy compositions. The one alloy tested, Pt-Au 70/30, corresponds to the peak in Figs. 6-9 (section 2) of potential vs. composition for the Pt-Au series (screening-solid electrode).

The Pd-Au 40/60 alloy is also interesting both for its performance which was comparable to platinum and for its apparent corrosion resistance. After 3000 hours of operation the performance level was only slightly below that of platinum. The performance of the other Pd-Au alloys was somewhat erratic but within the range of platinum performance nonetheless.

The Pt-Ag electrode which was a simple mixture of Pt and Ag_2O powders was very successful, indicating the importance of structural effects. The performance of the Pt-Os electrode was fair.

The noble metal mixtures prepared by the Bureau of Mines, Au-Pt-Pd and Ag-Pt-Pd, performed well but were not exceptional in view of the high loading required for their fabrication.

The nickel carbides, Bureau of Mines and Tyco preparations, showed low performance and deterioration (not as much as found in the floating electrode tests, however).
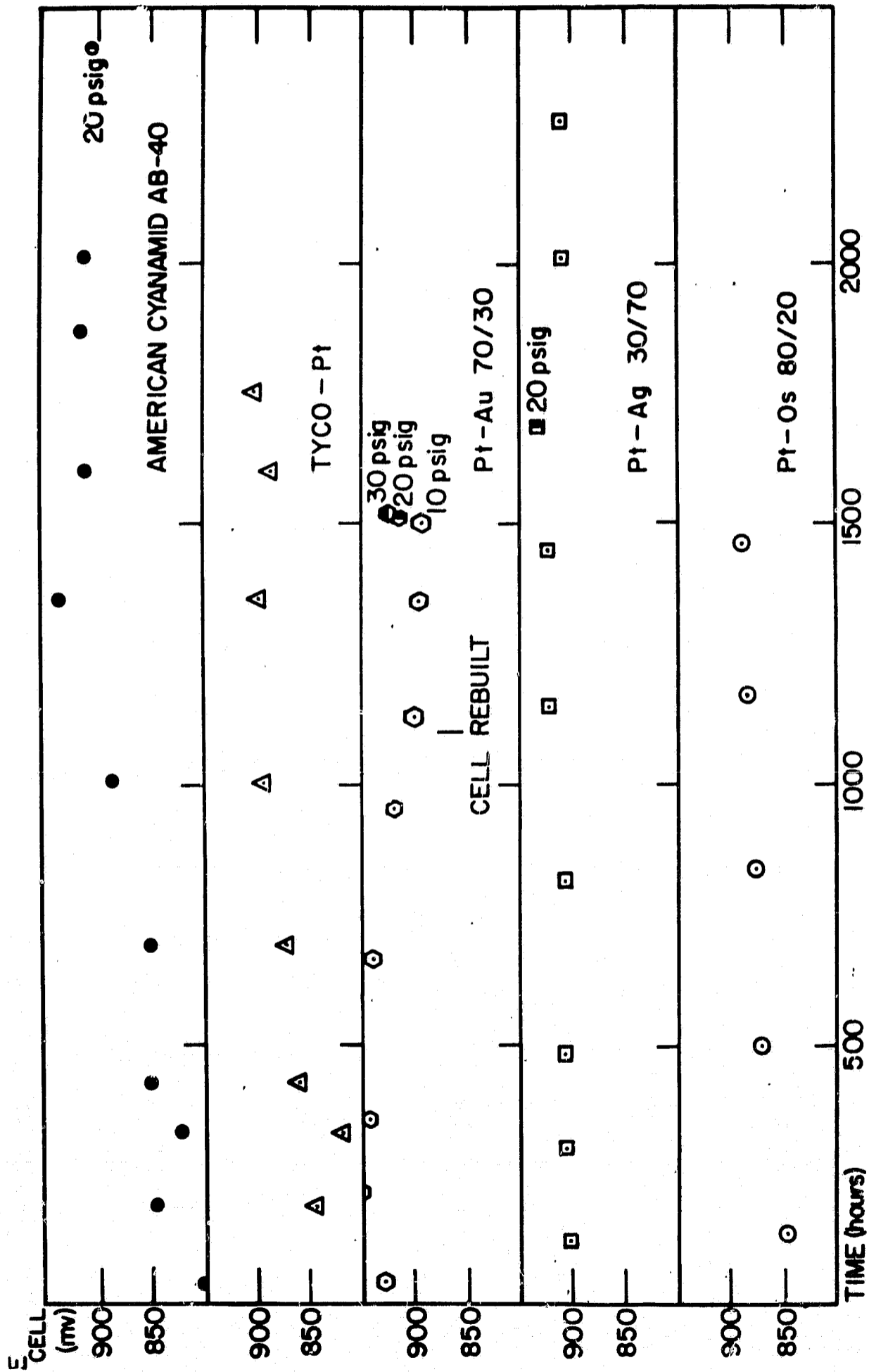
Life testing of cathodes

Cell voltage @ 100 ma/cm² vs. time

H₂ elect. - American Cyanamid AB-40
35% KOH, 80°C, 10 psig.

Fig. 29
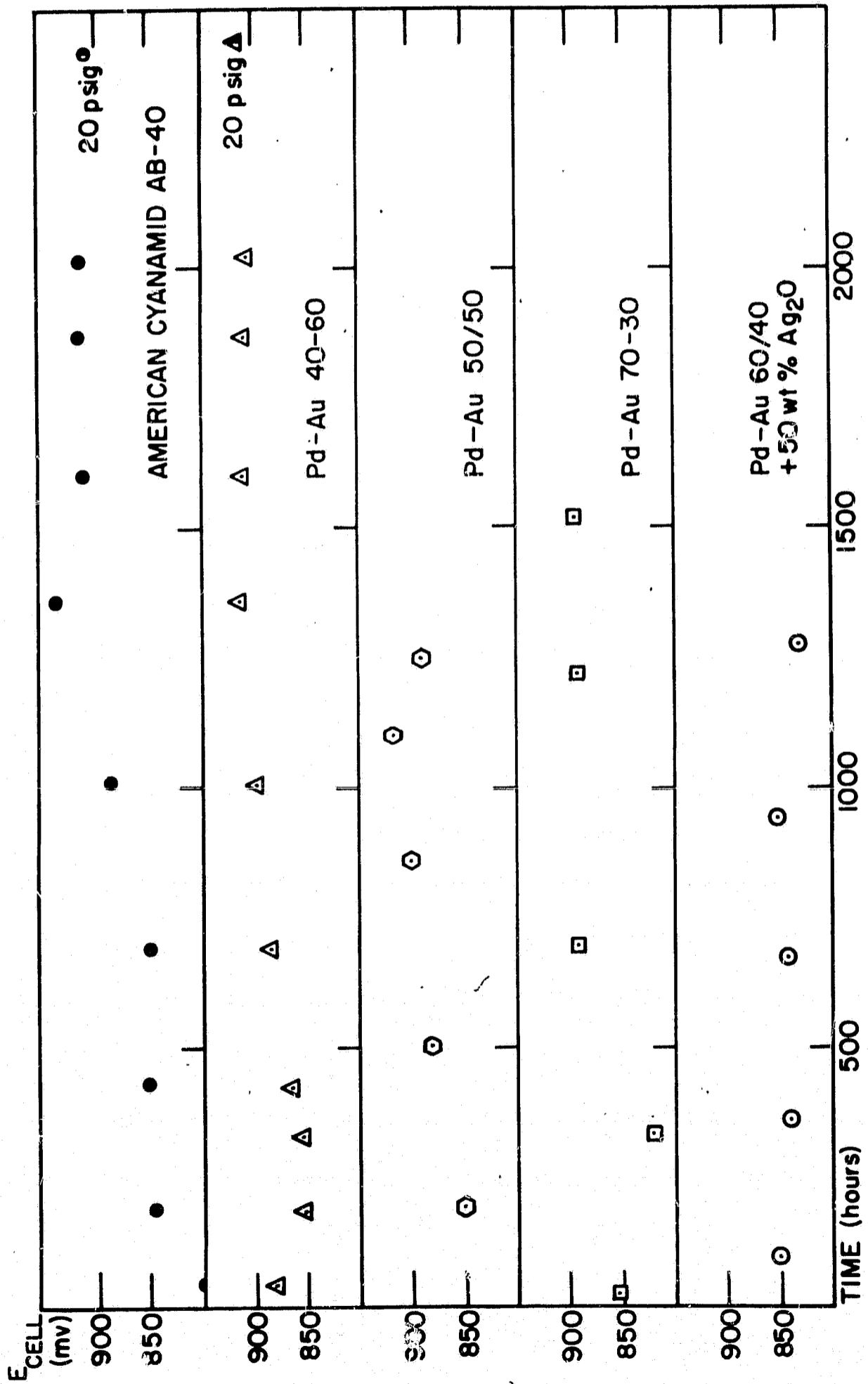
- 169 -

572F

Life testing of cathodes

Cell voltage @ 100 ma/cm^2 vs. time

H$_2$ elect. - American Cyanamid AB-40
35% KOH, 80°C, 10 psig.

Fig. 30

Fig. 31

Life testing of cathodes

Cell voltage @ 100 ma/cm^2 vs. time

H_2 elect. - American Cyanamid AB-40
35% KOH, 80°C, 10 psig.

572F
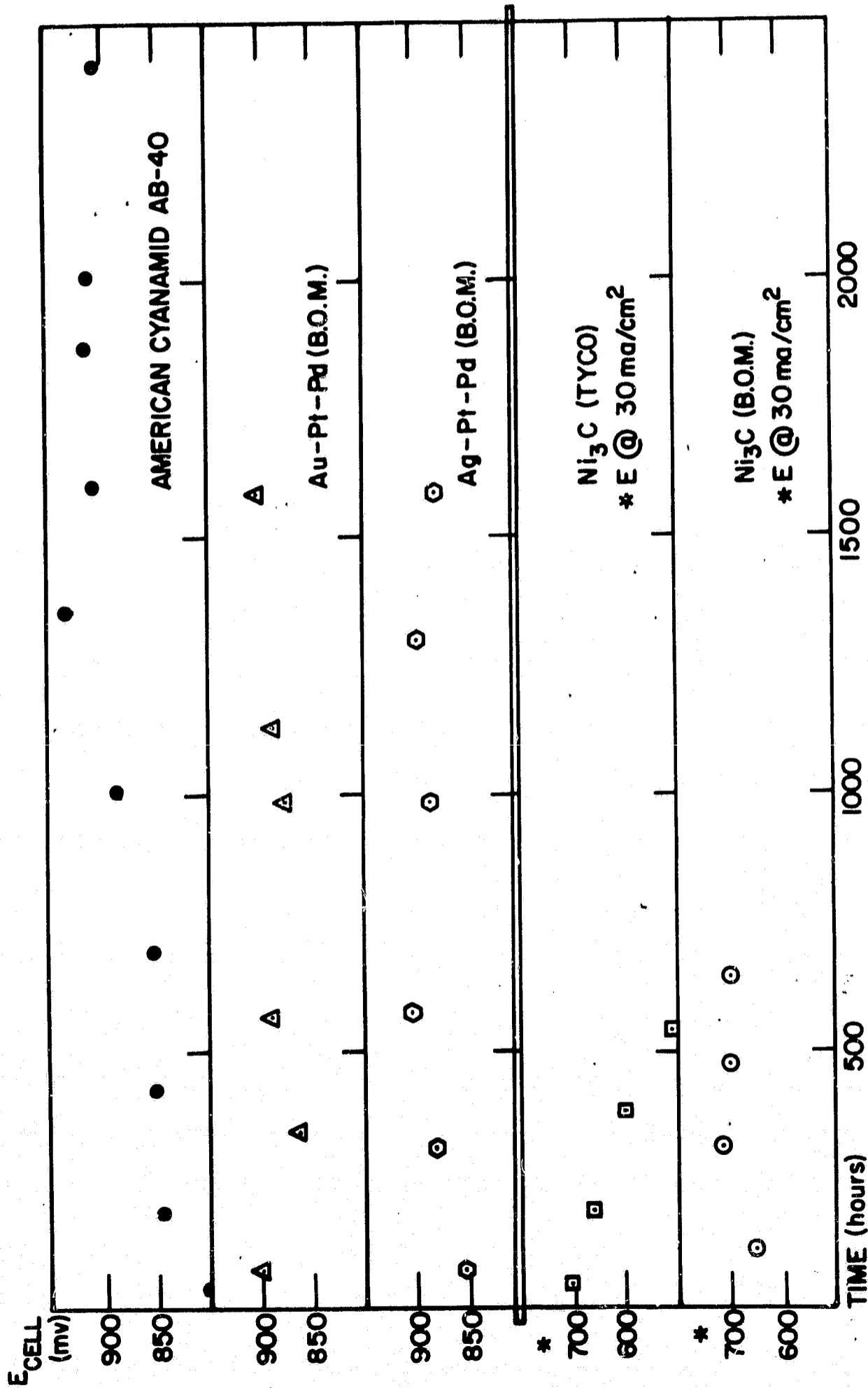
TABLE XXXI

Life Testing: Voltage-Current Data

American Cyanamid Pt-AB-40   40 mg/cm^2
80°C 35% KOH 10 psig

t	E (mv)	I (amps)	t	E (mv)	I (amps)
45 hrs	850	4.05	1003 hrs	846	7.05
	875	3.6		880	4.85
	895	2.83		900	3.84
	915	2.15		920	2.70
	935	1.6		940	1.80
	951	1.2		960	1.05
	975	0.75		980	0.64
	995	0.50			
			1361 hrs	910	7.62
190 hrs	850	4.87		925	6.14
	870	3.85		937	5.00
	890	3.15		947	4.05
	920	2.00		960	3.11
	940	1.40		975	2.00
	960	0.92		1000	1.00
	983	0.53			
			1600 hrs	888	7.18
330 hrs	850	4.02		910	5.14
	860	3.60		925	4.07
	875	2.80		940	2.97
	900	2.20		955	2.03
	920	1.64		980	1.02
	940	1.15			
	960	.75	1870 hrs	892	7.06
	980	.45		915	5.00
				926	4.07
427 hrs	850	5.15		938	3.15
	880	3.50		956	2.07
	902	2.82		980	0.95
	922	2.07			
	943	1.40	2012 hrs	880	7.10
	964	.90		910	5.12
	985	.52		923	4.03
				938	3.10
694 hrs	845	5.72		955	2.02
	860	4.54		980	0.97
	880	3.62			
	900	2.75			
	920	2.00			
	940	1.45			
	960	0.85			
	980	0.50			

TABLE XXXI (Cont.)

American Cyanamid

t	E (mv)	I (amps)
2422 hrs	877	7.00
(20 psig)	894	6.00
	907	5.00
	925	4.00
	942	3.15
	960	2.10
	992	1.00
2856 hrs	890	7.10
	900	6.00
	912	5.00
	925	4.00
	925	4.00
	938	3.00
	956	2.00
	980	1.00
3011 hrs	884	7.00
	895	6.00
	905	5.10
	918	4.05
	932	3.10
	952	2.00
	980	1.00

TABLE XXXI (Cont.)

TYCO Pt #73-79 (L-6) 20 ma/cm^2 30% PTFE

t	E (mv)	I (amps)	t	E (mv)	I (amps)
45 hrs	810	4.16	1362 hrs	870	6.98
	832	3.70		883	6.07
	852	3.14		897	5.03
	875	2.60		910	4.00
	895	2.04		925	2.98
	916	1.50		943	1.98
	937	1.04		970	0.95
	956	0.68		994	0.48
	977	0.42			
	995	0.25	1600 hrs	860	7.03
				885	5.04
190 hrs	847	4.77		900	4.00
	870	3.90		916	3.00
	892	3.05		936	2.00
	922	1.95		963	1.00
	942	1.40			
	962	0.92	1747 hrs	877	7.03
	982	0.53		900	5.06
				914	4.00
427 hrs	862	5.15		927	3.00
	879	3.82		945	2.00
	905	2.90		970	1.00
	923	2.05		992	0.50
	943	1.33			
	964	0.82			
	984	0.48			
694 hrs	860	6.00			
	880	4.54			
	900	3.45			
	920	3.44			
	940	1.67			
	960	1.05			
	980	0.65			
1003 hrs	867	7.05			
	890	5.30			
	905	4.36			
	920	3.28			
	940	2.15			
	960	1.25			
	980	0.75			

TABLE XXXI (Cont.)

Pt-Au 70/30 #F-20 (L-1) 20 mg/cm^2 20% PTFE

t	E (mv)	I (amps)	t	E (mv)	I (amps)
44 hrs	907	7.00	1166 hrs	880	7.00
	928	5.03		892	6.00
	942	4.00		900	5.00
	955	3.00		917	4.00
	977	2.00		930	3.00
	998	1.00		950	2.00
				974	1.00
210 hrs	925	7.88		990	0.50
	934	7.00			
	945	6.00	1345 hrs	873	7.00
	953	5.00		885	6.00
	967	4.00		897	5.00
	980	3.00		912	4.00
	996	2.00		927	2.95
	1016	1.00		945	2.00
				970	1.00
356 hrs	915	7.75			
	924	7.00	1500 hrs	870	7.00
	935	6.00		880	6.00
	943	5.00		894	5.00
	955	4.00		906	4.00
	967	3.00		923	3.00
	987	2.00		942	2.00
	1008	1.00		967	1.00
665 hrs	912	7.70	1502 hrs	890	7.00
	918	7.05	(20 psig)	915	5.00
	928	6.00		945	3.00
	940	5.00		990	1.00
	950	4.00			
	965	3.00	1504 hrs	905	7.00
	982	2.00	(30 psig)	925	5.00
	1003	1.00		953	3.00
				998	1.00
955 hrs	896	7.00			
	907	6.05			
	918	5.00			
	934	4.00			
	948	3.00			
	967	2.00			
	990	1.00			

TABLE XXXI (Cont.)

Pt-Ag 30/70 22 mg/cm^2 20% PTFE

t	E (mv)	I (amps)	t	E (mv)	I (amps)
122 hrs	867	7.95	1440 hrs	900	7.00
	900	5.30		924	5.00
	920	3.60		938	4.00
	940	2.40		950	3.00
	960	1.25		965	2.00
	980	0.50		985	1.00
482 hrs	907	5.15	1682 hrs	905	8.00
	917	4.25	(20 psig)	915	7.00
	932	3.17		925	6.00
	950	1.90		935	5.00
	960	1.38		945	4.00
	970	0.95		955	3.00
				974	2.00
817 hrs	875	8.00		992	1.00
	885	7.05			
	895	6.00	2010 hrs	880	7.95
	907	5.00		887	7.00
	920	4.00		898	6.00
	933	3.00		910	5.00
	950	2.00		920	4.00
	970	1.00		935	3.00
				950	2.00
1150 hrs	894	7.92		970	1.00
	902	7.00		988	0.50
	922	4.98			
	933	4.00	2275 hrs	880	7.95
	943	3.00		890	7.00
	958	2.00		900	5.95
	978	1.00		912	5.00
				925	4.00
				938	3.00
				953	2.00
				975	1.00

TABLE XXXI (Cont.)

Pt-Os 80/20 #F18(L-1) 25 mg/cm^2 30% PTFE

t	E (mv)	I (amps)	t	E (mv)	I (amps)
142 hrs	787	8.20	1170 hrs	860	7.03
	810	7.00		886	4.98
	840	5.38		900	4.00
	860	4.20		917	2.98
	880	3.45		937	2.00
	900	2.50		965	1.00
	920	1.75			
	940	1.20	1460 hrs	857	8.05
	960	0.76		865	7.09
	980	0.45		892	5.00
				908	4.00
502 hrs	870	5.15		923	3.00
	890	4.04		943	2.00
	907	3.92		972	1.00
	930	2.02			
	950	1.27			
	970	0.77			
	990	0.47			
837 hrs	838	8.00			
	850	7.10			
	863	6.00			
	875	5.03			
	892	4.00			
	910	3.00			
	928	2.00			
	957	1.00			
	983	0.50			

TABLE XXXI (Cont.)

Pd-Au 40/60 #F-13 (L-1) 28 mg/cm^2 20% PTFE

t	E (mv)	I (amps)	t	E (mv)	I (amps)
45 hrs	852	6.57	1003 hrs	867	7.07
	875	5.30		895	5.10
	895	4.17		900	4.64
	916	3.20		920	3.46
	937	2.25		940	2.24
	956	1.50		960	1.27
	975	0.90		980	0.60
	995	0.505			
			1361 hrs	882	8.00
190 hrs	850	5.17		892	7.02
	870	4.30		905	5.97
	892	3.37		915	5.00
	922	2.17		926	3.98
	942	1.55		940	3.00
	962	0.98		974	0.95
	983	0.62		987	0.50
330 hrs	852	5.10	1600 hrs	870	8.02
	860	4.36		907	5.03
	880	3.52		922	3.96
	900	2.72		937	3.00
	920	2.03		955	2.00
	940	1.40		975	1.00
	960	.88			
	980	.50	1870 hrs	886	7.00
				910	5.00
427 hrs	850	5.67		925	4.00
	878	4.00		938	3.00
	902	3.07		953	2.00
	922	2.26		975	1.00
	943	1.57			
	963	.97	2012 hrs	862	8.00
	983	.55		874	7.05
				900	5.00
694 hrs	860	6.40		917	4.00
	880	5.15		930	3.00
	900	3.92		950	2.00
	920	2.83		970	1.00
	940	1.87			
	960	1.12			
	980	0.60			

TABLE XXXI (Cont.)

Pd-Au 40/60

t	E (mv)	I (amps)
2443 hrs	875	8.00
(20 psig)	886	7.05
	902	6.00
	914	5.00
	927	4.00
	942	3.00
	960	2.00
	982	1.00
	1000	0.50
2756 hrs	862	8.00
	872	7.00
	885	6.00
	900	5.00
	914	4.00
	930	3.00
	947	2.00
	970	1.00
	985	0.50
3020 hrs	825	8.00
	840	7.00
	860	6.00
	875	5.00
	895	4.00
	915	3.00
	937	2.00
	963	1.00
	980	0.50

TABLE XXXI (Cont.)

Pd-Au 50/50 #F-15 (L-1) 23 mg/cm^2 20% PTFE

t	E (mv)	I (amps)	t	E (mv)	I (amps)
194 hrs	830	6. 10	1100 hrs	878	8. 12
	880	3. 94		918	5. 00
	900	3. 14		932	4. 00
	920	2. 44		945	3. 00
	940	1. 82		963	2. 00
	960	1. 26		985	1. 00
	980	0. 34			
			1250	854	7. 07
503 hrs	845	7. 10		887	5. 04
	865	5. 80		910	4. 00
	880	5. 15		927	3. 00
	900	3. 95		947	2. 00
	920	2. 95		973	1. 00
	960	1. 27		993	0. 50
	980	0. 75			
862 hrs	857	8. 00			
	870	7. 05			
	883	6. 04			
	900	4. 98			
	917	4. 00			
	933	3. 00			
	950	2. 00			
	975	1. 00			

TABLE XXXI (cont.)

Pd-Au 70/30 #F-17 (L-1) 24 mg/cm^2 10% PTFE

t	E (mv)	I (amps)	t	E	I
26 hrs	860	4.74	1222 hrs	863	6.85
	880	3.95		892	5.00
	900	3.11		907	4.06
	920	2.43		928	2.97
	940	1.82		948	2.00
	960	1.27		978	0.95
	980	0.85			
335 hrs	825	4.84	1512 hrs	867	6.98
	840	4.35		895	⌣.05
	860	3.70		910	4.00
	880	3.00		928	3.00
	900	2.45		948	2.00
	940	1.35		975	1.00
	980	0.60		995	0.50
695 hrs	865	6.53			
	890	5.00			
	907	4.07			
	930	2.98			
	952	2.00			
	983	1.00			
	1007	0.50			

TABLE XXXI (cont.)

Pd-Au 60/40 + 50 wt % Ag_2O 32 mg/cm^2 20% PTFE

t	E (mv)	I (amps)	t	E (mv)	I (amps)
98 hrs	810	7.05	940 hrs	770	7.94
	850	5.00		795	7.00
	870	4.00		825	6.00
	890	3.00		853	5.00
	916	2.00		880	4.00
	945	0.96		903	3.00
	965	0.50		930	2.00
				965	1.00
				987	0.50
360 hrs	795	6.95	1273 hrs	780	7.00
	840	5.00		812	6.00
	864	4.00		832	5.00
	890	3.00		860	4.00
	915	2.00		888	3.00
	950	1.00		920	2.00
	968	0.50		957	1.00
				985	0.50
672 hrs	780	7.94			
	805	7.00			
	827	6.00			
	843	5.00			
	865	4.00			
	887	3.00			
	920	2.00			
	957	1.00			
	980	0.50			

TABLE XXXI (cont.)

Au-Pt-Pd (B. O. M.) #107-R (L-1) 39 mg/cm^2 20% PTFE

t	E (mv)	I (amps)	t	E (mv)	I (amps)
76 hrs	875	6.96	983 hrs	850	6.96
	900	4.97		869	6.00
	914	4.04		878	5.00
	930	3.00		897	4.00
	948	1.97		914	3.00
	975	1.00		935	2.00
				964	1.00
				990	0.50
671 hrs	865	5.95	1384 hrs	878	7.00
	890	5.00		890	6.00
	905	4.00		902	5.00
	920	4.00		915	4.00
	920	3.00		932	3.00
	945	2.00		950	2.00
	970	1.00		973	1.00
				995	0.50

TABLE XXXI (cont.)

Ag-Pt-Pd (B. O. M.) #100-R (L-1) 38 mg/cm^2 20% PTFE

t	E (mv)	I (amps)	t	E	I
76 hrs	827	7.05	983 hrs	812	7.95
	856	4.98		845	7.05
	872	4.02		865	6.00
	886	2.97		885	5.00
	907	1.98		903	4.00
	930	1.00		920	3.00
	998	.47		935	2.00
				955	1.00
				970	0.50
671 hrs	883	7.10	1584 hrs	842	8.05
	904	4.95		852	7.05
	914	4.00		865	6.00
	930	3.00		880	5.00
	945	2.00		892	4.00
	967	1.00		908	3.00
	980	0.50		926	2.00
				950	1.00
				967	0.50

TABLE XXXI (cont.)

Ni_3C (B.O.M.) #54-C 56 mg/cm^2 20% PTFE

t	E (mv)	I (amps)	t	E (mv)	I (amps)
116 hrs	500	2.85	646 hrs	500	3.36
	520	2.67		550	2.90
	540	2.54		600	2.45
	560	2.35		650	1.95
	580	2.25		700	1.50
	600	2.10		750	1.00
	620	1.95		800	0.53
	640	1.80		850	0.15
	660	1.65			
	680	1.47			
	700	1.30			
	740	0.95			
	780	0.62			
	840	0.20			
478 hrs	510	3.70			
	540	3.36			
	600	2.72			
	640	2.30			
	680	1.86			
	725	1.40			
	762	1.00			
	805	0.60			
	840	0.25			

TABLE XXXI (cont.)

Ni_3C - TYCO #69 (L-1) 25 mg/cm^2 10% PTFE

t	E (mv)	I (amps)	t	E (mv)	I (amps)
190 hrs	500	3.15	530 hrs	500	1.50
	600	2.26		550	1.35
	700	1.35		600	1.17
	750	0.43		650	0.95
	800	0.50		700	0.78
	850	0.15		750	0.57
				800	0.37

SECTION 5

A MATHEMATICAL TREATMENT OF THE POROUS
PTFE BONDED ELECTRODES

I. INTRODUCTION

The theory of porous electrodes has been the object of many publications. A general discussion of the behavior of fully flooded and gas diffusion porous electrodes both for steady state and transient responses can be found in a recent monography by De Levie[19]. The present treatment is concerned only with the steady state behavior of gas diffusion electrodes, which although studied less than flooded electrodes, have also been the subject of attention in the last few years.

Four main models have been currently used to explain the behavior of the gas diffusion electrode: the Simple Pore Model, the Thin Film Model, the Surface Migration Model, and the Dual Scale of Porosity Model.

Two comments should be made at this point. First, the applicability of a certain model will depend on electrode structure; thus it can be expected that a model which applies to a Teflon bonded electrode will not apply to a Bacon sintered electrode and vice versa. Second, many of the models are microscopic models concerned with one element of the electrode producing the current, (such as a thin film or a finite contact meniscus, etc.). While the relationship between theory and the results obtained with the model system is straightforward, the way in which the electrode is composed by the simple elements is usually not clear at all. Thus a comparison between theory and results obtained with an actual electrode is virtually impossible. A few models, on the other hand, are macroscopic and treated as continuum systems. The application of these models is limited by their abstract nature. From this point of view, our model is an hybrid, with a microscopic consideration of elements (which are easily visualized in the total electrode) and with a macroscopic treatment of the elements of the electrodes ('flooded cylinders').

A. The Simple Pore Model

This model as developed by Austin, et al.[20], is a modification of the old theory[21] of the three-phase boundary according to which gas, metal and electrolyte came in contact in a boundary line.

In this model, as in the older one, the electrolyte does not cover the walls of the pore with a thin film, but its surface forms practically a 90° angle with the walls of the pore. In contrast to the old model, the gas, after diffusing through the pore to the electrolyte surface, dissolves and is transported to the submerged metallic electrode surface where it is consumed.

A similar model applies, according to Austin and Almaula[22], to the Teflon bonded electrode. These authors suggest for this electrode that only a thin layer near the plane electrode-electrolyte surface is wetted and takes part in reaction. Limiting currents and polarization are due to mass transfer of dissolved hydrogen to submerged platinum-black particles. According to these authors, only 2 - 5% of the electrode area is wetted. This is in contrast to our experiments[23] which show almost 100% wetting of the electrode surface area.

Srinivasan, Hurwitz and Bockris[24] have treated a one-dimensional Simple Pore Model in presence of activation, concentration and ohmic polarization. They suggested that a circulating system would greatly reduce concentration polarization and improve performance.

B. The Thin Film Model

According to Will[25, 26] the walls of a pore are covered by an electrolyte film. Reactant gas diffuses across the film and reacts on the pore wall (above the electrolyte bulk). Ionic migration along the electrolyte film defines the current distribution along the length of the pore and limits the length which is effective for current production.

Will has treated this model mathematically[26] for the case of diffusion and ohmic control and has experimentally[25] confirmed his conclusions using a pre-wetted, half immersed Pt-wire in H_2SO_4 under H_2 atmosphere. These conclusions are as follows:

(1)   At polarizations smaller than 10 mv, 99% of the current is produced in a zone of 0.35 mm from the electrolyte meniscus.

(2)   For polarizations smaller than 10 mv, a linear dependence of the total current on the applied potential is calculated which checks quantitatively with his experimental results on half immersed bright Pt electrodes in 8 N H_2SO_4 .

(3)   For polarization larger than 100 mv the current voltage curve is the type $i = K \sqrt{E}$.

(4)   The relative contributions of meniscus (if meniscus is assumed in addition to film) to the total current depend on film thickness and electrolyte concentration. For a film 1 μ thick 8 N H_2SO_4 and E = 0.4 v , the meniscus contributes 0.26 ma and the film 1.16 ma.

(5)   The reaction zone is confined to a narrow band close to the upper meniscus edge. In the numerical example given in 4, 0.35 mm of meniscus and 0.38 mm of film are responsible for 98% of the total current.

(6)   For a half immersed electrode, a film thickness of 1.5 μ is deduced.

In a more recent publication[27] Will has made confirming measurements using horizontal electrodes with rather thick (1 mm) electrolyte films. He concludes that considerable stirring ought to exist, to explain the lower than predicted concentration gradients along the film. It is questionable, however, whether the conclusions reached with these rather thick films can be scaled down to thin films. In addition, concentration gradients can be explained by a "distillation mechanism" (see ref. 33 and our assumption no. 4) on page   ).

Iczkowski[28] introduced, in his treatment of the Thin Film Model, activation polarization in addition to diffusion and ohmic polarization. He solved numerically his equations for the O_2-reduction in NaOH on Ni .

Rockett and Brown[29] also treated the complete case for the oxygen electrode of the Bacon fuel cell.

Srinivasan and Hurwitz[30] solved numerically the equations of the Thin Film Model with simultaneous activation, concentration and ohmic polarization using dimensionless parameters which allow rather general application.

Lindstrom[31] and Lindholm et al.[32] , have applied the Thin Film Model to porous electrodes of the Bacon type. An important contribution of this work is the consideration of transport limitations in gas phase. Differences of polarization between H_2-O_2 and Ar-O_2 mixtures at high drains confirm the importance of this limitation. This limitation will be important under certain conditions of current drain, gas dilution, and electrode geometry. It is interesting to note that conductivity and volume measurements of the electrolyte in the pore, as well as the effect of pressure differential on current, are interpreted by the Swedish workers as a "thinning out" of the film at higher pressures. The possibility that pressure may affect large amounts of electrolyte enclosed in small pores is not considered.

Bennion and Tobias[33] have studied the O_2-electrode according to the Thin Film Model under consideration of axial diffusion of electrolyte. These authors considered also the possibility that water transfer from one end of the film to the other may occur through the gas phase.

C. Variants to Thin Film Model

Models considering the shape of a meniscus can be considered as half-way between the Thin Film Model and the Simple Pore Model. An example is to be found in the work of Cahan[34] . This work can be discussed better by separating (1) the theory and experiments on "slit cell," (2) the extension to porous electrodes, and (3) the work on thin electrodes.

(1) Slit cell. This work is limited to the study, experimentally and theoretically, of the behavior of two partially immersed, parallel, smooth electrodes in an atmosphere of reactant gas. Cahan postulates, based on optical measurements, that a continuous Thin Film does not exist and proposes a Finite Contact Angle Model in which the current is drawn from the meniscus edge. The mathematical treatment, after suitable simplifications, is very similar to that of a Thin Film Model in presence of activation[28-30] but taking into account the geometry of the meniscus. A numerical solution

using a computer program has been obtained for H_2-oxidation and O_2-reduction on Pt in 1 N H_2SO_4. The theory agrees with the experimental results for the slit cell (although it should be noted that considerable uncertainty exists with regard to the i_o of both H_2- and O_2-electrode reaction on Pt electrodes in acid, so that this i_o could be considered as a calibration factor). Other conclusions reached by Cahan are as follows:

- (a) That current is proportional to square root of C (or p).
- (b) That current-potential curves are almost linear.
- (c) That the current in the slit cell is produced in a very small fraction of meniscus - 10^{-4} to 10^{-5} cm from tip.
- (d) That in some cases a "meniscus heating effect" can be observed.

(2) <u>Extension to porous electrodes.</u> Throughout the discussion of the behavior of the slit cell there is a tendency on Cahan's part to extend the conclusions to porous electrodes. Thus, from fact that only 10^{-4} to 10^{-5} cm length, from the tip of an ideal single meniscus of the slit cell is utilized to produce current, Cahan concludes that "99% or more of a uniformly distributed catalyst in a porous electrode is wasted, being out of the area of prime activity "[34].

We do not find any justification for the extension of the theory of a single very special meniscus to a porous electrode. Our work on the "flooded agglomerate model" of the Teflon bonded electrode will show that in some cases almost 100% utilization of heavily loaded electrodes is possible. Indeed, the experimental results for these electrodes can be explained better by assuming high utilization of catalyst.

(3) <u>Work on thin electrodes.</u> Electrodes consisting of a 50 Å layer of platinum (250 $\mu g/cm^2$ or less) deposited on Vycor have shown very high electrochemical performance as H_2-electrodes. These findings are constructed by Cahan as a confirmation that the real porous electrode works according to a Finite Contact Angle Model. We think that this work reflects the high exchange current of the hydrogen reaction and relatively good transport conditions. Such a thin structure could indeed be used as H_2-electrode

in acid if the problems of stability, H_2O removal and ohmic contact could be solved. From consideration of the surface area available in 50 Å films and the exchange current of O_2-electrode, it seems to us that a thin (50 - 200 Å) O_2-electrode, having the same performance as that of presently available electrodes is impossible using any of the known catalysts.

Borucka and Agar[35] have also treated the case of a defined meniscus using an electric conductance analog.

D.   The Surface Migration Mechanism

Migration of hydrogen on the surface of electrodes has been suggested by several authors[36-43] . It seems, however, that the surface diffusion coefficient determined by independent methods is too low[38] to contribute considerably to mass transport.

E.   Double Scale of Porosities Model

Burshtein and co-workers[39] have treated the Bacon type electrode, assuming that there is a spectrum of porosities, so that small pores are flooded -- a model theory initiated by Markin [24, 25]. Electrodes with an emphasized double scale of porosities have been constructed and tested experimentally. The fraction of flooded pores is adjusted by electrode design and by regulation of pressure differential. Flooding of small pores increases the ionic conductivity across the electrode and results in a deeper utilization than with the Thin Film Model. It should be noted that the experimental results of Brown and Rockett[38] with so-called "flooded electrodes" and the effect of pressure on activity observed by Lindstrom[31, 32] could be used to confirm the "double scale of porosity model," although these authors give a different interpretation.

Burshtein and co-workers in their statistical treatment of the electrode neglect the diffusion of dissolved species and use a linear relationship between local current density and voltage. They are unable to prove or disprove their theory based on the experimental data.

A quantitative treatment for a somewhat related model has been given by Grens II [42]. Grens considers gas filled macropores and electrolyte filled micropores. The electrode is represented by two one-dimensional continuum

systems (a macro- and a micro-pore system) which are joined by a series of "link-ing pores," the length of which is short compared with the length of the micro-pores. Some limitations of this treatment (which are not present in our treatment) are that diffusion is assumed to be linear and that migration of ionic species is considered. (It is <u>implicitly</u> assumed that concentration equalization in the micro-pore phase is not possible by evaporation and concentration; i.e. Q-term of ref. 17 is unity.) The diffusion of reactant gas is considered along the trans-veral direction of the electrode; no gas diffusion in the micropore phase per-pendicular to the micropore/macropore interface is considered. In effect, the thickness of flooded areas does not appear in treatment. Also, link pores are assumed, the dimensions of which are arbitrarily selected.

II. THE FLOODED AGGLOMERATE MODEL OF THE TEFLON BONDED ELECTRODE

A. Qualitative Description

The Teflon bonded electrode seems to us an ideal case of structure with double scale of porosity. According to a qualitative description by Giner [43,44] the working mechanism of this structure can be explained by assuming, as shown in Fig. 32, that the catalyst particles form porous (and electronically conductive) agglomerates which, under working conditions, are flooded with electrolyte. The catalyst agglomerates are kept together by the Teflon binder which creates hydrophobic gas channels. As current is drawn from the electrode, reactant gas diffuses through the channels, dissolves in the electrolyte contained in agglomerates, and after diffusing a certain distance, reacts on available sites of catalyst particles.

This qualitative explanation of the working mechanism based on the flooded agglomerate is confirmed by our own measurements which show (1) that the catalyst area in contact with electrolyte is the same when the Teflon bonded electrode is working as a gas diffusion cell electrode as when it is completely flooded with electrolyte *, (2) that the microporosity of the agglomerates is about 90%, i.e. 10% catalyst and 90% electrolyte. (Microporosities of about 80% have also been measured by Horowitz [45], who also assumes the same qualitative model.)

B. Mathematical Treatment

One way of quantitatively treating this working mechanism is to substitute flooded agglomerates by a porous cylinder of radius r_o and length h (as shown in Fig. 33), in which catalyst particles and electrolyte are homogeneously dispersed as a continuum. (Microporosity, θ, is defined as the volume of electrolyte per total volume of cylinder.) The porous cylinder is perpendicular to the external surface of the electrode. During operation, gas arrives at the cylinder in a direction perpendicular to its axis and diffuses to its center along the coordinate r, with simultaneous bulk re-

---

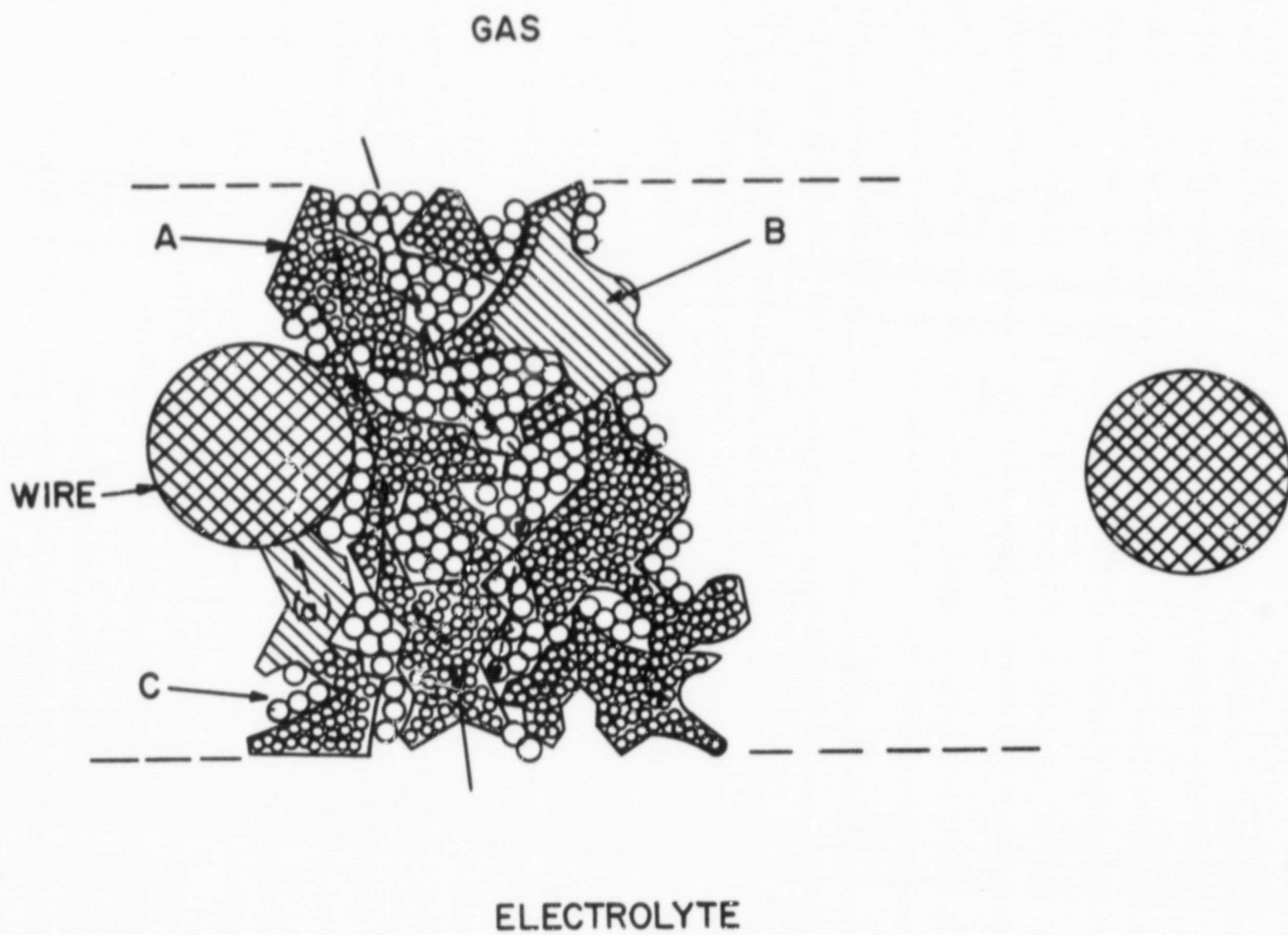* This is conflict with the value of 2 to 5% reported by Austin and Almaula [22].

Fig. 32 Schematic representation of a hydrophobic, porous electrode made of Teflon-bonded platinum black.

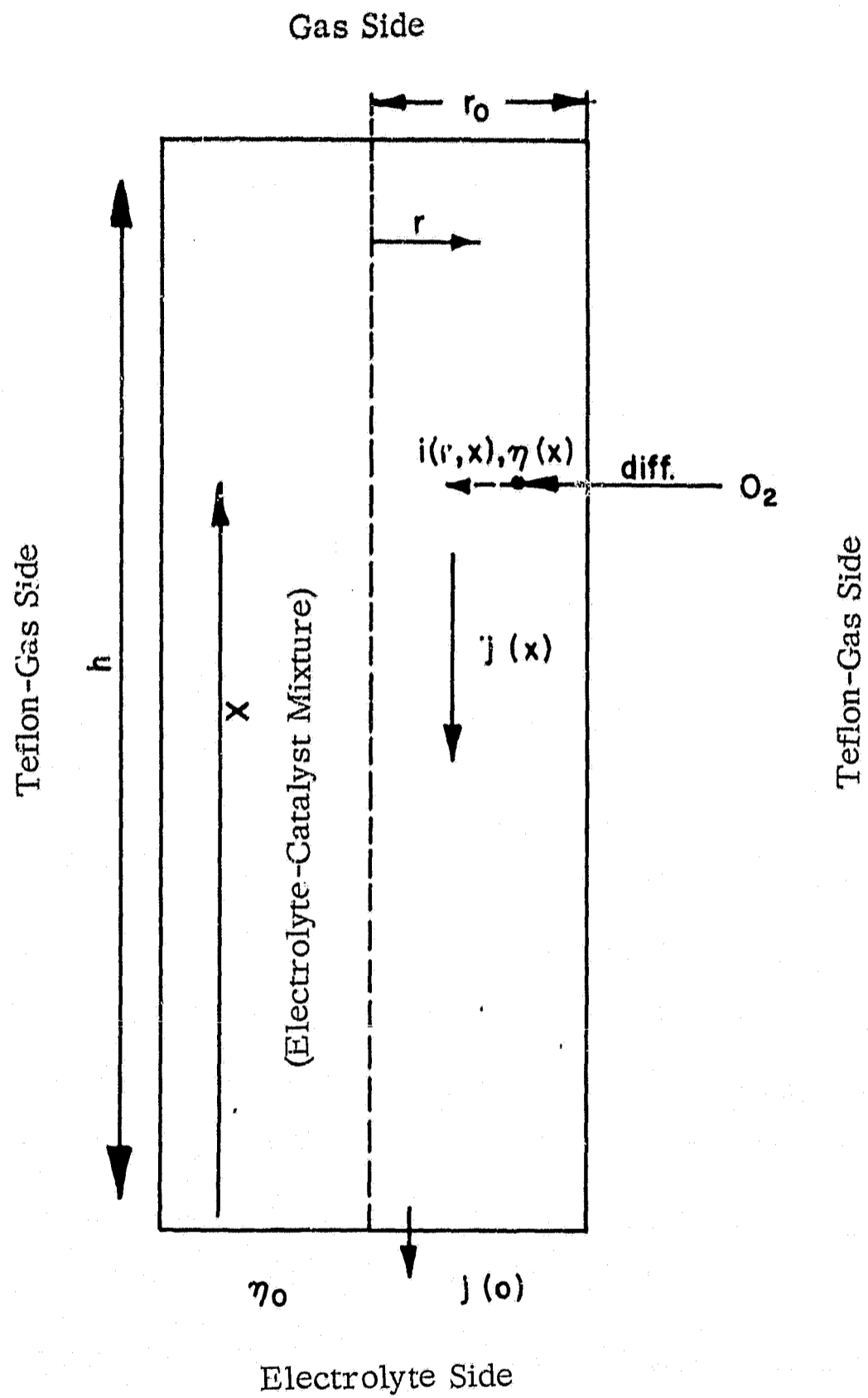A) Catalyst particle; B) Agglomerate; C) Teflon particle.

- 195 -

572F

Fig. 33 Schematic representation of flooded cylinder.

- 196 -

572F

action on catalyst particles in the diffusion path. Ionic current is conducted in the direction x parallel to the cylinder axis.

1. Assumptions

For the mathematical treatment we assume that:

(1) The electrode is made up of a number of porous cylinders of catalyst flooded with electrolyte. These cylinders are perpendicular to the external surface of the electrode.

(2) Electrolyte and catalyst are homogeneously mixed as a continuum.

(3) The intrinsic activity of the catalyst is constant throughout the cylinder.

(4) Equilibration of electrolyte concentration in cylinders occurs efficiently via an evaporation-condensation process.

(5) The local current density is directly proportional to the local concentration of reactant; i.e. an expression such as eq. (1) is pertinent.

(6) The voltage in the cylinder changes only in the axial direction and diffusion of dissolved gas occurs only in the radial direction.

(7) There are no transport limitation in the gas phase.

(8) There are no kinetic limitations in the process of gas dissolution.

(9) There is no electronic iR-drop in cylinders.

(10) There is no convention inside the cylinders.

In order to extend the theory of a single cylinder to the complete electrode we will further assume at this point that:

(11) The radius of all porous cylinders has the same value. (Under these conditions the number of cylinders per cm^2 of electrode (N) is related to a measurable macroscopic factor, which we will call macroporosity (β), by the expression $\beta = 1 - N\pi r_o^2$).

2. General Treatment

The local current density $i(r, x)$, i.e. current per unit of "real area," at a point (r, x) in the cylinder is assumed to be expressed by equation:

$$i = i_0 \left[\frac{C(x, r)}{C_o} \exp\left[\alpha z \eta(x) / \phi \right] - \exp\left[-(1 - \alpha) z \eta(x) / \phi \right] \right] \qquad (1)$$

The diffusion of the gas in the cylinder (with a simultaneous bulk consumption given by $i\gamma/nF$, γ = surface to volume ratio) follows the 2nd Fick's law for cylindric diffusion:

$$\bar{D} \frac{\partial^2 C(x, r, t)}{\partial r^2} + \bar{D} \frac{1}{r} \frac{\partial C(x, r, t)}{\partial r} - \frac{i\gamma}{nF} = \frac{\partial C(x, r, t)}{\partial t} \qquad (2)$$

At steady state:

$$\frac{\partial C(x, r, t)}{\partial t} = 0$$

and therefore:

$$\bar{D} \left\{ \frac{\partial^2 C}{\partial r^2} + \frac{1}{r} \frac{\partial C}{\partial r} \right\} = \frac{i\gamma}{nF} = \frac{\gamma i_0}{nF} \left\{ \frac{C(x, r)}{C_o} \exp \frac{\alpha z \eta(x)}{\phi} - \exp \frac{(\alpha - 1) z \eta(x)}{\phi} \right\} \qquad (3)$$

Boundary conditions:

$$\frac{\partial C}{\partial r} = 0 \text{ at } r = 0, \quad C = C_o \text{ at } r = r_o$$

The solution of this equation for the r-variation of C is straightforward:

$$C = C_0 \exp - \frac{z\,\eta}{\phi} + \text{(the solution of the homogeneous equation}$$

$$\frac{\partial^2 C}{\partial r^2} + \frac{1}{r}\,\frac{\partial C}{\partial r} - \left[\frac{\gamma\,i_0}{n\,F\,\bar{D}\,C_0}\,\exp\frac{\alpha z\eta}{\phi} \right] C = 0 \biggr) \quad (4)$$

The solution of the homogeneous equation can be expressed in terms of modified Bessel functions.

Since $\partial C/\partial r = 0$ at $r = 0$, the solution for C is:

$$C = C_0 \exp - \frac{z\,\eta}{\phi} + k_1 I_0 \left(\left[\frac{\gamma\,i_0\,r^2}{n\,F\,\bar{D}\,C_0}\,\exp\frac{\alpha z\,\eta}{\phi} \right]^{\frac{1}{2}} \right), \quad (5)$$

where I_0 is standard notation for the modified Bessel function of zero order and k_1 is a constant.

k_1 is fixed by the requirement that $C = C_0$ at $r = r_0$

$$k_1 = \frac{C_0\left[1 - \exp -\left(\frac{z\,\eta}{\phi}\right)\right]}{I_0 \left(\left[\dfrac{\gamma\,i_0\,r_0^{\,2}}{n\,F\,\bar{D}\,C_0}\,\exp\dfrac{\alpha z\,\eta}{\phi} \right]^{\frac{1}{2}} \right)} \quad (6)$$

$$\text{or} \quad k_1 = \frac{C_0\left[1 - \exp -\left(\frac{z\,\eta}{\phi}\right)\right]}{I_0\ (q)}$$

$$\text{with} \quad q = \left[\frac{\gamma\,i_0\,r_0^{\,2}}{n\,F\,\bar{D}\,C_0}\,\exp\frac{\alpha z\,\eta}{\phi} \right]^{\frac{1}{2}}$$

Thus equation (5) gives the variation of C with the radius of the cylinder (agglomerate) at a given value of x. E (or η) is only a function of x (coordinate in the axis direction) according to ohm's law:

$$\frac{d\eta}{dx} = -\frac{j(x)}{\pi r_o^2 \,\overline{\kappa}} \tag{7}$$

At the same time:

$$-\frac{dj(x)}{dx} = 2\pi\gamma \int_0^{r_o} i\, r\, dr \tag{8}$$

From equations (7) and (8):

$$\frac{d^2\eta}{dx^2} = \frac{2\gamma}{r_o^2\,\overline{\kappa}} \int_0^{r_o} i\, r\, dr . \tag{9}$$

The solution for C (equation (5)) can be used to solve equation (9) for η:
Thus multiplying equation (3) by r d r and integrating gives:

$$\overline{D}\, r_o \left[\frac{\partial C}{\partial r}\right]_{r=r_o} = \frac{\gamma}{nF} \int_0^{r_o} i\, r\, dr \tag{10}$$

from (9) and (10)

$$\frac{d^2\eta}{dx^2} = \frac{2\, n\, F\, \overline{D}}{\overline{\kappa}\, r_o} \left(\frac{\partial C}{\partial r}\right)_{r=r_o}$$

From solution (5):

$$\left[\frac{\partial C}{\partial r}\right]_{r=r_o} = k_1 \left[\frac{\gamma i_o}{n\,F\,\overline{D}C_o}\exp\frac{\alpha z\eta}{\phi}\right]^{\frac{1}{2}} I_o' \left(\left[\frac{\gamma i_o r_o^2}{n\,F\,\overline{D}\,C_o}\exp\frac{\alpha z\eta}{\phi}\right]^{\frac{1}{2}}\right) \tag{11}$$

Also $I_o'(x) = I_1(x)$, where I_1 is the modified Bessel function of order 1, or if we use previous definition of q, the equation for η is

$$\frac{d^2\eta}{dx^2} = \frac{2n\,F\bar{D}C_o}{r_o^2\,\bar{\kappa}}\left[1 - \exp\left(-\frac{z\,\eta}{\phi}\right)\right]\frac{q\,I_1(q)}{I_o(q)} \qquad (12)$$

Boundary conditions $\eta = \eta_o$ at $x = 0$, $d\eta/dx = 0$ at $x = h$.

At this stage it is convenient to introduce scaled variables. Define this by $\eta' = \frac{\eta}{\eta_o}$, $x' = \frac{x}{h}$ where η_o is the measurable overvoltage at the electrolyte.

Then

$$\frac{d^2\eta'}{dx'^2} = \frac{2n\,F\,\bar{D}\,C_o h^2}{\eta_o\,\bar{\kappa}\,r_o^2}\left[1 - \exp\left(-\frac{z\,\eta_o}{\phi}\,\eta'\right)\right]\frac{q\,I_1(q)}{I_o(q)} \qquad (13)$$

Boundary conditions: $\eta' = 1$ at $x' = 0$, $d\eta'/dx' = 0$ at $x' = I$.

It can be seen that equation (13) expresses η' only as a function of x' and a series of measurable constants. This equation can be solved with a relatively simple computer program. From this computer program we want to know:

(a) The local current at constant x' as a function of the cylinder radius. This is a measure of the depth utilization of the cylinder (or agglomerate), which is controlled mainly by diffusion.

(b) The current production at different values of x'. This is a measure of the depth of utilization of the electrode, which is controlled mainly by ohmic drop.

(c) The current density per unit area of electrode: i.e. the measurable current density.

Depth Utilization of Cylinder. The local current can be obtained from equation (1) since we know C (x, r) and η (r) from equations (5) and (13). Thus substituting solution (5) in equation (1) one obtains:

$$i = \frac{i_0 \, k_1}{C_0} \left(\exp \frac{\alpha z \eta}{\phi'} \right) I_0 \left(\left[\frac{\gamma i_0 \, r_0^2}{n F \bar{D} C_0} \exp \frac{\alpha z \eta}{\phi'} \right]^{\frac{1}{2}} \frac{r}{r_0} \right)$$ (14)

or

$$i = p \, I_0 \left(q \, \frac{r}{r_0} \right)$$ (15)

where p and q, which we will call distribution parameters, are suitably defined. From q the utilization of the catalyst as a function of r for a given x can be obtained, as shown in Fig. 34.

Depth Utilization of Electrode. Other information of a pertinent nature is the current production for different cross sections of the cylinder. This current is, of course, d j(x)/dx. The total current per cylinder across the surface x = constant, is

$$j \, (x) = - \pi \bar{\kappa} r_0^2 \frac{d\eta}{dx} ,$$ (16)

or expressed in nondimensional variables.

$$j \, (x) = - \frac{\pi \bar{\kappa} r_0^2 \, \eta_0}{h} \frac{d\eta'}{dx'} .$$ (17)

The current derivative:

$$\frac{dj}{dx} = - \frac{\pi \bar{\kappa} r_0^2 \, \eta_0}{h^2} \frac{d^2\eta'}{dx'^2}$$ (18)
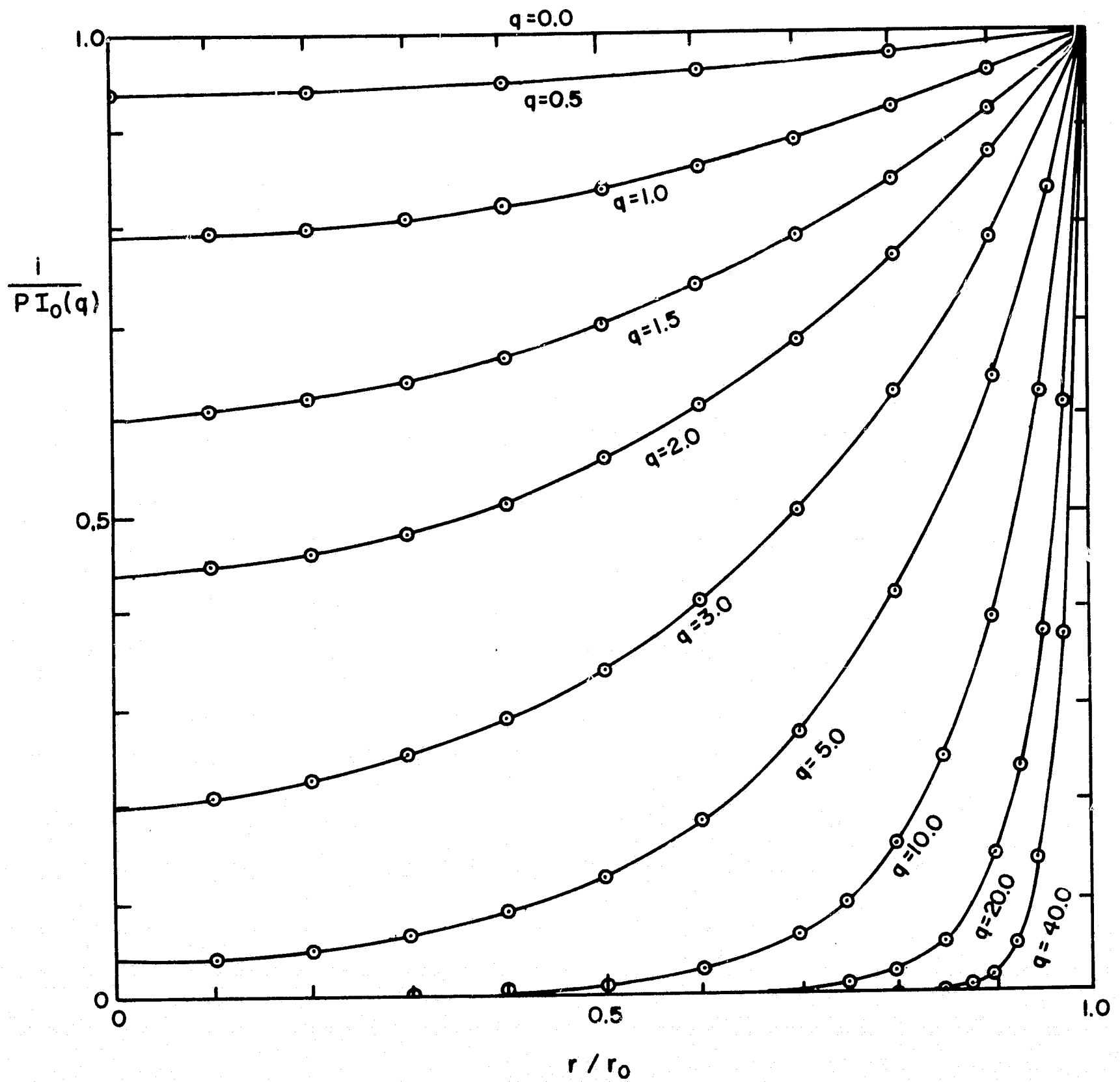
Fig. 34 Radial distribution of current in cylindric agglomerate
as function of second distribution parameter of Eq. 15.

Electrode Current Density.   The current density per unit area of electrode surface I(o) can be obtained from the total current of a cylinder j(o) by:

$$I(o) = j(o) \frac{1 - \beta}{\pi r_o^2} \qquad (19)$$

or

$$I(o) = \frac{-\bar{\kappa} \, \eta_o \, (1 - \beta)}{h} \left(\frac{d\eta'}{dx'} \right)_{x' = o} \qquad (20)$$

3. Application of the Model to Oxygen Electrode

In the first application of the model we have used the computer program to calculate (a) local current as function of cylinder radius, (b) current generated at different planes perpendicular to cylinder axis, and (c) measurable electrode current density.

The program, with pertinent comments, is presented in the Appendix.

We have fixed the following data which we feel is realistic for a Teflon bonded platinum electrode operating as oxygen electrode at 80° C in 30% KOH:

$$\eta_o = 0.3 \text{ volts}$$

$$\alpha = 0.5$$

$$n = 4 \text{ equiv/mol.}$$

$$D = 2 \times 10^{-5} \text{ cm}^2/\text{sec} \qquad \text{(extrapolated from ref. 48)}$$

$$\kappa = 0.75 \, \Omega^{-1}\text{cm}^{-1} \qquad (47)$$

$$S = 20 \text{ m}^2/\text{g} \qquad (23)$$

$$w = 20 \times 10^{-3} \text{ g/cm}^2 \qquad (23)$$

$$h = 0.02 \text{ cm} \qquad (23)$$

$$C_o = 5.5 \times 10^{-8} \text{ mol/cm}^3 \qquad (46)$$

$$z = 1$$

$$(\beta = 0.032)$$

$$\rho = 20 \text{ g/cm}^3$$

Indirect structural variables are:

$$\gamma = S\rho(1-\theta) = 2 \times 10^5 \text{ cm}^2/\text{g} \times 20 \text{ g/cm}^2 (1-\theta) = 4 \times 10^6 (1-\theta) \text{ cm}^{-1}$$

$$\beta = 1 - \frac{w}{\rho h (1-\theta)} \text{ , macroporosity, and}$$

$\bar{D} = \theta D$ and $\bar{\kappa} = \theta \kappa$. (The tortuosity factor is taken as unity for the purpose of the present example.)

As variables we have taken microporosity θ, cylinder radius r_o, and exchange current i_o.

The computer tabulations are reproduced in the Appendix. These tables were obtained for $\theta = 0.5, 0.7,$ and 0.9, $r = 10^{-3}$, 10^{-4} and 10^{-5} cm, $i_o = 10^{-6}$, 10^{-7}, and 10^{-8} A/cm^2 *. The columns of these tables show (a) position $= x/h$; (b) relative potential $= \dfrac{\eta}{\eta_o}$; (c) current in amps flowing through a plane x; (d) current derivative, i.e. current produced at the plane x; and (e) distribution parameter p, (see equation (15)), and distribution parameter q (see equation (15) and Fig. 34). At the end of each tabulation the measurable current density (in A/cm^2) is shown. Table XXXII shows a summary of effect of θ, r and i_o on electrode current density.

In all cases, decreasing the radius from 10^{-3} to 10^{-4} cm has a large effect on current, but a further decrease below 1 micron has little effect on performance. This finding, of course, applies only under the diffusion conditions of this example.

According to Table XXXII current densities higher than 150 ma/cm^2 are obtained for $i_o = 10^{-6}$ A/cm^2 and $r_o \leq 10^{-4}$ cm. For $r_o \leq 10^{-4}$ and $i_o < 10^{-7}$ the current density is proportional to i_o. These conditions correspond to high radial Pt utilization (small values of q). The exact range of high Pt-utilization will be discussed in the following.

---

* Our own work with smooth platinum in KOH solutions shows $i_o = 5 \times 10^{-7}$ A/cm^2 at $80°$C[49,50].

- 205 -

When the Pt is well utilized, the current is also independent of micro-porosity (θ). This is due to the fact that in this range the current from cylinder is directly proportional to $(1 - \theta)$, (Table XXXII), and the number of cylinders is inversely proportional to $(1 - \theta)$.

A summary of the internal voltage drop as a function of θ, i_o and r_o is given in Table XXXIII which shows that in all cases the internal voltage drop is small. For $\theta = 0.9$ and $r_o = 10^{-5}$ a voltage drop of only 11 mv between front and back of the electrode is observed, even if the current density is 386 ma/cm^2. Correspondingly, the current produced at the plane $x' = 1$ is only 10% lower than the current at $x' = 0$. For $\theta = 0.5$, on the other hand, the internal voltage drop is 55 mv and the current produced at the plane $x' = 1$, 58% lower than at the plane $x' = 0$. This relatively poor transversal utilization of the electrode with $\theta = 0.5$ explains in part why, for instance, at $i_o = 10^{-6}$ and $r_o = 10^{-4}$ the current for this value of θ is only half of the current when $\theta = 0.9$. The obvious solution of using electrodes of high degree of microporosity has to be re-examined after considering limitations of gas phase diffusion: Increase of microporosity (θ) at constant electrode loading (w) and thickness (h) results in an decrease of macroporosity (β) and therefore in a decrease of the residual volume. This volume includes volume of gas channels, of Teflon particles, and of wire screen, as shown in Table XXXIV. The fraction of gas volume in the residual volume is immaterial in the present treatment because we have assumed that diffusion in the gas phase is fast. But this assumption applies only under certain conditions of electrode structure, reactant gas concentration and current drain.

Table XXXV shows the value of the second distribution parameter which is a measure of the radial utilization of the agglomerates. The radial utilization is good when q is small. As shown in Fig. 34, the radial distribution is reasonably good for $q < 1$. Comparing the values of q in Table IV with the curves of Fig. 34 shows that for $r_o \leq 10^{-4}$ and $i_o \leq 10^{-6}$ radial utilization of catalyst in agglomerate is reasonably good.

- 206 -

TABLE XXXII

Effect of θ, r_o and i_o on Measurable Current Density (A/cm^2) at 300 mv Polarization

i_o (A/cm^2)	Cylinder Radius, r_o (cm)		
	10^{-3}	10^{-4}	10^{-5}
$\theta = 0.5$			
10^{-6}	.0258	.1691	.2451
10^{-7}	.0081	.0355	.0391
10^{-8}	.0022	.0042	.0043
$\theta = 0.7$			
10^{-6}	.0395	.2417	.3103
10^{-7}	.0120	.0394	.0414
10^{-8}	.0029	.0043	.0043
$\theta = 0.9$			
10^{-6}	.0766	.3484	.3865
10^{-7}	.0214	.0423	.0429
10^{-8}	.0038	.0043	.0043

TABLE XXXIII

Effect of θ, r_o and i_o on Internal Voltage Drop (mv)
at 300 mv Polarization

		Cylinder Radius, r_o (cm)		
	i_o (A/cm^2)	10^{-3}	10^{-4}	10^{-5}
$\theta = 0.5$				
	10^{-6}	6.81	41.78	55.75
	10^{-7}	2.14	9.25	10.14
	10^{-8}	0.59	1.12	1.14
$\theta = 0.7$				
	10^{-6}	4.49	26.19	32.43
	10^{-7}	1.37	4.46	4.46
	10^{-8}	0.34	0.49	0.48
$\theta = 0.9$				
	10^{-6}	2.25	10.08	11.12
	10^{-7}	0.63	1.25	1.12
	10^{-8}	0.11	0.13	0.13

TABLE XXXIV

Volume Distribution in Teflon Bonded Electrode
(w = 20 mg/cm^2, h = 0.02 cm, θ = 0.9, and 30% Teflon

Component	Volume x 10^3 cm^3/cm^2
Total electrode	20
Platinum	1
Wetted agglomerate	10
Residual volume (gas, Teflon, screen)	10
Teflon (density ~ 2.3)	3
Screen	2
Gas	5

TABLE XXXV

Effect of θ, r_0 and i_0 on Second Distribution Coefficient
q of Equation (15) for $x = 0.5$

Cylinder Radius, r_0 (cm)

i_0 (A/cm^2)	10^{-3}	10^{-4}	10^{-5}
$\theta = 0.5$			
10^{-6}	$3.0728 \times 10^{+1}$	2.4925	2.2801×10^{-1}
10^{-7}	9.9876	9.5772×10^{-1}	9.5269×10^{-2}
10^{-8}	3.1872	3.1772×10^{-1}	3.1770×10^{-2}
$\theta = 0.7$			
10^{-6}	$2.0393 \times 10^{+1}$	1.7923	1.7245×10^{-1}
10^{-7}	6.5682	6.4500×10^{-1}	6.4419×10^{-2}
10^{-8}	2.0896	2.0878×10^{-1}	2.0877×10^{-2}
$\theta = 0.9$			
10^{-6}	$1.0520 \times 10^{+1}$	1.0046	9.9838×10^{-2}
10^{-7}	3.3588	3.3467×10^{-1}	3.3464×10^{-2}
10^{-8}	1.0654	1.0653×10^{-1}	1.0654×10^{-2}

4. Discussion Based on Approximations

When applying the model to the oxygen electrode, the potential changes very little along the cylinder in most cases (Table XXXIII). The current derivative is almost constant -- a related result since this is a function of η'.

This result could have been anticipated from an examination of the three nondimensional variables in the basic equation (13).

(a) $\quad \dfrac{z\eta_o}{\phi} = 9.375$, or $\exp \dfrac{\alpha z \eta_o}{2\phi} \sim 10$

(b) $\quad \left(\dfrac{\gamma i_o r_o^2}{n F \bar{D} C_o}\right)^{\frac{1}{2}} \sim \left[\dfrac{i_o r_o^2 (1 - \theta) \times 10^{13}}{\theta}\right]^{\frac{1}{2}}$

(c) $\quad \dfrac{2n F \bar{D} C_o h^2}{\eta_o \bar{\kappa} r_o^2} \sim \dfrac{1.6 \times 10^{-9}}{r_o^2}$

The right hand side of equation (13) is small for the range of values of i_o and r_o of interest to us.

A valid approximation then is to suppose $\eta' = 1$ everywhere in calculating

$$\dfrac{d^2 \eta'}{dx'^2}$$

as a small constant.

This makes the current derivative approximately a constant, and the end current j(o) is just the integral of this constant

$$j(o) = + \dfrac{\pi \bar{\kappa} r_o^2 \eta_o}{h} \dfrac{d^2 \eta'}{dx'^2} \qquad (22)$$

The total current per unit area is

$$I(o) = \frac{2n \, F \, \bar{D} \, C_o \, h \, (1-\beta)}{r_o^{\,2}} \left[\frac{q \, I_1(q)}{I_o(q)} \right] \tag{23}$$

(The exponential term is neglected.)
Where now

$$q = \left(\frac{\gamma \, i_o \, r_o^{\,2}}{n \, F \, \bar{D} \, C_o} \right)^{\frac{1}{2}} \exp. \left(\frac{\alpha \, z \, \eta_o}{2\phi} \right) \sim 10 \left(\frac{10^{13}(1-\theta) \, i_o r_o^{\,2})}{\theta} \right)^{\frac{1}{2}}$$

Further analysis can be made under the following approximations, which are not always valid.

(1) q is small.

This is good when $r_o = 10^{-5}$, $i_o = 10^{-7}$ but is wrong for $r_o = 10^{-3}$, $i_o = 10^{-6}$.

For q small,

$$\frac{q I_1(q)}{I_o(q)} \simeq \frac{q^2}{2}$$

$$I(o) \simeq \gamma \, i_o \, h \, (1-\beta) \exp \left(\frac{\alpha \, z \, \eta_o}{\phi} \right) = S \, w \, i_o \, \exp \left(\frac{\alpha \, z \, \eta_o}{\phi} \right) \tag{24}$$

The electrode current density is independent of r_o. It is dependent on C_o through i_o.

Total current increases linearly with i_o, S and w.

Total current is independent of θ.

The Tafel parameter b for the porous electrode is the same as for the smooth electrode.

The basic situation is one in which C is roughly uniform across the electrode, and the I_o Bessel function is roughly = 1 everywhere.

(2) q large.

Approximation valid when $r_o = 10^{-3}$, $i_o = 10^{-6}$.

Distribution parameter q is large, so that the Bessel function's arguments vary widely across the cylinder. C is then much larger near the outer surface than in the center, and catalyst is not being so well utilized.

$$\frac{q I_1(q)}{I_0(q)} \simeq q$$

$$I(o) \simeq \frac{2h(1-\beta)}{r_o} \; (\gamma i_o n F \overline{D} C_o)^{\frac{1}{2}} \; \exp \left(\frac{\alpha z \eta_o}{2\phi} \right)$$

or

$$I(o) = \frac{2w}{\rho (1-\theta) r_o} \; (\gamma i_o n F \overline{D} C_o)^{\frac{1}{2}} \; \exp \left(\frac{\alpha z \eta_o}{2\phi} \right) \tag{25}$$

This does depend on r_o, increasing when r_o decreases. It increases like $C_o^{\frac{1}{2}}$ and $i_o^{\frac{1}{2}}$, (over-all then current is proportional to C_o).

The Tafel parameter b for the porous electrode is twice that for the smooth electrode.

Also:

$$I(o) \propto \frac{\theta^{\frac{1}{2}}}{(1-\theta)^{\frac{1}{2}}} \quad ,$$

i.e. increasing θ increases current.

C. Analysis Assumptions

The consideration of a Teflon bonded electrode with flooded agglomerates as a bunch of parallel flooded cylinders consisting of a continuum mixture of catalyst and electrolyte is a very simplified treatment of a very complex structure. Therefore, the applicability of the used assumptions is restricted to relatively narrow limits. It is necessary to know these limits in order to use the model safely in the pertinent cases and/or to modify the assumptions when we want to extend the model to other cases. An exact discussion of the assumptions and an extension of the application of the model by using less restrictive assumptions should be the object of future work. A preliminary discussion however will be given in the following:

1. Cylindric Configuration

The difference between a cylindric surface and any other surface as gas/agglomerate interface is reflected mostly on the accessibility of the interior of the agglomerate to diffusion. For comparison let's consider a porous planar agglomerate of a thickness $2 r_0$ perpendicaular to the external surface of the electrode.

Now instead of equation (2):

$$\frac{\partial^2 C}{\partial r^2} = \frac{\gamma i_0}{n F \bar{D}} \left\{ \frac{C(x,r)}{C_0} \exp \frac{\alpha z \eta}{\phi} - \exp \frac{(\alpha - 1) \eta}{\phi} \right\} \tag{26}$$

$$\therefore C = C_0 \exp -\frac{z \eta}{\phi} + \text{solution of the homogeneous equation}$$

$$\frac{\partial^2 C}{\partial r^2} = \frac{\gamma i_0}{n C_0 F \bar{D}} \left(\exp \frac{\alpha z \eta}{\phi} \right) C \tag{27}$$

This solution must be symmetric about $r = 0$.

$$\therefore C = C_0 \exp -\frac{z \eta}{\phi} + k_1 \cosh \left(\left[\frac{\gamma i_0}{n C_0 F \bar{D}} \exp \frac{\alpha z \eta}{\phi} \right]^{\frac{1}{2}} r \right) \tag{28}$$

Since

$$C = C_O \text{ at } r = r_O, \quad k_1 = \frac{C_O \left[1 - \exp\left(-\dfrac{z\eta}{\phi}\right)\right]}{\cosh\left(\left[\dfrac{\gamma i_O r_O^2}{n C_O F \bar{D}} \exp \dfrac{\alpha z \eta}{\phi}\right]^{\frac{1}{2}}\right)} \tag{29}$$

$$-\frac{dj}{dx} = 2\gamma \int_O^{r_O} i\,dr = 2n F \bar{D} \int_O^{r_O} \frac{\partial^2 C}{\partial r^2}\,dr = 2n F \bar{D} \left[\frac{\partial C}{\partial r}\right]_{r=r_O}$$

$$= \frac{2n F \bar{D} C_O}{r_O} \cdot \frac{q \sinh q}{\cosh q} \cdot \left[1 - \exp -\left(\frac{z\eta}{\phi}\right)\right], \tag{30}$$

where $q = \left(\dfrac{\gamma i_O^2 r_O^2}{nF \bar{D} C_O}\right)^{\frac{1}{2}} \exp \dfrac{\alpha z \eta}{2\phi}$ as before.

With equation (7) converted to $\dfrac{d\eta}{dx} = -\dfrac{j(x)}{2r_O \bar{\kappa}}$ \hfill (31)

$$\frac{d^2\eta}{dx^2} = \frac{nF \bar{D} C_O}{\kappa r_O^2} \left[1 - \exp\left(-\frac{z\eta}{\phi}\right)\right] \frac{q \sinh q}{\cosh q} \tag{32}$$

With the nondimensional variables as before

$$\frac{d^2\eta'}{dx'^2} = \frac{nF \bar{D} C_O h^2}{\eta_O \bar{\kappa} r_O^2} \left[1 - \exp\left(-\frac{z\eta_O \eta'}{\phi}\right)\right] \frac{q \sinh q}{\cosh q} \tag{33}$$

$$q = \left(\frac{\gamma i_O r_O^2}{nF \bar{D} C_O}\right)^{\frac{1}{2}} \exp \frac{\alpha z \eta_O}{2\phi} \cdot \eta'$$

The only difference between this and the case of cylindric geometry is the absence of the factor 2 on the right hand side, and the ratio of hyperbolic functions instead of Bessel functions.

The same nondimensional numbers appear.

Therefore with the same magnitudes of the physical variables as before, we would again have $d^2\eta'/dx'^2$ small and $\eta' \sim 1$ everywhere. Argue as before to

$$j(o) = \frac{2r_o \bar{\kappa} \, \eta_o}{h} \frac{d^2\eta'}{dx'^2} \tag{34}$$

$$\sim \frac{2nF\bar{D}C_o h}{r_o} \left[\frac{q \sinh q}{\cosh q}\right] \tag{35}$$

$$I(o) = \frac{nF\bar{D}C_o h}{r_o^2} (1-\beta) \left[\frac{q \sinh q}{\cosh q}\right]$$

Case (I). q small, $\sinh q \sim q$, $\cosh q \sim 1$: $\left[\frac{q \sinh q}{\cosh q}\right] \sim q^2$ $\qquad$ (36)

$$I(o) \sim \gamma i_o h (1-\beta) \exp\left(\frac{\alpha z \eta_o}{\phi}\right) \tag{37}$$

which is identical with the previous result for the cylindrical geometry. This is a consequence of the full utilization of the electrode material.

Case (II). q large, $\sinh q \sim \tfrac{1}{2} e^q$, $\cosh q \sim \tfrac{1}{2} e^q$: $\dfrac{q \sinh q}{\cosh q} \sim q$ $\qquad$ (38)

$$I(o) \sim \frac{h(1-\beta)}{r_o} \left(\gamma i_o nF \bar{D} C_o \right)^{\frac{1}{2}} \exp \left(\frac{\alpha z \eta_o}{2\phi} \right) \tag{39}$$

There is a factor 2 difference between this result and the previous one for cylindric diffusion which can be interpreted as a geometrical effect.

2. Continuum Distribution of Catalyst and Electrolyte

Such an assumption is acceptable if (a) the dimensions of the particles and pores making up the agglomerate are small compared with the radius of the agglomerate and (b) the dimension of the region where most of the current is produced is large compared with the dimensions of the catalyst particles and of the micropores. This second condition is of course more restrictive than the first condition and should suffice. For large values of q (i.e. for large values of i_o) the current is produced almost exclusively in the periphery of the cylinder; therefore, the continuum assumption can not be used for such a case as the hydrogen electrode.

As a consequence of the continuum distribution, a diffusion limiting current for an electrode of very high i_o, such as the hydrogen electrode, cannot be obtained mathematically with our model. This is easy to understand because assuming a continuum distribution of electrolyte and catalyst even on the external surface of the cylinder there are active catalyst sites which can be reached by the reactant gas without the hindrances of any diffusion path in the electrolyte.

Formally this problem can be solved by introducing a thin film of pure electrolyte around the cylinder. The model converts them for very high i_o to a Thin Film Model with the reaction localized on the surface of the cylinder, with diffusion through the thin film as the Thin Film Model, but with ionic current flowing mostly through the porous cylinder.

If the thickness of the thin film is δ and we now call C_o' the concentration of the reactant on the interface cylinder thin film to differentiate from C_o solubility of gas, all the previous equations apply if C_o is substituted by C_o'. In addition we will have the following relation between C_o and C_o'

$$- \frac{d\,j\,(x)}{d\,x} = \frac{n\,\overline{F}\,D\,(C_o - C_o')\,2\,\pi\,r_o}{\delta}$$

A computer program with an additional equation could of course be easily written. The merit of this approach is doubtful, however, since δ is not known. This correction will be necessary when $C_o' - C_o$ is large. According to the following equation

$$C_o' - C_o = \frac{1}{2\,n\,\pi\,F\,\overline{D}}\left(\frac{\delta}{r_o}\right)\frac{d\,j\,(x)}{d\,x}$$

$C_o' - C_o$ is large when $\left(\dfrac{\delta}{r_o}\right)$ is large and/or $\dfrac{d\,j\,(x)}{d\,x}$ is large (high i_o exp $\dfrac{\alpha\,z\,F}{RT}$ η values).

For the oxygen electrode example treated above with $C_o = 5.5 \times 10^{-8}$:

$$\frac{C_o'}{C_o} = 1 = \frac{4 \times 10^5}{\theta} \times \left(\frac{\delta}{r_o}\right) \times \frac{d\,j\,(x)}{d\,x}$$

with $\dfrac{d\,j\,(x)}{d\,x}$ printed out by computer.

For $\theta = 0.5$:

Difference becomes significant

for $\dfrac{\delta}{r_o} = \dfrac{1}{10}$ when $\left|\dfrac{d\,j}{d\,x}\right| \sim 10^{-5}$ or

for $\dfrac{\delta}{r_o} = \dfrac{1}{100}$ when $\left|\dfrac{d\,j}{d\,x}\right| \sim 10^{-4}$

The effect is not likely to be significant for $r_o = 10^{-5}$ cm may have an effect for $r_o = 10^{-4}$ cm only if $i_o = 10^{-6}$ and $\left(\dfrac{\delta}{r_o}\right) = \dfrac{1}{10}$.

For $\theta = 0.9$:

Effect should be significant only for $\dfrac{\delta}{r_o} = \dfrac{1}{10}$, $r_o = 10^{-3}$, $i_o = 10^{-6}$ and is not very significant for smaller $\dfrac{\delta}{r_o}$, r_o or i_o .

A more definite approach is of course to consider a noncontinuum dispersion of catalyst, conserving the rest of the assumptions. In this regard a physical understanding of the effect of agglomerate structure on tortuosity factor (both conductive and diffusive) would be very useful.

3. Constant Intrinsic Activity of the Catalyst Throughout the Cylinder

This assumption seems reasonable, although it is possible that under certain conditions a larger amount of bulk area is located in the core of the agglomerate. This could be handled mathematically by an expression relating γ to r_o .

When large values of q exist (i.e. high values of i_o , r_o and η and/or low values of D and C_o), it may be advisable to form agglomerates with porous noncatalytic cores. This will result in significant savings of the catalyst.

4. Equilibration of Electrolyte Concentration in Cylinder Via Gas Phase

Due to the small diameter of cylinder compared with its length, this assumption seems more reasonable than the assumption (implicit in ref. 42) that concentration equalization occurs only via ionic migration in the axial direction of the flooded micropore system. * As a consequence of evaporation and condensation, electrolyte transport to the gas side of the oxygen electrode should be expected. A compensating counter flow of electrolyte from the gas side to the electrolyte side can be expected also. Indeed, the often observed "weeping" of oxygen electrodes could be explained at least partially by this mechanism.

---

* This is independent of the fact that our assumptions greatly simplify the mathematical treatment.

5. Direct Relationship Between Local Current and Local
Concentration of Reactant

Modification of this assumption does not change the model
basically. If needed, another concentration dependence can be used, but
the mathematics will be considerably different since the differential equation
(3) will cease to be linear.

6. No Radial Voltage Drop and Axial Concentration Difference

These assumptions seem reasonable since h is very large com-
pared with r_o .

7. No Transport Limitation in the Gas Phase

Transport limitations should be small in the case of thin electrodes
(h ~ 0.2 mm), high O_2-pressures (P_{O_2} > 0.75 atm), moderate currents
(i < 200 ma/cm^2), and high gas porosity. If these conditions are exceeded,
gas diffusion hindrances have to be considered. Such a consideration could
be done with relative ease since the assumption is not essential to the model.

Consideration of gas diffusion hindrances in our model is indeed ad-
visable when trying to optimize structures for high current drains. Experi-
mentally, the effect of O_2-partial pressure should be studied.

8. The Process of Gas Dissolution is Not Kinetically Limited

This assumption seems reasonable. Kinetic expression for solu-
bility could be considered in the treatment of the model but does not seem
necessary.

9. No Electronic iR Drop in Cylinder

Such an assumption seems reasonable; however, it should be
tested when trying to optimize electrodes for high current drains.

10. Absence of Convection

Convection has been found to occur in free menisci[34]; it seems
unlikely that it occurs at an appreciable degree inside of a porous agglomerate.

11. All Cylinders Have the Same Radius

This assumption is to some extent justified by the high degree of
lateral interlocking of the agglomerates. The effect of varying the radius

of agglomerates in translating the results of a cylinder to the electrode should however be investigated in subsequent work.

D. List of Symbols

C, $C(r, x)$, $C(r, x, t)$ Concentration of reactant gas at a point (r, x), mol $\times$ cm^{-1}

C_o Solubility of reactant gas, mol $\times$ cm^{-1}

D Diffusion coefficient of reactant gas in liquid, cm^2 $\times$ cm^{-1}

$\bar{D}$ Effective diffusion coefficient of reactant gas in liquid; affected by microporosity and tortuosity

F Faraday constant

h Thickness of electrode, cm

i, $i(r, x)$ Local real current density   A $\times$ cm^{-2}

i_o "Real" exchange current density, A $\times$ cm^{-2}

I_o Bessel function of order zero

I_1 Bessel function of order one

$I(o)$ Electrode current density   A $\times$ cm^{-2}

j, $j(x)$ Current flowing through plane x of cylinder, A

$j(o)$ Total current produced by cylinder, A

k_1 Integration constant

N Number of cylinders in one cm^2 of electrode

n Number of electrons involved in electrode reaction

p First distribution parameter (see equation (15) and Fig. 3)

q Second distribution parameter (see equation (15) and Fig. 3)

R Gas constant

r Radial coordinate in cylinder, cm

r_o Radius of cylinder, cm

S Surface area of catalyst,   m^2 $\times$ g^{-1}

T	Absolute temperature, $^\circ$K
w	Catalyst load in electrode, g x cm^{-2}
x	Axial coordinate in cylinder (also in electrode), cm
x'	Scaled axial coordinate
z	Stoichiometric number
α	Transfer coefficient
β	Macroporosity
γ	Surface to volume ratio, cm^{-1}
δ	Electrolyte outer layer, cm
η , $\eta(x)$	Overvoltage at plane (x), volt
η_o	Measured overvoltage, at plane x = 0, volt
η'	Scaled overvoltage ($\eta' = \eta/\eta_o$)
θ	Microporosity
κ	Ionic conductivity, ohm^{-1}cm^{-1}
$\bar{\kappa}$	Effective ionic conductivity, affected by microporosity and tortuosity, ohm^{-1}cm^{-1}
ρ	Catalyst density g x cm^{-3}
ϕ	RT/F , volt

REFERENCES

1. See, for example, M. L. B. Rao, A. Damjanovic, and J. O'M. Bockris, J. Phys. Chem. 67, 2508 (1963); J. P. Hoare, J. Electrochem. Soc. 111, 232 (1964); A. Kranse, J. Slawck, and Z. Winowski, Z. Physik. Chem. 40, 261 (1964).

2. M. Stern and A. C. Makrides, J. Electrochem. Soc. 107, 782 (1960).

3. J. Giner, J. Electrochem. Soc. 111, 377 (1964).

4. Fourth Quarterly Report, this contract.

5. R. Parsons, Trans. Faraday Soc. 47, 1332 (1951).

6. G. Bianchi, F. Mazza, and S. Trasatti, Proc. Second Int. Cong. on Metallic Corrosion, 1966.

7. M. L. Kronenberg, J. Electroanal. Chem. 12, 168 (1966).

8. J. H. Fishman and E. F. Rissmann, Extended Abstracts, Spring Meeting of The Electrochemical Society, San Francisco, May 1965.

9. M. L. B. Rao, A. Damjanovic, and J. Bockris, J. Phys. Chem. 67, 2508 (1963).

10. S. Z. Beer and Y. R. Sandler, J. Electrochem. Soc. 112, 113 (1965).

11. J. Turkevich, J. Hillier, and P. C. Stevenson, Disc. Faraday Soc., 11, 55 (1951).

12. Final Report, Contract No. DA 44-009-AMC-410(T), January 1967.

13. J. Leicester and M. J. Redman, J. Appl. Chem. 12, 356 (1962).

14. J. F. Schultz, L. J. E. Hofer, E. M. Cohn, K. C. Stein, and R. B. Anderson, Bulletin 578, 1959, Bureau of Mines, Synthetic Liquid Fuels from the Hydrogenation of CO; Bulletin 612, 1963, Bureau of Mines, Nitrides and Carbonitrides of Iron as Catalysts in the Fischer Tropsch Synthesis.

15. Bureau of Mines' reports, Q-1 through Q-7, July 1966 to March 1968, Contract No. NASW 12300.

16. L. W. Niedrach, H. R. Alford, J. Electrochem. Soc. 112, 117 (1965).

17. Irani and Callis, Particle Size: Measurement Interpretation and Application (New York: Wiley and Sons, 1963), p. 9.

18. G. Feuillade, Proc. Int. Meeting on Fuel Cells, Brussells 1965, Vol. IV, p. 49, Contract NASA-W 12,300.

19. R. DeLevie, Electrochemical Response of Porous Electrodes, Advances in Electrochemistry and Electrochemical Engineering, Vol. 6, P. Delahay, ed., p. 329, Interscience (1967).

20. L. G. Austin, M. Ariet, R. D. Walker, G. B. Wood, and R. H. Comyn, I&EC Fundamentals $\underline{4}$, 321 (1965).

21. A. Schmid, Helv. Chim. Acta $\underline{1}$, 169 (1933).

22. L. G. Austin and S. Almaula, J. Electrochem. Soc. $\underline{114}$, 927 (1967).

23. J. Giner, J. M. Parry, S. M. Smith, Meeting of The Electrochemical Society in Montreal, 1968, Abstract No. 328.

24. S. Srinivasan, H. D. Hurwitz, and J. O'M. Bockris, J. Chem. Phys. $\underline{46}$, 3108 (1967).

25. F. G. Will, J. Electrochem. Soc. $\underline{110}$, 145 (1963).

26. F. G. Will, J. Electrochem. Soc. $\underline{110}$, 152 (1963).

27. F. G. Will, Comptes Rendus des Deuxiemes Journees Internationales D'Etude des Piles a Combustible, Bruxels, p. 89 (1967).

28. R. P. Iczkowski, J. Electrochem. Soc. $\underline{111}$, 1078 (1964).

29. J. A. Rockett and R. Brown, J. Electrochem. Soc. $\underline{113}$, 207 (1966).

30. S. Srinivasan and H. D. Hurwitz, Electrochim. Acta $\underline{12}$, 495 (1967).

31. O. Lindström, Meeting Am. Chem. Soc. Div. Fuel Cell Chemistry, September 1967.

32. I. Lindholm and I. Edwardsson, Reports by ASEA to National Aeronautics and Space Administration, Washington, on Contract No. NASW-1536.

33. D. N. Bennion and C. W. Tobias, J. Electrochem. Soc. $\underline{113}$, 593 (1966).

34. B. D. Cahan, The Mechanism of Electrode Reaction on Porous Surfaces, Doctoral thesis, University of Pennsylvania.

35. A. Borucka and J. N. Agar, Electrochim. Acta $\underline{11}$, 603 (1966).

36. E. Justi, M. Pilkuhn, W. Scheibe, and A. Winsel, High Drain Hydrogen-Diffusion Electrodes Operating at Ambient Temperature and Low Pressure, Verl. Akad. Wissenschaft v.d. Lit, Wiesbaden (1959).

37. E. Justi and A. Winsel, Fuel Cells, Kalte Verbiennung, 245 Steiner, Wiesbaden (1962).

38. R. Brown and J. A. Rockett, J. Electrochem. Soc. 113, 865 (1966).

39. R. Chs. Burshtein, V. X. Markin, A. G. Pshenichnikov, V. A. Chismadgev and Y. G. Chirkov, Electrochim. Acta 9, 773 (1964).

40. V. S. Markin, Izv. ANSSR Otd. Khim. Nauk. 9, 1690 (1963).

41. V. S. Markin, ibid., 11, 1923 (1963).

42. E. A. Grens, II, I&EC Fundamentals 5, 542 (1966).

43. J. Giner, Report to U. S. Army Engineer Research and Development Laboratories, Fort Belvoir, Virginia, on Contract No. DA 44-009-AMC-410(T).

44. J. Giner, Proc. 21st Annual Power Sources Conf., p. 10 (1967).

45. H. H. Horowitz, J. Electrochem. Soc. 114, 650 (1967).

46. R. E. Davis, G. L. Horvatz, and C. W. Tobias, Electrochim. Acta 12, 287 (1967).

47. M. A. Klochko and M. M. Godneva, Russian Journal of Inorganic Chemistry 4, 968 (1959).

48. R. D. Walker, Jr., Fourth Semiannual Report on NASA Research Grant NGR 10-005-022, August 31, 1967.

49. J. Giner, J. M. Parry, and L. Swette, Proc. 5th Biennial Symp. on Fuel Cells, ACS; to be published in Advances in Chemistry series no. 90, Washington, D. C. (1968).

50. Report Q-8, June 1967, by Tyco Laboratories to National Aeronautics and Space Administration Headquarters on Contract No. NASW-1233.

III. APPENDIX

A. NOTES ON THE PROGRAM

The basic problem to be solved numerically is that of integrating the nondimensional equation

$$\frac{d^2\eta'}{dx'^2} = \frac{2nF\bar{D}C_o h^2}{\eta_o \bar{\kappa} r_o^2} \left[1 - \exp\left(-\frac{z\eta_o}{\phi} \cdot \eta' \right) \right] \frac{q I_1(q)}{I_o(q)}$$

where $q = \left(\frac{\gamma i_o r_o^2}{nF\bar{D}C_o} \right)^{\frac{1}{2}} \exp\left\{ \left(\frac{\alpha z \eta_o}{2\phi} \right) \eta' \right\}$

subject to the boundary conditions

$$\eta' = 1 \quad \text{at} \quad x' = o,$$

$$\frac{d\eta'}{dx'} = o \quad \text{at} \quad x' = 1.$$

The solution is required in the range $o \leq x' \leq 1$, and so we have a non-linear equation with 2 point boundary conditions. Such an equation has to be solved iteratively.

The method used is the "η" method described in L. Fox, Numerical Solution of Two-point Boundary Problems in Ordinary Differential Equations. Oxford University Press, 1957, p. 87.

Our equation is basically of the form

$$\frac{d^2 y}{dx^2} = f(y) \qquad \text{where } y = \eta', \ x = x' \text{ and } f \text{ is defined suitably.}$$

Suppose $Y(x)$ is an approximate solution.

Suppose $z(x)$ describes the error in this solution.

Then $y = Y + z$ is the true solution.

Substitute this in the governing equation

$$\frac{d^2z}{dx^2} - \left[\frac{\partial f}{\partial y}\right]_{y=Y} z = f(Y) - \frac{d^2Y}{dx^2}$$

if we neglect all but the first order terms in z. This is a linear equation for z. Given Y, z can be calculated from this equation and then $Y + z$ is the improved solution. The iteration can be repeated as often as required.

Difference Scheme

The range 0 to 1 is subdivided in intervals of 1/20N by tabular points, where N is an integer that can be varied
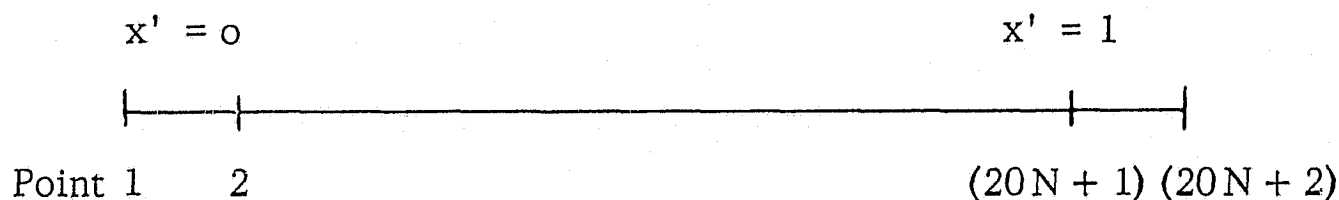
They are numbered as shown. One point beyond the physical range at $x' = 1 + 1/20N$ is taken so as to accommodate the zero derivative boundary condition at $x' = 1$.

At the I'th point of the range for I = 2 to (20N + 1) the differential equation is approximated by the difference equation

$$(1 - \frac{1}{12}h^2 f'(Y_{I+1})) z_{I+1} + (-2 - \frac{5}{6}h^2 f'(Y_I)) z_I + (1 - \frac{1}{12}h^2 f'(Y_{I-1})) z_{I-1}$$

$$= \frac{1}{12}h^2 f(Y_{I+1}) + \frac{5}{6}h^2 f(Y_I) + \frac{1}{12}h^2 f(Y_{I-1}) - Y_{I+1} + 2Y_I - Y_{I-1}$$

where the subscripts refer to the points where variables are evaluated. Here the prime refers to the derivative and $h = 1/(20 N)$ is the step length. The above is well known to be the most accurate 3-point difference scheme possible. The error is of the order of h^6. (Fox, p. 68)

The initial approximate solution is taken as $Y = (1 - x)^2$, which satisfies both boundary conditions. Thereafter we solve the above difference equation for z, and ensure that the boundary conditions are satisfied by making

$$z_1 = 0, \quad z_{20N + 2} = z_{20N}.$$

Note that, because of the simple form of one problem, the solution must be symmetric about $x' = 1$ so that the second requirement here ensures that the boundary condition of vanishing first derivative at $x' = 1$ is satisfied with the same degree of accuracy as the rest of our difference scheme.

The method described above converges rapidly. Currently, the iteration is continued until the correction z is less than 10^{-5} at all points, though this could be changed by just altering the number in the order

IF (XM - 0.00001) 34, 34, 37.

The input must be of the following form

Card 1: α, z, C_o, ϕ 　　　　　　　FORMAT (7E 10. 4)

Card 2: κ, D, η_o, h (length of cylinder)　　　　"

Card 3: 4 integers in FORMAT (4I3)

(1) N for number $(20N + 2)$ of integration points. $(2 \leq N \leq 25)$

(2) Number of values of θ to be used.

(3) Number of values of r_o to be used.

(4) Number of values of i_o to be used.

Card 4:   Values of θ FORMAT (7E 10.4)

Card 5:   Values of r_0 "

Card 6:   Values of i_0 "

More than one card can be used for values of θ, r_0, i_0 as needed.
These sets of cards may be repeated.
Program can be stopped by ending with a card 1 with $\alpha < 0$.

B. PROGRAM

```
      PROGRAM ELECTROD
      DIMENSION A(502),B(502),C(502),D(502),BE(502),Q(502),X(502),Y(502),
     1,Z(502),YA(502),YB(502),TH(20),RX(20),EC(20)
    1 FORMAT(7E10.4)
    2 FORMAT(/3H N=,I3,13H IS TOO LARGE)
    3 FORMAT(/21H TRANSFER COEFFICIENT,F10.4,22H STOICHIOMETRIC NUMBER,F
     210.4)
    4 FORMAT(/14H CONCENTRATION,E12.4,30HMOL CM-3 DIFFUSION COEFFICIENT,
     1E12.4,9H CM2SEC-1)
    5 FORMAT(/24H SURFACE TO VOLUME RATIO,E12.4,24H CM-1 IONIC CONDUCTIV
     2ITY,E12.4,10H OHM-1CM-1)
    6 FORMAT(/16H CYLINDER LENGTH,E12.4,17H CM END POTENTIAL,E12.4,6H VO
     3LTS)
    7 FORMAT(2F12.5,4E12.4)
    8 FORMAT(//13H RESULT AFTER,I3,11H ITERATIONS)
    9 FORMAT(35H NO CONVERGENCE AFTER 20 ITERATIONS)
   10 FORMAT(//77H       POSITION   RELATIVE   CURRENT      CURRENT
     7DISTRIBUTION PARAMETERS)
   11 FORMAT(49H                    POTENTIAL   IN AMPS     DERIVATIVE)
   12 FORMAT(//I4,18H POINT INTEGRATION)
   13 FORMAT(8I3)
   14 FORMAT(/21H MICROPOROSITY THETA=,F10.4)
   15 FORMAT(/16H CYLINDER RADIUS,E12.4,22H CM   EXCHANGE CURRENT,E12.4,
     59H AMPSCM-2)
   16 FORMAT(//30H TOTAL CURRENT PER CM2 IN AMPS,F12.4)
      F=96500.
      EN=4.
  101 READ 1,ALPHA,ZE,CO,PHI
      IF (ALPHA) 100,102,102
  102 READ 1,AK,DD,ET,AH
      PRINT 3,ALPHA,ZE
      PRINT 4,CO,DD
      PRINT 6,AH,ET
      READ 13,N,NTHET,NR,NIO
      IF (N-25) 103,103,104
  104 PRINT 2,N
      GO TO 101
  100 STOP
  103 L=20*N+2
      READ 1,(TH(I),I=1,NTHET)
      READ 1,(RX(I),I=1,NR)
      READ 1,(EC(I),I=1,NIO)
      DO 150 JX=1,NTHET
      DBAR=TH(JX)*DD
      BK=TH(JX)*AK
      GAMMA=4.0E06*(1.-TH(JX))
      PRINT 14,TH(JX)
      PRINT 5,GAMMA,AK
      DO 150 JY=1,NR
      RO=RX(JY)
      DO 150 JZ=1,NIO
      EI=EC(JZ)
      PRINT 15,RO,EI
      XA=ZE*ET/PHI
      XB=SQRTF((GAMMA*EI*RO*RO)/(EN*F*DBAR*CO))
      XC=(2.*EN*F*DBAR*CO*AH*AH)/(ET*BK*RO*RO)
```

```
      XD=0.5*ALPHA*XA
      AJ=(-3.1415927*RO*RO*BK*ET)/AH
      NL=L-2
      DO 20 I=1,L
      X(I)=(I-1.)/NL
   20 Y(I)=(1.-X(I))**2
      NL=L-1
      PRINT 12, NL
      H=X(2)
      VA=XC*H*H/12.
      M=0
   27 DO 22 I=1,L
      P=XB*EXPF(XD*Y(I))
      CALL BESI(P,2,RC)
      CALL BESI (P,0,RA)
      RB=P*(RA-RC)/2.
      VB=1.-EXPF(-XA*Y(I))
      VC=P*RB/RA
      YA(I)=VA*VB*VC
      VD=((2.*RB+P*RC)*RA-P*RB*RB)/(RA**2)
   22 YB(I)=VA*(XA*VC*(1.-VB)+VB*VD*XB*XD*EXPF(XD*Y(I)))
      DO 23 I=2,NL
      A(I)=1.-YB(I-1)
      B(I)=-2.-10.*YB(I)
      C(I)=1.-YB(I+1)
   23 D(I)=YA(I-1)+10.*YA(I)+YA(I+1)-Y(I+1)+2.*Y(I)-Y(I-1)
      A(NL)=2.*A(NL)
      BE(1)=0.
      Q(1)=0.
      DO 28 I=2,NL
      W=B(I)-A(I)*BE(I-1)
      BE(I)=C(I)/W
   28 Q(I)=(D(I)-A(I)*Q(I-1))/W
      Z(NL)=Q(NL)
      DO 30 I=2,NL
      K=L-I
   30 Z(K)=Q(K)-BE(K)*Z(K+1)
      XM=0.
      DO 32 I=2,NL
      YC=ABSF(Z(I))
      IF(XM-YC) 33,32,32
   33 XM=YC
   32 CONTINUE
      M=M+1
      DO 35 I=2,NL
   35 Y(I)=Y(I)+Z(I)
      Y(L)=Y(L-2)
      IF (XM-0.00001) 34,34,37
   37 IF (M-20) 27,31,31
   31 PRINT 9
   34 PRINT 8,M
      PRINT 10
      PRINT 11
      DO 38 I=1,NL,N
      QA=XB*EXPF(XD*Y(I))
      CALL BESI(QA,0,RES)
```

```
      CALL BESI(QA,1,RB)
      RB=RB*QA*XC*(1.-EXPF(-XA*Y(I)))/RES
      DEX=-3.1415927*BK*ET*RB*((RO/AH)**2)
      P=EI*EXPF(ALPHA*XA*Y(I))*(1.-EXPF(-XA*Y(I)))/RES
      IF (I-NL) 41,40,40
   41 IF(I-1) 42,42,43
   43 DERIV=AJ*(2.*(Y(I+1)-Y(I-1))-(Y(I+2)-Y(I-2))/4.)/(3.*H)
      GO TO 38
   42 YC=H*(YB(1)+0.875)
      DERIV=AJ*(Y(2)-(Y(3)+15.)/16.-4.5*YA(1))/YC
      SAVE=(-DERIV*ET*BK)/(1000.*AH*AH*AJ*(1.-TH(JX)))
      GO TO 38
   40 DERIV=0.
   38 PRINT 7,X(I),Y(I),DERIV,DEX,P,QA
      PRINT 16, SAVE
  150 CONTINUE
      GO TO 101
       END
```

```
      SUBROUTINE BESI(X,N,BI)
    1 FORMAT(34H NEGATIVE ORDER OF BESSEL FUNCTION)
    2 FORMAT(37H NEGATIVE ARGUMENT OF BESSEL FUNCTION)
      IER=0
      BI=1.0
      IF(N)    150,15,10
   10 IF (X) 160,20,20
   15 IF(X) 160,145,20
   20 TOL=1.E-6
      IF (X-12.)    40,40,30
   30 IF (X-FLOATF(N)) 40,40,110
   40 XX=X/2.
   50 TERM=1.0
      IF (N) 70,70,55
   55 DO 60 I=1,N
      FI=I
      IF (ABSF(TERM)-1.E-25)    56,60,60
   56 IER=0
      BI=0.0
      RETURN
   60 TERM=TERM*XX/FI
   70 BI=TERM
      XX=XX*XX
      DO 90 K=1,1000
      IF (ABSF(TERM)-ABSF(BI*TOL)) 145,145,80
   80 FK=K*(N+K)
      TERM=TERM*(XX/FK)
   90 BI=BI+TERM
      GO TO 144
  110 FN=4*N*N
      XX=1./(8.*X)
      TERM=1.
      BI=1.
      DO 130 K=1,30
      IF(ABSF(TERM)-ABSF(TOL*BI)) 140,140,120
  120 FK=(2*K-1)**2
      TERM=TERM*XX*(FK-FN)/FLOATF(K)
  130 BI=BI+TERM
      GO TO 40
  140 PI=3.141592653
      BI=BI*EXPF(X)/SQRTF(2.*PI*X)
      GO TO 144
  150 IER=1
      GO TO 144
  160 IER=2
  144 IF(IER-1) 145,146,147
  146 PRINT 1
      GO TO 145
  147 PRINT 2
  145 RETURN
      END
```

C. COMPUTER TABULATIONS, 81 POINT INTEGRATION

$\theta = 0.5$, cylinder radius 10^{-3} cm, $i_0 = 10^{-6}$ A/cm^2
Result after 3 iterations

POSITION	RELATIVE POTENTIAL	CURRENT IN AMPS	CURRENT DERIVATIVE	DISTRIBUTION PARAMETERS	
0.00000	1.00000	8.1003-007	-4.1987-005	1.9749-017	3.1983+001
0.05000	0.99777	7.6815-007	-4.1764-005	2.3033-017	3.1816+001
0.10000	0.99565	7.2649-007	-4.1554-005	2.6624-017	3.1659+001
0.15000	0.99366	6.8504-007	-4.1357-005	3.0505-017	3.1511+001
0.20000	0.99178	6.4378-007	-4.1172-005	3.4653-017	3.1372+001
0.25000	0.99001	6.0269-007	-4.0999-005	3.9034-017	3.1243+001
0.30000	0.98837	5.6177-007	-4.0839-005	4.3604-017	3.1123+001
0.35000	0.98683	5.2101-007	-4.0690-005	4.8313-017	3.1011+001
0.40000	0.98542	4.8039-007	-4.0553-005	5.3100-017	3.0908+001
0.45000	0.98412	4.3990-007	-4.0427-005	5.7899-017	3.0814+001
0.50000	0.98293	3.9953-007	-4.0313-005	6.2638-017	3.0728+001
0.55000	0.98185	3.5927-007	-4.0210-005	6.7241-017	3.0651+001
0.60000	0.98089	3.1911-007	-4.0118-005	7.1630-017	3.0582+001
0.65000	0.98005	2.7903-007	-4.0037-005	7.5728-017	3.0522+001
0.70000	0.97932	2.3903-007	-3.9967-005	7.9458-017	3.0469+001
0.75000	0.97870	1.9909-007	-3.9908-005	8.2749-017	3.0425+001
0.80000	0.97819	1.5921-007	-3.9860-005	8.5538-017	3.0389+001
0.85000	0.97779	1.1937-007	-3.9822-005	8.7769-017	3.0361+001
0.90000	0.97751	7.9563-008	-3.9796-005	8.9396-017	3.0341+001
0.95000	0.97734	3.9776-008	-3.9780-005	9.0386-017	3.0329+001
1.00000	0.97729	0.0000+000	-3.9774-005	9.0718-017	3.0325+001

TOTAL CURRENT PER CM2 IN AMPS   0.0258

$\theta = 0.5$, cylinder radius 10^{-3} cm, $i_0 = 10^{-7}$ A/cm^2
Result after 3 iterations

POSITION	RELATIVE POTENTIAL	CURRENT IN AMPS	CURRENT DERIVATIVE	DISTRIBUTION PARAMETERS	
0.00000	1.00000	2.5310-007	-1.2805-005	3.4610-009	1.0114+001
0.05000	0.99930	2.4030-007	-1.2783-005	3.5042-009	1.0097+001
0.10000	0.99864	2.2753-007	-1.2762-005	3.5457-009	1.0082+001
0.15000	0.99801	2.1478-007	-1.2742-005	3.5852-009	1.0067+001
0.20000	0.99742	2.0205-007	-1.2723-005	3.6228-009	1.0053+001
0.25000	0.99687	1.8933-007	-1.2706-005	3.6584-009	1.0040+001
0.30000	0.99635	1.7663-007	-1.2690-005	3.6919-009	1.0028+001
0.35000	0.99587	1.6395-007	-1.2674-005	3.7233-009	1.0016+001
0.40000	0.99543	1.5128-007	-1.2660-005	3.7526-009	1.0006+001
0.45000	0.99502	1.3863-007	-1.2648-005	3.7797-009	9.9964+000
0.50000	0.99464	1.2599-007	-1.2636-005	3.8046-009	9.9876+000
0.55000	0.99430	1.1336-007	-1.2625-005	3.8272-009	9.9797+000
0.60000	0.99400	1.0074-007	-1.2616-005	3.8476-009	9.9726+000
0.65000	0.99373	8.8126-008	-1.2608-005	3.8656-009	9.9664+000
0.70000	0.99350	7.5522-008	-1.2600-005	3.8812-009	9.9610+000
0.75000	0.99330	6.2925-008	-1.2594-005	3.8945-009	9.9564+000
0.80000	0.99314	5.0333-008	-1.2589-005	3.9054-009	9.9527+000
0.85000	0.99302	3.7746-008	-1.2585-005	3.9139-009	9.9498+000
0.90000	0.99293	2.5162-008	-1.2583-005	3.9200-009	9.9477+000
0.95000	0.99288	1.2580-008	-1.2581-005	3.9236-009	9.9465+000
1.00000	0.99286	0.0000+000	-1.2580-005	3.9248-009	9.9460+000

TOTAL CURRENT PER CM2 IN AMPS   0.0081

$\theta = 0.5$, cylinder radius 10^{-3} cm, $i_o = 10^{-8}$ A/cm^2

After 3 iterations

POSITION	RELATIVE POTENTIAL	CURRENT IN AMPS	CURRENT DERIVATIVE	DISTRIBUTION PARAMETERS	
0.00000	1.00000	7.0001-008	-3.5136-006	1.8918-007	3.1983+000
0.05000	0.99981	6.6489-008	-3.5116-006	1.8923-007	3.1968+000
0.10000	0.99962	6.2978-008	-3.5097-006	1.8928-007	3.1955+000
0.15000	0.99945	5.9469-008	-3.5079-006	1.8933-007	3.1942+000
0.20000	0.99929	5.5962-008	-3.5062-006	1.8938-007	3.1930+000
0.25000	0.99913	5.2457-008	-3.5047-006	1.8942-007	3.1918+000
0.30000	0.99899	4.8953-008	-3.5032-006	1.8946-007	3.1907+000
0.35000	0.99886	4.5450-008	-3.5018-006	1.8950-007	3.1897+000
0.40000	0.99873	4.1949-008	-3.5005-006	1.8953-007	3.1888+000
0.45000	0.99862	3.8449-008	-3.4994-006	1.8956-007	3.1880+000
0.50000	0.99852	3.4950-008	-3.4983-006	1.8959-007	3.1872+000
0.55000	0.99842	3.1452-008	-3.4974-006	1.8962-007	3.1865+000
0.60000	0.99834	2.7955-008	-3.4965-006	1.8964-007	3.1859+000
0.65000	0.99826	2.4459-008	-3.4957-006	1.8966-007	3.1853+000
0.70000	0.99820	2.0963-008	-3.4951-006	1.8968-007	3.1848+000
0.75000	0.99814	1.7469-008	-3.4945-006	1.8970-007	3.1844+000
0.80000	0.99810	1.3974-008	-3.4941-006	1.8971-007	3.1841+000
0.85000	0.99807	1.0480-008	-3.4937-006	1.8972-007	3.1838+000
0.90000	0.99804	6.9867-009	-3.4935-006	1.8972-007	3.1836+000
0.95000	0.99803	3.4932-009	-3.4933-006	1.8973-007	3.1835+000
1.00000	0.99802	0.0000+000	-3.4933-006	1.8973-007	3.1835+000

TOTAL CURRENT PER CM2 IN AMPS   0.0022

$\theta = 0.5$, cylinder radius 10^{-4} radius 10^{-4} cm, $i_o = 10^{-6}$ A/cm^2

Result after 4 iterations

POSITION	RELATIVE POTENTIAL	CURRENT IN AMPS	CURRENT DERIVATIVE	DISTRIBUTION PARAMETERS	
0.00000	1.00000	5.3123-008	-3.5136-006	1.8918-005	3.1983+000
0.05000	0.98546	4.9684-008	-3.3664-006	1.9295-005	3.0911+000
0.10000	0.97187	4.6386-008	-3.2331-006	1.9588-005	2.9942+000
0.15000	0.95920	4.3214-008	-3.1124-006	1.9809-005	2.9066+000
0.20000	0.94741	4.0157-008	-3.0031-006	1.9969-005	2.8274+000
0.25000	0.93645	3.7204-008	-2.9042-006	2.0079-005	2.7558+000
0.30000	0.92634	3.4345-008	-2.8150-006	2.0147-005	2.6912+000
0.35000	0.91702	3.1571-008	-2.7346-006	2.0183-005	2.6330+000
0.40000	0.90847	2.8874-008	-2.6623-006	2.0192-005	2.5808+000
0.45000	0.90068	2.6244-008	-2.5977-006	2.0181-005	2.5341+000
0.50000	0.89361	2.3676-008	-2.5401-006	2.0156-005	2.4925+000
0.55000	0.88727	2.1162-008	-2.4892-006	2.0122-005	2.4557+000
0.60000	0.88163	1.8695-008	-2.4446-006	2.0081-005	2.4235+000
0.65000	0.87669	1.6270-008	-2.4060-006	2.0039-005	2.3955+000
0.70000	0.87242	1.3881-008	-2.3730-006	1.9997-005	2.3717+000
0.75000	0.86883	1.1523-008	-2.3455-006	1.9958-005	2.3518+000
0.80000	0.86590	9.1887-009	-2.3232-006	1.9924-005	2.3357+000
0.85000	0.86363	6.8745-009	-2.3061-006	1.9896-005	2.3233+000
0.90000	0.86201	4.5749-009	-2.2939-006	1.9875-005	2.3145+000
0.95000	0.86104	2.2850-009	-2.2866-006	1.9862-005	2.3093+000
1.00000	0.86072	0.0000+000	-2.2842-006	1.9858-005	2.3075+000

TOTAL CURRENT PER CM2 IN AMPS   0.1691

θ = 0.5, cylinder radius 10^{-4} cm, i_o = 10^{-7} A/cm^2

Result after 3 iterations

POSITION	RELATIVE POTENTIAL	CURRENT IN AMPS	CURRENT DERIVATIVE	DISTRIBUTION PARAMETERS	
0.00000	1.00000	1.1146-008	-6.0760-007	8.5319-006	1.0114+000
0.05000	0.99693	1.0543-008	-5.9982-007	8.4374-006	1.0041+000
0.10000	0.99403	9.9465-009	-5.9256-007	8.3489-006	9.9734-001
0.15000	0.99130	9.3574-009	-5.8579-007	8.2660-006	9.9098-001
0.20000	0.98874	8.7748-009	-5.7949-007	8.1887-006	9.8504-001
0.25000	0.98634	8.1983-009	-5.7365-007	8.1167-006	9.7951-001
0.30000	0.98410	7.6273-009	-5.6825-007	8.0500-006	9.7439-001
0.35000	0.98202	7.0616-009	-5.6328-007	7.9885-006	9.6965-001
0.40000	0.98010	6.5006-009	-5.5873-007	7.9319-006	9.6530-001
0.45000	0.97834	5.9440-009	-5.5458-007	7.8803-006	9.6133-001
0.50000	0.97674	5.3914-009	-5.5082-007	7.8335-006	9.5772-001
0.55000	0.97529	4.8423-009	-5.4745-007	7.7913-006	9.5448-001
0.60000	0.97400	4.2963-009	-5.4446-007	7.7539-006	9.5159-001
0.65000	0.97286	3.7532-009	-5.4183-007	7.7210-006	9.4905-001
0.70000	0.97187	3.2126-009	-5.3957-007	7.6926-006	9.4686-001
0.75000	0.97104	2.6740-009	-5.3766-007	7.6687-006	9.4502-001
0.80000	0.97036	2.1371-009	-5.3611-007	7.6491-006	9.4351-001
0.85000	0.96983	1.6016-009	-5.3491-007	7.6340-006	9.4234-001
0.90000	0.96945	1.0672-009	-5.3405-007	7.6232-006	9.4151-001
0.95000	0.96923	5.3342-010	-5.3354-007	7.6167-006	9.4101-001
1.00000	0.96915	0.0000+000	-5.3336-007	7.6146-006	9.4084-001

TOTAL CURRENT PER CM2 IN AMPS   0.0355

θ = 0.5, cylinder radius 10^{-4} cm, i_o = 10^{-8} A/cm^2

Result after 3 iterations

POSITION	RELATIVE POTENTIAL	CURRENT IN AMPS	CURRENT DERIVATIVE	DISTRIBUTION PARAMETERS	
0.00000	1.00000	1.3317-009	-6.7360-008	1.0585-006	3.1983-001
0.05000	0.99963	1.2644-009	-6.7246-008	1.0567-006	3.1955-001
0.10000	0.99928	1.1972-009	-6.7138-008	1.0550-006	3.1929-001
0.15000	0.99896	1.1301-009	-6.7035-008	1.0534-006	3.1905-001
0.20000	0.99864	1.0631-009	-6.6939-008	1.0519-006	3.1881-001
0.25000	0.99835	9.9623-010	-6.6849-008	1.0505-006	3.1860-001
0.30000	0.99808	9.2942-010	-6.6765-008	1.0492-006	3.1839-001
0.35000	0.99783	8.6270-010	-6.6686-008	1.0480-006	3.1820-001
0.40000	0.99759	7.9605-010	-6.6614-008	1.0469-006	3.1803-001
0.45000	0.99738	7.2947-010	-6.6547-008	1.0459-006	3.1787-001
0.50000	0.99718	6.6295-010	-6.6487-008	1.0449-006	3.1772-001
0.55000	0.99700	5.9649-010	-6.6432-008	1.0441-006	3.1759-001
0.60000	0.99684	5.3008-010	-6.6383-008	1.0433-006	3.1747-001
0.65000	0.99670	4.6372-010	-6.6340-008	1.0426-006	3.1737-001
0.70000	0.99658	3.9740-010	-6.6302-008	1.0421-006	3.1728-001
0.75000	0.99648	3.3112-010	-6.6270-008	1.0416-006	3.1720-001
0.80000	0.99639	2.6486-010	-6.6245-008	1.0412-006	3.1714-001
0.85000	0.99633	1.9862-010	-6.6224-008	1.0409-006	3.1709-001
0.90000	0.99628	1.3241-010	-6.6210-008	1.0406-006	3.1705-001
0.95000	0.99625	6.6200-011	-6.6202-008	1.0405-006	3.1703-001
1.00000	0.99624	0.0000+000	-6.6199-008	1.0405-006	3.1703-001

TOTAL CURRENT PER CM2 IN AMPS   0.0042

$\theta = 0.5$, cylinder radius 10^{-5} cm, $i_O = 10^{-6}$ A/cm^2

Result after 4 iterations

POSITION	RELATIVE POTENTIAL	CURRENT IN AMPS	CURRENT DERIVATIVE	DISTRIBUTION PARAMETERS	
0.00000	1.00000	7.6995-010	-6.7360-008	1.0585-004	3.1983-001
0.05000	0.97914	7.0578-010	-6.1155-008	9.6211-005	3.0457-001
0.10000	0.96001	6.4730-010	-5.5963-008	8.8131-005	2.9121-001
0.15000	0.94246	5.9359-010	-5.1586-008	8.1306-005	2.7948-001
0.20000	0.92638	5.4391-010	-4.7872-008	7.5506-005	2.6914-001
0.25000	0.91165	4.9766-010	-4.4704-008	7.0551-005	2.6001-001
0.30000	0.89819	4.5435-010	-4.1991-008	6.6303-005	2.5193-001
0.35000	0.88592	4.1355-010	-3.9660-008	6.2650-005	2.4479-001
0.40000	0.87477	3.7492-010	-3.7653-008	5.9503-005	2.3848-001
0.45000	0.86468	3.3815-010	-3.5926-008	5.6792-005	2.3291-001
0.50000	0.85562	3.0299-010	-3.4440-008	5.4458-005	2.2801-001
0.55000	0.84753	2.6920-010	-3.3165-008	5.2454-005	2.2373-001
0.60000	0.84037	2.3659-010	-3.2077-008	5.0744-005	2.2001-001
0.65000	0.83413	2.0499-010	-3.1156-008	4.9296-005	2.1681-001
0.70000	0.82876	1.7423-010	-3.0387-008	4.8066-005	2.1410-001
0.75000	0.82426	1.4417-010	-2.9755-008	4.7092-005	2.1185-001
0.80000	0.82060	1.1468-010	-2.9251-008	4.6298-005	2.1004-001
0.85000	0.81777	8.5630-011	-2.8867-008	4.5694-005	2.0865-001
0.90000	0.81575	5.6908-011	-2.8596-008	4.5268-005	2.0767-001
0.95000	0.81455	2.8400-011	-2.8436-008	4.5015-005	2.0708-001
1.00000	0.81414	0.0000+000	-2.8383-008	4.4932-005	2.0689-001

TOTAL CURRENT PER CM2 IN AMPS   0.2451

$\theta = 0.5$, cylinder radius 10^{-5} cm, $i_O = 10^{-7}$ A/cm^2

Result after 3 iterations

POSITION	RELATIVE POTENTIAL	CURRENT IN AMPS	CURRENT DERIVATIVE	DISTRIBUTION PARAMETERS	
0.00000	1.00000	1.2269-010	-6.8131-009	1.0830-005	1.0114-001
0.05000	0.99662	1.1593-010	-6.7062-009	1.0660-005	1.0034-001
0.10000	0.99344	1.0927-010	-6.6070-009	1.0502-005	9.9595-002
0.15000	0.99044	1.0271-010	-6.5148-009	1.0356-005	9.8898-002
0.20000	0.98763	9.6240-011	-6.4295-009	1.0221-005	9.8248-002
0.25000	0.98499	8.9850-011	-6.3508-009	1.0096-005	9.7643-002
0.30000	0.98254	8.3536-011	-6.2782-009	9.9804-006	9.7084-002
0.35000	0.98027	7.7292-011	-6.2117-009	9.8747-006	9.6567-002
0.40000	0.97817	7.1111-011	-6.1509-009	9.7782-006	9.6093-002
0.45000	0.97624	6.4988-011	-6.0957-009	9.6906-006	9.5661-002
0.50000	0.97449	5.8918-011	-6.0459-009	9.6114-006	9.5269-002
0.55000	0.97291	5.2895-011	-6.0013-009	9.5406-006	9.4916-002
0.60000	0.97149	4.6913-011	-5.9617-009	9.4778-006	9.4602-002
0.65000	0.97025	4.0969-011	-5.9271-009	9.4228-006	9.4327-002
0.70000	0.96918	3.5058-011	-5.8973-009	9.3755-006	9.4090-002
0.75000	0.96827	2.9173-011	-5.8723-009	9.3357-006	9.3890-002
0.80000	0.96752	2.3312-011	-5.8519-009	9.3034-006	9.3726-002
0.85000	0.96695	1.7468-011	-5.8361-009	9.2783-006	9.3600-002
0.90000	0.96654	1.1638-011	-5.8249-009	9.2604-006	9.3509-002
0.95000	0.96629	5.8166-012	-5.8181-009	9.2498-006	9.3455-002
1.00000	0.96621	0.0000+000	-5.8159-009	9.2462-006	9.3437-002

TOTAL CURRENT PER CM2 IN AMPS   0.0391

$\theta = 0.5$, cylinder radius 10^{-5} cm, $i_o = 10^{-8}$ A/cm^2

Result after 3 iterations

POSITION	RELATIVE POTENTIAL	CURRENT IN AMPS	CURRENT DERIVATIVE	DISTRIBUTION PARAMETERS	
0.00000	1.00000	1.3481-011	-6.8209-010	1.0854-006	3.1983-002
0.05000	0.99963	1.2799-011	-6.8090-010	1.0836-006	3.1955-002
0.10000	0.99928	1.2119-011	-6.7978-010	1.0818-006	3.1929-002
0.15000	0.99894	1.1440-011	-6.7872-010	1.0801-006	3.1904-002
0.20000	0.99863	1.0762-011	-6.7772-010	1.0785-006	3.1880-002
0.25000	0.99833	1.0084-011	-6.7678-010	1.0770-006	3.1858-002
0.30000	0.99806	9.4079-012	-6.7591-010	1.0756-006	3.1838-002
0.35000	0.99780	8.7324-012	-6.7510-010	1.0743-006	3.1818-002
0.40000	0.99756	8.0577-012	-6.7435-010	1.0731-006	3.1801-002
0.45000	0.99735	7.3837-012	-6.7366-010	1.0720-006	3.1784-002
0.50000	0.99715	6.7104-012	-6.7303-010	1.0710-006	3.1770-002
0.55000	0.99697	6.0377-012	-6.7246-010	1.0701-006	3.1756-002
0.60000	0.99680	5.3654-012	-6.7195-010	1.0693-006	3.1744-002
0.65000	0.99666	4.6937-012	-6.7150-010	1.0686-006	3.1734-002
0.70000	0.99654	4.0224-012	-6.7111-010	1.0680-006	3.1724-002
0.75000	0.99643	3.3515-012	-6.7078-010	1.0675-006	3.1717-002
0.80000	0.99635	2.6808-012	-6.7052-010	1.0670-006	3.1710-002
0.85000	0.99628	2.0104-012	-6.7031-010	1.0667-006	3.1705-002
0.90000	0.99623	1.3402-012	-6.7016-010	1.0665-006	3.1702-002
0.95000	0.99621	6.7005-013	-6.7007-010	1.0663-006	3.1700-002
1.00000	0.99620	0.0000+000	-6.7004-010	1.0663-006	3.1699-002

TOTAL CURRENT PER CM2 IN AMPS   0.0043

$\theta = 0.7$, cylinder radius 10^{-3} cm, $i_o = 10^{-6}$ A/cm^2

Result after 3 iterations

POSITION	RELATIVE POTENTIAL	CURRENT IN AMPS	CURRENT DERIVATIVE	DISTRIBUTION PARAMETERS	
0.00000	1.00000	7.4498-007	-3.8152-005	9.9880-013	2.0938+001
0.05000	0.99853	7.0690-007	-3.8018-005	1.0640-012	2.0866+001
0.10000	0.99714	6.6894-007	-3.7891-005	1.1295-012	2.0798+001
0.15000	0.99583	6.3111-007	-3.7772-005	1.1948-012	2.0734+001
0.20000	0.99459	5.9340-007	-3.7659-005	1.2596-012	2.0674+001
0.25000	0.99343	5.5579-007	-3.7554-005	1.3233-012	2.0618+001
0.30000	0.99234	5.1829-007	-3.7457-005	1.3856-012	2.0565+001
0.35000	0.99134	4.8087-007	-3.7366-005	1.4460-012	2.0517+001
0.40000	0.99040	4.4355-007	-3.7282-005	1.5041-012	2.0472+001
0.45000	0.98954	4.0631-007	-3.7205-005	1.5594-012	2.0431+001
0.50000	0.98876	3.6914-007	-3.7135-005	1.6115-012	2.0393+001
0.55000	0.98805	3.3204-007	-3.7072-005	1.6601-012	2.0359+001
0.60000	0.98742	2.9499-007	-3.7015-005	1.7046-012	2.0329+001
0.65000	0.98686	2.5800-007	-3.6966-005	1.7449-012	2.0303+001
0.70000	0.98637	2.2106-007	-3.6923-005	1.7804-012	2.0280+001
0.75000	0.98596	1.8416-007	-3.6886-005	1.8110-012	2.0260+001
0.80000	0.98563	1.4729-007	-3.6856-005	1.8364-012	2.0244+001
0.85000	0.98537	1.1044-007	-3.6833-005	1.8564-012	2.0232+001
0.90000	0.98518	7.3617-008	-3.6817-005	1.8708-012	2.0223+001
0.95000	0.98507	3.6805-008	-3.6807-005	1.8795-012	2.0218+001
1.00000	0.98503	0.0000+000	-3.6804-005	1.8824-012	2.0216+001

TOTAL CURRENT PER CM2 IN AMPS   0.0395

$\theta = 0.7$, cylinder radius 10^{-3} cm, $i_o = 10^{-7}$ A/cm^2

Result after 3 iterations

POSITION	RELATIVE POTENTIAL	CURRENT IN AMPS	CURRENT DERIVATIVE	DISTRIBUTION PARAMETERS	
0.00000	1.00000	2.2599-007	-1.1388-005	9.1373-008	6.6211+000
0.05000	0.99955	2.1461-007	-1.1375-005	9.1765-008	6.6142+000
0.10000	0.99913	2.0324-007	-1.1362-005	9.2137-008	6.6076+000
0.15000	0.99873	1.9188-007	-1.1351-005	9.2489-008	6.6015+000
0.20000	0.99836	1.8054-007	-1.1340-005	9.2822-008	6.5956+000
0.25000	0.99800	1.6920-007	-1.1330-005	9.3136-008	6.5902+000
0.30000	0.99767	1.5788-007	-1.1320-005	9.3429-008	6.5851+000
0.35000	0.99737	1.4656-007	-1.1311-005	9.3703-008	6.5803+000
0.40000	0.99708	1.3526-007	-1.1303-005	9.3957-008	6.5759+000
0.45000	0.99682	1.2396-007	-1.1295-005	9.4191-008	6.5719+000
0.50000	0.99658	1.1267-007	-1.1288-005	9.4405-008	6.5682+000
0.55000	0.99636	1.0138-007	-1.1282-005	9.4599-008	6.5649+000
0.60000	0.99617	9.0101-008	-1.1277-005	9.4772-008	6.5619+000
0.65000	0.99600	7.8827-008	-1.1272-005	9.4925-008	6.5593+000
0.70000	0.99585	6.7557-008	-1.1267-005	9.5058-008	6.5570+000
0.75000	0.99573	5.6292-008	-1.1264-005	9.5171-008	6.5551+000
0.80000	0.99562	4.5029-008	-1.1261-005	9.5263-008	6.5535+000
0.85000	0.99554	3.3770-008	-1.1258-005	9.5334-008	6.5523+000
0.90000	0.99549	2.2512-008	-1.1257-005	9.5386-008	6.5514+000
0.95000	0.99545	1.1256-008	-1.1256-005	9.5416-008	6.5509+000
1.00000	0.99544	0.0000+000	-1.1256-005	9.5427-008	6.5507+000

TOTAL CURRENT PER CM2 IN AMPS   0.0120

$\theta = 0.7$, cylinder radius 10^{-3} cm, $i_o = 10^{-8}$ A/cm^2

Result after 3 iterations

POSITION	RELATIVE POTENTIAL	CURRENT IN AMPS	CURRENT DERIVATIVE	DISTRIBUTION PARAMETERS	
0.00000	1.00000	5.5581-008	-2.7860-006	4.4580-007	2.0938+000
0.05000	0.99989	5.2795-008	-2.7850-006	4.4574-007	2.0932+000
0.10000	0.99979	5.0010-008	-2.7840-006	4.4569-007	2.0927+000
0.15000	0.99969	4.7227-008	-2.7831-006	4.4563-007	2.0922+000
0.20000	0.99960	4.4444-008	-2.7822-006	4.4559-007	2.0918+000
0.25000	0.99951	4.1662-008	-2.7814-006	4.4554-007	2.0914+000
0.30000	0.99943	3.8881-008	-2.7806-006	4.4550-007	2.0910+000
0.35000	0.99935	3.6101-008	-2.7799-006	4.4546-007	2.0906+000
0.40000	0.99928	3.3321-008	-2.7793-006	4.4542-007	2.0902+000
0.45000	0.99922	3.0542-008	-2.7787-006	4.4538-007	2.0899+000
0.50000	0.99916	2.7764-008	-2.7781-006	4.4535-007	2.0896+000
0.55000	0.99910	2.4986-008	-2.7776-006	4.4532-007	2.0894+000
0.60000	0.99906	2.2209-008	-2.7772-006	4.4530-007	2.0891+000
0.65000	0.99901	1.9432-008	-2.7768-006	4.4528-007	2.0889+000
0.70000	0.99898	1.6655-008	-2.7764-006	4.4526-007	2.0888+000
0.75000	0.99895	1.3879-008	-2.7761-006	4.4524-007	2.0886+000
0.80000	0.99892	1.1103-008	-2.7759-006	4.4523-007	2.0885+000
0.85000	0.99890	8.3268-009	-2.7757-006	4.4521-007	2.0884+000
0.90000	0.99889	5.5511-009	-2.7756-006	4.4521-007	2.0883+000
0.95000	0.99888	2.7756-009	-2.7755-006	4.4520-007	2.0883+000
1.00000	0.99888	0.0000+000	-2.7755-006	4.4520-007	2.0883+000

TOTAL CURRENT PER CM2 IN AMPS   0.0029

$\theta = 0.7$, cylinder radius 10^{-4} cm, $i_o = 10^{-6}$ A/cm^2

Result after 4 iterations

POSITION	RELATIVE POTENTIAL	CURRENT IN AMPS	CURRENT DERIVATIVE	DISTRIBUTION PARAMETERS	
0.00000	1.00000	4.5565-008	-2.7860-006	4.4580-005	2.0938+000
0.05000	0.99107	4.2821-008	-2.7026-006	4.4088-005	2.0504+000
0.10000	0.98269	4.0157-008	-2.6261-006	4.3593-005	2.0105+000
0.15000	0.97483	3.7567-008	-2.5558-006	4.3104-005	1.9738+000
0.20000	0.96750	3.5044-008	-2.4915-006	4.2626-005	1.9402+000
0.25000	0.96066	3.2582-008	-2.4327-006	4.2163-005	1.9094+000
0.30000	0.95432	3.0177-008	-2.3790-006	4.1719-005	1.8812+000
0.35000	0.94846	2.7822-008	-2.3303-006	4.1298-005	1.8555+000
0.40000	0.94307	2.5514-008	-2.2861-006	4.0901-005	1.8323+000
0.45000	0.93815	2.3249-008	-2.2463-006	4.0531-005	1.8112+000
0.50000	0.93367	2.1020-008	-2.2106-006	4.0189-005	1.7923+000
0.55000	0.92965	1.8826-008	-2.1789-006	3.9878-005	1.7755+000
0.60000	0.92606	1.6661-008	-2.1509-006	3.9597-005	1.7606+000
0.65000	0.92291	1.4523-008	-2.1266-006	3.9347-005	1.7477+000
0.70000	0.92019	1.2407-008	-2.1057-006	3.9130-005	1.7366+000
0.75000	0.91790	1.0311-008	-2.0882-006	3.8946-005	1.7273+000
0.80000	0.91602	8.2297-009	-2.0741-006	3.8795-005	1.7197+000
0.85000	0.91457	6.1613-009	-2.0631-006	3.8677-005	1.7138+000
0.90000	0.91353	4.1024-009	-2.0553-006	3.8593-005	1.7097+000
0.95000	0.91291	2.0496-009	-2.0507-006	3.8542-005	1.7072+000
1.00000	0.91270	0.0000+000	-2.0491-006	3.8525-005	1.7064+000

TOTAL CURRENT PER CM2 IN AMPS   0.2417

$\theta = 0.7$, cylinder radius 10^{-4} cm, $i_o = 10^{-7}$ A/cm^2

Result after 3 iterations

POSITION	RELATIVE POTENTIAL	CURRENT IN AMPS	CURRENT DERIVATIVE	DISTRIBUTION PARAMETERS	
0.00000	1.00000	7.4332-009	-3.8840-007	9.7581-006	6.6211-001
0.05000	0.99854	7.0460-009	-3.8588-007	9.6983-006	6.5984-001
0.10000	0.99715	6.6614-009	-3.8351-007	9.6420-006	6.5770-001
0.15000	0.99584	6.2790-009	-3.8128-007	9.5890-006	6.5569-001
0.20000	0.99461	5.8988-009	-3.7919-007	9.5395-006	6.5380-001
0.25000	0.99346	5.5206-009	-3.7725-007	9.4932-006	6.5204-001
0.30000	0.99238	5.1442-009	-3.7544-007	9.4502-006	6.5039-001
0.35000	0.99138	4.7696-009	-3.7376-007	9.4103-006	6.4887-001
0.40000	0.99045	4.3967-009	-3.7222-007	9.3736-006	6.4746-001
0.45000	0.98960	4.0252-009	-3.7081-007	9.3400-006	6.4617-001
0.50000	0.98883	3.6550-009	-3.6953-007	9.3094-006	6.4500-001
0.55000	0.98813	3.2861-009	-3.6837-007	9.2819-006	6.4394-001
0.60000	0.98750	2.9182-009	-3.6734-007	9.2573-006	6.4299-001
0.65000	0.98695	2.5513-009	-3.6644-007	9.2357-006	6.4216-001
0.70000	0.98647	2.1853-009	-3.6565-007	9.2170-006	6.4144-001
0.75000	0.98606	1.8200-009	-3.6499-007	9.2013-006	6.4083-001
0.80000	0.98573	1.4553-009	-3.6445-007	9.1884-006	6.4033-001
0.85000	0.98547	1.0910-009	-3.6404-007	9.1784-006	6.3995-001
0.90000	0.98529	7.2716-010	-3.6374-007	9.1713-006	6.3967-001
0.95000	0.98518	3.6352-010	-3.6356-007	9.1670-006	6.3951-001
1.00000	0.98514	0.0000+000	-3.6350-007	9.1656-006	6.3945-001

TOTAL CURRENT PER CM2 IN AMPS   0.0394

$\theta = 0.7$, cylinder radius 10^{-4} cm, $i_0 = 10^{-8}$ A/cm^2

Result after 3 iterations

POSITION	RELATIVE POTENTIAL	CURRENT IN AMPS	CURRENT DERIVATIVE	DISTRIBUTION PARAMETERS	
0.00000	1.00000	8.1004-010	-4.0708-008	1.0739-006	2.0938-001
0.05000	0.99984	7.6935-010	-4.0678-008	1.0731-006	2.0930-001
0.10000	0.99969	7.2869-010	-4.0649-008	1.0724-006	2.0922-001
0.15000	0.99955	6.8805-010	-4.0622-008	1.0717-006	2.0915-001
0.20000	0.99941	6.4744-010	-4.0596-008	1.0710-006	2.0909-001
0.25000	0.99928	6.0686-010	-4.0572-008	1.0704-006	2.0903-001
0.30000	0.99917	5.6630-010	-4.0550-008	1.0698-006	2.0897-001
0.35000	0.99906	5.2576-010	-4.0529-008	1.0692-006	2.0891-001
0.40000	0.99895	4.8524-010	-4.0510-008	1.0687-006	2.0886-001
0.45000	0.99886	4.4474-010	-4.0492-008	1.0683-006	2.0882-001
0.50000	0.99877	4.0425-010	-4.0476-008	1.0678-006	2.0878-001
0.55000	0.99870	3.6378-010	-4.0461-008	1.0674-006	2.0874-001
0.60000	0.99863	3.2333-010	-4.0448-008	1.0671-006	2.0870-001
0.65000	0.99857	2.8288-010	-4.0437-008	1.0668-006	2.0867-001
0.70000	0.99851	2.4245-010	-4.0427-008	1.0665-006	2.0865-001
0.75000	0.99847	2.0203-010	-4.0418-008	1.0663-006	2.0863-001
0.80000	0.99843	1.6161-010	-4.0411-008	1.0661-006	2.0861-001
0.85000	0.99840	1.2121-010	-4.0406-008	1.0660-006	2.0859-001
0.90000	0.99838	8.0802-011	-4.0402-008	1.0659-006	2.0858-001
0.95000	0.99837	4.0401-011	-4.0400-008	1.0658-006	2.0858-001
1.00000	0.99836	0.0000+000	-4.0399-008	1.0658-006	2.0858-001

TOTAL CURRENT PER CM2 IN AMPS   0.0043

$\theta = 0.7$, cylinder radius 10^{-5} cm, $i_0 = 10^{-6}$ A/cm^2

Result after 4 iterations

POSITION	RELATIVE POTENTIAL	CURRENT IN AMPS	CURRENT DERIVATIVE	DISTRIBUTION PARAMETERS	
0.00000	1.00000	5.8483-010	-4.0708-008	1.0739-004	2.0938-001
0.05000	0.98858	5.4520-010	-3.8598-008	1.0185-004	2.0385-001
0.10000	0.97795	5.0756-010	-3.6729-008	9.6948-005	1.9883-001
0.15000	0.96806	4.7167-010	-3.5073-008	9.2595-005	1.9427-001
0.20000	0.95887	4.3735-010	-3.3601-008	8.8728-005	1.9014-001
0.25000	0.95037	4.0442-010	-3.2293-008	8.5290-005	1.8639-001
0.30000	0.94252	3.7271-010	-3.1131-008	8.2233-005	1.8299-001
0.35000	0.93530	3.4211-010	-3.0099-008	7.9517-005	1.7992-001
0.40000	0.92868	3.1248-010	-2.9183-008	7.7108-005	1.7715-001
0.45000	0.92266	2.8371-010	-2.8374-008	7.4977-005	1.7467-001
0.50000	0.91721	2.5570-010	-2.7660-008	7.3100-005	1.7245-001
0.55000	0.91232	2.2836-010	-2.7036-008	7.1454-005	1.7048-001
0.60000	0.90798	2.0160-010	-2.6492-008	7.0024-005	1.6876-001
0.65000	0.90417	1.7535-010	-2.6025-008	6.8793-005	1.6726-001
0.70000	0.90089	1.4953-010	-2.5629-008	6.7749-005	1.6598-001
0.75000	0.89812	1.2407-010	-2.5300-008	6.6883-005	1.6490-001
0.80000	0.89587	9.8905-011	-2.5035-008	6.6185-005	1.6404-001
0.85000	0.89412	7.3977-011	-2.4831-008	6.5648-005	1.6337-001
0.90000	0.89288	4.9222-011	-2.4687-008	6.5269-005	1.6289-001
0.95000	0.89213	2.4583-011	-2.4602-008	6.5042-005	1.6260-001
1.00000	0.89188	0.0000+000	-2.4573-008	6.4967-005	1.6251-001

TOTAL CURRENT PER CM2 IN AMPS   0.3103

$\theta = 0.7$, cylinder radius 10^{-5} cm, $i_o = 10^{-7}$ A/cm^2

Result after 3 iterations

POSITION	RELATIVE POTENTIAL	CURRENT IN AMPS	CURRENT DERIVATIVE	DISTRIBUTION PARAMETERS	
0.00000	1.00000	7.7944-011	-4.0908-009	1.0845-005	6.6211-002
0.05000	0.99847	7.3868-011	-4.0615-009	1.0768-005	6.5973-002
0.10000	0.99701	6.9820-011	-4.0340-009	1.0695-005	6.5749-002
0.15000	0.99564	6.5799-011	-4.0082-009	1.0626-005	6.5538-002
0.20000	0.99435	6.1803-011	-3.9840-009	1.0562-005	6.5341-002
0.25000	0.99315	5.7831-011	-3.9615-009	1.0503-005	6.5156-002
0.30000	0.99202	5.3880-011	-3.9406-009	1.0447-005	6.4984-002
0.35000	0.99097	4.9949-011	-3.9213-009	1.0396-005	6.4824-002
0.40000	0.99000	4.6037-011	-3.9035-009	1.0349-005	6.4677-002
0.45000	0.98911	4.2141-011	-3.8873-009	1.0306-005	6.4542-002
0.50000	0.98829	3.8262-011	-3.8725-009	1.0267-005	6.4419-002
0.55000	0.98756	3.4396-011	-3.8592-009	1.0232-005	6.4308-002
0.60000	0.98690	3.0543-011	-3.8473-009	1.0200-005	6.4209-002
0.65000	0.98633	2.6701-011	-3.8369-009	1.0173-005	6.4122-002
0.70000	0.98582	2.2868-011	-3.8279-009	1.0149-005	6.4047-002
0.75000	0.98540	1.9044-011	-3.8203-009	1.0129-005	6.3984-002
0.80000	0.98505	1.5227-011	-3.8141-009	1.0112-005	6.3932-002
0.85000	0.98479	1.1416-011	-3.8093-009	1.0099-005	6.3891-002
0.90000	0.98459	7.6082-012	-3.8059-009	1.0090-005	6.3863-002
0.95000	0.98448	3.8034-012	-3.8038-009	1.0085-005	6.3845-002
1.00000	0.98444	0.0000+000	-3.8032-009	1.0083-005	6.3840-002

TOTAL CURRENT PER CM2 IN AMPS   0.0414

$\theta = 0.7$, cylinder radius 10^{-5} cm, $i_o = 10^{-8}$ A/cm^2

Result after 3 iterations

POSITION	RELATIVE POTENTIAL	CURRENT IN AMPS	CURRENT DERIVATIVE	DISTRIBUTION PARAMETERS	
0.00000	1.00000	8.1439-012	-4.0929-010	1.0856-006	2.0938-002
0.05000	0.99984	7.7347-012	-4.0898-010	1.0848-006	2.0930-002
0.10000	0.99969	7.3259-012	-4.0869-010	1.0840-006	2.0922-002
0.15000	0.99954	6.9173-012	-4.0841-010	1.0833-006	2.0915-002
0.20000	0.99941	6.5091-012	-4.0815-010	1.0826-006	2.0909-002
0.25000	0.99928	6.1010-012	-4.0791-010	1.0819-006	2.0902-002
0.30000	0.99916	5.6932-012	-4.0768-010	1.0813-006	2.0897-002
0.35000	0.99905	5.2857-012	-4.0747-010	1.0808-006	2.0891-002
0.40000	0.99895	4.8783-012	-4.0727-010	1.0803-006	2.0886-002
0.45000	0.99885	4.4711-012	-4.0709-010	1.0798-006	2.0882-002
0.50000	0.99877	4.0641-012	-4.0693-010	1.0793-006	2.0877-002
0.55000	0.99869	3.6572-012	-4.0678-010	1.0790-006	2.0873-002
0.60000	0.99862	3.2505-012	-4.0664-010	1.0786-006	2.0870-002
0.65000	0.99856	2.8439-012	-4.0653-010	1.0783-006	2.0867-002
0.70000	0.99850	2.4375-012	-4.0642-010	1.0780-006	2.0864-002
0.75000	0.99846	2.0311-012	-4.0634-010	1.0778-006	2.0862-002
0.80000	0.99842	1.6248-012	-4.0627-010	1.0776-006	2.0860-002
0.85000	0.99839	1.2185-012	-4.0621-010	1.0775-006	2.0859-002
0.90000	0.99837	8.1232-013	-4.0617-010	1.0774-006	2.0858-002
0.95000	0.99836	4.0615-013	-4.0615-010	1.0773-006	2.0857-002
1.00000	0.99836	0.0000+000	-4.0614-010	1.0773-006	2.0857-002

TOTAL CURRENT PER CM2 IN AMPS   0.0043

$\theta = 0.9$, cylinder radius 10^{-3} cm, $i_0 = 10^{-6}$ A/cm^2

Result after 3 iterations

POSITION	RELATIVE POTENTIAL	CURRENT IN AMPS	CURRENT DERIVATIVE	DISTRIBUTION PARAMETERS	
0.00000	1.00000	4.8127-007	-2.4364-005	2.0576-008	1.0661+001
0.05000	0.99926	4.5693-007	-2.4319-005	2.0867-008	1.0643+001
0.10000	0.99856	4.3263-007	-2.4278-005	2.1146-008	1.0625+001
0.15000	0.99790	4.0837-007	-2.4238-005	2.1414-008	1.0609+001
0.20000	0.99728	3.8416-007	-2.4201-005	2.1668-008	1.0593+001
0.25000	0.99669	3.5997-007	-2.4166-005	2.1909-008	1.0579+001
0.30000	0.99615	3.3582-007	-2.4133-005	2.2136-008	1.0565+001
0.35000	0.99564	3.1170-007	-2.4103-005	2.2350-008	1.0553+001
0.40000	0.99517	2.8762-007	-2.4075-005	2.2549-008	1.0541+001
0.45000	0.99473	2.6355-007	-2.4049-005	2.2733-008	1.0530+001
0.50000	0.99434	2.3952-007	-2.4026-005	2.2903-008	1.0520+001
0.55000	0.99398	2.1550-007	-2.4005-005	2.3057-008	1.0512+001
0.60000	0.99366	1.9151-007	-2.3986-005	2.3196-008	1.0504+001
0.65000	0.99338	1.6753-007	-2.3969-005	2.3318-008	1.0497+001
0.70000	0.99314	1.4357-007	-2.3954-005	2.3425-008	1.0491+001
0.75000	0.99293	1.1962-007	-2.3942-005	2.3516-008	1.0486+001
0.80000	0.99276	9.5682-008	-2.3932-005	2.3590-008	1.0482+001
0.85000	0.99263	7.1754-008	-2.3924-005	2.3649-008	1.0478+001
0.90000	0.99253	4.7832-008	-2.3919-005	2.3690-008	1.0476+001
0.95000	0.99248	2.3915-008	-2.3916-005	2.3715-008	1.0475+001
1.00000	0.99246	0.0000+000	-2.3914-005	2.3723-008	1.0474+001

TOTAL CURRENT PER CM2 IN AMPS   0.0766

$\theta = 0.9$, cylinder radius 10^{-3} cm, $i_0 = 10^{-7}$ A/cm^2

Result after 3 iterations

POSITION	RELATIVE POTENTIAL	CURRENT IN AMPS	CURRENT DERIVATIVE	DISTRIBUTION PARAMETERS	
0.00000	1.00000	1.3448-007	-6.7511-006	1.6390-006	3.3713+000
0.05000	0.99979	1.2773-007	-6.7471-006	1.6397-006	3.3697+000
0.10000	0.99960	1.2098-007	-6.7433-006	1.6403-006	3.3681+000
0.15000	0.99941	1.1424-007	-6.7397-006	1.6409-006	3.3667+000
0.20000	0.99924	1.0750-007	-6.7363-006	1.6414-006	3.3653+000
0.25000	0.99908	1.0077-007	-6.7331-006	1.6419-006	3.3640+000
0.30000	0.99892	9.4035-008	-6.7301-006	1.6424-006	3.3628+000
0.35000	0.99878	8.7307-008	-6.7274-006	1.6428-006	3.3617+000
0.40000	0.99865	8.0581-008	-6.7248-006	1.6432-006	3.3606+000
0.45000	0.99853	7.3857-008	-6.7225-006	1.6436-006	3.3597+000
0.50000	0.99842	6.7135-008	-6.7203-006	1.6439-006	3.3588+000
0.55000	0.99832	6.0416-008	-6.7184-006	1.6443-006	3.3580+000
0.60000	0.99823	5.3699-008	-6.7166-006	1.6445-006	3.3573+000
0.65000	0.99815	4.6983-008	-6.7151-006	1.6448-006	3.3567+000
0.70000	0.99808	4.0268-008	-6.7138-006	1.6450-006	3.3561+000
0.75000	0.99802	3.3555-008	-6.7126-006	1.6452-006	3.3557+000
0.80000	0.99797	2.6843-008	-6.7117-006	1.6453-006	3.3553+000
0.85000	0.99794	2.0131-008	-6.7110-006	1.6454-006	3.3550+000
0.90000	0.99791	1.3421-008	-6.7105-006	1.6455-006	3.3548+000
0.95000	0.99789	6.7101-009	-6.7102-006	1.6456-006	3.3547+000
1.00000	0.99789	0.0000+000	-6.7101-006	1.6456-006	3.3546+000

TOTAL CURRENT PER CM2 IN AMPS   0.0214

$\theta = 0.9$, cylinder radius 10^{-3} cm, $i_o = 10^{-8}$ A/cm^2

Result after 3 iterations

POSITION	RELATIVE POTENTIAL	CURRENT IN AMPS	CURRENT DERIVATIVE	DISTRIBUTION PARAMETERS	
0.00000	1.00000	2.4002-008	-1.2012-006	8.3199-007	1.0661+000
0.05000	0.99996	2.2800-008	-1.2011-006	8.3188-007	1.0660+000
0.10000	0.99993	2.1599-008	-1.2009-006	8.3178-007	1.0659+000
0.15000	0.99990	2.0398-008	-1.2007-006	8.3168-007	1.0658+000
0.20000	0.99986	1.9198-008	-1.2006-006	8.3159-007	1.0658+000
0.25000	0.99983	1.7997-008	-1.2004-006	8.3151-007	1.0657+000
0.30000	0.99981	1.6797-008	-1.2003-006	8.3143-007	1.0656+000
0.35000	0.99978	1.5596-008	-1.2002-006	8.3135-007	1.0656+000
0.40000	0.99976	1.4396-008	-1.2000-006	8.3128-007	1.0655+000
0.45000	0.99974	1.3196-008	-1.1999-006	8.3122-007	1.0654+000
0.50000	0.99972	1.1996-008	-1.1998-006	8.3116-007	1.0654+000
0.55000	0.99970	1.0796-008	-1.1997-006	8.3111-007	1.0653+000
0.60000	0.99968	9.5964-009	-1.1997-006	8.3106-007	1.0653+000
0.65000	0.99967	8.3966-009	-1.1996-006	8.3102-007	1.0653+000
0.70000	0.99966	7.1969-009	-1.1995-006	8.3098-007	1.0652+000
0.75000	0.99965	5.9973-009	-1.1995-006	8.3095-007	1.0652+000
0.80000	0.99964	4.7977-009	-1.1994-006	8.3093-007	1.0652+000
0.85000	0.99963	3.5982-009	-1.1994-006	8.3091-007	1.0652+000
0.90000	0.99963	2.3988-009	-1.1994-006	8.3090-007	1.0652+000
0.95000	0.99962	1.1993-009	-1.1994-006	8.3089-007	1.0652+000
1.00000	0.99962	0.0000+000	-1.1994-006	8.3089-007	1.0652+000

TOTAL CURRENT PER CM2 IN AMPS 0.0038

$\theta = 0.9$, cylinder radius 10^{-4} cm, $i_o = 10^{-6}$ A/cm^2

Result after 4 iterations

POSITION	RELATIVE POTENTIAL	CURRENT IN AMPS	CURRENT DERIVATIVE	DISTRIBUTION PARAMETERS	
0.00000	1.00000	2.1888-008	-1.2012-006	8.3199-005	1.0661+000
0.05000	0.99665	2.0695-008	-1.1847-006	8.2223-005	1.0578+000
0.10000	0.99349	1.9518-008	-1.1692-006	8.1309-005	1.0500+000
0.15000	0.99052	1.8357-008	-1.1548-006	8.0453-005	1.0427+000
0.20000	0.98772	1.7209-008	-1.1414-006	7.9655-005	1.0359+000
0.25000	0.98511	1.6074-008	-1.1290-006	7.8912-005	1.0295+000
0.30000	0.98267	1.4950-008	-1.1175-006	7.8224-005	1.0237+000
0.35000	0.98040	1.3838-008	-1.1070-006	7.7589-005	1.0182+000
0.40000	0.97832	1.2736-008	-1.0973-006	7.7006-005	1.0133+000
0.45000	0.97640	1.1643-008	-1.0885-006	7.6474-005	1.0087+000
0.50000	0.97466	1.0559-008	-1.0806-006	7.5991-005	1.0046+000
0.55000	0.97308	9.4819-009	-1.0734-006	7.5557-005	1.0009+000
0.60000	0.97167	8.4117-009	-1.0671-006	7.5171-005	9.9762-001
0.65000	0.97044	7.3474-009	-1.0616-006	7.4832-005	9.9473-001
0.70000	0.96936	6.2883-009	-1.0568-006	7.4539-005	9.9223-001
0.75000	0.96846	5.2336-009	-1.0528-006	7.4293-005	9.9013-001
0.80000	0.96772	4.1825-009	-1.0495-006	7.4092-005	9.8841-001
0.85000	0.96714	3.1343-009	-1.0469-006	7.3936-005	9.8708-001
0.90000	0.96673	2.0883-009	-1.0451-006	7.3824-005	9.8613-001
0.95000	0.96649	1.0438-009	-1.0441-006	7.3758-005	9.8556-001
1.00000	0.96641	0.0000+000	-1.0437-006	7.3735-005	9.8537-001

TOTAL CURRENT PER CM2 IN AMPS 0.3484

$\theta = 0.9$, cylinder radius 10^{-4} cm, $i_0 = 10^{-7}$ A/cm^2
Result after 3 iterations

POSITION	RELATIVE POTENTIAL	CURRENT IN AMPS	CURRENT DERIVATIVE	DISTRIBUTION PARAMETERS	
0.00000	1.00000	2.6564-009	-1.3453-007	1.0555-005	3.3713-001
0.05000	0.99959	2.5220-009	-1.3428-007	1.0536-005	3.3681-001
0.10000	0.99921	2.3878-009	-1.3404-007	1.0517-005	3.3650-001
0.15000	0.99884	2.2539-009	-1.3382-007	1.0500-005	3.3622-001
0.20000	0.99850	2.1202-009	-1.3360-007	1.0483-005	3.3594-001
0.25000	0.99818	1.9867-009	-1.3340-007	1.0468-005	3.3569-001
0.30000	0.99787	1.8534-009	-1.3322-007	1.0453-005	3.3545-001
0.35000	0.99759	1.7203-009	-1.3304-007	1.0440-005	3.3523-001
0.40000	0.99733	1.5873-009	-1.3288-007	1.0428-005	3.3503-001
0.45000	0.99709	1.4545-009	-1.3274-007	1.0416-005	3.3484-001
0.50000	0.99688	1.3218-009	-1.3260-007	1.0406-005	3.3467-001
0.55000	0.99668	1.1893-009	-1.3248-007	1.0397-005	3.3451-001
0.60000	0.99650	1.0568-009	-1.3238-007	1.0388-005	3.3438-001
0.65000	0.99635	9.2451-010	-1.3228-007	1.0381-005	3.3425-001
0.70000	0.99621	7.9227-010	-1.3220-007	1.0374-005	3.3415-001
0.75000	0.99610	6.6011-010	-1.3213-007	1.0369-005	3.3406-001
0.80000	0.99600	5.2801-010	-1.3207-007	1.0365-005	3.3399-001
0.85000	0.99593	3.9596-010	-1.3203-007	1.0361-005	3.3393-001
0.90000	0.99588	2.6396-010	-1.3199-007	1.0359-005	3.3389-001
0.95000	0.99585	1.3197-010	-1.3198-007	1.0357-005	3.3386-001
1.00000	0.99584	0.0000+000	-1.3197-007	1.0357-005	3.3386-001

TOTAL CURRENT PER CM2 IN AMPS   0.0423

$\theta = 0.9$, cylinder radius 10^{-4} cm, $i_0 = 10^{-8}$ A/cm^2

POSITION	RELATIVE POTENTIAL	CURRENT IN AMPS	CURRENT DERIVATIVE	DISTRIBUTION PARAMETERS	
0.00000	1.00000	2.7214-010	-1.3624-008	1.0826-006	1.0661-001
0.05000	0.99996	2.5851-010	-1.3622-008	1.0824-006	1.0660-001
0.10000	0.99992	2.4489-010	-1.3619-008	1.0822-006	1.0659-001
0.15000	0.99988	2.3127-010	-1.3617-008	1.0820-006	1.0658-001
0.20000	0.99985	2.1766-010	-1.3614-008	1.0819-006	1.0657-001
0.25000	0.99981	2.0405-010	-1.3612-008	1.0817-006	1.0656-001
0.30000	0.99978	1.9043-010	-1.3610-008	1.0815-006	1.0656-001
0.35000	0.99975	1.7682-010	-1.3608-008	1.0814-006	1.0655-001
0.40000	0.99973	1.6321-010	-1.3607-008	1.0813-006	1.0654-001
0.45000	0.99970	1.4961-010	-1.3605-008	1.0811-006	1.0654-001
0.50000	0.99968	1.3600-010	-1.3604-008	1.0810-006	1.0653-001
0.55000	0.99966	1.2240-010	-1.3602-008	1.0809-006	1.0652-001
0.60000	0.99964	1.0879-010	-1.3601-008	1.0808-006	1.0652-001
0.65000	0.99962	9.5193-011	-1.3600-008	1.0807-006	1.0652-001
0.70000	0.99961	8.1592-011	-1.3599-008	1.0807-006	1.0651-001
0.75000	0.99960	6.7992-011	-1.3599-008	1.0806-006	1.0651-001
0.80000	0.99959	5.4392-011	-1.3598-008	1.0806-006	1.0651-001
0.85000	0.99958	4.0795-011	-1.3598-008	1.0805-006	1.0651-001
0.90000	0.99958	2.7196-011	-1.3597-008	1.0805-006	1.0650-001
0.95000	0.99957	1.3598-011	-1.3597-008	1.0805-006	1.0650-001
1.00000	0.99957	0.0000+000	-1.3597-008	1.0805-006	1.0650-001

TOTAL CURRENT PER CM2 IN AMPS   0.0043

$\theta = 0.9$, cylinder radius 10^{-5} cm, $i_O = 10^{-6}$ A/cm^2

Result after 4 iterations

POSITION	RELATIVE POTENTIAL	CURRENT IN AMPS	CURRENT DERIVATIVE	DISTRIBUTION PARAMETERS	
0.00000	1.00000	2.4287-010	-1.3624-008	1.0826-004	1.0661-001
0.05000	0.99629	2.2937-010	-1.3390-008	1.0640-004	1.0569-001
0.10000	0.99279	2.1609-010	-1.3172-008	1.0467-004	1.0482-001
0.15000	0.98949	2.0302-010	-1.2970-008	1.0308-004	1.0402-001
0.20000	0.98640	1.9014-010	-1.2784-008	1.0160-004	1.0327-001
0.25000	0.98352	1.7745-010	-1.2612-008	1.0023-004	1.0257-001
0.30000	0.98082	1.6492-010	-1.2454-008	9.8980-005	1.0192-001
0.35000	0.97833	1.5253-010	-1.2310-008	9.7832-005	1.0133-001
0.40000	0.97603	1.4029-010	-1.2178-008	9.6785-005	1.0079-001
0.45000	0.97392	1.2817-010	-1.2058-008	9.5835-005	1.0029-001
0.50000	0.97200	1.1617-010	-1.1950-008	9.4978-005	9.9838-002
0.55000	0.97027	1.0427-010	-1.1854-008	9.4211-005	9.9433-002
0.60000	0.96872	9.2460-011	-1.1768-008	9.3533-005	9.9073-002
0.65000	0.96736	8.0731-011	-1.1693-008	9.2939-005	9.8758-002
0.70000	0.96618	6.9070-011	-1.1629-008	9.2429-005	9.8486-002
0.75000	0.96519	5.7469-011	-1.1575-008	9.2000-005	9.8257-002
0.80000	0.96437	4.5917-011	-1.1531-008	9.1651-005	9.8070-002
0.85000	0.96374	3.4404-011	-1.1497-008	9.1381-005	9.7925-002
0.90000	0.96329	2.2920-011	-1.1473-008	9.1188-005	9.7821-002
0.95000	0.96302	1.1455-011	-1.1458-008	9.1073-005	9.7759-002
1.00000	0.96293	0.0000+000	-1.1453-008	9.1035-005	9.7739-002

TOTAL CURRENT PER CM2 IN AMPS   0.3865

$\theta = 0.9$, cylinder radius 10^{-5} cm, $i_O = 10^{-7}$ A/cm^2

Result after 3 iterations

POSITION	RELATIVE POTENTIAL	CURRENT IN AMPS	CURRENT DERIVATIVE	DISTRIBUTION PARAMETERS	
0.00000	1.00000	2.6926-011	-1.3642-009	1.0854-005	3.3713-002
0.05000	0.99959	2.5563-011	-1.3615-009	1.0833-005	3.3680-002
0.10000	0.99920	2.4203-011	-1.3590-009	1.0813-005	3.3649-002
0.15000	0.99883	2.2845-011	-1.3567-009	1.0795-005	3.3620-002
0.20000	0.99848	2.1490-011	-1.3545-009	1.0777-005	3.3593-002
0.25000	0.99815	2.0136-011	-1.3524-009	1.0760-005	3.3567-002
0.30000	0.99785	1.8785-011	-1.3505-009	1.0745-005	3.3543-002
0.35000	0.99756	1.7435-011	-1.3487-009	1.0731-005	3.3521-002
0.40000	0.99730	1.6088-011	-1.3470-009	1.0717-005	3.3500-002
0.45000	0.99705	1.4741-011	-1.3455-009	1.0705-005	3.3481-002
0.50000	0.99683	1.3397-011	-1.3441-009	1.0694-005	3.3464-002
0.55000	0.99663	1.2053-011	-1.3428-009	1.0684-005	3.3448-002
0.60000	0.99645	1.0711-011	-1.3417-009	1.0675-005	3.3434-002
0.65000	0.99630	9.3697-012	-1.3407-009	1.0667-005	3.3422-002
0.70000	0.99616	8.0295-012	-1.3398-009	1.0661-005	3.3411-002
0.75000	0.99604	6.6900-012	-1.3391-009	1.0655-005	3.3402-002
0.80000	0.99595	5.3512-012	-1.3385-009	1.0650-005	3.3394-002
0.85000	0.99588	4.0130-012	-1.3380-009	1.0646-005	3.3389-002
0.90000	0.99582	2.6751-012	-1.3377-009	1.0644-005	3.3385-002
0.95000	0.99579	1.3375-012	-1.3375-009	1.0642-005	3.3382-002
1.00000	0.99578	0.0000+000	-1.3375-009	1.0642-005	3.3381-002

TOTAL CURRENT PER CM2 IN AMPS   0.0429

$\theta = 0.9$, cylinder radius 10^{-5} cm, $i_o = 10^{-8}$ A/cm^2

Result after 3 iterations

POSITION	RELATIVE POTENTIAL	CURRENT IN AMPS	CURRENT DERIVATIVE	DISTRIBUTION PARAMETERS	
0.00000	1.00000	2.7251-012	-1.3643-010	1.0857-006	1.0661-002
0.05000	0.99996	2.5887-012	-1.3641-010	1.0855-006	1.0660-002
0.10000	0.99992	2.4523-012	-1.3638-010	1.0853-006	1.0659-002
0.15000	0.99988	2.3159-012	-1.3636-010	1.0851-006	1.0658-002
0.20000	0.99985	2.1796-012	-1.3634-010	1.0849-006	1.0657-002
0.25000	0.99981	2.0433-012	-1.3631-010	1.0847-006	1.0656-002
0.30000	0.99978	1.9070-012	-1.3629-010	1.0846-006	1.0656-002
0.35000	0.99975	1.7707-012	-1.3628-010	1.0844-006	1.0655-002
0.40000	0.99973	1.6344-012	-1.3626-010	1.0843-006	1.0654-002
0.45000	0.99970	1.4982-012	-1.3624-010	1.0842-006	1.0654-002
0.50000	0.99968	1.3619-012	-1.3623-010	1.0841-006	1.0653-002
0.55000	0.99966	1.2257-012	-1.3622-010	1.0840-006	1.0652-002
0.60000	0.99964	1.0895-012	-1.3620-010	1.0839-006	1.0652-002
0.65000	0.99962	9.5326-013	-1.3619-010	1.0838-006	1.0652-002
0.70000	0.99961	8.1707-013	-1.3618-010	1.0837-006	1.0651-002
0.75000	0.99960	6.8088-013	-1.3618-010	1.0836-006	1.0651-002
0.80000	0.99959	5.4470-013	-1.3617-010	1.0836-006	1.0651-002
0.85000	0.99958	4.0853-013	-1.3617-010	1.0836-006	1.0651-002
0.90000	0.99958	2.7235-013	-1.3616-010	1.0835-006	1.0650-002
0.95000	0.99957	1.3618-013	-1.3616-010	1.0835-006	1.0650-002
1.00000	0.99957	0.0000+000	-1.3616-010	1.0835-006	1.0650-002

TOTAL CURRENT PER CM2 IN AMPS   0.0043

INDEX OF CATALYST MATERIALS